Imperial College London

Aberrant RNA replication of highly pathogenic avian influenza viruses and its impact on the mammalian-associated cytokine storm

Rebecca Louise Penn

Supervised by Professor Wendy Barclay and Professor Cecilia Johansson

Department of Infectious Disease

Faculty of Medicine

Submitted for the Degree of Doctor of Philosophy

Author's declaration

I, Rebecca Penn, declare that the work presented in this thesis is entirely my own, except where otherwise stated. Any material from other sources has been properly acknowledged.

Copyright declaration

Acknowledgements

Firstly, I would like to thank my supervisors Wendy and Cecilia for allowing me the opportunity to conduct a PhD with them; both have been incredibly supportive throughout the past four years. Special thanks to Wendy who always made time to discuss my project even whilst guiding the government during a global pandemic! Thanks for making me feel a valued member of your lab and always believing in me.

Thanks also to the MRC for funding my PhD and letting me join the doctoral training program.

I'm thankful to all members of the Barclay lab who not only contributed to my progression as a scientist but also made my time here enjoyable. Even when experiments failed or I felt overwhelmed, I could always count on group members to suggest alternative experiments, keep the snack box topped up and cheer me up (often involving a trip to the pub) – thank you all!!

I'm thankful to all my friends who I haven't seen as much as I would have liked to – your understanding about my absence is much appreciated!

Finally, I'm grateful to my family. My parents for always asking for updates on my PhD and asking me constantly if I've finished yet? My brother for making me laugh. My twin sister who said I was mad to do a PhD (she speaks from experience), but is always happy to offer advice, listen to my woes and put me back on track!

To my children – Libby and Rowan. Thanks for reminding me that there is life outside the lab and for constantly being super fun! I apologise for the many times when Mummy was working and couldn't join you in your adventures.

To my husband, Andy, you were the one who encouraged me to follow my dream even though it meant we would be worse off financially and would make family life a bit more stressful for everyone. You have always supported me and your unwavering belief that I can do this, has ultimately got me through it. Thank you.

Abstract

Highly pathogenic avian influenza viruses (HPAIVs) such as the H5N1 subtype, can sporadically cross the species barrier from their natural host (aquatic waterfowl) into mammalian species including humans with often fatal outcomes. Mammalian HPAIV pathogenesis is associated with an overzealous innate immune response characterised by elevated levels of pro-inflammatory cytokines, referred to as a "cytokine storm." Aberrant RNAs including defective viral genomes (DVGs) and mini viral RNAs (mvRNAs) are made by the viral polymerase in error during replication and cytokine induction is associated with their emergence *in vivo*. High viral replication of HPAIVs within myeloid immune cells could also trigger inappropriate levels of type I interferon (IFN) and pro-inflammatory cytokines.

Here we investigated the role that aberrant replication of HPAIVs has in the mammalian-associated cytokine storm. Firstly, we demonstrated that viruses containing the internal genes of H5N1 did not generate higher levels of vRNA in macrophages than those containing internal genes from an H1N1pdm09 virus. Next, by manipulating the levels of DVGs in H5N1 recombinant viruses, high DVG stocks displayed reduced viral replication but increased type I IFN and pro-inflammatory cytokines in various cell types. In BALB/c mice, DVG levels in the initial virus inoculum as well as their amplification kinetics during the infection, impacted pro-inflammatory cytokine levels, viral load, and pathogenesis. Furthermore, we showed that HPAIV polymerases generated aberrant RNAs *de novo* and limiting NP increased mvRNA synthesis. Finally, we showed that the introduction of human adapting amino acid residues into the H5N1 PB2 protein led to increased type I IFN *in vitro* but did not impact severity in mice. Overall, our results suggest that the timing and levels of aberrant RNAs generated during infection contribute to H5N1 pathogenesis. This knowledge could help guide better treatments and highlights the need to consider aberrant RNA replication products in future research.

Contents

Figures

Tables

List of acronyms and abbreviations

3P Trimeric viral RNA-dependent RNA polymerase (PB1, PB2 and PA)

50-92 A/turkey/England/50-92/1991 (H5N1)

ANOVA Analysis of variance

APC Antigen presenting cell

ANP32A/B Acidic leucine-rich nuclear phosphoprotein family member A/B

ARDS Acute respiratory distress syndrome

AUC Area under the curve

BAL Bronchoalveolar lavage

bp Base pair

BM Bone marrow

BMDM Bone marrow derived macrophage (murine)

CARD Caspase-activation and recruitment domain

cDNA Complementary DNA

cRNA Complementary RNA

cRNP Complementary ribonucleoprotein

CIP Calf intestinal alkaline phosphatase

DNA deoxyribonucleic acid

dsRNA double stranded RNA

Eng/09 A/England/195/2009 (Pdm09 H1N1)

FCS Foetal calf serum

FL Full-length

GAPDH Glyceraldehyde 3-phosphate dehydrogenase

GM-CSF Granulocyte-macrophage colony-stimulating factor

GM-DC Granulocyte-macrophage colony-stimulating factor derived dendritic cell (murine)

gs/GD goose/Guangdong lineage

HA Haemagglutinin

HP Highly pathogenic

HPAIV Highly pathogenic avian influenza virus

h.p.i Hours post infection

hMDM Human monocyte derived macrophage

IAV Influenza A virus

IFN Interferon

IL-1β Interleukin-1β

IL-6 Interleukin-6

IL-8 Interleukin-8

IP-10 Interferon gamma-induced protein 10

LP Low pathogenic

LRT Lower respiratory tract

ISG Interferon stimulated gene

M1 Matrix protein 1

M2 Matrix protein 2

MCP-1 Monocyte chemoattractant protein-1

M-CSF Macrophage colony-stimulating factor

MerTK Proto-oncogene tyrosine-protein kinase MER

MIP-1β Macrophage inflammatory protein-1β

MOI Multiplicity of Infection

mRNA messenger RNA

mvRNA mini viral RNA

Mx Myxovirus resistance protein

NA Neuraminidase

NEP Nuclear export protein

NGS Next generation sequencing

NP Nucleoprotein

NS1 Non-structural 1

NS2/NEP Non-structural 2/Nuclear export protein

nt Nucleotide

PAMP Pathogen associated molecular pattern

PA Polymerase acidic protein

PB1 Polymerase basic protein 1

PB2 Polymerase basic protein 2

PBS Phosphate buffered saline

PCR Polymerase chain reaction

PFU Plaque forming Unit

Poly I:C Polyinosinic: polycytidylic acid

PR8 A/Puerto Rico/8/1934 (H1N1)

PRR Pattern recognition receptor

qRT-PCR Quantitative reverse transcriptase polymerase chain reaction

RBC red blood cell

RG Reverse genetics

RIG-I Retinoic acid inducible gene

RNA Ribonucleic acid

RNP Ribonucleoprotein

RT-PCR Reverse transcriptase polymerase chain reaction

SA Sialic acid

SARS CoV-2 Severe acute respiratory syndrome coronavirus 2

SF Serum free

svRNA Small viral RNA

Tky/05 A/turkey/Turkey/1/2005 (H5N1)

TNF-α Tumour necrosis factor-α

TPCK L-(tosylamido-2-phenyl) ethyl chloromethyl ketone

URT Upper respiratory tract

UTR Untranslated region

vRNA Viral RNA

vRNP Viral ribonucleoprotein complex

WSN A/Wilson-Smith/1933 (H1N1) Neurotropic

WT Wildtype

ZBP1 Z-DNA binding protein 1

Zbtb46 Zinc finger and BTB domain containing 46 gene

Chapter 1 Introduction

1.1 Zoonotic viruses, novel hosts and virulence

There are numerous infectious viral diseases in humans that have a zoonotic origin; COVID-19 (caused by SARS CoV-2) resulted in the ongoing global pandemic currently responsible for over 6 million deaths worldwide (Cascella et al., 2022). Other zoonotic viruses that have recently caused outbreaks in humans are monkeypox in Africa, Europe, UK and Northern America (Adalja & Inglesby, 2022) and Marburg virus in Ghana (Hussain, 2022). Unsurprisingly, zoonotic viral infections remain a serious threat to public health; all priority pathogens currently listed on the WHO R&D blueprint fall into this category (Mehand et al., 2018). This is due to the severe infections that these viruses often cause when they spill-over into the human population; rabies virus if left untreated is always fatal (Ward & Brookes, 2021), HPAIV H5N1 has a case fatality rate (CFR) of approx. 50% (Wille & Barr, 2022), Ebola has a CFR of 25-90% (World Health Organization, 2019) and both Nipah and Hendra viruses (HeV) have CFR ranging from 50-100% (Marsh & Wang, 2012). However, many of these viruses do not cause mortality in their natural host species with some exhibiting only mild or even sub-clinical symptoms. For example, HPAIV H5N1 can be asymptomatic in wild and domestic duck species (Kim et al., 2009), and HeV manifests no noticeable signs of disease in *Pteropid* bats (Woon et al., 2020; Young et al., 1996). This makes identifying potential pandemic threats and successfully limiting transmission in the animal reservoirs more difficult. This could explain why an important feature of eradicated/nearly eradicated human infectious diseases (smallpox, polio) are their lack of host species other than humans (Baum, 2008).

When zoonotic viruses infect a new host, in most cases there is no onward transmission Indeed, it is well established that once zoonotic viruses have infected a new host species, they acquire specific mutations allowing for adaptation to the novel cell environment. A well characterised example of this is human immunodeficiency virus type-1 (HIV-1) group M. The precursor virus (monkey simian immunodeficiency virus, SIV) overcame the restriction factor APOBEC3 by mutations in the virally encoded Vif protein (Etienne et al., 2015) as well as changes in the viral capsid protein to allow interaction with chimpanzee RanBP2 (Meyerson et al., 2018), thus allowing transmission into the chimpanzee population (SIVcpz). This resulting SIVcpz virus acquired further mutations to overcome both the human restriction factors APOBEC3H and Tetherin, thereby emerging in humans as HIV-1 group M (Sauter et al.,

2009; Zhang et al., 2017). A pro-viral host factor has been identified as being key for the adaptation of avian influenza viruses (AIVs) to successfully replicate in mammalian cells-acidic nuclear phosphoprotein 32 family member A (ANP32A). A specific mutation in the viral polymerase basic 2 subunit (PB2) of the RNA dependent RNA polymerase complex (RdRp) at position 627 allows compatibility with the human version of ANP32A (Long et al., 2016). It is therefore apparent that many viruses on initial transfer to a novel host are ill-adapted.

A common belief is that viruses that establish and eventually persist in a novel species will become less virulent over time as they adapt to their host. One of the best cited examples is the myxoma virus that causes myxomatosis in European rabbits. This was deliberately introduced into the invasive European rabbit population inhabiting Australia in the 1950s as a method of biological control (Ratcliffe et al., 1952). It was highly effective, causing 99% mortality and eventually becoming endemic. Later strains circulating in the late 1950s-1960s showed a reduction in virulence, attributed to the natural selection of rabbits with enhanced innate resistance to the disease (Fenner & Woodroofe, 1965; Marshall & Fenner, 1958). However, more recent work suggests that circulating strains are not evolving to become a mild disease as seen in the natural host. In fact, to overcome resistance, some strains have evolved to become more immunosuppressive, leading to immune collapse (Kerr et al., 2017). It therefore seems that adaptation to a novel host does not necessarily lead to an overall reduction in virulence as there is a continuing evolutionary “arms race” between hosts and pathogens which is sometimes referred to as the Red Queen hypothesis.

One zoonotic virus that has a long history with infecting humans is influenza A virus (IAV). It is proposed that all currently circulating seasonal human IAVs are descended in some way from the 1918 H1N1 virus (Patrono et al., 2022). This 1918 H1N1 virus originated from birds, although how long this virus was circulating in humans prior to the start of the pandemic and whether it was in another mammalian host beforehand is still unresolved due to the paucity of sequencing data (Taubenberger et al., 2006). This virus caused a catastrophic pandemic from 1918-1919 across the globe resulting in high mortality rates. Through gradual adaption to the human host this has resulted in its long-term establishment in the human population and lessening of severity. Influenza A viruses therefore serve as a great model to try to understand the complex relationship between the host and virus after a jump into a new species and the mechanisms governing alterations in pathogenesis.

1.2 The Influenza virus

The Orthomyxovirus family includes Influenza A, B, C and D with only the former two being responsible for annual epidemics in humans. Influenza C can also infect humans but usually only presents with mild symptoms (Sederdahl & Williams, 2020) and Influenza D is only known to circulate in swine or cattle (Liu et al., 2020). Influenza A viruses can be categorised into subtypes based on both the antigenic and genetic properties of the haemagglutinin (HA) and neuraminidase (NA) protein. All of the currently identified influenza A subtypes have been either isolated in wild waterfowl (H1-16, N1-9) (Diskin et al., 2020) or bats (H17N10 and H18N11) (Tong et al., 2012), but some subtypes can infect a variety of other hosts (Figure 1.1). Only Influenza A virus is associated with causing pandemics and will be discussed in greater detail.

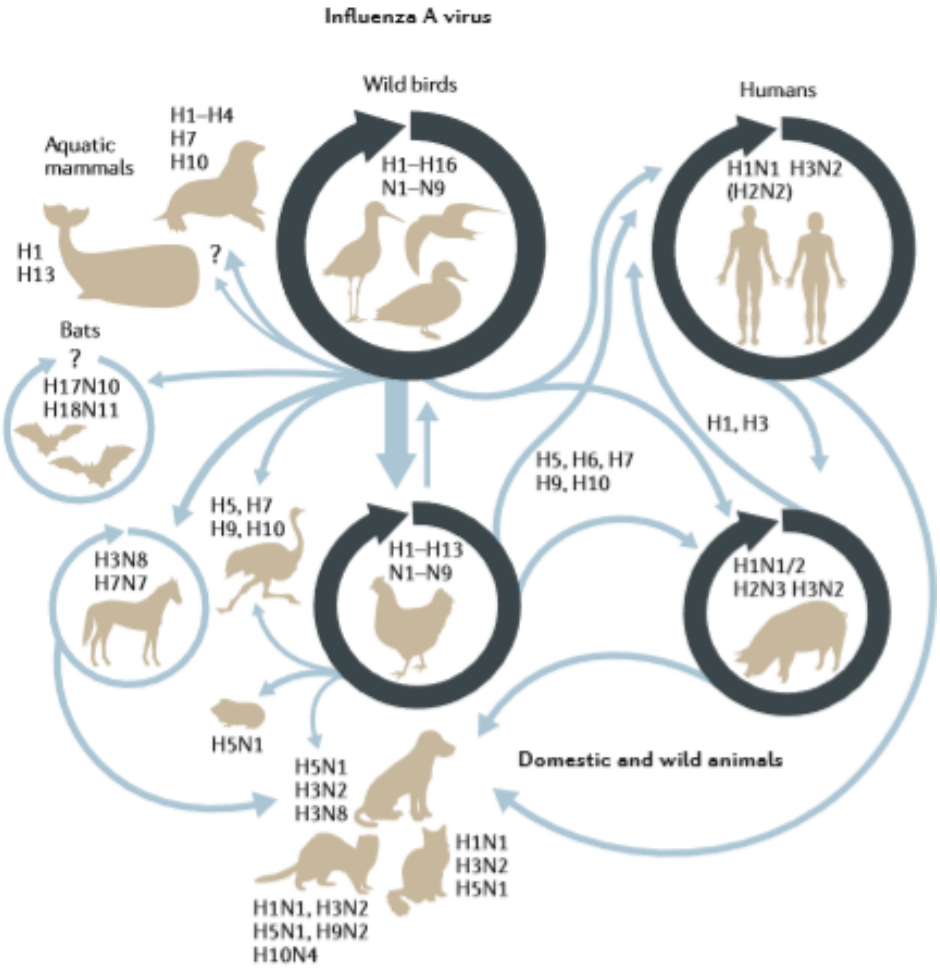

Figure 1.1. Host species of IAV. The main reservoir for H1-H16 and N1-N9 subtypes are wild waterfowl but multiple different species can be infected although specific adaptive mutations may need to occur before transmission is established (represented by blue arrows). When subtypes have become endemic in a

particular species this is indicated by a circle. Figure taken from (Long et al., 2019), with permission of the rights holder, SNCSC.

Influenza A viruses are constantly evolving, and two main mechanisms are employed to essentially evade host immunity and increase viral fitness. The first is antigenic drift, where due to the lack of proof-reading ability by the viral RNA dependent RNA polymerase, errors occur during replication, believed to be approx. one error per viral genome (Drake, 1993). This leads to the viral population during an infection comprising of many different variant viruses termed a "quasispecies", some of which will be selected for if they enhance viral fitness in the given environment. If these variant viruses contain point mutations in the HA or NA which fall in antigenic sites, this could lead to a reduction in affinity to host antibodies raised against the original infecting virus (Barbezange et al., 2018). Therefore, a gradual "drift" from the original virus strain occurs, resulting in pre-existing antibodies no longer being effective, termed immune escape. Antigenic drift is responsible for the need to update the influenza vaccine on an annual basis and occurs in both the currently circulating IAV subtypes in humans, H1N1 and H3N2 (Carrat & Flahault, 2007). These are referred to as seasonal influenza strains due to the timing of epidemics, typically in the winter months of temperate climates (Lofgren et al., 2007).

Antigenic shift is the second mechanism by which viruses can evade pre-existing immunity. This relies on coinfection of the same cell with two distinct influenza A strains. A novel strain is created by the process of reassortment, where the genes from the two different viruses can recombine due to the segmented nature of the influenza genome. In instances where the HA alone or HA and NA are acquired from a different strain to those found naturally in the host, an antigenically distinct virus is generated, rendering the host immunologically naïve (Webster & Govorkova, 2014). It is therefore hardly surprising that antigenic shift has been responsible for most influenza pandemics in humans.

1.3 Influenza virion and encoded proteins

The influenza A virion (depicted in Figure 1.2) is pleomorphic, either forming a spherical or elongated filamentous form that is dependent on a variety of factors including origin, passage

history, virus strain and the matrix 1 (M1) or matrix 2 (M2) protein (Dadonaite et al., 2016). A host-derived lipid membrane surrounds the virion and embedded within this are the transmembrane proteins; haemagglutinin (HA), neuraminidase (NA), and M2. A matrix of M1 protein associates with the lipid membrane and provides structural integrity for the virion, thus protecting the viral genome. The HA and NA are the two surface glycoproteins performing vital functions in cell entry and release as well as being key targets for host immunity (Gamblin & Skehel, 2010). The M2 protein serves as an ion channel, modulating the pH across the membrane thereby facilitating the release of the viral genome required for replication. Virions also incorporate host proteins donated from the host cell membrane during the budding process (Hutchinson et al., 2014).

The IAV viral genome consists of eight negative sense single-stranded RNA segments, encoding for ten core proteins as well as some accessory proteins which vary according to the strain (Samji, 2009). These viral RNA segments form viral ribonucleoproteins (vRNPs) which are made up of the gene segment, nucleoprotein (NP) and the trimeric polymerase complex (Polymerase Basic 1 (PB1), Polymerase Basic 2 (PB2), and Polymerase Acidic (PA) protein). Not all gene segments encode only one protein; currently all segments except for the HA segment have been shown to encode multiple proteins (Pinto et al., 2021). This is achieved either through alternative mRNA splicing, alternative translation initiation sites, or ribosomal frameshifting. Schematics of the influenza virion, vRNA, vRNPs and mRNAs are depicted in Figure 1.2. A summary of both the core and accessory proteins of IAV and the functions they perform are listed in Table 1.1.

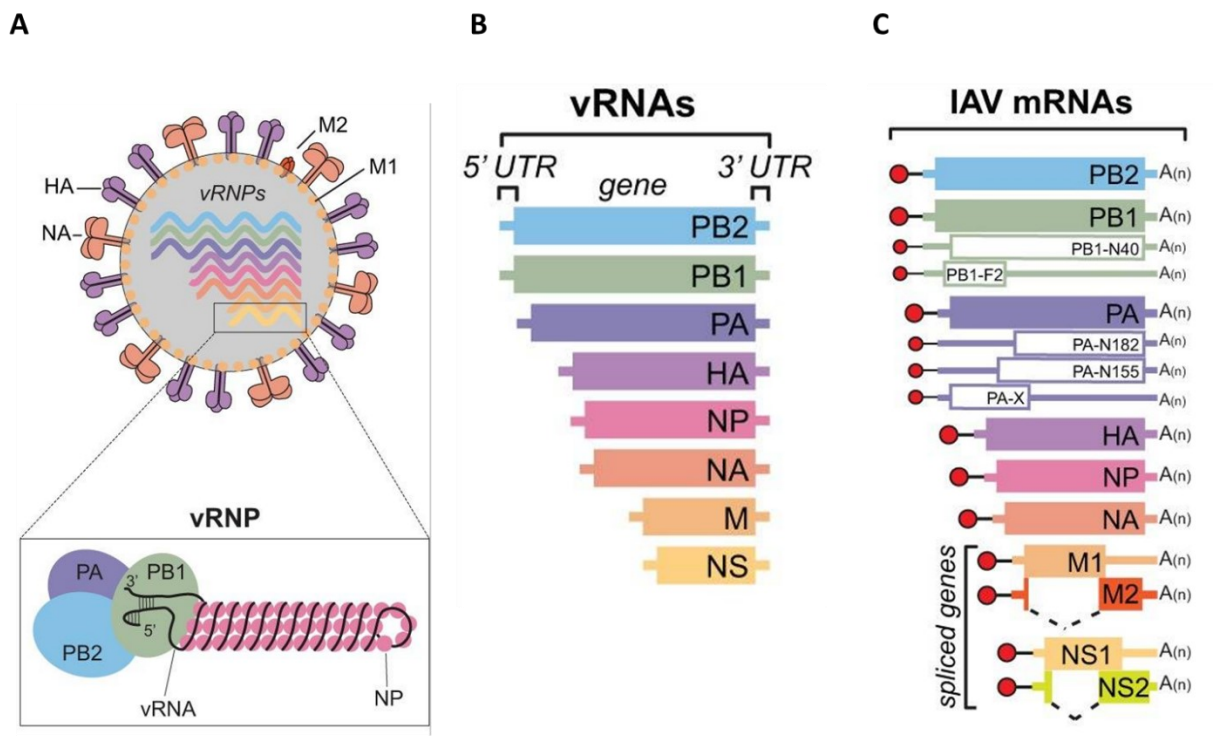

Figure 1.2. The Influenza A virus. A) Schematic of an influenza A virion. The surface glycoproteins HA and NA are shown, alongside M2, as well as the eight vRNPs, and the matrix protein M1 required for structural support. A single vRNA gene segment is shown below wrapped around multiple copies of NP with the conserved promoter regions in the 5′ and 3′ untranslated regions (UTRs) forming a panhandle structure which is bound by the trimeric viral polymerase. B) Schematic representation of the eight vRNA gene segments of IAV. The 5′ and 3 UTRs are represented with a line, and the box corresponds to the coding region within each vRNA. C) Diagram of the viral mRNAs that are transcribed from the IAV (left) vRNA templates. Boxes indicate the viral gene product encoded by each mRNA whereas dashed lines represent the alternative splicing of the IAV M and NS transcripts. Red circles denote the 5′ M7 pppG cap and black lines represent the 10–13 nucleotide-long host-derived primers that are obtained by the cap-snatching mechanism of the viral polymerase. A(n) corresponds to the 3′ poly-A tail produced. Empty boxes display transcripts that encode nonessential accessory proteins identified in most strains. Figure adapted from (Dou et al., 2018).

Segment	Proteins encoded	Function
PB2	Polymerase basic protein 2	Viral polymerase subunit that binds to the 5' caps of cellular pre-mRNAs
	PB2-S1	Only found in H1N1 strains pre-2009. Possibly acts as an inhibitor of RIG-I signalling pathway
PB1	Polymerase basic protein 1	Viral polymerase subunit that contains the core enzymatic activity
	PB1-F2	Promotes pro-inflammatory response and apoptosis
	PB1-N40	Currently unknown function
PA	Polymerase acidic protein	Viral polymerase subunit responsible for cleaving the 10-13nt downstream of the 5' cap on pre-mRNAs used as primers for the initiation of viral transcription
	PA-X	Has endonuclease activity and aids host-cell shutoff
	PA-N155	Supports viral replication in avian cells (Wang et al., 2018)
	PA-N182	Supports viral replication in avian cells (Wang et al., 2018)
HA	Haemagglutinin	Forms homotetramers embedded in the membrane of virion. Mediates binding to sialic acid-containing cellular receptors as well as fusion necessary for releasing the viral genome
NP	Nucleoprotein	Protein that covers the vRNA to form vRNPs which also associate with the trimeric viral polymerase
	eNP	Virulence factor for H1N1 strains

Segment	Protein encoded	Function
NA	Neuraminidase	Has sialidase activity which cleaves through mucins in the respiratory tract and releases newly synthesised virions from the surface of infected cells
	NA43	Currently unknown function (Machkovech et al., 2019)
M	Matrix 1	Export of vRNPs from nucleus, viral assembly and budding
	Matrix 2	Forms an ion channel allowing acidification of the viral core, also helps with membrane scisson for viral budding
	M42	Supports viral replication (Wise et al., 2012)
NS	Non-structural protein 1	Nuclear export of viral mRNAs, broad-spectrum IFN antagonist
	Non-structural protein 2/Nuclear export protein	Nuclear export of vRNPs, enhancement of polymerase activity
	NS3	Unknown function but seems to be expressed in a host specific manner (Selman et al., 2012)

Table 1.1. Summary of the major functions of proteins encoded from the IAV genome. Adapted from (Pinto et al., 2021) with additional functions referenced accordingly.

1.4 The influenza replication cycle

The core steps of the influenza replication cycle are depicted in Figure 1.3 and explored in more detail below.

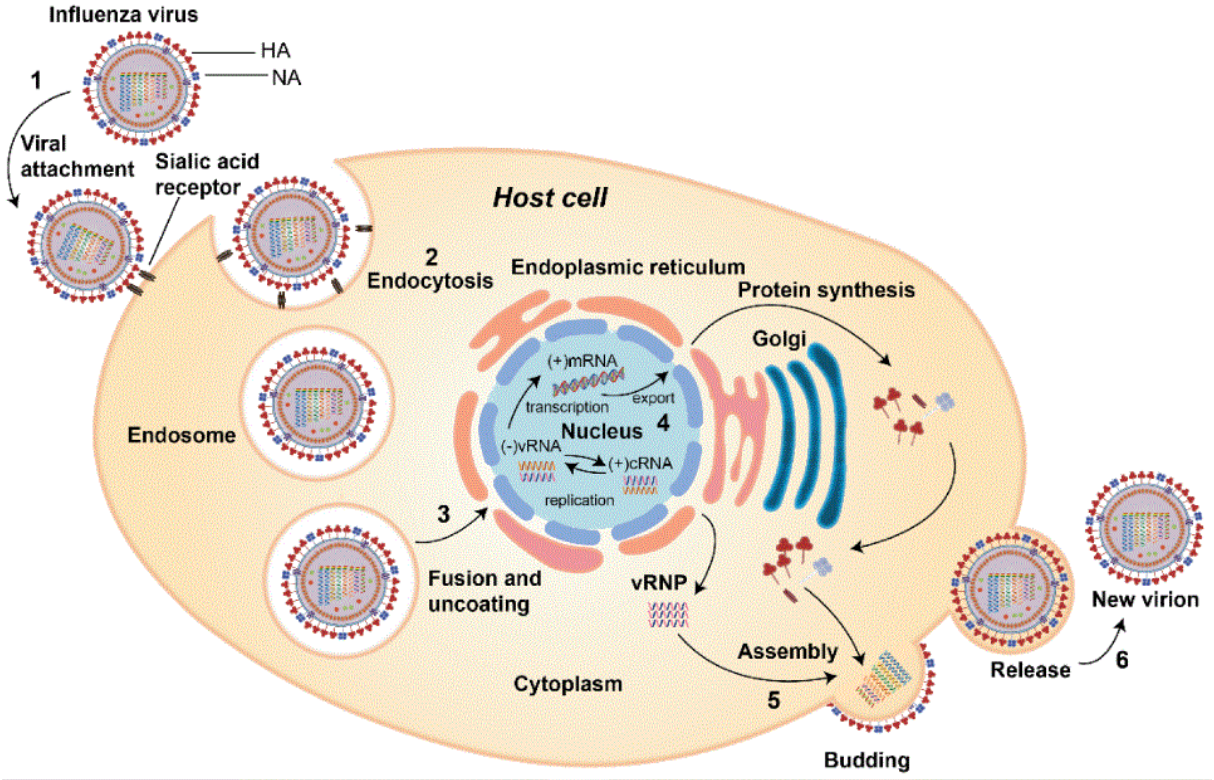

Figure 1.3. The replication cycle of influenza A virus. (1) virus attaches to target cell by HA binding to sialic acid receptor (2) virus enters the cell via the endosome by endocytosis (3) the virions are uncoated and fusion with the endosomal membrane occurs (4) vRNPs enter the nucleus where transcription and replication of the viral RNA genome takes place before vRNPs are then exported into the cytoplasm (5) the viral components assemble and new virions bud from the membrane (6) Newly formed virions are released from the cell. Image taken from (Nuwarda et al., 2021).

1.4.1 Attachment and entry

The first stage of the influenza A replication cycle is to attach to host cells, mediated by the HA protein. Binding of HA is through recognition of sialic acid containing receptors on the target cell surface. These sialic acids are located at the termini of numerous host glycolipids or glycoproteins and are usually α-linked to the penultimate galactose of the oligosaccharide glycan chain (Matrosovich et al., 2013). Influenza A viruses use both α2,3 and α2,6 linkages but show receptor preferences depending on host species (Connor et al., 1994; Rogers & Paulson, 1983). Human influenza viruses preferentially bind to sialic acid with an α2,6 linkage,

which are predominantly located on human respiratory upper airway cells (Kumlin et al., 2008), whereas avian viruses bind to those with an α2,3 linkage highly expressed on the duck intestinal mucosa as well as human alveolar macrophages (Franca et al., 2013; Yu et al., 2011). The nature of these linkages is therefore one of the determinants in host range (Long et al., 2019).

The next step following attachment is internalisation of the virion so it can enter the host cell. This is usually achieved through clathrin mediated endocytosis, a process which exposes the virion to a drop in pH (Matlin et al., 1981). This low pH inside the endosome results in a conformational change in the HA protein, exposing the fusion peptide that mediates the fusion of the viral and endosomal membranes. A pore is formed, and this coupled with an influx of protons into the virion through the M2 ion channel, allows for the release of vRNPs from the endosome into the cytoplasm (Hamilton et al., 2012). These vRNPs are then transported to the nucleus by utilising host proteins such as importins, where they can initiate the replication process (Staller & Barclay, 2021).

1.4.2 Replication

Upon entry into the nucleus, the viral polymerase both transcribes the vRNA to generate messenger RNA (mRNA) and replicates the vRNA through a positive sense complementary RNA (cRNA) intermediate (Te Velthuis & Fodor, 2016). The 5' and 3' termini of both vRNA and cRNA are highly conserved as these are the binding site for the viral polymerase and therefore serve as the viral promoter (Fodor et al., 1994). This promotor region is often referred to as a panhandle structure but can adopt other conformations such as a corkscrew or hook structure when the polymerase is bound (Flick & Hobom, 1999; Fodor et al., 1995). Primary transcription occurs first, as replication requires *de novo* polymerase complexes for stabilisation of the cRNA (Vreede et al., 2004). Figure 1.4 summarises the replication process and we explore each step in more detail below.

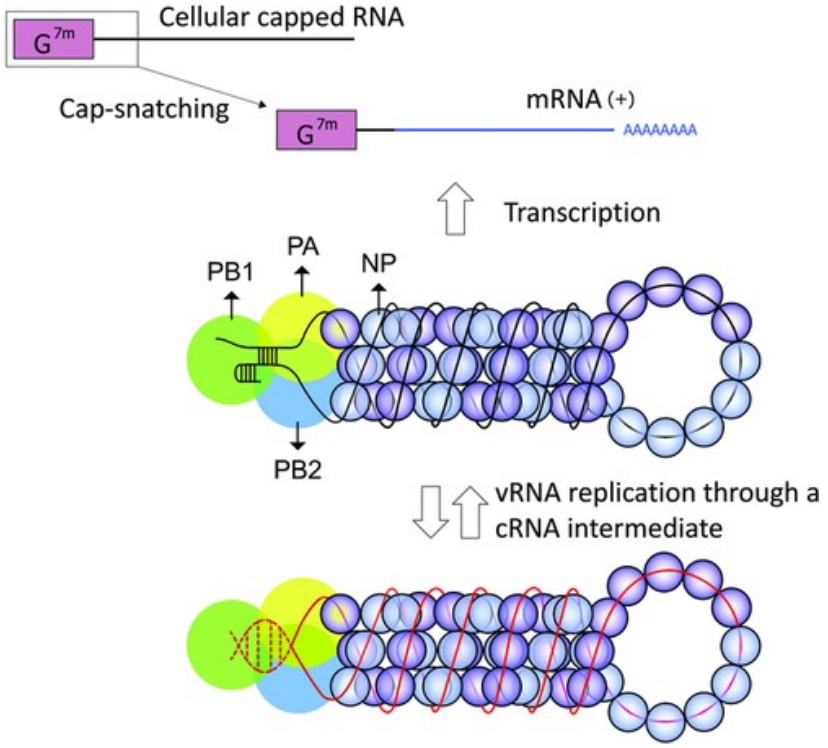

Figure 1.4. Schematic summarising influenza vRNA, cRNA and mRNA synthesis. The vRNP is depicted with black vRNA (top) and the cRNP with red cRNA (bottom) The termini of the vRNA are shown with the 5' end forming a hook structure whereas the conformation for the cRNP promoter region is unspecified. Figure taken from (Stevaert & Naesens, 2016).

1.4.2.1 Generation of mRNA

The negative sense vRNA is transcribed into positive sense mRNA by a primer dependent process. These primers are acquired through "cap-snatching" where initially PB2 binds to the 5' cap of host pre-mRNAs (Guilligay et al., 2008). This is followed by PA which has endonuclease activity (Dias et al., 2009), cleaving the host RNA 10-13nt downstream of the 5' cap. These short, capped RNA products are then used to prime transcription generating mRNA from the vRNA template. This process is highly dependent on the host transcriptional machinery. Association of host RNA polymerase II (Pol II) with the viral polymerase is essential as Pol II is the source of these stolen capped transcripts (Engelhardt et al., 2005; Walker & Fodor, 2019).

For the host cell machinery to translate viral mRNA, in addition to a 5’ cap, it must also acquire a 3’ polyadenylated (polyA) tail. This is achieved through stuttering of the viral polymerase on a short stretch (5-7nt) of uracils near the 5’ end of the vRNA (Poon et al., 1999). Preferential processing of viral mRNAs is achieved through inhibition of host gene expression, termed “host shutoff” mediated by PA-X and NS1 (Jagger et al., 2012; Khaperskyy et al., 2016; Nacken et al., 2021).

1.4.2.2 Generation of cRNA

Unlike mRNA synthesis, generation of cRNA is a primer independent process. Terminal initiation begins when the 3’ vRNA enters the active site of PB1 and a pppApG dinucleotide is incorporated onto the U and C nucleotides at position 1 and 2 of the 3’ vRNA terminus (Deng et al., 2006). This is supported by a priming loop located on the PB1 subunit that helps with stabilisation of the complex (Te Velthuis et al., 2016). To complete cRNA synthesis, the replicating polymerase forms a dimer with an encapsidating polymerase, bridged by the host factor ANP32 (Carrique et al., 2020). Once the 5’ end of the nascent cRNA is released, it is captured by the encapsidating polymerase, initiating NP encapsidation to form newly formed cRNP complexes.

1.4.2.3 Generation of vRNA

cRNA acts as a template for the synthesis of vRNA, which largely proceeds similarly to cRNA synthesis albeit with some important differences. Firstly, the initiation of vRNA synthesis by the cRNA promoter differs; an internal initiation and realignment mechanism is utilised referred to as “prime-and-realign”. Here, a pppApG dinucleotide is templated by the U and C nucleotides at position 4 and 5, followed by the dinucleotide being realigned to the U and C at positions 1 and 2 prior to elongation (Deng et al., 2006). This process is critically dependent on the flexibility of the PB1 priming loop which must undergo conformational changes to permit elongation (Oymans & Te Velthuis, 2018). There is also the requirement for the replicating polymerase to form a dimer with a trans-activating polymerase (Fan et al., 2019; York et al., 2013). As vRNA is also encapsidated to form nascent vRNPs, current models suggest that dimers also need to occur with an encapsidating polymerase (Carrique et al., 2020).

1.4.3 vRNP export, packaging, budding and release of progeny virions

Once synthesised in the nucleus, the nascent vRNPs must transport to the cytoplasm to be packaged and assembled into new virions. The major pathway that allows export through the nuclear pore complex (NPC) is the Chromosome Region Maintenance 1 (CRM1) mediated export pathway and this is utilised by the vRNPs. Both NEP and M1 are required for nuclear export (Shimizu et al., 2011) as well as host factors such as Rab11 for transport to the plasma membrane (Eisfeld et al., 2011)

A fully infectious virion must contain all eight influenza segments. The exact mechanism detailing how this is achieved is still not fully elucidated but there are two models proposed. One suggests segments are incorporated randomly (Bancroft & Parslow, 2002), whereas others propose a more regulated process where there is specificity in the selection of segments (Hutchinson et al., 2010). There is more compelling evidence for the latter model; transmission electron microscopy (TEM) of vRNPs show a 7+1 arrangement of one central vRNP surrounded by seven other vRNPs, with most virions displaying this formation (Noda et al., 2006). Cis-acting packaging signals have been identified in the conserved 5' and 3' termini as well as within segment specific regions of all eight segments (Eisfeld et al., 2015; Shafiuddin & Boon, 2019). Interestingly, RNA-RNA interactions between the segments which are not located in the packaging signals, have also been implicated (Dadonaite et al., 2019; Gavazzi et al., 2013).

The IAV membrane proteins, which are incorporated into the viral envelope, are synthesized by ribosomes associated with the ER membrane. HA emerges from the ER as a fusion incompetent precursor termed HA0 and must be cleaved into the subunits HA1 and HA2 prior to fusion by endogenous proteases. This either occurs en route to the plasma membrane or at the plasma membrane (Dou et al, 2018). The budding process appears to be mediated by the vRNPs and the viral proteins HA, NA, M1, M2 but is still not completely defined. Accumulation of HA and NA at the cell membrane initiates budding, whilst M2 has a role in membrane scisson (Rossman et al., 2010). The vRNP bound M1 proteins interact with the HA and NA short cytoplasmic tails, M1 polymerization occurs and forms the structure of the virion (Ruigrok et al., 2001).

Finally, NA cleaves sialic acid thereby inhibiting virion aggregation, preventing binding by HA, and releasing the virion from the membrane (Palese et al., 1974). NA has also an important role in cleaving sialic acids in the mucus layer, thus enabling viral egress as well as ingress (Cohen et al., 2013).

1.5 Pandemic Influenza

Since the start of the 20th Century, there have been five influenza pandemics in humans occurring in 1918, 1957, 1968, 1977 and 2009 (Figure 1.5). The most devastating was the 1918 pandemic which resulted in 50 million deaths worldwide (Johnson & Mueller, 2002). This pandemic or "Spanish flu" was caused by the adaption of an existing avian H1N1 virus to humans whereas the influenza strains that caused the other pandemics arose from antigenic shift (apart from the 1977 H1N1 strain). The sequence of the 1977 H1N1 virus showed highly similar homology to H1N1 strains from the 1950s that were no longer circulating, leading to the hypothesis that this outbreak was caused by accidental laboratory release or unintentionally through vaccine trials (Rozo & Gronvall, 2015).

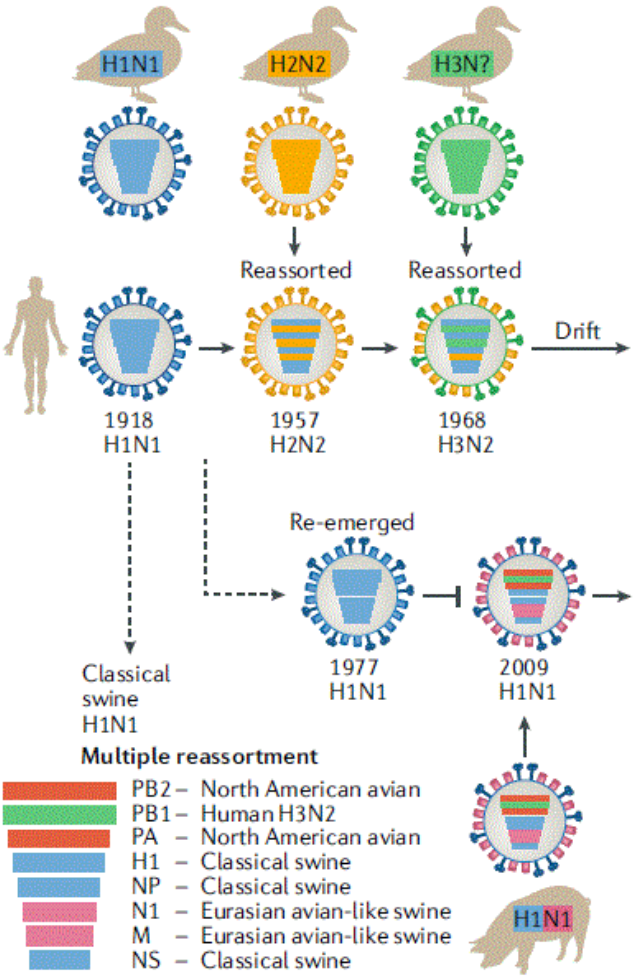

Figure 1.5. The composition of pandemic IAV strains. All segments of the 1918 pandemic H1N1 virus are believed to originate from an avian source. The 1957 H2N2 pandemic strain was from reassortment of segments from an avian H2N2 strain and the 1918 strain. Reassortment of this virus with a H3 avian strain resulted in the 1968 H3N2 pandemic virus strain. In 1977, a H1N1 strain genetically similar to earlier H1N1 strains from the 1950s emerged. The 2009 pandemic H1N1 strain arose due to multiple reassortment events with IAV strains of human, avian and swine origin. Image taken from Long et al. (2019), with permission of the rights holder, SNCSC.

As antigenic shift results in a complete exchange of HA and/or NA genes, there is limited pre-existing immunity in the human population, thereby increasing transmission. A common feature of pandemics is a shift in the age distribution of mortality; typically, younger age groups are more susceptible, in contrast with seasonal influenza where most deaths occur in 65+ year olds (Cromer et al., 2014; Simonsen et al., 1998). The most extreme example of this was observed during the 1918 pandemic where alongside the very young and elderly, high

case fatality rates were also observed in healthy 20-40 year olds (Morens & Taubenberger, 2018). This discrepancy in susceptible age groups has been attributed to differences in several factors including history of influenza exposure, transmissibility, and virulence. It should be noted that not all pandemics are associated with grossly elevated virulence, for example the H1N1 2009 pandemic virus had an estimated CFR of 0.02% and generally displayed similar symptoms to seasonal influenza strains (Simonsen et al., 2013). However, the 1918 pandemic displayed clinical manifestations that were not typical for current seasonal influenza strains. Alongside mild upper respiratory tract symptoms, in some individuals, an acute aggressive pneumonia was observed presenting with necrosis to the epithelia, pulmonary oedema, haemorrhage and severe tissue damage to the lungs, typically resulting in death within 5 days (Taubenberger et al., 2001). Secondary bacterial lung infections were also common, reflective of the pre-antibiotic era (Wolbach, 1919). Heliotrope cyanosis, a blue/black skin discolouration due to inadequate oxygen was reported and was associated with acute respiratory distress syndrome (ARDS) and mortality (Shanks, 2015).

Genetic characterisation has been performed by directly sequencing the 1918 virus from frozen and fixed lung tissue samples (Basler et al., 2001; Reid et al., 2002; Reid et al., 2000; Taubenberger et al., 1997). This has enabled researchers to effectively reconstruct the 1918 H1N1 virus and directly infect animal models to evaluate pathogenesis. Both studies in BALB/c mice (Tumpey et al., 2005) and macaques (Kobasa et al., 2007), demonstrated that following infection there was enhanced inflammation in the lung, oedema, and ARDS, mirroring the pathology reported in humans. This indicates that the high virulence by this 1918 H1N1 virus is not solely associated with host immunity and that viral genetic features contributed to its lethality.

1.6 Highly Pathogenic Avian Influenza Viruses (HPAIVs)

Some avian influenza strains are described as low pathogenicity (LP) or high pathogenicity (HP) and this subsequent distinction of being either a low pathogenic avian influenza virus (LPAIV) or a highly pathogenic avian influenza virus (HPAIV) is defined according to their pathogenicity in chickens and/or the molecular characteristics of the HA protein. LPAIVs possess a single arginine or lysine at the cleavage site connecting HA1 and HA2, whereas HPAIVs contain a multi-basic cleavage site with the motif RXR/KR (Vey et al., 1992). The

presence of a multi-basic cleavage site allows the infection to spread beyond the respiratory tract as cleavage is mediated by ubiquitous proteases which are present in a broad range of host cells (Horimoto et al., 1994). This contrasts with LPAIVs, where only trypsin-like proteases can cleave HA0 and these are only expressed in enteric or respiratory epithelia (Garten & Klenk, 2008). Currently only viruses belonging to the H5 and H7 subtypes are deemed HPAIVs, but not all viruses belonging to these subtypes are, some are LPAIVs. Generally, HPAIVs that have infected humans lead to a more severe disease than LPAIVs, although LPAIV H7N9 viruses that emerged in China in 2013 have enhanced severity in humans (Tang & Chen, 2013).

1.6.1 H5N1 infections in humans

H5N1 infection in humans were first documented in 1997 when an outbreak occurred in poultry workers in Hong Kong (Yuen et al., 1998). The H5N1 strain responsible was referred to as the goose/Guangdong lineage (gs/GD) or Asian lineage virus. Resultant Asian lineage H5N1 HPAIVs have caused ongoing outbreaks of severe disease in a wide range of hosts including poultry and humans. They have undergone continual evolution and reassortment leading to the diversification of several clades and are endemic in poultry found in Asian and African countries (Wille & Barr, 2022). One notable clade which has caused recent outbreaks across the globe including in Europe, is 2.3.4.4 which has further been divided into eight subclades (a-h), based on their HA gene. Furthermore, although the H5 HA is usually paired with the N1 NA, in this 2.3.4.4 clade, the HPAIV H5 Gs/GD has undergone frequent reassortment with LPAIVs resulting in viruses bearing N2, N5, N6 or N8 NAs which are referred to as H5NX (Smith et al., 2015). H5N1 viruses belonging to clade 2.3.4.4.b have been the predominant strain globally since October 2021 and form 16 different genotypes (Cui et al., 2022). This virus is particularly concerning due to the sheer number of wild birds that have been infected-over 400,000 non-poultry birds died in 2,600 outbreaks, which was double the number reported in the last 2016-17 wave (Miller, 2022).

A total of 863 human cases of H5N1 have been reported globally since 2003, 455 of which were fatal (UK Health Security Agency, 2022). In all human cases, sporadic poultry to human transmission has occurred accompanied with limited and non-sustained human-human transmission (Abdel-Ghafar et al., 2008). Although there are cases of asymptomatic H5N1 human infections such as recently reported in the UK (Oliver et al., 2022), many result in a

severe infection. Most laboratory confirmed cases of H5N1 are from hospitalised patients, a proportion of which progressed to ARDS and multiorgan failure (Lai et al., 2016). Similar to the 1918 H1N1 virus, severe lung pathology is often observed including diffuse alveolar damage (DAD), extensive lung consolidation and pulmonary haemorrhage (Ng et al., 2006; Yuen et al., 1998). A defining feature of severe H5N1 infection is the spread of virus to beyond the respiratory tract; virus antigen and viral RNA has been detected in autopsy samples in both brain neurons and lymphocytes (Gu et al., 2007). This has been largely attributed to the multi-basic cleavage site in the HA which extends virus tropism (Luczo et al., 2015; Schrauwen et al., 2012). Dysregulation of the immune system is also a hallmark; both lymphopenia and hypercytokinemia are frequently reported (de Jong et al., 2006; Liem et al., 2009). Hypercytokinemia or "cytokine storm" is a severe systemic inflammatory syndrome that results in elevated levels of cytokines and immune cell hyperactivation triggered by some pathogens, cancers, autoimmune conditions, treatments, and genetic disorders. It commonly leads to multi-organ failure and is associated with high mortality rates (Fajgenbaum & June, 2020). Blunting the cytokine storm is therefore essential but immunomodulators may be counterproductive if their use prohibits or delays the inhibition of viral replication (Yuen & Wong, 2005).

1.6.2 Mammalian models of H5N1 infection

Mammalian models for assessing H5N1 pathogenesis include mice, ferrets, and non-human primates. Although differences are observed between species, there are some universal clinical features shared between them. One is the aberrant innate immune response described in human infections. High levels of pro-inflammatory cytokines in the lungs and blood have been reported for mice (Maines et al., 2008; Szretter et al., 2007), ferrets (Cameron et al., 2008; Maines et al., 2012) and macaques (Baskin et al., 2009). Interestingly, a modelling study comparing the transcriptional regulatory networks in macaque and mouse H5N1 infections showed that in both species there was high statistical enrichment in genes associated with hypercytokinemia (McDermott et al., 2011). Like observed for human infections, high lymphocyte depletion in peripheral blood has also been reported in multiple species (Belser et al., 2011; Tumpey et al., 2000). Other common clinical manifestations typically conserved in mammalian models are severe lung pathology, dissemination outside

the respiratory tract, high viral load and a higher mortality rate than seasonal influenza viruses (Belser & Tumpey, 2013). However, HPAIVs that may cause only moderate disease in one animal model may cause lethality in another at a comparable inoculum dose. Additionally, as previously mentioned, intravenous pathogenicity index tests in chickens are not always predictive of virulence in mammals.

Use of transgenic mice has allowed investigation of how specific cytokines and chemokines modulate pathogenesis, and while useful, has also emphasised the redundancy in the host immune system (Szretter et al., 2007). Furthermore, the use of animal models has been invaluable for identifying key amino acids encoded by the viral genome that confer high virulence, adaptation, or both.

1.6.3 Adaptation of H5N1 to mammalian hosts

As viruses are essentially intracellular parasites, completion of their cellular replication cycle relies on molecular interactions with host proteins at multiple stages. Therefore, for a virus to successfully infect, replicate, and transmit to a novel host, a series of host-specific adaptations must occur. For influenza, firstly the HA protein must be able to bind and infect the host cell (Matrosovich et al., 2013). Additionally, the vRNP complex must be able to replicate the virus genome which is heavily reliant on host factors such as ANP32 (Long et al., 2016), and importins which ensure targeting to the nucleus (Gabriel et al., 2011). They must also effectively counteract the host specific immune response such as through acquiring mutations or deletions in viral proteins such as PB1-F2 (Smith & McCullers, 2013) NS-1 (Li et al., 2006) and PA-X (Lutz IV et al., 2020). The mechanisms of adaptation are still not fully understood, and all viral proteins may potentially be involved. Table 1.2 lists just a few of the mutations observed encoded by viral genes from mammalian animals or cell lines following infection with HPAI H5.

Viral gene	Mutation	Phenotype	References
HA	103Y, 156A	Contributes to airborne transmissibility between ferrets	(Herfst et al., 2012)
PB1	473V, 598P	Enhanced viral replication in mammalian cells	(Xu et al., 2012)
	622G	Enhanced viral replication in mammalian cells Increased virulence *in vivo*	(Feng et al., 2016)
PB2	627K	Enhanced viral replication in mammalian cells Increased virulence in vivo	(Mase et al., 2006) (Fornek et al., 2009) (Mok et al., 2009)
	249G, 309D, T339M	Enhanced replication in human lung epithelial cells (A549)	(Yamaji et al., 2015b)
	591K, 701N	Enhanced viral replication in mammalian cells Increased virulence in vivo	(Li et al., 2014)
	158G	Increased virulence in vivo	(Zhou et al., 2011)
PA	343S, 347E	Enhanced viral replication in mammalian cells Increased virulence *in vivo.*	(Zhong et al., 2018)
	44I, 127A, 241Y, 343T, 573V	Enhanced viral replication in human lung epithelial cells (A549) Increased virulence *in vivo.*	(Yamaji et al., 2015a)

Table 1.2. Common mutations observed following infection with HPAIV H5N1 viruses in mammalian animal models or cell lines

1.7 The innate immune response to IAV

The innate immune response is an imposing barrier to viruses. Host cells respond to viral infection by limiting viral replication, inhibiting the spread of the virus from the infected cell, and upregulating the production of antiviral proteins in neighbouring cells in preparation for future infection. This is achieved through viral recognition via specialised host cellular receptors which activate numerous signalling cascades that orchestrate a plethora of

defensive responses. In this section we will explore the impressive functions of the innate immune response to IAV in further detail.

1.7.1 Recognition of IAV: The role of Pattern Recognition Receptors (PRRs)

IAV detection is mediated through PRRs which are expressed in host cells and recognise specific pathogen associated molecular patterns (PAMPs). As the name implies, these PAMPS are not found in the uninfected host but are specifically found in various pathogens. Types of PAMPS include viral nucleic acids, viral glycoproteins, and bacterial products such as flagellin and LPS (Mogensen, 2009). Individual PRRs are specialised at detecting a subset of PAMPs and are localised on specific cell types and cellular locations. This results in distinct PPRs differentially recognising different types of pathogens (Thompson et al., 2011). IAV is recognised by different classes of PRRs which are briefly summarised below:

- **Toll-like receptors (TLRs):** There are ten functional TLR family members in humans (TLR1-10) and twelve in mice (TLR1-9, 11-13) (Fitzgerald & Kagan, 2020). These are located both within endosomes and the surface of plasma membranes and can detect a wide array of PAMPs. Detection of IAV in humans is mainly associated with TLR3, and TLR7 which both detect viral RNA species (Iwasaki & Pillai, 2014). These are primarily located in the endosomes of cells of myeloid origin, with TLR7 predominantly expressed in plasmacytoid dendritic cells (pDCs) (Ito et al., 2005). TLR3 is also expressed in human respiratory epithelial cells (Guillot et al., 2005). Other TLRs that have demonstrated activity in humans following IAV infection are TLR8 and TLR9 in monocytes and pharyngeal epithelial cells respectively (de Marcken et al., 2019; Han et al., 2014; Lee et al., 2014). As TLR9 recognises unmethylated CpG motifs, it is likely that rather than directly sensing IAV RNA, this receptor instead recognises DAMPs (damage associated molecular patterns) such as mitochondrial DNA, which has been shown for other RNA viruses such as Dengue virus (DENV) (Lai et al., 2018).

- **Retinoic acid-inducible gene 1 (RIG-I) (RLR) like receptors:** These are cytosolic sensors that detect intermediates of virus replication such as RNA with 5’ triphosphates or double-stranded RNA (dsRNA). This family consists of RIG-I, Melanoma-associated

differentiation protein 5 (MDA-5) and Laboratory of genetics and physiology 2 (LGP2). RIG-I recognises short regions of blunt-ended dsRNA with a terminal 5' di (5'pp) or triphosphate (5'ppp) moiety (Goubau et al., 2014; Hornung et al., 2006), whereas MDA-5 does not require the presence of a 5' ppp/5' pp group and recognises longer regions of dsRNA (Kato et al., 2006). LGP2 is considered a regulator of antiviral responses for both MDA5 and RIG-I (Satoh et al., 2010). In mammalian cells, activation of RIG-I has been shown to be crucial in mounting an effective antiviral response to influenza A infection (Loo et al., 2008). Furthermore, defects in RIG-I are associated with severe human infections (Jørgensen et al., 2018). The influenza panhandle promoter, with its 5'-ppp and short stretch of dsRNA has been shown to be a strong activating ligand for RIG-I (Liu et al., 2015; Rehwinkel et al., 2010) and RIG-I ligands are sensed during active viral replication (Killip et al., 2014). As IAV replication occurs in the nucleus, explaining how these newly synthesised RNAs were accessible to the cytosolic RIG-I remained puzzling. This was solved by Liu et al. (2018), who demonstrated that RIG-I was also present in the nucleus and sensed nuclear vRNA synthesis. Interestingly, Baum et al. (2010), showed that the shorter genome segments or short aberrant RNA replication products termed defective viral genomes (DVGs) preferentially associated with RIG-I. Additionally, a recent study identified IFN-γ-inducible protein-16 (IFI16), as a positive regulator of RIG-I signalling achieved by enhancing its expression through recruitment of RNA pol II to the RIG-I promoter as well as by facilitating RIG-I binding to IAV vRNAs (Jiang et al., 2021).

- **Nucleotide-binding oligomerization domain (NOD)-like receptors (NLRs):** These are cytosolic receptors that form multiprotein inflammasome complexes consisting of an NLR, the adaptor ASC and pro-caspase 1. Through activation of the inflammasome, autocatalytic processing of pro-caspase 1 occurs, resulting in the cleavage of pro-IL-1β and pro-IL-18 into secreted IL-1β and IL-18. NLRP3 is the most documented inflammasome activated during influenza infection (Kuriakose & Kanneganti, 2017). Activation of the inflammasomes requires two signals-a priming signal for the transcription of IL-1β and IL-18 and a second signal that assembles the inflammasome complex and subsequent secretion of IL-1β and IL-18. For influenza virus, signal 1 is triggered by the sensing of vRNA through TLRs or RIG-I and signal 2 by a virally encoded

protein such as M2 (Ichinose et al.) PB1-F2 (McAuley et al., 2013) or NP (Kim et al., 2022). In addition to cytokine secretion, activation of the inflammasome can also trigger multiple cell death pathways such as apoptosis, necroptosis, pyroptosis and ferroptosis (Huang et al., 2021).

In addition to the IAV sensors mentioned above, recent research has shown that Z-DNA binding domain protein 1 (ZBP1) can bind to IAV RNAs, where it can initiate a range of cell death pathways and pro-inflammatory cytokine induction (Kesavardhana et al., 2017; Kuriakose et al., 2016; Mo & Han, 2021; Wang et al., 2019). Interestingly, the binding profile for ZBP1 is remarkably similar to RIG-I, showing a preference for the shorter IAV segments and DVGs (Thapa et al., 2016). As ZBP1 binds Z-form DNA and RNA, it is assumed that vRNAs and DVGs assume this confirmation although how this is achieved is still not defined (Zhang et al., 2020).

1.7.2 Signalling pathways following IAV sensing

Sensing of IAV through these various PRRs, initiate signalling cascades that utilise a wide range of adaptor proteins and post-translational modifications, all resulting in the activation of transcription factors that either initiate the transcription of pro-inflammatory cytokines or type I IFNs or both. Figure 1.6 summarises the main signalling pathways involved in an IAV infected cell in a simplified schematic. As RIG-I is ubiquitously expressed and is believed to be the main sensor for activating the type I IFN response following IAV infection, RIG-I signalling will be explored in greater depth.

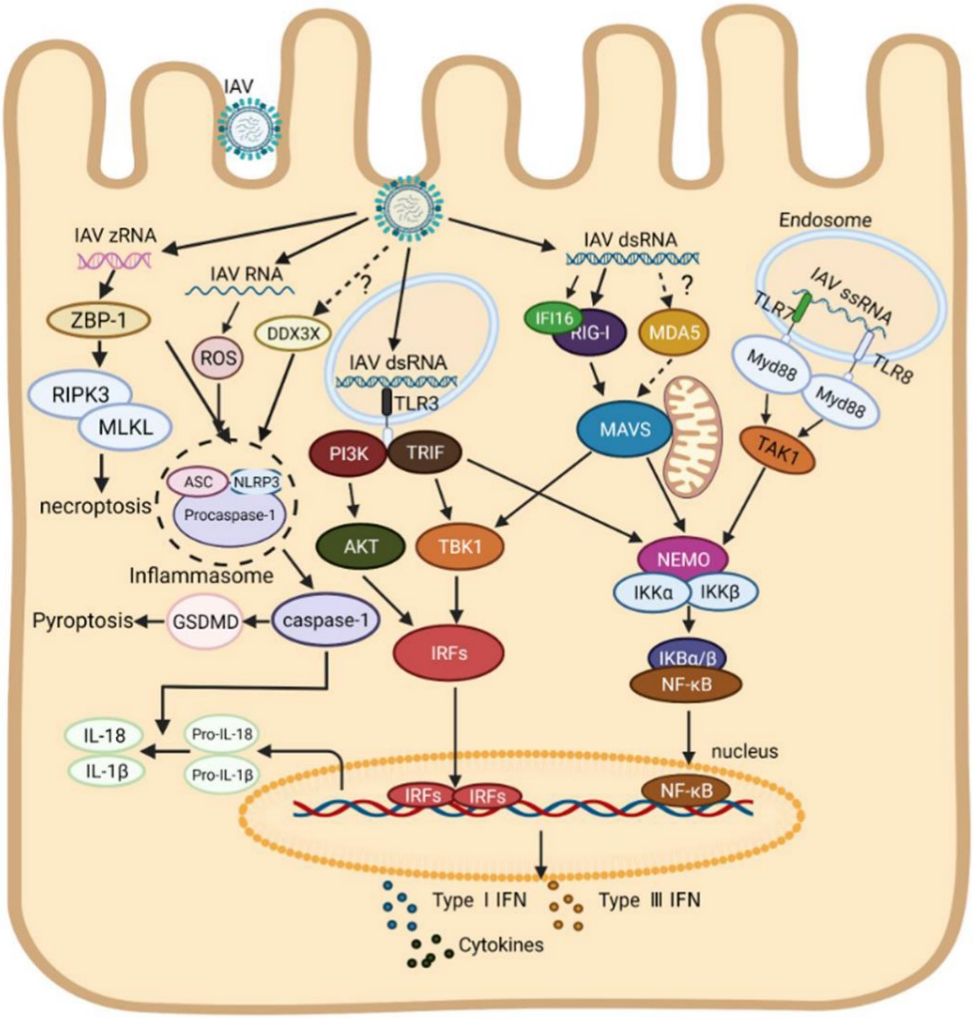

Figure 1.6. Schematic of innate immune signalling pathways triggered by IAV RNA in mammalian cells. Influenza viral single stranded RNA in the endosome is sensed by TLR7/8 recruiting the MyD88 adapter resulting in the production of pro-inflammatory cytokines through the TAK1-IKK-NF-κB signalling pathway. Influenza viral double-stranded RNA in the endosome is sensed by TLR3 where signalling is mediated through TRIF and PI3K adapters, inducing the production of IFN through the TKB1-IRFs signalling pathway. The transcription factor NF-κβ is also activated by binding to TRIF, inducing the expression of pro-inflammatory cytokines. Viral dsRNA in the cytoplasm is sensed by RIG-I, facilitated by IFI16, leading to activation of NF-κB and phosphorylation of IRFs by binding to the adaptor protein MAVS. RIG-I has also been shown to bind to ssRNA with a 5' triphosphate moiety (Pichlmair et al., 2006). IAV RNA can also be sensed by NLRP3, which forms inflammasomes, secreting IL-1β and IL-18 and/or promoting pyroptosis. ZBP1 senses IAV Z-RNA and via binding to RIPK3 mediates MLKL driven necroptosis as well as regulating NLRP3 inflammasome activation. It should be noted that pyroptosis and apoptosis have also been implicated to be activated via binding to IAV Z-RNAs but are not depicted here. The dashed lines for sensing through MDA5 or DDX3X signify that there is no direct evidence to demonstrate that IAV RNA can be recognized by these sensors in mammals. Abbreviations: MyD88, Myeloid differentiation primary response 88; TAK1, Transforming growth factor-β (TGF-β)-activated

kinase 1; NF-κβ, Nuclear factor kappa-light chain enhancer of B cells; TRIF, TIR-domain-containing adapter-inducing interferon-β; TBK1, Tank-binding protein 1; P3IK, Phosphatidylinositol-3-kinase; AKT, also known as Protein kinase B (PKB); IRFs, Interferon regulatory factors; RIPK3, Receptor interacting Serine/Threonine Kinase 3, NEMO, NF-kappaB essential modulator; MAVS, Mitochondrial anti-viral signalling protein; ROS, reactive oxygen species; MLKL, mixed lineage kinase domain-like pseudokinase; ASC, Apoptosis associated speck-like protein containing a CARD; GSDMD, Gasdermin D. Image taken from (Li et al., 2022).

1.7.2.1 RIG-I Signalling

In an uninfected cell, RIG-I adopts an inactive state where caspase activation and recruitment domains (CARDs) are bound by the alpha-helical insertion domain (Hel2i). RIG-I constantly surveys RNAs in the cellular environment and will transiently bind to host cellular RNAs, but this association is not strong enough to dislodge Hel2i (Kowalinski et al., 2011). This only occurs when RIG-I binds to appropriate RNAs such as 5'-ppp dsRNA and is modulated by ATP hydrolysis (Rawling et al., 2015). Upon binding to RIG-I, a massive conformational change is activated releasing the CARDs. The E3 ligases, tripartite motif containing 25 (TRIM25) or Riplet ubiquitinates these CARDs causing oligomerisation as well as ensuring that they cannot revert to their previous auto-repressive confirmation (Gack et al., 2007; Hayman et al., 2019; Oshiumi et al., 2010). Subsequently, activated RIG-I associates with a downstream protein residing in the mitochondrial outer membrane- MAVS. This leads to a conformational change in MAVS and nucleates MAVS oligomerisation which is necessary for binding to the TNF associated recruitment factors (TRAFs) which in turn recruits both TBK1 and the IKB kinase complex (IKK). Through phosphorylation and ubiquitination, signalling through these adaptor proteins results in activation of the transcription factors factors IRF3, IRF7 and NF-KB. These translocate to the nucleus where they promote both type I and III IFN and pro-inflammatory cytokine expression (Rehwinkel & Gack, 2020).

1.7.2.2 The Interferons

Interferons (IFNs) were first discovered to interfere with the replication of influenza virus over sixty years ago (Isaacs & Lindenmann, 1957). There are three classes of IFN-type I, type II and type III. Most of the recognised antiviral responses against IAV are attributed to type I and III IFN (Galani et al., 2017). More recently an emerging antiviral role for IFN II has been

recognised; Fong et al. (2022) demonstrated inhibition of IAV replication by exposing cells to type II IFN prior to infection mediated through impaired binding of HA to sialic acid.

Mammalian type I IFNs constitute numerous distinct genes of IFN-α (thirteen in humans), IFN-β (one in humans) as well as IFN-ω, -ε, -τ, -δ, -κ. Only IFN-α/β are virally induced so for the remainder of this thesis, type I IFN will be used to only denote IFN-α/β. IFN-γ is the only member of type II IFN (Billiau & Matthys, 2009), and type III IFNs constitute IFN-λ1, IFN-λ2, IFN-λ3 and IFN-λ4 in humans (Kotenko et al., 2003; Prokunina-Olsson et al., 2013). The production of type I and III IFNs leads to the expression of IFN-stimulated genes by activation of the Janus kinase (JAK)- signal transducers and activators of transcription (STAT)-signalling pathway which will be discussed in more detail later. Type II IFN is only produced by specific cells of the immune system (Schroder et al., 2004), type III IFN is predominantly produced by epithelial cells (Kotenko et al., 2019), and type I IFN is believed to be made by all cells, with plasmacytoid dendritic cells producing high amounts of IFN-α (Ali et al., 2019). There is some redundancy in the type I and type III IFN response; an extremely similar gene induction profile is observed between IFN-α and IFN-λ in both murine and human airway epithelial cells (Crotta et al., 2013). However, one important distinction to make is that type I IFNs also mediate inflammation by the recruitment of innate immune cells and promoting pro-inflammatory cytokine production, whereas this is not associated with type III IFNs (Davidson et al., 2016; Makris et al., 2017).

1.7.2.3 Pro-inflammatory cytokines and chemokines

Activation of PRRs can also lead to the expression of pro-inflammatory cytokines and chemokines such as Il-6, TNF-α, IL-1β, CCL2 (MCP-1) and CXCL10 (IP-10). Alongside IFNs, these pro-inflammatory cytokines/chemokines are responsible for controlling the lung environment during infection (Tisoncik et al., 2012). Many of the cytokines secreted exert pleiotropic roles on cells and depending on the context can have both pro and anti-inflammatory roles. For example, in IAV infection, Il-6 trans-signalling through its soluble receptor (sIL-6R) has been linked to pro-inflammatory effects whereas classical signalling through its membrane bound receptor (IL-6Rα) mediates anti-inflammatory effects (Scheller et al., 2011). IL-6 and IFN-α kinetics have been associated with the occurrence of clinical symptoms such as fever (Hayden et al., 1998), but are also crucial for mounting appropriate antiviral responses and promoting lung repair (Yang et al., 2017). Broadly speaking, pro-inflammatory cytokines and chemokines

both activate and recruit leukocytes into the site of infection, where these newly recruited cells will also release pro-inflammatory cytokines thus amplifying the inflammatory response. When tightly regulated, this inflammatory response promotes viral clearance but if not, can lead to immunopathology (Tavares et al., 2017).

1.7.2.4 IFNAR signalling and ISGs

One of the main effects mediated through activation of both the RLR and TLR pathway is the signalling of type I IFNs. Here secreted IFN-α or IFN-β can bind to their shared receptor (IFNAR) which initiates signalling through the JAK-STAT pathway. As the IFNAR receptor is ubiquitously expressed, type I IFNs have a broad range of target cells.

The canonical IFNAR pathway is activated once type I IFNs are bound by IFNAR2, triggering the heterodimerisation between IFNAR1 and IFNAR2. Here, the IFNAR bound JAK1 and TYK2 through a series of autophosphorylation steps, cause the dimerisation of STAT1 and STAT2 allowing dissociation. These STAT heterodimers translocate to the nucleus with interferon regulatory factor 9 (IRF9) where they form the interferon-stimulated gene factor 3 (ISG3) complex (Schreiber & Piehler, 2015). Transcription of interferon stimulated genes (ISGs) is mediated through this ISGF3-complex binding to a specific DNA binding region called the interferon-stimulated response element (ISRE) which is located at the promotor (Schneider et al., 2014). Type III IFNs (IFN λ), also signal through the JAK/STAT pathway although this is activated through binding initially to the Interferon Lambda receptor 1 (IFNLR1). Both however, result in activation of ISGs. Some genes containing ISREs do not actually respond directly to IFN, instead they respond to transcription factors such as IRF3 and IRF7 activated through detection of viral infection by PRRs (Schoggins & Rice, 2011).

Numerous ISGs have been identified, many of which have antiviral functions, targeting various stages of the virus lifecycle (De Veer et al., 2001). There appears to be some selectivity for the ISGs upregulated; viruses all activate a unique but slightly overlapping ISG signature (Schoggins & Rice, 2011). The below table provides a summary of some key ISGs with demonstrated antiviral activity against IAV infections.

ISG	Function	References
Myxovirus resistance gene (Mx) A (Humans) Mx1 (Mice)	• Binds to NP, inhibits transport of vRNPs and NP into nucleus • Contributes to activation of inflammasome	(Xiao et al., 2013) (Lee et al., 2019)
Interferon Induced Transmembrane Protein 3 (IFITM3)	• Inhibits the fusion of viral and endosomal membranes-blocking release of vRNPs	(Desai et al., 2014)
Viperin	• Inhibiting virion budding process by disrupting the composition of lipid rafts	(Wang et al., 2007)
ISG15 (ubiquitin and ubiquitin-like modifier family)	• Conjugates a variety of proteins termed ISGylation, disrupting activity of target cell/altering localisation but exact mechanisms still largely undefined. • ISG15 conjugation inhibits IAV replication in human respiratory cells	(Perng & Lenschow, 2018) (Hsiang et al., 2009)

Table 1.3. A small selection of ISGs upregulated following IAV infection and how they function.

1.7.3 The Innate Immune cells

Specialised cells of the innate immune system (leukocytes), play an important role in responding to an IAV infection and are vital to the outcome of infection. These include dendritic cells, macrophages, monocytes, neutrophils, natural killer (NK) cells and innate lymphoid cells, all of which have unique functions for defending against invading pathogens, one of which is the secretion of specific cytokines/chemokines. By the release of a large range of pro-inflammatory and immunoregulatory cytokines and chemokines they can either alert or effectively disable the immune system (Lamichhane & Samarasinghe, 2019). Under normal circumstances, these innate immune cells help to maintain pulmonary homeostasis leading to minimal tissue damage and viral clearance but in certain circumstances, an overzealous response occurs leading to uncontrolled inflammation and immunopathology. Table 1.4 summarises the functions of key innate immune cells during an IAV infection with examples from the literature on how they contribute to either protection or pathogenesis.

Cell	Description	Contributes to *Protection* or **Pathogenesis** in IAV infection
Monocytes	• Migrate to the lung mediated by MCP-1 • Under inflammatory conditions can differentiate into monocyte derived macrophages and dendritic cells • Release type I IFN and pro-inflammatory cytokines • Can activate T-cells	• *Following IAV infection, recruited monocytes differentiate into monocyte derived dendritic cells which secrete high levels of type I IFN and upregulate antiviral ISGs and RIG-I (Cao et al., 2012)* • **Reducing inflammatory CCR2+ monocytes is associated with a better outcome in mice following a severe IAV infection (Lin et al., 2014)** • **High monocyte recruitment to the lung and increased MCP-3, IFN-α2, and IL-10 is predictive of clinical severity (Oshansky et al., 2014)**
Macrophages	• Multiple subtypes-comprising both resident and monocyte derived populations • Phagocytose infected/dying cells and cell debris • Produce pro-inflammatory cytokines • Restore tissue homeostasis • Can activate T-cells	• *Experimental depletion of alveolar macrophages in mice results in higher viral titres and mortality following IAV infection (Tate et al., 2010)* • **Monocyte-derived macrophages induce high levels of pro-inflammatory cytokines especially TNF-α (Cheung et al., 2002)** • **Monocyte derived macrophages can be productively infected with some H5N1 viruses, aiding viral dissemination (Westenius et al., 2018)** • **TRAIL-expressing macrophages induce alveloar epithelial cell apoptosis contributing to lung leakage (Herold et al., 2008)**
Dendritic cells	• Multiple subtypes-comprising both resident and monocyte derived populations • Can migrate to lymph nodes	• *pDCs lead to IFN-a production and an antiviral state (Jewell et al., 2007)* • *Experimental depletion of tipDCs reduces viral clearance due to decreased CD8+ T cell response (Aldridge Jr et al., 2009)*

	• Main cell involved in antigen presentation to T-cells • Phagocytose infected/dying cells and cell debris • Produce pro-inflammatory cytokines • Plasmacytoid DCs (pDCs) secrete high amounts of IFN-a, ISG induction and promote B cell responses	• **pDCs can contribute to sustained IFN-a signalling which can lead to uncontrolled inflammation (Davidson et al., 2014)** • **High levels of monocyte derived inflammatory DCs (tipDCs) in the lung are associated with increased mortality in mice (Aldridge Jr et al., 2009).** • **High replication in GM-DCs (cDCs and mDC) by a virus containing the H5N1 internal genes, correlating with excessive pro-inflammatory cytokine production (Li et al., 2018)**
Neutrophils	• Recruited to site of infection, mediated largely by the chemokine IL-8 • Involved in a large array of functions aimed at pathogen clearance such as phagocytosis, release of cytotoxic granules, pro-inflammatory cytokine production, formation of reactive oxygen species, undergoing a specialised programmed cell death (NETosis) resulting in the formation of extracellular traps (NETs)	• *Depletion of neutrophils prior to a severe IAV infection increased weight loss in mice (Tate et al., 2011)* • **NET formation impaired in H5N1 IAV infection compared to H1N1 infection (Chan et al., 2020)** • **H5N1 viral proteins and RNA found in neutrophils isolated from infected patients could aid viral dissemination and/or contribute to neutropenia (Zhao et al., 2008)** • **Depletion of MIP-2 led to reduced neutrophils in the lung following IAV infection, less severe lung pathology and less rapid weight loss in mice (Sakai et al., 2000)**

Table 1.4. A table highlighting the functions of key innate immune cells and a summary of studies supporting a role for protection or pathogenesis during IAV infection.

1.8 Adaptive Immunity

Whilst this thesis focuses on the early immune response which corresponds to innate immunity, the adaptive immune response is crucial for viral clearance and responding to re-infection. Specialised adaptive immune cells include T-lymphocytes and B-lymphocytes as well as Natural Killer cells with memory type functions (Sun et al., 2009). T-lymphocytes can be broadly characterised into two subsets: CD8+ lymphocytes and CD4+ lymphocytes. The former can directly kill virus infected cells by the secretion of granzymes or perforin to mediate pore formation and apoptosis or via the expression of surface molecules that can trigger cell death such as FasL or TRAIL. CD8+ T-lymphocytes can also release pro-inflammatory cytokines such as TNF which can promote the cell death of infected cells (Schmidt & Varga, 2018). In contrast, CD4+ T-lymphocytes are crucial for the activation of B-lymphocyte responses. After clearing viral pathogens, 90-95% virus-specific T-lymphocytes undergo apoptosis, whilst the remainder become long-lived memory cells (Welsh & McNally, 1999). Importantly, these memory T-lymphocytes can provide cross-protection against other subtypes of influenza A virus as they typically recognise epitopes of the highly conserved internal proteins (Lee et al., 2008).

The humoral arm of the adaptive immune response is mediated through antibody producing B-lymphocytes and is exploited in the seasonal annual inactivated influenza vaccine (Keshavarz et al., 2019). The major influenza antigens that are recognised by antibodies are the two surface antigens-HA and NA. Neutralising antibodies directed against the HA head block receptor attachment and thus entry into cells, whereas those directed against NA block the release of virions from the cell surface (Padilla-Quirarte et al., 2019). Antibodies provide protection against re-infection with the same influenza strain but offer poor protection against other strains (Cox, 2013). Additionally, antibody dependent cell mediated cytotoxicity (ADCC) can also occur where antibodies facilitate targeting killing of infected cells (Gao et al., 2020).

1.9 Aberrant RNA synthesis

In addition to making full length copies of vRNA or cRNA, the IAV RNA polymerase can also synthesise other RNA replication products. These are all truncated versions of the vRNA or

cRNA template and include defective viral genomes (DVGs), mini viral RNAs (mvRNAs) and small viral RNAs (svRNAs) (Figure 1.7). The latter are only derived from the 5' end of vRNA, are 22-27 nucleotides in length and have been proposed to act as a switch between transcription and replication (Perez et al., 2010). In contrast, DVGs and mvRNAs are copies of the genome with a large central region missing, whilst retaining both the 3' and 5' termini so can still be replicated. DVGs are typically >180 nt in length, whereas mvRNAs are substantially shorter, only between 56-125nt in length (Te Velthuis et al., 2018). Due to their shorter length, mvRNAs can be made independently of NP, implying that they do not form canonical vRNP structures (Turrell et al., 2013).

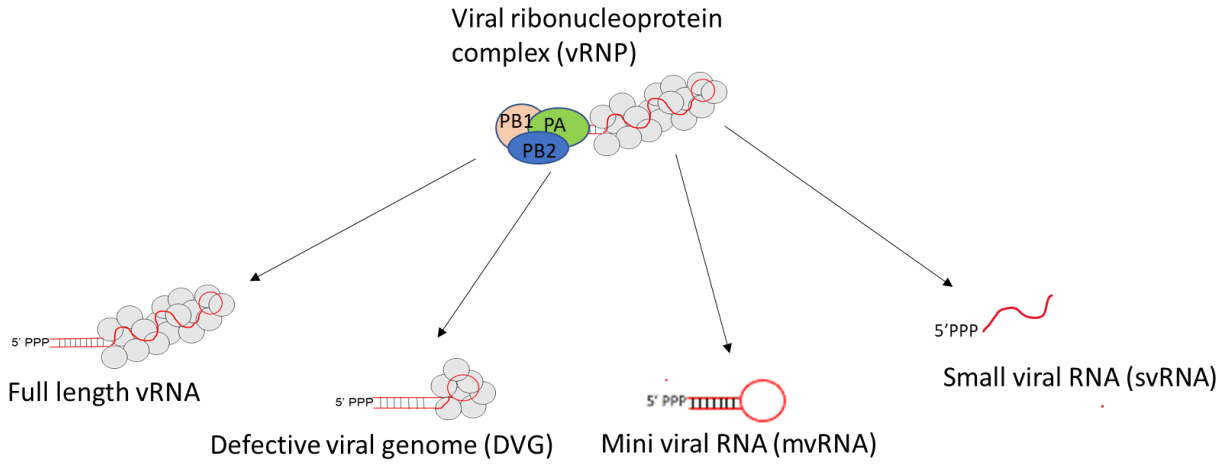

Figure 1.7. The four different RNAs produced by the IAV polymerase. Adapted from (Weis & Te Velthuis, 2021).

DVGs are not unique to IAV, they have been characterised from a broad range of both RNA and DNA viruses (Addetia et al., 2021; Li et al., 2011; Saira et al., 2013; Sun et al., 2015). Originally believed to be artifacts created by passaging viruses at high MOI *in vitro* (von Magnus, 1954), these are now known to be generated during both natural and experimental viral infections (Felt et al., 2021; Genoyer & Lopez, 2019; Martin et al., 2019). Different types of DVGs have been characterised but most are missing large parts of the viral genome. The two most common types are deletion DVGs and copy-back DVGs (cbDVGs). Deletion DVGs (such as those generated by IAV) retain the 5' and 3' termini, and RNA structural elements necessary for replication, but lack a central region. cbDVGs are formed when the viral polymerase dissociates from the template strand and proceeds to use the nascent strand as

template instead, forming a duplicated region in the reverse complement which generates a panhandle structure (Vignuzzi & Lopez, 2019).

The mechanisms by which the viral polymerase make DVGs is still not fully understood. One theory is that these aberrant RNAs arise as a result of the viral polymerase lacking proof reading ability and are simply stochastic mistakes. Numerous studies have shown that there is huge diversity in DVGs produced during an infection (Alnaji et al., 2021; Martin et al., 2019). However, others have shown specific "hot-spots" for DVG generation. Sun et al. (2019), demonstrated that particular regions of the RSV genome were more prone to generate cbDVGs and identified specific nucleotides necessary for their formation. There is compelling evidence for a copy choice mechanism to be responsible for the formation of IAV DVGs. This is where the viral polymerase loses association with the template v/c RNA whilst maintaining association with the nascent v/c RNA and "jumps" to a complementary sequence of the template where elongation proceeds (shown schematically in Figure 1.8). Numerous studies have identified identical nucleotides surrounding the breakpoint region and the other side of the deleted region and hypothesise that these direct repeats may promote DVG formation (Jennings et al., 1983; Lui et al., 2019; Saira et al., 2013). Mutations in IAV proteins such as PA, M and NS2/NEP have also been implicated in the generation of DVGs in cell culture (Fodor et al., 2003; Odagiri et al., 1994; Pérez-Cidoncha et al., 2014). Furthermore, avian adapted mutations within the influenza viral polymerase were demonstrated to increase the levels of mvRNAs generated in human cells, suggesting that these mutations conferred a reduced ability for functional replication thereby increasing aberrant RNAs (Te Velthuis et al., 2018).

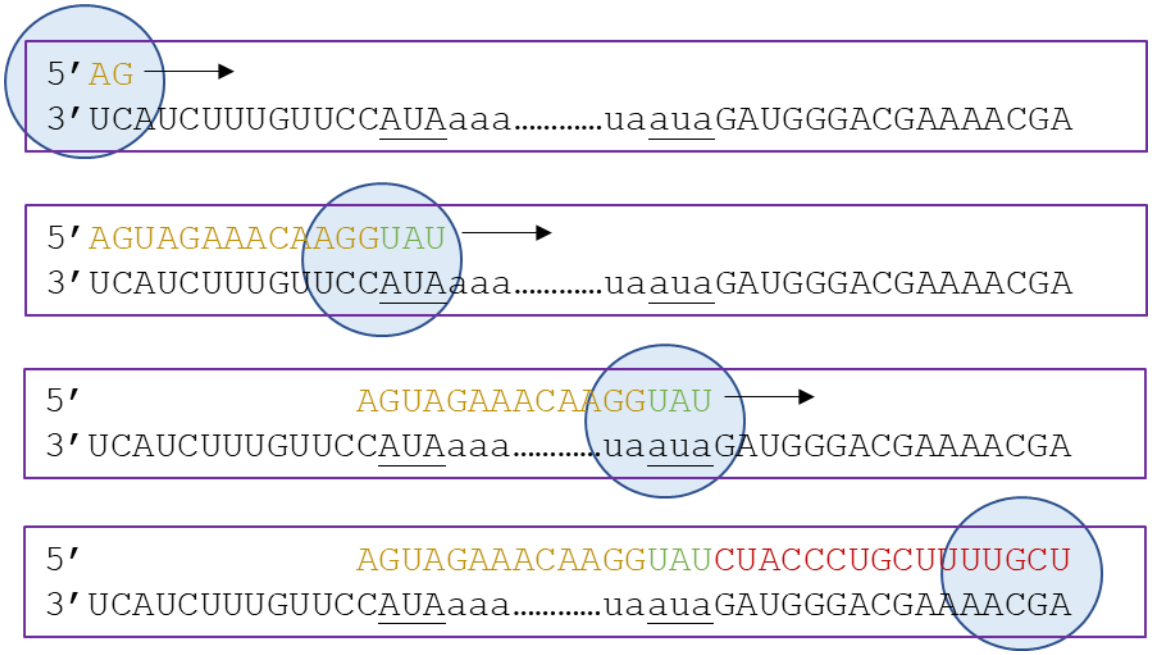

Figure 1.8. A model of how Influenza DVGs/mvRNAs are made via a copy-choice mechanism. The viral polymerase (blue circle) initiates replication at the 3' end of the vRNA template (black). Elongation proceeds until the polymerase dissociates from the template by an unknown mechanism at the underlined AUA sequence. The polymerase re-joins at another AUA sequence downstream in the vRNA template and elongation proceeds. Uppercase denotes the copied template vRNA, whereas lowercase denotes the "skipped" template. Gold represents the nascent RNA before the copy choice, green for the nucleotides involved in re-annealing with the template vRNA and red for the RNA produced after the copy choice. Figure adapted from (Te Velthuis et al., 2018), with permission of the rights holder, SNCSC.

IAV Internal deletion DVGs typically retain the 3' and 5' termini where identified packaging signals reside so therefore can be incorporated into new virions. However, the virions containing a DVG will be non-infectious since they lack the full protein coding capacity for a viral protein. However, if a fully infectious particle or a particle containing the complementary full-length sequence co-infects the same cell, they can provide the missing viral proteins. In such dual-infected cells, it has been demonstrated that DVGs will often outcompete the full-length genomes and will therefore accumulate to higher levels which sequentially results in more DVG containing virions than WT virions (Frensing et al., 2013). These non-infectious particles are often referred to as defective interfering particles (DIPs), due to their interference with standard viral replication by competing with full length segments for polymerase components and packaging, which ultimately leads to a reduction in viral titre i*n vitro* (Frensing et al., 2014). In contrast, mvRNAs are not packaged (Te Velthuis et al., 2018).

Alongside interference with standard replication, DVGs have been shown to trigger type I IFN (López, 2014). For IAV, this latter feature is shared with mvRNAs (Te Velthuis et al., 2018) which is hardly surprising considering that both these aberrant RNAs retain the panhandle promoter and 5' triphosphate moiety. In contrast, svRNAs do not contribute to type I IFN induction (Perez et al., 2010). Interestingly, influenza DVGs and mvRNAs may be the main activators of the type I IFN response rather than the full-length v or cRNA. This is supported by work from (Killip et al., 2014) where they showed that both incoming genomes and progeny vRNPs were poor activators of IFN-β. This was also observed by Liu et al. (2019); only incoming DVGs activated RIG-I and not the full-length genomes.

In vivo RSV and IAV infections have demonstrated that type I IFN and pro-inflammatory cytokines are induced only once DVG levels are detectable (Tapia et al., 2013). Furthermore, high levels of DVGs present in virus stocks used to conduct animal studies typically lead to a mild disease, and high levels of DVGs detected in humans with H1N1pdm09 strains have been shown to correlate to less severe infections (Swieton et al., 2020; Vasilijevic et al., 2017). It has also been shown that in numerous animal models, administration of influenza DIPs prophylactically can protect against IAV challenge (Dimmock et al., 2012; Hein et al., 2021a; Huo et al., 2020).

1.10 The cytokine storm in HPAIV H5N1 mammalian infections

Clinical data from H5N1 human infections, show high serum concentrations of IL-6, IFN-γ, IP-10, Il-8, and TNF-α (de Jong et al., 2006; To et al., 2001). This is also mirrored in animal models; mice infected with H5N1 have elevated IL-1β, IFN-γ, TNF-α and IL-6 (Xu et al., 2006), ferrets have upregulation of IP-10 and IFN response gene expression (Cameron et al., 2008) and macaques demonstrate high levels of type I IFNs, IL-6, TNF-α and IP-10 (Baskin et al., 2009). The high levels of cytokines and chemokines lead to the excessive recruitment and activation of innate immune cells including neutrophils, macrophages, and dendritic cells into the lung, further amplifying pro-inflammatory cascades. This imbalance of inflammatory mediators results in immunopathology such as the death of lung epithelial cells, alveolar and endothelial cells, leading to further complications such as hypoxia and pulmonary oedema (Tisoncik et al., 2012). The H5N1 induced cytokine storm is invariably associated with severe clinical

symptoms and has a critical role in the development of both acute lung injury (ALI) and ARDS (Bhatia & Moochhala, 2004).

How HPAIVs can induce a cytokine storm in mammalian species is still poorly understood. One hypothesis was that these viruses had a poorly functioning NS1 protein. As H5N1 viruses can replicate very efficiently even in the presence of high levels of type I IFN, it was argued that H5N1 viruses were perhaps resistant to their antiviral effects. Research published by Seo et al. (2002), confirmed this and mapped this resistant phenotype to a D92E substitution in the NS1 segment. However, Ngunjiri et al. (2012), failed to recapitulate these findings using the same viruses and cell lines; D92E H5N1 viruses were sensitive to IFNs. Additionally, another study showed that in a mouse model, type I IFN signalling was required for controlling H5N1 replication and extrapulmonary spread (Szretter et al., 2009). Furthermore, the H5N1 NS1 protein is fully functional in human cells and behaves similarly to human adapted strains (Hayman et al., 2007; Li et al., 2018).

Perhaps the most well-characterised virulence marker in H5 HPAIVs is the multi-basic cleavage site of the HA protein, enabling viral replication outside the respiratory tract. However, this is not an absolute requirement for high pathogenicity as the 1918 H1N1 virus contained a monobasic cleavage site (Tumpey et al., 2005). Other key virulence markers associated with this glycoprotein are changes in binding preferences from α-2-6 sialic acid to α 2-3 sialic acid (Rogers & Paulson, 1983), changes in the level of glycosylation (Zhao et al., 2017) and an increased pH of activation for endosomal fusion (DuBois et al., 2011).

Several studies link high virulence to specific amino acid changes within the viral polymerase genes (see table 1.2). Adaptive mutations within the polymerase genes are crucial for supporting efficient replication in novel host cells but are often associated with increased virulence. This is hardly surprising; a virus that can rapidly replicate to high viral titres could outpace the immune system leading to the host succumbing to infection. Extending viral replication within a range of cell types has also been linked to the cytokine storm. Prior work has shown that some H5N1 strains can replicate and secrete more pro-inflammatory cytokines within certain innate immune cells (Cheung et al., 2002; Westenius et al., 2018) (also refer to table 1.4). Indeed, a previous study from our laboratory found that a virus containing H5N1 internal genes was highly pathogenic in mice, induced hypercytokinemia but did not replicate to higher viral loads in the lung than a human adapted strain (Li et al., 2018).

The high virulence observed was rather due to increased replication in myeloid immune cells which drove the production of high levels of pro-inflammatory cytokines. This could not be mapped to one polymerase gene segment alone, rather the replication activity of the whole vRNP complex was responsible (Li et al., 2018).

It is currently unknown to what role DVGs or mvRNAs may have in infections where innate immune responses become uncontrolled such as in the H5N1 induced cytokine storm in mammalian hosts. Could aberrant RNA replication products instead of triggering innate immunity for an effective host response instead contribute to pathogenicity by amplifying inflammation? Additionally, are aberrant RNAs more likely to be generated when the viral polymerase is poorly adapted to the host cell environment? Intriguingly, a higher abundance of mvRNAs were generated in human cells by the H5N1 HPAIV polymerase compared to a mammalian-adapted influenza polymerase (Te Velthuis et al., 2018). This same study also demonstrated that high levels of mvRNAs were detected in the lungs of ferrets infected with either a HPAIV H5N1 or the 1918 pandemic H1N1 strain, correlating with increased cell death and pro-inflammatory cytokine expression (Te Velthuis et al., 2018). Furthermore, another study identified a novel protein encoded by a DVG derived from the PB2 segment of an H5N1 virus strain, and this was shown to induce high levels of type I IFN in cell culture and led to enhanced disease severity in a mouse model (Boergeling et al., 2015).

1.11 Thesis Aims

In this thesis, we seek to understand the contribution of aberrant RNA replication by HPAIV polymerases to the innate immune response and infection outcome.

The aims of this thesis are outlined below:

- To determine whether viruses containing the internal genes of a HP H5N1 replicate to high levels in murine and human macrophages
- To investigate how DVGs modulate innate immune responses in various cell types
- To demonstrate how levels of DVGs generated by viruses containing the internal genes of a HP H5N1 impact pathogenicity in the mouse model
- Uncover whether a HPAIV polymerase makes aberrant RNA replication products and identify viral factors that can promote their formation

Chapter 2 Materials and Methods

2.1 Materials

2.1.1 Cells

Cell line/Primary cells	Description	Source
HEK293T (293T)	Human kidney cells expressing large T antigen of SV40	ATCC
MDCK	Madin Darby canine kidney cell	ATCC
A549	Human epithelial lung cell line	ATCC
A549 IFN-β luc	Human epithelial lung cell line stably expressing firefly luciferase reporter gene under the control of IFN-β promoter	Barclay lab stock (Hayman et al., 2006)
L929	Mouse fibroblast cell line	ATCC
MEFs	Immortalised mouse embryonic fibroblasts ZBP1-/- reconstituted with WT ZBP1	Prof. Jan Rehwinkel, University of Oxford (Maelfait et al., 2017)
ZBP1-/- MEFs	Immortalised mouse embryonic fibroblasts ZBP1-/-	
ZBP1 Zα1α2^{mut} MEFs	Immortalised mouse embryonic fibroblasts containing ZBP1 with the mutations N46A and Y50A in Zα1 and N122A and Y126A in Zα2.	
GM-DCs	Primary murine bone marrow derived dendritic cells cultured with GM-CSF	BALB/c mice (this study)
BMDMs	Primary murine bone marrow derived macrophages cultured with L929 conditioned media	BALB/c mice (this study)
hMDMs	Human monocyte derived macrophages. CD14+ monocytes were derived from a 54-year-old African American male generated in the presence of human macrophage colony-stimulating factor (hMCSF).	Lonza

Table 2.1. List of cell lines/primary cells used.

2.1.2 Oligonucleotides, probes and Taqman gene expression assays

Primer name	Primer/Probe sequence (5'-3')	Function
Uni12	AGCRAAAGCAGG	cDNA synthesis/RT-PCR
Tagged Uni12	GGCCGTCATCGGCCATTAGCRAAAGCAGG	cDNA synthesis, RT-PCR (as above but incorporates tag at 5' end)
MBT Uni12	ACGCGTGATCAGCRAAAGCAGG	NGS
MBT Uni13	ACGCGTGATCAGTAGAAACAAGG	
Tag Forward	GGCCGTCATCGGCCATT	RT-PCR (FL and DVGs)
Tky/05 PB1 Terminal Forward	AGCGAAAGCAGGCAAACC	
Tky/05 PB1 Terminal Reverse	AGTAGAAACAAGGCATTTTTTCACG	
Tky/05 PB2 Terminal Forward	AGCGAAAGCAGGTCAAATATATTC	
Tky/05 PB2 Terminal Reverse	AGTAGAAACAAGGTCGTTTTTAAAC	
Tky/05 PA Terminal Forward	AGCGAAAGCAGGTACTGATTC	
Tky/05 PA Terminal Reverse	AGTAGAAACAAGGTACTTTTTTGG	
Hoffman PB2 Forward	TATTGGTCTCAGGGAGCGAAAGCAGGTC	
Hoffman PB2 Reverse	ATATGGTCTCGTATTAGTAGAAACAAGGTCGTTT	
Hoffman PB1 Forward	TATTCGTCTCAGGGAGCGAAAGCAGGCA	
Hoffman PB1 Reverse	ATATCGTCTCGTATTAGTAGAAACAAGGCATTT	

Hoffman PA Forward	TATTCGTCTCAGGGAGCGAAAGCAGGTAC	
Hoffman PA Reverse	ATATCGTCTCGTATTAGTAGAAACAAGGTACTT	
Tky/05 PB1 683 Forward	AWACRATGACCAAAGATGC	RT-PCR (FL only)
Tky/05 PB1 1225 Reverse	AACATGCCCATCATCATTCC	
Tky/05 PA 735 Forward	TTTAGAGCCTATGTGGATGG	
Tky/05 PA 1470 Reverse	TATGTATTCTGTGGCTCGC	
Tky/05 PB2 420 Forward	GAAAGGTTAAAACATGGAACC	RT-PCR (FL only)/Sanger sequencing
Tky/05 PB2 758 Reverse	ATGTACACACTGCTTGTTCC	
Tky/05 PB2 771 Forward	GACGATGTTGACCAG	Sanger sequencing
Tky05 PB2 1410 Forward	GACATGACTCCCAGC	
Tky/05 9N SDM Forward	GCGGGACTGTGACATTAGATTTCTTAATTCC	Site Directed Mutagenesis for creating mutations in Tky/05 PB2
Tky/05 9N SDM Reverse	GCGGGACTGTGACATTAGATTTCTTAATTCC	
Tky/05 81M SDM Forward	CTCTGGAGCAAGATGAATGATGCTGG	
Tky/05 81M SDM Reverse	CCAGCATCATTCATCTTGCTCCAGAG	
Tky/05 PB2 pCAGGS SC Forward	TATATATAGCGGCCGCGCCACCATGGAGAGAAT AAAGG	Subcloning Tky/05 PB2 into pCAGGS
Tky/05 PB2 pCAGGS SC Reverse	TTAATTAACTCGAGCTAATTGATGGCCATCC	
PR8 NA vRNA tagged Forward	GGCCGTCATGGTGGCGAATGAAACCATAAAAAG TTGGAGGAAG	cDNA synthesis Tagged NA vRNA
PR8 NA vRNA Forward (tag)	GGCCGTCATGGTGGCGAAT	qRT-PCR
PR8 NA vRNA Reverse	CCTTCCCCTTTTCGATCTTG	
M gene Forward	GACCRATCCTGTCACCTCTGA	
M gene Reverse	AGGGCATTYTGGACAAAKCGTCTA	
M gene probe	FAM-TGCAGTCCTCGCTCACTGGGCACG-BHQ1	
Human IFN-β Forward	GCCGCATTGACCATCT	
Human IFN-β Reverse	CACAGTGACTGTTACTCCT	
Human Il-8 Forward	AGCTGGCCGTGGCTCTCT	
Human Il-8 Reverse	CTGACATCTAAGTTCTTTAGCACTCCTT	
Human TNF-α Forward	GCCAGAGGGCTGATTAGAGA	
Human TNF-α Reverse	CAGCCTCTTCTCCTTCCTGAT	
Human IP-10 Forward	CTGACTCTAAGTGGCATT	
Human IP-10 Reverse	TGATGGCCTTCGATTCTG	
Human GAPDH Forward	ATTCCACCCATGGCAAATTC	
Human GAPDH Reverse	CGCTCCTGGAAGATGGTGAT	
Murine GAPDH Forward	TGTGTCCGTCGTGGATCTGA	
Murine GAPDH Reverse	TTGCTGTTGAAGTCGCAGGAG	
Murine IL-6 Forward	GACAAAGCCAGAGTCCTTCAGAGAG	
Murine IL-6 Reverse	CTAGGTTTGCCGAGTAGATCTC	
Murine TNF-α Forward	GGCAGGTCTACTTTGGAGTCATTG	
Murine TNF-α Reverse	ACATTCGAGGCTCCAGTGAATTCGG	
Murine ZBP1 Forward	GACGACAGCCAAAGAAGTGA	
Murine ZBP1 Reverse	GAGCTATGTCTTGGCCTTCC	

Table 2.2. List of oligonucleotide primers and probes used in this thesis. Primers were synthesised by either MWG Eurofins or Merk and all were diluted in sterile dH2O to 100pmol/µl (100µM).

Name	Reference	Species
IFN-α5	Mm00833976_s1	Mouse
GAPDH	Mm99999915_g1	Mouse
MerTK	Mm99999915_g1	Mouse
Zbtb46	Mm00511327_m1	Mouse

Table 2.3 List of Taqman gene expression assays used. All obtained from ThermoFisher.

2.1.3 Plasmids

Name	Plasmid Description	Source
pPol I Tky/05 PB2	pPol I vector expressing Tky/05 segment 1 cDNA	Prof. Ron Fouchier, Erasmus
pPol I Tky/05 PB1	pPol I vector expressing Tky/05 segment 2 cDNA	
pPol I Tky/05 PA	pPol I vector expressing Tky/05 segment 3 cDNA	
pPol I Tky/05 NP	pPol I vector expressing Tky/05 segment 5 cDNA	
pPol I Tky/05 M	pPol I vector expressing Tky/05 segment 7 cDNA	
pPol I Tky/05 NS	pPol I vector expressing Tky/05 segment 8 cDNA	
pCAGGS Tky/05 PB2	pCAGGS vector expressing Tky/05 PB2 protein	Barclay lab stock (Dr Jason Long)
pCAGGS Tky/05 PB1	pCAGGS vector expressing Tky/05 PB1 protein	
pCAGGS Tky/05 PA	pCAGGS vector expressing Tky/05 PA protein	
pCAGGS Tky/05 NP	pCAGGS vector expressing Tky/05 NP protein	
pPol I PR8 HA	pPol I vector expressing PR8 segment 4 cDNA	Barclay lab stock
pPol I PR8 NA	pPol I vector expressing PR8 segment 6 cDNA	
pPol I Eng/09 PB2	pPol I vector expressing Eng/09 segment 1 cDNA	
pPol I Eng/09 PB1	pPol I vector expressing Eng/09 segment 2 cDNA	
pPol I Eng/09 PA	pPol I vector expressing Eng/09 segment 3 cDNA	
pPol I Eng/09 NP	pPol I vector expressing Eng/09 segment 5 cDNA	
pPol I Eng/09 M	pPol I vector expressing Eng/09 segment 7 cDNA	
pPol I Eng/09 NS	pPol I vector expressing Eng/09 segment 8 cDNA	
pCAGGS Eng/09 PB2	pCAGGS vector expressing Eng/09 PB2 protein	
pCAGGS Eng/09 PB1	pCAGGS vector expressing Eng/09 PB1 protein	
pCAGGS Eng/09 PA	pCAGGS vector expressing Eng/09 PA protein	
pCAGGS Eng/09 NP	pCAGGS vector expressing Eng/09 NP protein	
pPol I Tky/05 PB2 9N	pPol I vector expressing Tky/05 segment 1 cDNA with 9N mutation	This study
pPol I Tky/05 PB2 81M	pPol I vector expressing Tky/05 segment 1 cDNA with 81M mutation	
pPol I Tky/05 PB2 9N + 81M (DM)	pPol I vector expressing Tky/05 segment 1 cDNA with 9N and 81M mutation	
pCAGGS Tky/05 PB2 9N	pCAGGS vector expressing Tky/05 PB2 protein with 9N mutation	
pCAGGS Tky/05 PB2 81M	pCAGGS vector expressing Tky/05 PB2 protein with 81M mutation	
pCAGGS Tky/05 PB2 9N + 81M (DM)	pCAGGS vector expressing Tky/05 PB2 protein with 9N and 81M mutation	
pPol I DVG 1 Tky/05 PB1 (479nt)	pPol I vector expressing 479nt long DVG cDNA derived from Tky/05 segment 1	
pPol I DVG 2 Tky/05 PB2 (425nt)	pPol I vector expressing 425nt long DVG cDNA derived from Tky/05 segment 2	
pPol I DVG 3 Tky/05 PB2 (584nt)	pPol I vector expressing 584nt long DVG cDNA derived from Tky/05 segment 2	
pPol I DVG 4 Tky/05 PA (361nt)	pPol I vector expressing 361nt long DVG cDNA derived from Tky/05 segment 3	
pPol I DVG 5 Tky/05 PA (388nt)	pPol I vector expressing 388nt long DVG cDNA derived from Tky/05 segment 1	

Table 2.4. List of plasmid constructs.

2.1.4 Reporter Constructs

Name	Reporter Description	Source
IFN-β luc	Firefly luciferase reporter gene under the control of IFN-β promoter	Prof. Steve Goodbourn, St Georges, London
pPol I firefly luciferase	Human minigenome luciferase reporter	Barclay lab stock (Dr Olivier Moncorge)
Renilla pCAGGS	Renilla luciferase (used as a transfection control)	Barclay lab stock

Table 2.5. List of reporter constructs.

2.1.5 Viruses

Virus Full Name	Virus Short Name	Genetic Constellation	Comments
6:2 A/turkey/Turkey/1/2005	6:2 Tky/05	6:2. All internal genes from Tky/05, HA and NA from A/Puerto Rico/8/1934 (PR8)	Tky/05 = HPAIV H5N1 PR8 = lab adapted H1N1. All rescued for this study
6:2 A/turkey/Turkey/1/2005 PB2 9N	6:2 Tky/05 9N		
6:2 A/turkey/Turkey/1/2005 PB2 81M	6:2 Tky/05 81M		
6:2 A/turkey/Turkey/1/2005 PB2 9N + 81M	6:2 Tky/05 DM		
7:1 A/turkey/Turkey/1/2005	7:1 Tky/05	7:1. All internal genes and NA from Tky/05, HA from PR8.	Tky/05 = HPAIV H5N1 PR8 = lab adapted H1N1. Existing laboratory stock (incorrectly labelled as 6:2)
7:1 A/turkey/Turkey/1/2005 LOW	7:1 Tky/05 LOW		Tky/05 = HPAIV H5N1 PR8 = lab adapted H1N1. Passage of 7:1 Tky/05 at low MOI
7:1 A/turkey/Turkey/1/2005 HIGH	7:1 Tky/05 HIGH		Tky/05 = HPAIV H5N1 PR8 = lab adapted H1N1. Passage of 7:1 Tky/05 at high MOI
6:2 A/England/195/2009	6:2 Eng/09	6:2. All internal genes from Eng/09, HA and NA from PR8	Eng/09 = H1N1pdm09 PR8 = lab adapted H1N1. Rescued for this study
5:3 A/turkey/England/50-92/1991 PB2 627E (WT)	5:3 50-92 E	5:3. PB2, PB1, PA, NS, and NP from 50-92, HA, NA and M from PR8	50-92 = HPAIV H5N1 PR8 = lab adapted H1N1. Existing laboratory stock
5:3 A/turkey/England/50-92/1991 PB2 627K	5:3 50-92 K		

Table 2.6. List of viruses.

2.1.6 Media and Buffers

Name	Recipe	Use
Cell culture media (10% DMEM)	Dulbecco's Modified Eagle Medium (DMEM) with L-glutamine and sodium pyruvate (Gibco) 10% Heat inactivated foetal calf serum (FCS) (BioSera) 1% non-essential amino acids (NEAA) (Gibco) 1% Penicillin/Streptomycin (P/S) (Gibco)	Maintenance of cell lines (HEK293T, A549, MDCK, MEFs)
A549 IFN-β luc cell culture media	As above but with addition of 2mg/ml Geneticin (G418) (Gibco)	Maintenance of A549 IFN-β luc cell line
Virus Infection Media	As cell culture media but with no FCS and the addition of 1µg/ml TPCK-treated trypsin (Worthington)	Virus growth media for propagation/infection
L929 cell culture media	RPMI 1640 medium (Gibco) 10% Heat inactivated FBS 1% P/S	To propagate L929 cells to generate M-CSF
BMDM media	RPMI 1640 medium 10% Heat inactivated FBS 50µM β-mercaptoethanol (Gibco) 1% L-glutamine (Gibco) 1% P/S 20% L929 conditioned media (cell supernatant)	For differentiating murine BM cells into BMDMs
2% BMDM infection media	RPMI 1640 medium 2% Heat inactivated FBS 50µM β-mercaptoethanol 1% L-glutamine 1% P/S	For viral infections in murine BMDCs
GM-DC media	RPMI 1640 medium 10% Heat inactivated FBS 50µM β-mercaptoethanol 1% L-glutamine 1% P/S 1% NEAA 40ng/ml rmGM-CSF (R&D Systems)	For differentiating murine BM cells into GM-DCs
2% GM-DC infection media	RPMI 1640 medium 2% Heat inactivated FBS 50µM β-mercaptoethanol 1% L-glutamine 1% P/S 1% NEAA	For virus infections in murine GM-DCs
hMDM media	X-Vivo 15 medium (Lonza) 10% Heat inactivated FBS 25 ng/ml of M-CSF (Gibco)	For culturing hMDMs
Plaque assay overlay	100ml 10X Minimal Essential Medium (MEM) (Gibco) 28ml 7.5% BSA Fraction V (Gibco) 10ml 1% L-glutamine (Gibco) 20ml 7.5% NaHCO3 (Gibco) 10ml 1M HEPES (Gibco) 5ml 1% DEAE Dextran (Merck) 10ml 1% P/S 517ml dH2O	For plaque assays in MDCK cells

	2% agarose in dH2O 7.5ml 2% agarose added to 17.5ml overlay	
Crystal Violet solution	100ml crystal violet (Merck) 300ml ethanol 1.6L dH2O	For staining plaque assays
LB (Luria Bertani) Broth	1% tryptone 0.5% yeast extract 0.5% NaCl 0.1% glucose dH2O	Growth of *E.coli* for generation of plasmids
SOC	2% tryptone 0.5% yeast extract 10mM NaCl 2.5mM KCl 10mM MgCl2 10mM MgSO4.7H20 20mM glucose	Growth of *E.coli* for selection of plasmids
TAE buffer	40mM Tris-acetate pH 8 1mM EDTA	DNA gel electrophoresis

Table 2.7. List of cell culture media and buffers used.

2.2 Methods

2.2.1 Plasmid constructs and cloning

2.2.1.1 Site directed mutagenesis

For site-directed mutagenesis, PCR reactions were set up using primers containing the desired mutation and pPolI Tky/05 PB2 WT plasmid. PCR reactions in 25µl volumes were prepared as follows: 100ng pPolI Tky05 PB2 WT plasmid, 1x KOD buffer, 1.5mM $MgSO_4$, 0.2mM dNTPs, 0.6µM forward primer, 0.6µM reverse primer and 0.02U/µl KOD DNA polymerase. PCR cycling conditions were 95°C for 2 mins, followed by 30 cycles of 95°C for 20 secs, 55°C for 20 secs, 68°C for 7 mins and a single 2 min step at 68°C. SDM PCR products were DpnI digested by incubating PCR products with 1µl DpnI enzyme and 3µl cutsmart buffer (NEB) at 37°C for 3 hours. Reactions were used in bacterial transformations as described in 2.2.1.8.

2.2.1.2 Subcloning inserts from pPolI plasmids into pCAGGS

100ng of pPolI Tky/05 PB2 9N, 81M or 9N + 81M plasmid was used in PCR reaction using primers to incorporate NotI and XhoI restriction sites. PCR reactions were set up as follows: 1x KOD buffer, 1.5mM MgSO4, 0.2mM dNTPs, 0.3µM forward primer, 0.3µM reverse primer and 0.02U/µl KOD DNA polymerase. PCR cycling conditions were 95°C for 2 mins, followed by 35 cycles of 95°C for 20 secs, 60°C for 15secs and 70°C for 1 min and a single 2 min step at

70°C. Full length bands were gel purified and double digests using NotI and XhoI (NEB) were performed in 50µl reactions containing 44µl purified PCR product, 1µl XhoI, 0.5µl NotI and 4.5µl cutsmart buffer. Reactions were incubated at 37°C for 3 hours, followed by PCR purification (Monarch). Ligations were performed as described in 2.2.1.7 using XhoI and NotI digested Tky/05 PB2 pCAGGS as destination vector.

2.2.1.3 TOPO cloning of DVGs

PCR products ranging from 300 to 1000 bp (DVGs) were gel purified (Monarch) and cloned into the PCR II-blunt TOPO Vector (Thermofisher Scientific). Briefly, 4µl of gel purified PCR products were added to a mix containing 1µl 1.2M $NaCl_2$:0.06M $MgCl_2$ salt solution and 1µl PCR-II blunt TOPO vector. These were incubated at room temperature for 5 mins before being placed on ice prior to transformation which is described in 2.2.1.8.

2.2.1.4 Subcloning of DVGs into pPolI plasmids

PB1, PB2 and PA DVGs previously cloned into TOPO vectors were subcloned into the pPolI vector using Hoffman segment specific primers containing BsaI or BsmBI restriction sites. 100ng of DVG TOPO clone plasmid was incubated with 1x KOD buffer, 1.5mM MgSO4, 0.2mM dNTPs, 0.3µM forward primer, 0.3µM reverse primer and 0.02U/µl KOD DNA polymerase. PCR cycling conditions were 95°C for 2 minutes followed by 35 cycles of 95°C for 20 seconds, 60°C for 10 seconds, 70°C for 50 seconds and a final step of 70°C for 5 minutes. PCR products were gel purified (Monarch) and digests performed in 20µl reactions in water containing 10µl PCR purified product, 1µl enzyme and 2µl Cutsmart buffer (NEB). These were incubated at either 37°C (BsaI) or 55°C (BsmBI) for 1 hour. Reactions were performed where 1µg empty pPolI plasmid was also digested and subsequently treated with 1µl Antartic Phosphatase (NEB) at 37°C for 30 minutes to prevent religation of the linearised vector. All digested products were gel purified and ligation performed (see 2.2.1.7).

2.2.1.5 Agarose gel electrophoresis

DNA fragments were separated on 1% or 2% agarose gels diluted with 0.5X TAE buffer and supplemented with 1X Gel Red (Cambridge Bioscience). DNA was loaded with 6x Gel loading dye (NEB) and gels were run in 0.5X TAE buffer. Samples were run alongside either 50/100bp or 1kb DNA ladders (Invitrogen) at 100V until the bands had sufficiently separated. DNA was visualised using a UV trans-illuminator.

2.2.1.6 DNA purification

DNA fragments were cut from the agarose gel under UV light, and DNA extracted using a gel extraction kit (Monarch) following the manufacturer's instructions. DNA digested with restriction enzymes or PCR products were purified using the PCR purification kit (Monarch). DNA fragments were eluted with 35-50µl sterile water.

2.2.1.7 DNA ligation

Ligation reactions were performed in a total volume of 20µl. Typically 4µl of digested insert and 0.5-1µl of digested vector was ligated with 1µl T4 ligase and 2µl T4 ligase buffer (NEB). The reaction mixture was incubated at 16°C between 6-16 hrs and then used to transform competent bacterial cells.

2.2.1.8 Transforming competent bacterial cells

1-2µl of the DNA ligation, ~100ng of plasmid, 2µl DpnI digested SDM reaction or 2µl TOPO cloning reaction was mixed with 20µl DH5α chemically competent *E. coli* (NEB) and incubated on ice for 30 minutes. Cells were heat shocked for 30-45 seconds at 42°C and replaced on ice for 5 minutes. 250µl of pre-warmed SOC media (Invitrogen) was added to the cells and incubated for 1 hour at 37°C in a shaking incubator (225rpm). 50-100µl was spread on to pre-warmed LB agar plates containing 1% Ampicillin or Kanamycin and incubated overnight at 37°C. Colonies were picked and grown in LB supplemented with Ampicillin (100µg/ml) or Kanamycin (50µg/ml) for TOPO cloning.

2.2.1.9 Plasmid purification

Miniprep (up to 20µg). Bacterial cells grown in 5ml LB (100µg/ml Ampicillin) were pelleted by centrifugation at 3000xg for 5 minutes. The supernatant was discarded and DNA purified by the Monarch plasmid miniprep kit (NEB) following the manufacturer's instructions. DNA was eluted with 30µl sterile water and stored at 20°C. The concentration and quality of DNA was determined by nanodrop spectrophotometer.

Maxiprep (up to 500µg). 250ml of LB supplemented with 100µg/ml Ampicillin was inoculated with 200µl bacterial cells and incubated at 37°C for 16 hours. Cells were pelleted by centrifugation at 3000xg for 20minutes. The supernatant was discarded and DNA purified by the QIAfilter Plasmid Maxi kit (Qiagen) following the manufacturer's instructions. DNA was

eluted with 1ml sterile water and stored at 20°C. The concentration and quality of DNA was determined by nanodrop spectrophotometer.

2.2.2 Cell lines and transfections

2.2.2.1 Cell culture

MDCKs, A549s, HEK293Ts, ZBP1 +/+ MEFs, ZBP1 -/- MEFs and ZBP1 Zα1α2mut MEFs were maintained in 10% DMEM. A549 IFN-β luc cells were maintained as above but supplemented with G418 for selection. All cells were grown at 37°C and 5% CO_2. Cell lines were trypsinised and passaged at least twice a week.

2.2.2.2 Generation of murine BMDMs and GM-DCs

Methods were adapted from Trouplin et al. (2013) for BMDM generation and Madaan et al. (2014) for GM-DC generation. The femur and tibia of six-to-eight week old female BALB/c mice were removed and cleaned of any flesh. Bone marrow cells were subsequently flushed from the bones, filtered through a nylon cell strainer (Falcon) and washed with PBS. Cells were centrifuged at 1500rpm for 7 minutes and the pellet resuspended in ACK lysis buffer (Gibco) for removal of erythrocytes. BM cells were counted using Trypan blue (Thermo Fisher) and following another centrifugation step at 1500rpm, 7 mins, cells were resuspended in either 1ml of BMDC media at a cell density of 4 x 10^6 cells/ml (for BMDMs) or resuspended in 1ml of GM-DC media at a cell density of 1 x 10^7 cells/ml (for GM-DCs). 1ml cell suspensions were added to 90mm non-treated cell culture petri dishes (Thermo Fisher) and 9ml GM-DC media was added to the GM-DCs or 9ml BMDM media to the BMDMs for differentiation. On day 3 of BMDM culture, non-adherent cells were removed and fresh BMDM media containing the same concentration of L929 cell supernatant was added. On day 3 of GM-DC culture, 50% of the culture media was removed and replaced with fresh GM-DC media containing rmGM-CSF. On day 7, cells were harvested for further experimental use. BMDMs were trypsinised prior to counting whereas the supernatant was collected for GM-DCs. Both GM-DCs and macrophages were seeded at 1.25 × 10^5 cells per well in 96-well plates and rested for 24 hours prior to infection.

2.2.2.3 Transfections

All transfections were performed using Lipofectamine 3000 reagent (Invitrogen) according to the manufacturer's instructions, apart from transfections of plasmids for RG which are described in 2.2.3.2. The ratio of DNA:reagent were scaled up accordingly. All dilutions were performed in Opti-MEM (Invitrogen). For transfection of RNA into A549 IFN-β luc cells (~2 x 10^5 cells), equal amounts of Polyinosinic:polycytidylic acid (Poly I:C) (InvivoGen) was co-transfected to serve as a positive control.

2.2.2.4 Minigenome polymerase assays

To measure polymerase activity, 0.1µg PB1, 0.1µg PB2, 0.05µg PA and 0.2µg NP pCAGGS expression plasmids, together with 0.1µg of the minigenome firefly reporter plasmid (PolI Firefly luciferase) and 0.025µg of a pCAGGS expression plasmid encoding Renilla luciferase, were transfected into ~2 x 10^5 HEK293T cells. Transfections were also performed where the PB2 pCAGGS plasmid or PB1 pCAGGS was omitted (2P) and empty pCAGGS transfected instead. 24 hours post transfection, cells were lysed in passive lysis buffer (Promega) and luciferase activity measured using the dual luciferase assay system (Promega) with a FLUOstar Omega plate reader (BMG Labtech). Values were normalised to Renilla.

2.2.2.5 vRNP reconstitution assays

pCAGGS expression plasmids encoding PB1 (0.1µg), PB2 (0.1µg), PA (0.05µg) (3P) and NP (0.2µg) from Tky/05 were transfected into ~2 x 10^5 HEK293T cells, alongside 0.1µg pPolI plasmids containing either a Tky/05 polymerase full length segment or a polymerase DVG. Transfections were also performed where the PB2 pCAGGS plasmid or PB1 pCAGGS was omitted (2P) and empty pCAGGS transfected instead. 24 hours later, appropriate volumes of miRNA lysis buffer (Promega) or Trizol (Thermo Fisher) was added for RNA extraction.

2.2.2.6 Minigenome driven luciferase IFN expression assays

Tky/05 pCAGGS expression plasmids encoding PB1 (0.1µg), PB2 (0.1µg), PA (0.05µg) (3P) and NP (0.2µg) were transfected into ~ 4 x 10^5 HEK293T cells, alongside 0.1µg of a pPolI plasmid containing either a Tky/05 polymerase full length segment or a polymerase DVG. Additionally, 0.1µg of a firefly luciferase reporter plasmid under the control of the IFNB promoter was co-transfected as well as 0.025µg of a pCAGGS expression plasmid encoding Renilla luciferase. Transfections were also performed minus the addition of the PB2 pCAGGS plasmid (2P). To

ensure total DNA amounts were equivalent, empty pCAGGS was transfected instead. 24 hours later, cells were lysed in passive lysis buffer (Promega) and the luciferase measured by the dual luciferase assay system (Promega) using a FLUOstar Omega plate reader (BMG Labtech). Values were normalised to Renilla and expressed as fold increase over 2P.

2.2.3 Viruses and viral infections

2.2.3.1 Biosafety

All work was approved by the local genetic manipulation (GM) safety committee of Imperial College London, St Mary's Campus (centre number GM77), and the Health and Safety Executive of the United Kingdom and carried out in accordance with the approved guidelines.

2.2.3.2 Virus

All virus stocks were originally rescued by reverse genetics and grown on MDCK cells at 37°C and 5% CO2. Briefly, 12 plasmids (8 pPol1 plasmids and 4 polymerase protein expression "helper" pCAGGs plasmids) were transfected into HEK293T cells seeded in 12-well plates. On the day of transfection, media were removed and replaced with 500µl Opti-MEM (Gibco). 0.5µg of each pPolI plasmid, PB2 and PB1 pCAGGS, 0.25µg PA pCAGGS and 1µg NP pCAGGS were added together. In a separate reaction, 20µl X-tremeGENE 9 (Roche) was added to 230µl Opti-MEM and incubated for 5 mins at room temperature. The DNA mix was then added and incubated with the X-tremeGENE 9 mix for a further 20 minutes at room temperature, before being added, drop-wise, to the HEK293T monolayer. The transfections were incubated overnight at 37**°**C, 5% CO_2. The following day, a confluent layer of MDCK cells were trypsinised and resuspended in 20ml 10% DMEM. The transfected HEK293T cells were washed gently in PBS and detached by pipetting 1ml of the MDCK cell suspension into the HEK293T well. After the cells were dislodged, an additional 4mls of the MDCK suspension was added and this mix was transferred to a 25cm^2 flask. These were allowed to adhere for 6 hours at 37**°**C, 5% CO_2. Cells were washed gently in serum-free DMEM, to remove any FCS, and then 5 ml serum-free DMEM with 1µg/ml TPCK trypsin (Worthington) was added. Cultures were incubated at 37°C, 5% CO_2 for at least 3-6 days until cytopathic effect (CPE) was observed. Virus rescues were harvested from the supernatant and cell debris was removed by centrifugation at 2000rpm for 10 minutes. The resulting aliquots were stored at -80**°**C. To make viral stocks, rescued viruses were further passaged once in MDCK cells at either an MOI of 0.0001 (6:2 Tky/05, 6:2 Tky/05 9N, 6:2 Tky/05 81M, 6:2 Tky/05 DM, 6:2 Eng/09, 7:1 Tky/05 LOW) or at an MOI of 0.01

(7:1 Tky/05 HIGH) and harvested 48 hours later. After harvesting, all viruses were clarified by centrifugation and stored at -80°C. Viral titres were determined by plaque assay and Sanger sequencing performed on at least one full genome segment for verification.

2.2.3.3 Virus titration by plaque assay.

12 well plates were seeded to form a confluent monolayer of MDCK cells on the day of infection. The media were removed, and cells washed twice in PBS. Virus was diluted in SF DMEM in a 10-fold dilution series. 200µl of virus was added to each well and incubated at 37°C, 5% CO_2. After 1 hour, the inoculum was removed and 1ml of flu overlay/agarose mix was added to each well. After 3 days incubation at 37°C, 5 % CO_2. the overlay was removed, and cells fixed/stained using Crystal Violet stain for at least 30 minutes. Crystal Violet was rinsed from the plates and plaques counted to determine plaque forming units (PFU)/ml.

2.2.3.4 Infectivity/total particle ratio

For determination of Infectivity/total particle ratios, we followed the method as described in (Xue et al., 2016). Briefly, plaque assays were performed and PFU per 25µl were calculated to quantify infectious particles. A haemagglutination (HA) assay was performed for quantification of total particles. A two-fold dilution series of virus was performed in PBS, followed by incubation with equal amounts of 0.7% turkey red blood cells. HA titres were determined by counting the last well in which clear haemagglutination was observed and calculated as HA titre/25µl.

2.2.3.5 Viral growth curves

MDCK and A549 cells were seeded in 6-well plates and infected by viruses diluted in SF media at either an MOI of 0.001 (MDCK) or 0.01 (A549) when cells were confluent. Cells were maintained in serum-free medium with the addition of 1 µg/ml TPCK trypsin (Worthington). Supernatants were taken at indicated time points and stored at -80°C until viral quantification by plaque assay on MDCK cells.

2.2.3.6 Virus infections in A549 and A549 IFN-β luc cells

24-well plates of confluent A549 or A549 IFN-β luc cells were infected with viruses diluted in SF media with an MOI of 1 in triplicate. Virus inoculums were incubated for 1 hour, removed and replaced with 2% DMEM. For A549 cells supernatants were harvested at specified time

points and cells washed in PBS prior to lysis in Trizol. Both supernatants and cell lysates were stored at -80°C. For infections in the A549 IFN-β luc cells, cells were washed in PBS before the addition of passive lysis buffer (Promega). One freeze/thaw cycle was performed to aid with lysis and luciferase was measured using the luciferase assay system (Promega) with a FLUOstar Omega plate reader (BMG Labtech).

2.2.3.7 Virus infections in murine BMDMs and GM-DCs

Viruses were diluted in SF RPMI and infected at 1 or 10 MOI (determined by plaque assay) or mock infected. After 1 hour, viral inoculums were removed and washed x1 in PBS before the addition of 2% BMDM infection media (BMDMs) or 2% GM-DC infection media (GM-DCs). At appropriate time points supernatants were collected, cells washed once in PBS and cells lysed with Trizol (Thermofisher Scientific) and frozen at -80°C.

2.2.3.8 Virus infections in hMDMs

Cells were seeded in 24-well plates at 5 x 10^5 /well in hMDM media and rested for 48 hrs at 37°C, 5 % CO_2. Viruses were diluted in SF DMEM and infected at 1 MOI (determined by plaque assay) or mock infected. After 1 hour, viral inoculums were removed and cells washed x2 in PBS before replenishing with hMDM media. At desired time points (0, 6 and 24 hrs), supernatant was removed and collected as x2 250 µl aliquots and stored at -80°C. Cells were washed in PBS before the addition of 350 µl buffer RLT and β-mercaptoethanol for RNA extraction using Qiagen RNeasy Plus Micro Kit.

2.2.3.9 Cell viability in ZBP1 +/+, ZBP1 -/- and ZBP1 Zα1α2mut MEFs

Triplicate wells of a 96-well plate of confluent ZBP1 +/+, ZBP1 -/- and ZBP1 Zα1α2mut MEFs were infected with an MOI of 1 PFU/cell. After 1 hr, virus inoculums were removed and replaced with 2% DMEM and cells were incubated for 24 hours at 37°C, 5% CO_2. Cell titre glow lysis buffer (Promega) was added to all wells and luciferase was measured using the luciferase assay system (Promega) with a FLUOstar Omega plate reader (BMG Labtech).

2.2.3.10 IFN-B quantification by ELISA

IFN-β concentrations from A549 cell supernatants was measured with VeriKine human IFN-β ELISA kit (PBL, cat 42400).

2.2.4 In vivo

2.2.4.1 Ethics statement

All animal research described in this study was approved by the Animal Welfare and Ethical Review Board (AWERB) at Imperial College London and carried out under a United Kingdom Home Office License, P48DAD9B4 in accordance with the approved guidelines.

2.2.4.2 Mouse experiments

Six- to eight-week-old female BALB/c (Envigo RMS UK Ltd) mice were maintained in pathogen-free conditions until experimental use. Isoflurane was used to anesthetise mice prior to intranasal infection with 10^5 PFU influenza virus in a 25µl/35µl volume or sterile PBS (mock). Animals were monitored, weighed daily, and culled if weight dropped below 80% of original weight measured on day 0. Lungs were harvested at designated time points, or when culled due to exceeding acceptable weight loss threshold. For experiment 1 (6:2 Tky/05, 6:2 Eng/09, 6:2 Tky/05 PB2 DM and 7:1 Tky/05) lungs were split into two, weighed and either suspended in 1 ml of PBS (for plaque assays) or 350µl cOmplete mini protease inhibition buffer (1 tablet in 10 ml PBS, Roche) (for ELISA) and homogenized using 2.8 mm beads in Precellys 2ml tubes (VWR) with a Minilys personal homogeniser (Bertin Technologies). The lungs homogenised in protease inhibition buffer were spun for 10 min at 11,000rpm at 4°C and supernatant was transferred into a fresh reaction tube containing 650µl protease inhibitor buffer. All were stored at -80°C prior to analysis. For experiment 2 (6:2 Tky/05, 7:1 Tky/05 LOW and 7:1 Tky/05 HIGH), lungs were spilt equally into three, weighed and either suspended in 1ml of PBS (for plaque assays) 1ml Trizol (RNA extraction) or 350µl protease inhibition buffer prior to homogenisation and processed as stated for exp 1. All aliquots were stored at -80°C. Bronchoalveolar lavage fluid (BAL) was collected by instilling the lungs with PBS. Supernatant was collected after centrifugation and assayed.

2.2.4.3 Chemokine and Cytokine quantification by ELISA

IFN-γ, IL-6, TNF, IP-10, MCP-1, and MIP-1β quantities in 100µl BAL fluid were determined by the Meso Scale Discovery as a 10-spot U-PLEX kit (K15069L-2). The concentration of IFN-α, TNF and IL-1β from mouse lung tissue homogenates were measured using the following ELISA kits: Quantikine mouse TNF ELISA kit (R&D systems, cat MTA00B), VeriKine mouse IFN-α ELISA kit (PBL, cat 42120) and Quantikine mouse IL-1β/IL-1F2 kit (R&D systems, cat MLB00C).

2.2.5 RNA extraction, cDNA synthesis and RT-PCR/RT-qPCR

2.2.5.1 RNA extraction from virus stocks

750µl Trizol LS (Thermofisher Scientific) was added to 250µl of virus stocks and incubated at room temperature for 10 minutes. Subsequently, 200µl chloroform was added followed by centrifugation at 11,000rpm at 4°C for 20 minutes. The aqueous phase was removed, equal volumes of 100% ethanol added, mixed and loaded onto the Zymo RNA clean and concentrator 5 columns and RNA obtained by following the manufacturers protocol.

2.2.5.2 RNA extraction from cells and murine lungs

Total RNA was extracted by adding appropriate volumes of chloroform to Trizol cell/tissue lysate and centrifuging at 11,000rpm at 4°C for 20 minutes. The aqueous phase was then removed and equal volumes of 100% ethanol was added, subsequently mixed and loaded onto either the Zymo RNA clean and concentrator 5 columns (for BMDMs and GM-DCs) or the Zymo RNA miniprep columns (for murine lung homogenates or A549 cells) and RNA obtained by following the manufacturers protocol. On column DNase I treatment was performed on all RNA samples.

2.2.5.3 RNA extraction from hMDMs

RNA was extracted from both hMDM supernatants and total RNA was extracted from cells. For supernatants, 1ml Trizol LS was added, followed by 200µl chloroform and incubated for 10 minutes at room temperature. Samples were centrifuged at 12,000rpm at 4°C for 20 minutes. The aqueous phase was carefully removed into a new labelled tube, mixed with 500µl isopropanol and incubated at room temperature for 10 minutes before centrifuging at 12,000rpm for 10 minutes. The supernatant was discarded and to the tube 1ml of 75% ethanol was added prior to centrifugation at 10,000rpm for 5 minutes at 4°C. The supernatant was again discarded, and the pellet was washed in 75% ethanol three times. On the final wash, samples were spun at 10,000rpm for 7 minutes at 4°C. The supernatant was removed, and the pellet was air-dried for 10 minutes. The pellet was resuspended in 30µl RNAse-free water and incubated at 55°C for 10 minutes prior to storage at -80°C. For RNA extraction from cells, cells were lysed in 350µl RLT plus buffer (+ β-Mercaptoethanol) (Qiagen) and transferred to a gDNA Eliminator spin column, which was placed in a collection tube, and centrifuged for 30

seconds at 10,000rpm. The flow-through was collected and mixed with 350 µl of 70% ethanol. This was then used for subsequent RNA processing using the RNeasy Plus Micro Kit (Qiagen).

2.2.5.4 RNA extraction from transfected cells

Total RNA was extracted either by lysing cells in Trizol or LBA + TG buffer (Promega). For Trizol cell lysates, chloroform was added and centrifuged at 11,000rpm at 4°C for 20 minutes. The aqueous phase was then removed, equal volumes of 100% ethanol added, mixed and loaded onto the Zymo RNA clean and concentrator 5 columns and RNA obtained by following the manufacturers protocol. For cells lysed in LBA + TG buffer, these were loaded onto QIAShredder spin column (Qiagen) and centrifuged at 11,000rpm at 4°C for 2 minutes and cleared lysate was then used for subsequent RNA processing using the Reliaprep miRNA cell and tissue miniprep system (Promega).

2.2.5.5 CIP treatment of RNA

Reactions for CIP treatments were performed in x2 20µl volumes each consisting of: 1µg RNA, 1µl quickCIP enzyme (NEB), 2µl cutsmart buffer and 15µl water. A further x2 20µl reactions were set up where 1µl water was used instead of the enzyme to serve as negative controls. All reactions were incubated at 37°C for 10 minutes followed by a further 2 minutes at 80°C. Duplicate reactions were pooled and diluted in 160µl water to obtain 200µl volumes. 600µl Trizol was added, and RNA extracted in the same manner as 2.2.5.4.

2.2.5.6 RT-qPCR for M gene detection

RT-qPCR was performed using the 7500 real time PCR system (ABI) in 20µl reactions using AgPath-ID One-step RT-PCR reagents (Thermo Fisher). A mastermix containing 10µl RT-PCR buffer (2x), 0.8µM forward primer (5' GACCRATCCTGTCACCTCTGA 3'), 0.8µM reverse primer (5' AGGGCATTYTGGACAAAKCGTCTA 3'), 0.4µM probe (5' FAM-TGCAGTCCTCGCTCACTGGGCACG-BHQ1 5') and 1µl RT-PCR enzyme mix (25x) was prepared and 5µl RNA added. The following cycling conditions were used: 45°C for 10 min, 1 cycle; 95°C for 10 min, 1 cycle; 95°C for 15 s then 60°C for 45s, 40 cycles. Threshold cycle (Ct) values for the target M gene was determined per sample. Absolute M gene copy numbers were calculated based on a standard curve.

2.2.5.7 RT-qPCR for NA vRNA quantification

Equal amounts (100ng) of RNA were subjected to cDNA synthesis using RevertAid reverse transcriptase (Thermo Fisher). 12µl reactions were prepared using 100ng RNA, water and either 1µl 5' tagged vRNA NA primer (for NA vRNA) or 1µl Oligo (dT) (for GAPDH). These were incubated at 65°C for 5 minutes before being transferred to ice. A mix containing 4µl 5xRT buffer, 2µl dNTPs and 1µl RevertAid minus H RT was added to each reaction and all were incubated at 50°C for 60 minutes. Negative controls where no primer, no RT and no template were also performed. A 148bp NA vRNA amplicon was amplified in qRT-PCR using tagged NA vRNA forward primer and NA vRNA reverse primer as follows: SYBR green PCR mixes containing 5µl FAST SYBR green master mix (Applied Biosystems), 0.2µM forward primer, 0.2µM reverse primer and 5µl of 2.5ng cDNA. qPCR analysis was carried out in duplicate on a Viia 7 real-time PCR system (Thermo Fisher) using the following cycling conditions: 95°C for 10 minutes followed by 40 cycles of 95°C for 15 seconds and 60°C for 1 minute. Fold changes in gene expression relative to mock infected controls were calculated using the 2-ΔΔCT method with GAPDH expression as internal control. Melt curves were analysed to confirm the absence of non-specific binding.

2.2.5.8 RT-PCR for full length genome and DVG detection

cDNA was made using Uni12 primer and Superscript IV (Life Technologies). Briefly mixes were made consisting of: 1µl 2µM Uni12 primer, 1µl 10mM dNTP mix and appropriate amount of water to total 13µl with the addition of either 500ng (A549 cells), 100ng (BMDMs/GM-DCs) or 2µg (murine lung homogenates) of total RNA. After an incubation step at 65°C for 5 minutes to denature RNA, mixes were put on ice for 1 minute and subsequently 4µl 5 x buffer, 1µl 0.1M DTT, 1µl water and 1µl Superscript IV (200U/µl) were added. Mixes were incubated at 50°C for 10 minutes followed by a further 10 minutes at 80°C. For cDNA synthesis from viral stocks, 3µl RNA was added in each RT reaction which were performed as above. PCR reactions were performed in a total volume of 25µl using KOD Taq polymerase (Novagen). This consisted of 1x KOD buffer, 1.5mM MgSO4, 0.2mM DNTPs, 0.3µM forward and reverse primers and 0.02U/µl KOD polymerase and 2-3µl RT reaction. To detect both DVGs and full genomes, terminal Tky/05 polymerase primers or Hoffman primers were used. For FL genome only, primers complimentary to an internal region of the genome were used. A Hot-start touchdown PCR was used to minimise non-specific priming (Korbie & Mattick, 2008) with the

following cycling conditions: 95°C for 2 minutes, followed by the touchdown step comprising 12 cycles of 95°C for 20 seconds, 10 seconds of 68-57°C which decreased by 1°C each cycle and finally 70°C for 10-50 seconds depending on amplicon length. This was immediately followed by 25 cycles of 95°C for 20 seconds, 50°C for 10 seconds, 70°C for 10-50 seconds depending on amplicon length. The final extension step was performed at 70°C for 3-5 mins.

2.2.5.9 Transcription factor gene expression in murine BM derived cells by qRT-PCR

For qPCR detection of murine MerTK and Zbtb46 in BMDMs and GM-DCs, cDNA was synthesised using the high-capacity cDNA reverse transcription kit (Applied Biosystems) with random primers. Briefly, reactions were set up containing: 2µl 10XRT buffer, 0.8µl 100mM dNTP mix, 2µl 10X RT random primers, 1µl Multiscribe reverse transcriptase and 4.2µl water. Equal volumes (10µl) of diluted RNA at a concentration of 100ng were added and reactions incubated at 25°C for 10 minutes, 37°C for 120 minutes and 85°C for 5 minutes. PCR reactions were set up as follows: 1µl 20X Taqman gene expression assay, 10µl 2X Taqman gene expression mastermix, 5µl water and 4µl of diluted cDNA at a concentration of 20ng. MerTK and Zbtb46 Taqman gene expression assays were used alongside GAPDH (Thermo Fisher). qPCR analysis was carried out in duplicate on a Viia 7 real-time PCR system (Thermo Fisher) and the following cycling conditions were used: 50°C for 2 minutes, 95°C for 10 minutes followed by 40 cycles at 95°C for 15 seconds followed by 1 minute at 60°C. Fold changes in gene expression relative to GAPDH were calculated.

2.2.5.10 Cytokine/Chemokine detection by qRT-PCR

For qPCR detection of cytokines, cDNA was either synthesised by using the high-capacity cDNA reverse transcription kit (Applied Biosystems) using random primers for gene expression using Taqman assays (as described in 2.2.5.8), RevertAid reverse transciptase using Oligo (dT) (Thermo Fisher) for gene expression using gene specific primers (as described in 2.2.5.6) or the QuantiTect Reverse Transcription Kit (Qiagen) for gene expression in hMDMs. 50ng of RNA extracted from hMDMs was used in the RT step and were performed as follows: 2µl 7x gDNA Wipeout Buffer was added to 11µl water for genomic elimination reaction and incubated at 42°C for 5 minutes. 1µl Quantiscript Reverse Transcriptase, 1µl RT primer mix and 4µl 5x Quantiscript RT Buffer was added to the genomic elimination reaction and incubated at 42°C for 30 minutes, then 95°C for 3 minutes. qPCR was performed in the hMDMs by using PowerUp SYBR Green master mix as follows: 2µl 25ng cDNA was mixed

with 5µl PowerUp SYBR Green Master Mix (Applied Biosystems), 0.3µl 10µM forward primer, 0.3µl 10µM reverse primer and 2µl water. PCR cycling conditions were: 95°C for 5 minutes, followed by 40 cycles of 15 seconds at 95°C, 20 seconds at 57°C and 20 seconds at 72°C. This was followed by x3 15 second single steps at 95°C, 60°C and 95°C. Cycles were run on the 7900HT Fast Real-Time PCR System (Applied Biosystems). 500ng total RNA (A549 cells), or 100-200ng total RNA (BMDMs/GM-DCs) were used in cDNA reactions. The mRNA level of murine TNF-α, Il-6 and GAPDH in BMDMs/GM-DCs, human IFN-β and GAPDH in A549 cells and human IFN-β, IL-8, TNF-α, IL-6, IP-10 and GAPDH were quantified with SYBR green PCR mix (Applied Biosystems) as previously described in 2.2.5.6. To detect murine IFN-α5 mRNA, a Taqman gene expression assay was used alongside GAPDH. As previously described in 2.2.5.8. qPCR analysis was carried out in duplicate on a Viia 7 real-time PCR system (Thermo Fisher). Fold changes in gene expression relative to mock infected controls were calculated using the 2-ΔΔCT method with GAPDH expression as an internal control.

2.2.6 Sanger sequencing, NGS and Bioinformatics

2.2.6.1 Sanger sequencing

5µl purified DNA at either 100ng/µl (plasmid) or 1-10ng/µl (purified PCR product) was added to 5µl 5µM relevant primer and sent for Sanger sequencing, performed by Eurofins.

2.2.6.2 NGS from murine lungs

NGS analysis was performed using RNA from two murine lungs for each group (7:1 Tky/05, HIGH, 7:1 Tky/05 LOW and 6:2 Tky/05) per time point (6, 24, 48, 96 h.p.i.) All eight genome segments were amplified using 2µg total RNA in cDNA reactions using 2µM MBTUni-12 primer and SSIV (Invitrogen). For PCR amplification, 2µl cDNA was incubated with 10µM MBTUni-12 and 10µM MBTUni-13 primer with KOD polymerase (Merck) and the following cycling conditions used: 95°C for 2 minutes followed by 25 cycles of 95°C for 20 seconds, 57°C for 10 seconds, 70°C for 50 seconds and a terminal extension of 72°C for 5 mins. All samples were purified using the Monarch PCR cleanup kit (NEB), prior to dilution to 20ng in 50µl. Samples were fragmented using the Covaris M220 ultrafocused sonicator (Covaris). The NEBnext Ultra II DNA library prep kit (NEB) was used for library construction. Adapters were diluted 1:10 with 10nM Tris/NaCl and after ligation, AMPure XP beads (Beckman-Coulter) were used for

the clean-up step with no size selection. 6 PCR cycles were performed for PCR enrichment by adding index and universal primers using NEBnext multiplex oligos for Illumina (NEB). Another clean-up step was performed using the AMPure XP beads and libraries were pooled at an equimolar ratio following quantification by Qubit (Thermofisher Scientific). Libraries were sequenced with pair-ended 2x150nt reads on an Illumina MiSeq using V2 Chemistry, performed by the Imperial BRC Genomics Facility.

2.2.6.3 Bioinformatics

Raw sequences for NGS data were deposited at http://www.ebi.ac.uk/ena, project number PRJEB56225. For NGS from murine lungs, fastq files were generated and demultiplexed with the bclfastq v2.20 conversion software (Illumina). One set of sequencing reads from each pair (R1) were analyzed by ViReMa (v0.10) (Routh & Johnson, 2014) to detect junction spanning reads (DVGs). Read support cutoff (RSC) of >30 was used to minimise the number of inaccurate junctions; all other parameters were set to default settings. For verification of sequencing results, alignments were performed to compare to the reference genome in Geneious R6. For aligning DVGs/mvRNAs to the reference genome, the gap open penalty was set to 3 and the gap extension penalty set to 0 to permit the alignment of large central deletions.

2.2.6.4 Statistical analysis

Statistics throughout this study were performed using GraphPad Prism version 9.0 (Graphpad Software) and are described in the figure legends. P-values less than 0.05 were considered significant.

Chapter 3 Aberrant replication and cytokine responses in IAV infected innate immune cells

3.1 Introduction

Whilst respiratory epithelial cells are the main target cells for IAV infection in mammals and produce new infectious virions, other cell types can also be infected, albeit not always productively. Both macrophages and dendritic cells act as APCs, presenting antigen either via phagocytosis of infected epithelial cells or through direct infection. They also both secrete cytokines and are key orchestrators of the innate immune response. Indeed, although the absolute numbers of dendritic cells in the lung is low, the levels of cytokines they can produce is considerable (Banchereau et al., 2000). Immunohistochemical techniques have detected viral proteins within macrophages, monocytes, and dendritic cells following IAV infection both *in vitro* and *in vivo,* demonstrating at least virus entry and primary rounds of transcription and gene expression (Ioannidis et al., 2012; Manicassamy et al., 2010). Furthermore, animal models of HPAIV infection have demonstrated an influx of white blood cells into the lung associating with high levels of pro-inflammatory cytokines (Perrone et al., 2008; Xu et al., 2006).

As mammalian infections with HPAIVs such as the H5N1 subtype are often associated with hypercytokinemia, resulting in extensive tissue damage, ARDS and ultimately high fatality rates (Belser & Tumpey, 2013; de Jong et al., 2006; Xu et al., 2006), trying to understand the virological mechanisms behind the cytokine storm is of paramount importance. Both macrophages and dendritic cells have been implicated in the IAV-induced cytokine storm (Guo & Thomas, 2017), and past studies have tried to address whether HPAIV H5N1 viruses replicate to a greater extent within these innate immune cells. Many of these focus on whether replication is productive (release of new influenza virions) or abortive (failure to release viral progeny) and have shown conflicting results. For example, one study showed that a subset of H5N1 viruses were able to replicate productively in the murine macrophage cell line RAW264.7 and murine alveolar macrophages, whereas other subtypes were not (Cline et al., 2013). Conversely a study by (Chan et al., 2012), showed that H5N1 infection of murine BMDMs resulted in abortive replication whereas H1N1 virus replication was productive. Infections in human macrophages and dendritic cells show a similar discordance

(Short et al., 2012). However, there is agreement that most IAV strains can replicate abortively within macrophages and dendritic cells, as measured by increasing quantities of influenza protein or viral RNA over the experimental time course.

Although productive replication could contribute to increasing viral dissemination and therefore enhance virulence, even abortive replication can still induce cytokine responses. Accumulation of viral RNA within the cell act as a PAMP to trigger cell signalling pathways leading to the production of pro-inflammatory cytokines. Indeed, alveolar macrophages are programmed to detect and respond to pathogens rapidly due to a higher basal expression level of PRRs when compared to epithelial cells (Ma et al., 2019). Analysis of pro-inflammatory cytokine induction by H5N1 strains compared to seasonal strains in macrophages and dendritic cells, again shows divergent results although numerous studies indicate that H5N1 strains elicit a stronger pro-inflammatory response than their seasonal counterparts (Chan et al., 2012; Cheung et al., 2002; S. M. Lee et al., 2009; Sandbulte et al., 2008; Westenius et al., 2018). We have also previously shown in our laboratory that following infection of murine GM-DCs with a recombinant virus bearing the H5N1 internal genes, 6:2 Tky/05, high levels of IFN-α and other pro-inflammatory cytokines were produced; significantly higher than those induced by recombinant viruses containing mammalian-adapted internal genes as well as a virus engineered to be restricted for replication in myeloid cells (Li et al., 2018).

The aim of this chapter is to therefore establish whether the 6:2 Tky/05 virus replicates and produces higher levels of type I IFN and pro-inflammatory cytokines in dendritic cells and macrophages compared to a more mammalian adapted IAV strain, 6:2 Eng/09. We will generate primary murine GM-DCs (phenotypically similar to monocyte derived and conventional DCs) and BMDMs (phenotypically similar to macrophages) and challenge these cells with the recombinant viruses in order to assess viral replication and cytokine induction. Additionally, we will also conduct infections in primary human macrophages.

3.2 Results

3.2.1 The 6:2 Tky/05 and 6:2 Eng/09 viruses can activate the IFN-β promoter and replicate to similar levels in human lung epithelial cells

The 6:2 Tky/05 and 6:2 Eng/09 viruses are recombinant viruses containing the six internal genes either from the HPAIV H5N1 A/turkey/Turkey/1/2005 strain or the H1N1pdm09 A/England/195/2009 strain respectively. Both viruses contain the HA and NA genes from the laboratory adapted strain A/Puerto Rico/8/34 (PR8). This ensures both viruses have the same host and cell tropism, and acts as an important safety measure as the PR8 virus and viruses with the PR8 HA and NA are attenuated for humans (Beare et al., 1975) and are also not a threat to domestic poultry (Shelton, unpublished). Thus, experiments can be conducted at BSL2. We have previously shown in our laboratory that the 6:2 Tky/05 virus did not activate the IFN-β promoter to higher levels than the 6:2 Eng/09 strain in lung epithelial cells (Li et al., 2018). To confirm these findings, we infected the A549 IFN-β luc cell line with the two recombinant strains at an MOI of 3 and measured luciferase activity 24 hours later (Figure 3.1A). We again observed that the 6:2 Tky/05 virus did not induce higher IFN-β promoter activity than the 6:2 Eng/09 strain. We also wished to ascertain whether there was any difference in vRNA load at this time within the epithelial cells between these two viruses. We therefore extracted total RNA and performed RT-qPCR to determine vRNA levels (Figure 3.1B). We used RT primers that incorporated a 5' tag, followed by PCR using the tag sequence in the forward primer to ensure elimination of any non-specific products generated through self-priming (as described in (Staller et al., 2019)). We found that the vRNA of 6:2 Tky/05 and 6:2 Eng/09 viruses accumulated to similar levels.

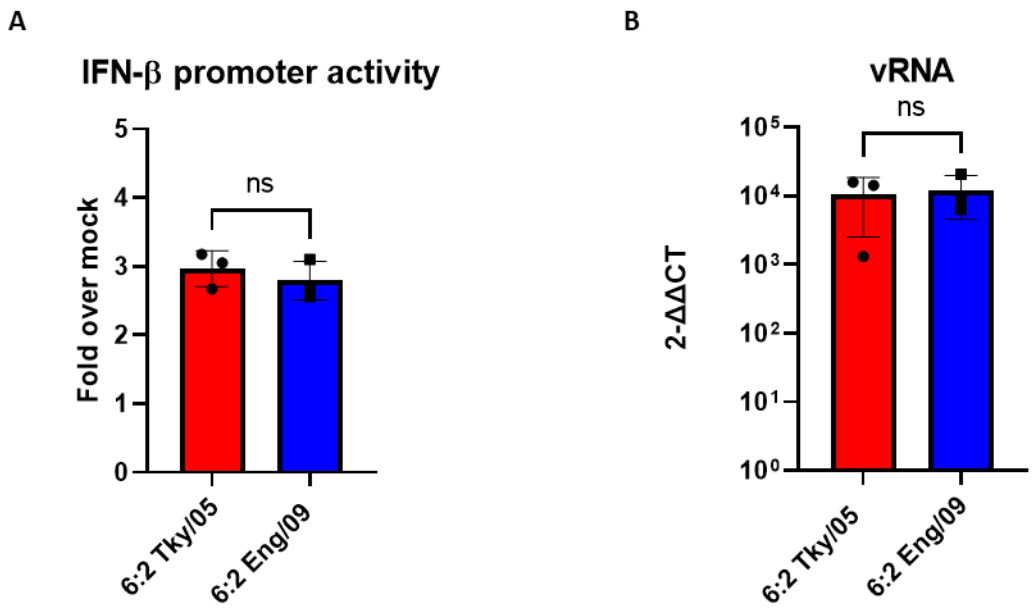

Figure 3.1. IFN-β promoter activity and viral replication in lung epithelial (A549) cells. A) A549 IFN-β luciferase cells were infected with 6:2 Tky/05, 6:2 Eng/09 virus at an MOI of 3 or mock infected and at 24 h.p.i., cells were lysed, and luciferase measured. Data represents mean ± SD (n=3). B) RNA was extracted from infections in A), DNAse I on-column treated, and concentration measured by spectrophotometry. Equal amounts of total RNA (100 ng) were used to generate cDNA using RevertAid reverse transcriptase and tagged primers against NA vRNA or Oligo(dT). qPCR was performed using Fast SYBR green master mix and primers to amplify NA vRNA or GAPDH. Relative expression was calculated by the 2 -ΔΔ CT method normalised to the GAPDH housekeeping gene and shown as fold increase over the mock infected cells. Data represents mean ± SD (n=3 biological replicates) performed in technical duplicates. Differences between 6:2 Tky/05 and 6:2 Eng/09 were calculated by a two-tailed unpaired student's t-test.

3.2.2 Generation and characterisation of BMDMs and GMDCs

To examine the replication and cytokine response in immune cells following infection with the 6:2 Tky/05 and 6:2 Eng/09 viruses, we generated murine BMDMs and GM-DCs. To do this, we propagated murine bone marrow derived cells in media supplemented with different growth factors to generate phenotypically distinct cell populations (schematically shown in Figure 3.2).

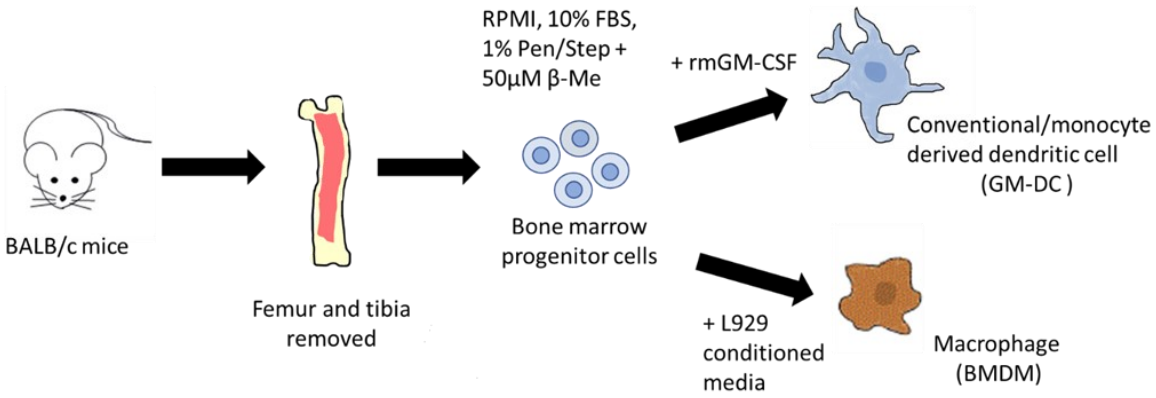

Figure 3.2. Generation of BMDMs and GM-DCs. Bone marrow progenitor cells were flushed out from the tibia and femur of BALB/c mice and propagated in media either containing 40ng/µl rmGM-CSF for GM-DCs or 20% L929 conditioned media for BMDMs. Both GM-DCs and BMDMs were harvested at day 7 and seeded in 96-well plates prior to infection. L929 conditioned media contains M-CSF and has been routinely used to differentiate bone marrow progenitor cells into macrophages (Englen et al., 1995; Trouplin et al., 2013).

To ensure differentiation, flow cytometry is typically used to analyse surface expression markers, but upregulation of transcription factors can also be employed. MerTK is primarily found on the macrophage cell surface, correlating with the expression of mRNA transcripts, although it is also expressed by dendritic cells, albeit at lower levels (Behrens et al., 2003; Gautier et al., 2012; Helft et al., 2015). Zbtb46 expression is only associated with dendritic cells (Satpathy et al., 2012). To verify that our cell populations represent BMDMs and GM-DCs respectively, we differentiated both cell types and 24 hrs later, total RNA was extracted, and RT-qPCR performed (Figure 3.3).

As expected, the BMDMs expressed MerTK and there were undetectable levels of Zbtb46 (Figure 3.3A). The GM-DCs expressed both MerTK and Zbtb46, although Zbtb46 expression was higher (Figure 3.3B). Of note there is known heterogeneity that arises when culturing BM cells with GM-CSF as monocyte derived macrophages can also be obtained (Erlich et al., 2019; Helft et al., 2015). Therefore, our results confirm that there was successful propagation of both BMDMs and GM-DCs and the methods for their generation are suitable for use in further experiments.

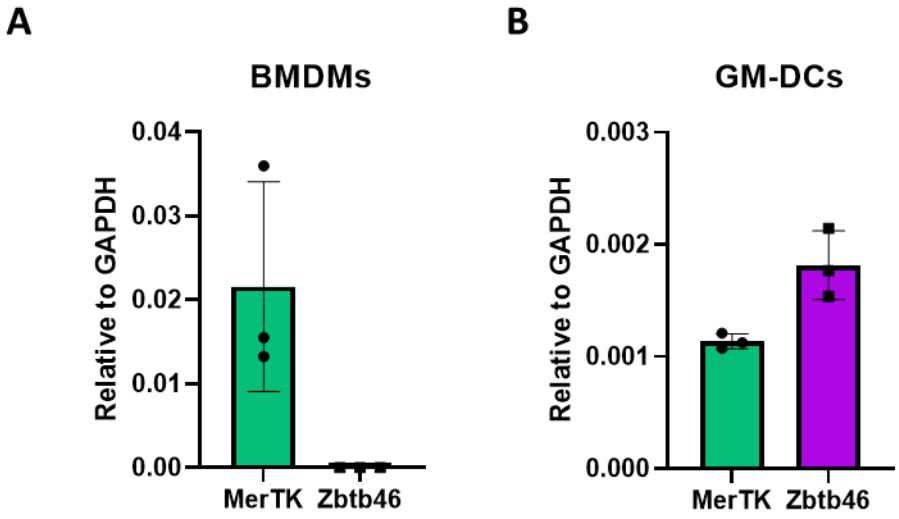

Figure 3.3. Gene expression analysis to confirm BMDM and GM-DC populations. A) BMDM or B) GM-DC cells were generated and 24 hrs later, RNA was extracted, DNAse I on-column treated, and concentration measured by spectrophotometry. Equal amounts of RNA (100 ng) were used to generate cDNA using high capacity reverse transcriptase kit and random primers. qPCR was performed using murine MerTK, Zbtb46 and GAPDH Taqman gene expression assays. Relative expression to the GAPDH housekeeping gene was calculated. Data represents mean ± SD (n=3 biological replicates) performed in technical duplicates.

3.2.3 The 6:2 Tky/05 and 6:2 Eng/09 viruses replicate to similar levels in GM-DCs and BMDMs

In an initial experiment we cultured both BMDMs and GM-DCs and infected them with the 6:2 Tky/05 and 6:2 Eng/09 virus at an MOI of 10. Total RNA was extracted 8 h.p.i and the concentration measured by spectrophotometry. As the individual RNA yields were low, RNA from two wells were pooled prior to subsequent RT-qPCR analysis using primers for PR8 NA vRNA as described previously. We found no difference in the levels of vRNA between the 6:2 Tky/05 virus and 6:2 Eng/09 virus in either the GM-DCs or the BMDMs (Figure 3.4). We also observed noticeably higher levels of vRNA in the GM-DCs than the BMDMs. Despite this increased permissively in the GM-DCs, we focused on BMDMs for further experiments due to obtaining higher yields during culturing.

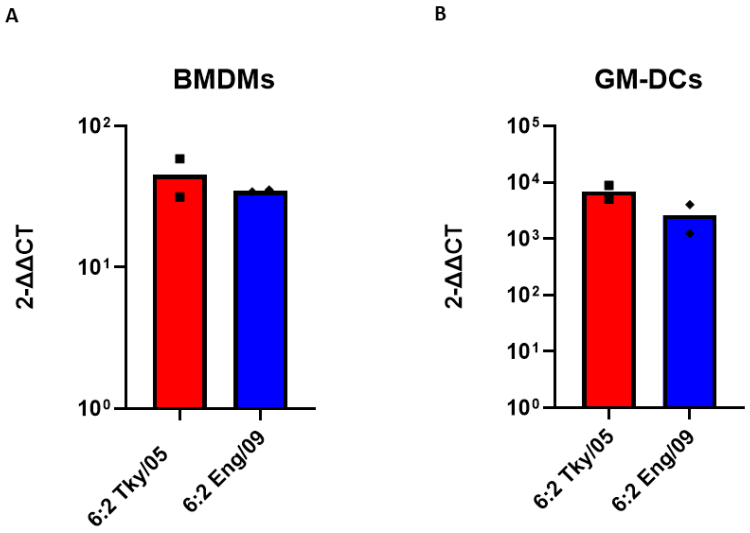

Figure 3.4. Viral replication of 6:2 Tky/05 and 6:2 Eng/09 virus in GM-DCs and BMDMs. Following differentiation, GM-DCs (A) and BMDMs (B) were infected with 6:2 Tky/05 and 6:2 Eng/09 at an MOI of 10, or mock infected in quadruplicate. RNA was extracted at 8 h.p.i, DNAse I on-column treated, and concentration measured by spectrophotometry. RNA was pooled from two wells to ensure sufficient yields for RT-qPCR. Equal amounts of RNA (100 ng) were used to generate cDNA using RevertAid reverse transcriptase and tagged primers against NA vRNA or Oligo(dT). qPCR was performed using Fast SYBR green master mix and primers to amplify NA vRNA or GAPDH. Relative expression was calculated by the 2 -ΔΔ CT method normalised to the GAPDH housekeeping gene and shown as fold increase over the mock infected cells. Data represents mean (n=2 biological replicates) performed in technical duplicates. Statistical analysis was not performed due to small sample size.

To ensure we were measuring genuine replication within these cells and not just residual input viral RNA, we performed a further experiment where we infected BMDMs with the 6:2 Tky/05 and 6:2 Eng/09 virus. We also included two additional viruses: 6:2 Tky/05 NPmir142mir and 7:1 Tky/05 LOW. The 6:2 Tky/05 NPmir142 is compromised in its ability to replicate within myeloid cells due to containing four copies of a microRNA target sequence in the NP gene that is only expressed in myeloid cells (Langlois et al., 2012) and has been used in our laboratory previously (Li et al., 2018). The 7:1 Tky/05 LOW virus[1] was generated from a stock that had a high genome copy number to PFU ratio, indicative of a high DVG content,

[1] The 7:1 Tky/05 virus was an existing laboratory stock that had been passaged multiple times under different MOI conditions and was labelled as a 6:2 virus (PR8 HA and NA). Prior to use, initial sanger sequencing analysis of this stock only focused on the polymerase and HA genes, so this virus was believed to have a 6:2 gene constellation for most of the experiments in this thesis. Later NGS data (chapter 5) indicated that viruses derived from this original stock contained the NA gene from Tky/05 and not PR8. Subsequent sanger sequencing of all eight genome segments confirmed this.

and was generated by passaging the original stock at a low MOI (0.0001). The inclusion of this virus was to establish whether any DVGs present in this stock could alter the replication or cytokine induction compared to the standard 6:2 Tky/05 virus. All viruses replicated within the BMDMs as shown by an increase in vRNA between 8 and 24hrs (Figure 3.5). As expected, replication was reduced for the 6:2 Tky/05 NP142mir virus and was undetectable at the early time point (8 hrs). There was also a noticeable reduction in the vRNA levels for the 7:1 Tky/05 virus which was originally intriguing (see footnote) but is presumably due to the PR8 specific NA primers sub-optimally binding to the Tky NA segment. At 24 h.p.i, there was only a 2-fold increase in NA vRNA produced by the 6:2 Tky/05 virus when compared to the 6:2 Eng/09 virus. Overall, these findings suggest that the 6:2 Tky/05 virus does not replicate to higher levels than the 6:2 Eng/09 virus in either murine GM-DCs or BMDMs.

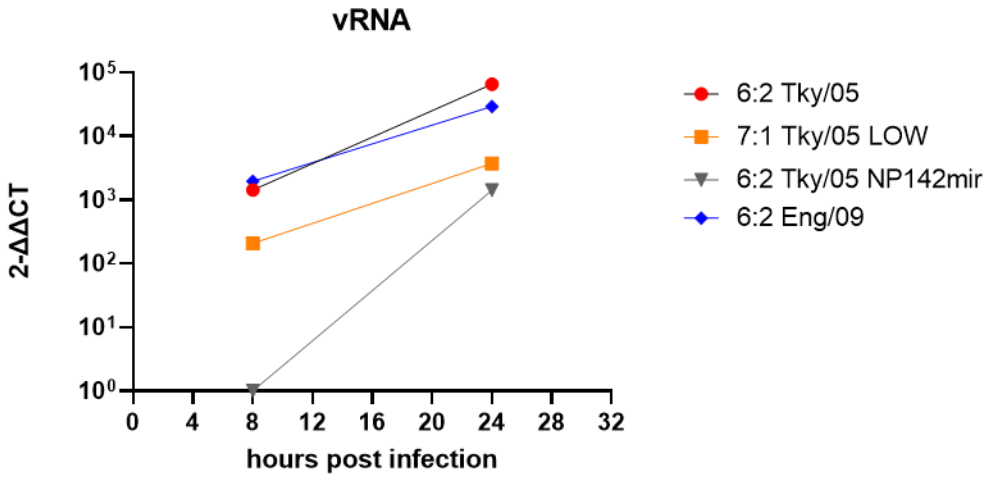

Figure 3.5. Viral replication of 6:2 Tky/05 and 6:2 Eng/09 virus in BMDMs. Following differentiation, BMDMs were infected with 6:2 Tky/05, 7:1 Tky/05 LOW, 6:2 Tky/05 NP142mir and 6:2 Eng/09 at an MOI of 10, or mock infected in quadruplicate. RNA was extracted at 8 and 24 h.p.i, DNAse I on-column treated, and concentration measured by spectrophotometry. RNA was pooled from two wells to ensure sufficient yields for RT-qPCR. Equal amounts of RNA (100 ng) were used to generate cDNA using RevertAid reverse transcriptase and tagged primers against NA vRNA or Oligo(dT). qPCR was performed using Fast SYBR green master mix and primers to amplify NA vRNA or GAPDH. Relative expression was calculated by the 2 -ΔΔ CT method normalised to the GAPDH housekeeping gene and shown as fold increase over the mock infected cells. Data represents mean (n=2 biological replicates) performed in technical duplicates. Statistical analysis was not performed due to small sample size.

3.2.4 DVGs are detected in the BMDMs following IAV infection

As aberrant replication products such as DVGs can act as PAMPs and have been shown to induce innate immune responses (Genoyer & Lopez, 2019; Tapia et al., 2013), we wished to ascertain whether any were generated in the BMDMs following infection with the influenza viruses. As the 7:1 Tky/05 LOW stock was generated from a virus stock that had a high genome to PFU ratio, we suspected that this virus stock still retained DVGs and these would be amplified in the BMDMs. We therefore amplified RNA extracted from the BMDMs at both 8 and 24 h.p.i, using primers that target the 5' and 3' end of the PB1 segment and analysed these on an agarose gel (Figure 3.6). As IAV DVGs typically contain a large central deletion these primers should amplify any PB1 DVGs. We chose to analyse the PB1 segment because IAV DVGs typically arise from the polymerase segments (Noble & Dimmock, 1995). Indeed, we saw PCR products that were between approx. 450nt-700nt long were generated from all viral infections. There was a very intense band of just below 500nt in size at 8 h.p.i that was stronger at 24 h.p.i generated by the 7:1 Tky/05 LOW virus.

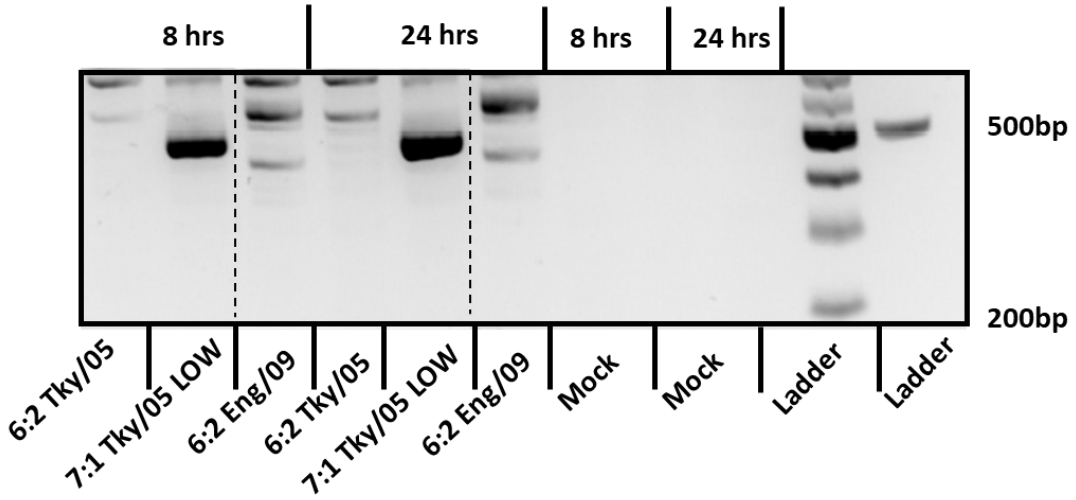

Figure 3.6. IAV DVGs detected in the BMDMs. BMDMs were either infected with an MOI of 10 for viruses or mock infected in quadruplicate as in Figure 5.5. Total cellular RNA was extracted at 8 and 24 h.p.i and RNA was pooled from two wells. RNA was DNAse I on-column treated, and concentration measured by spectrophotometry. 100ng of RNA was used for cDNA synthesis with Superscript IV RT and Uni12 primer that targets the 3' end of vRNA. PCR was then performed using KOD polymerase and Hoffman primers that target the conserved 3' and 5' termini of PB1 vRNA and products ran on a 1.5% agarose gel with GelRed. Both 100bp and 1kb ladders were used. Lanes on gel were rearranged for conformity and boundaries are indicated with dotted lines.

3.2.5 All viruses containing H5N1 internal genes induced higher secretion of IFN-α than the 6:2 Eng/09 virus

Next, we wished to investigate cytokine induction in the BMDMs that were infected with the 6:2 Tky/05, 7:1 Tky/05 LOW, 6:2 Tky/05 NPmir142 and 6:2 Eng/09 virus. We chose two key proinflammatory cytokines which have been implicated to be elevated in the cytokine storm: -IL-6 and TNF-α (Karki & Kanneganti, 2021; Perrone et al., 2010; Tisoncik et al., 2012). Total RNA was extracted 24 h.p.i and RT-qPCR performed (Figure 3.7A and B). The 6:2 Tky/05 and the 6:2 Eng/09 virus showed similar induction of mRNA expression for both IL-6 and TNF-α. Interestingly, the 7:1 Tky05 LOW showed the highest mRNA expression and this was vastly increased for IL-6. We also determined the concentration of secreted IFN-α by performing ELISA on the BMDM supernatants (Figure 3.7C). Only the 6:2 Tky/05 and 7:1 Tky/05 LOW virus showed detectable levels of secreted IFN-α protein, with the 7:1 Tky/05 LOW virus secreting statistically higher levels than the 6:2 Tky/05 virus. The 6:2 Tky/05 NPmir142 virus which replicated poorly, did not induce IL-6 or TNF-α mRNA expression nor any detectable IFN-α protein (Figures 3.7A-C).

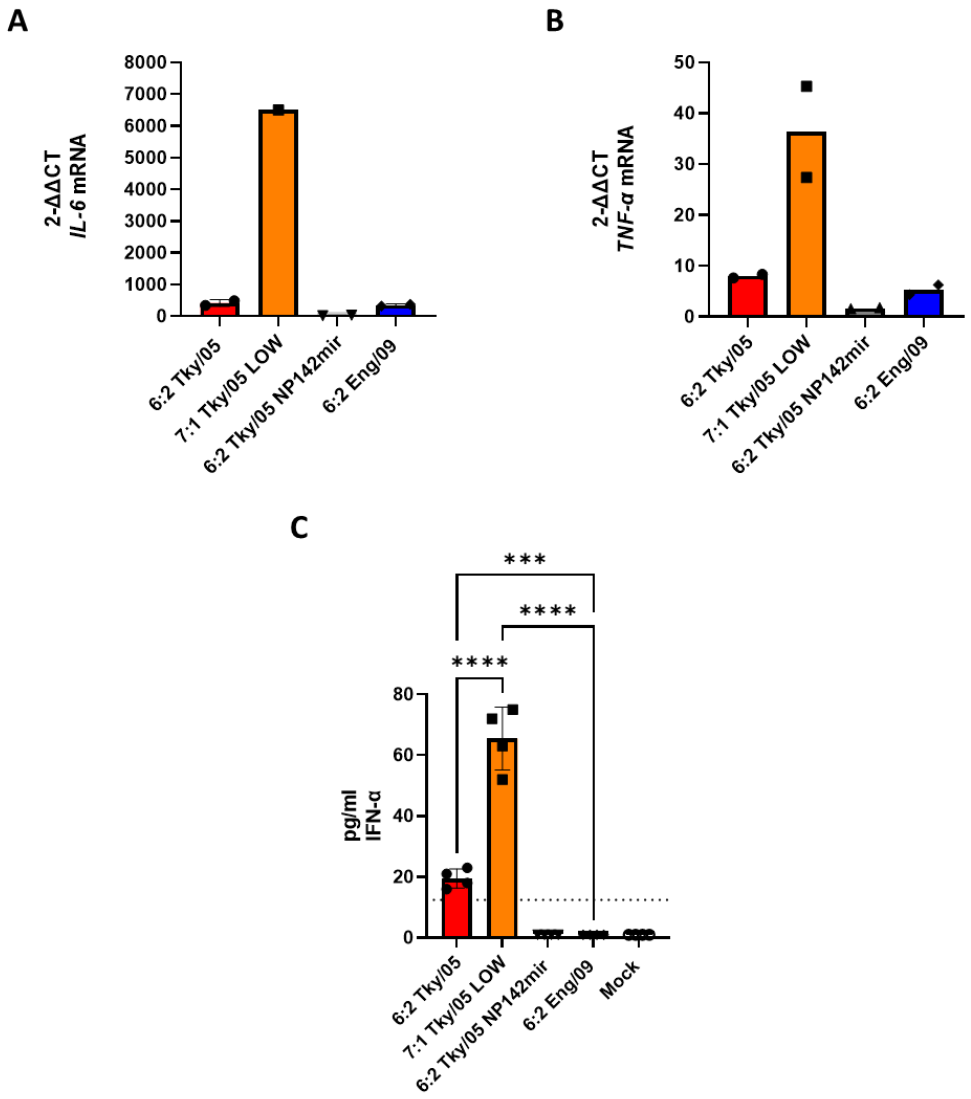

Figure 3.7. Cytokine expression and IFN-α secretion in BMDMs. BMDMs were either infected with an MOI of 10 for viruses or mock infected in quadruplicate. 24 h.p.i, supernatants were collected, and total cellular RNA extracted. RNA was pooled from two wells to ensure sufficient yields for RT-qPCR analysis whereas supernatants were analysed separately. RNA was DNAse I on-column treated, and concentration measured by spectrophotometry. Equal amounts of RNA (100 ng) were used to generate cDNA using RevertAid reverse transcriptase and primer for Oligo(dT). qRT-PCR performed using Fast SYBR green master mix and primers targeting GAPDH and A) Il-6 (B) TNF-α. Relative expression was calculated by the 2 -ΔΔ CT method normalised to the GAPDH housekeeping gene and shown as fold increase over the mock infected cells. C) IFN-α levels in cell supernatants harvested at 24 h.p.i determined by ELISA. Variance among groups was calculated by one-way ANOVA with Tukey post hoc test for multiple comparisons (* p<0.001, ****, p<0.0001. Only comparisons between the 7:1 Tky/05, 6:2 Tky/05 and 6:2 Eng/09 are shown. Statistical analysis on A-B was not performed due to small sample size (n=2). Error bars depict mean + SD. Data from C forms part of Figure 4 in (Penn et al., 2022).**

3.2.6 Replication and cytokine expression in human monocyte derived macrophages

Next, we infected commercially obtained hMDMs that had been generated by culturing CD14+ monocytes from one donor with human macrophage colony stimulating factor (hM-CSF). To analyse virus replication, the hMDMs were infected with both the 6:2 Tky/05 and 6:2 Eng/09 at an MOI of 1. Total RNA was extracted from infected cells at 0, 6, and 24 hrs. In addition, supernatants were collected at the same time and quantification of the M gene copy number was performed on both cell lysates and the supernatants (Fig 3.8). Unfortunately, the total RNA yield was too low for analysis at 24 hrs, however it is apparent that both the 6:2 Tky/05 and 6:2 Eng/09 virus were able to replicate within the hMDMs as M gene copy numbers/µl increased between 0 and 6 hrs (Fig 3.8A) This is in stark contrast to the RNA obtained from the supernatant which showed no detectable M gene copies at 6 h.p.i for either virus (Fig 3.8B). At 24 h.p.i, one of the two supernatants obtained from the 6:2 Tky/05 infected hMDM showed a low M gene copy number of 802, whereas for the other replicate there was no M gene copies detected which was also observed for the 6:2 Eng/09 virus. These results suggest that replication is abortive which we confirmed by plaque assay as no infectious particles were detected (data not shown).

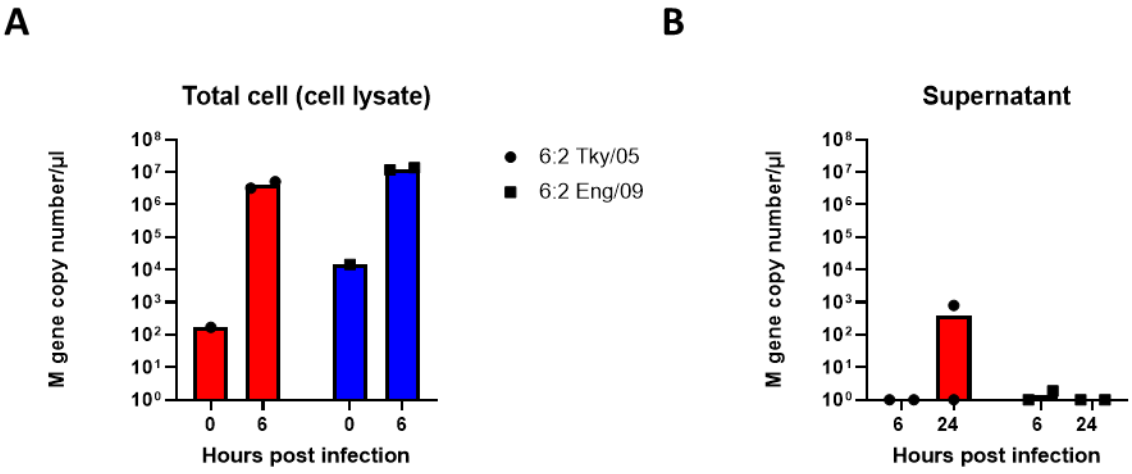

Figure 3.8. Replication of 6:2 Tky/05 and 6:2 Eng/09 viruses in hMDMs. hMDMs were infected with 6:2 Eng/09 and 6:2 Tky/05 at an MOI of 1 and at 0, 6, and 24 h.p.i, total RNA was extracted as well as RNA from the supernatants. RNA from cell lysates and supernatants were DNAse I on-column treated and used in a one-step qRT-PCR using primers and probe for M gene. Quantification of M gene copy number/µl in A) cell lysates B) supernatants. Statistical analysis was not performed due to small sample size (n = 2 biological replicates

apart from 0-hour time point where n = 1). RNA extractions and qPCR analysis were performed by Miss Ziyun Zhang. The data from this figure was used for Supplementary Figure 2 in (Zhang et al., 2022).

Having established that both recombinant influenza viruses were able to replicate their RNA in the hMDMs, we examined whether infection led to the early induction of pro-inflammatory cytokines and type I IFN. Gene expression of the pro-inflammatory cytokines/chemokines IL-6, TNF-α, IL-8 and IP-10 as well as IFN-β were assessed by RT-qPCR at 6 h.p.i (Fig 3.9). Both the 6:2 Tky/05 and 6:2 Eng/09 virus resulted in increased gene expression over that of uninfected (mock) cells for all cytokines analysed although this was minimal for IL-8. All mRNA levels were higher for the 6:2 Eng/09 virus than the levels seen with the 6:2 Tky/05 infection for all genes measured. An IFN-α ELISA on the supernatants of both the 6:2 Tky/05 and 6:2 Eng/09 infected cells were also performed. Only detectable levels (22pg/ml) of IFN-α protein in 1 of the 2 supernatants harvested at 24 h.p.i from the 6:2 Tky/05 infected hMDMs was observed (data not shown, level of detection= 12.5pg/ml).

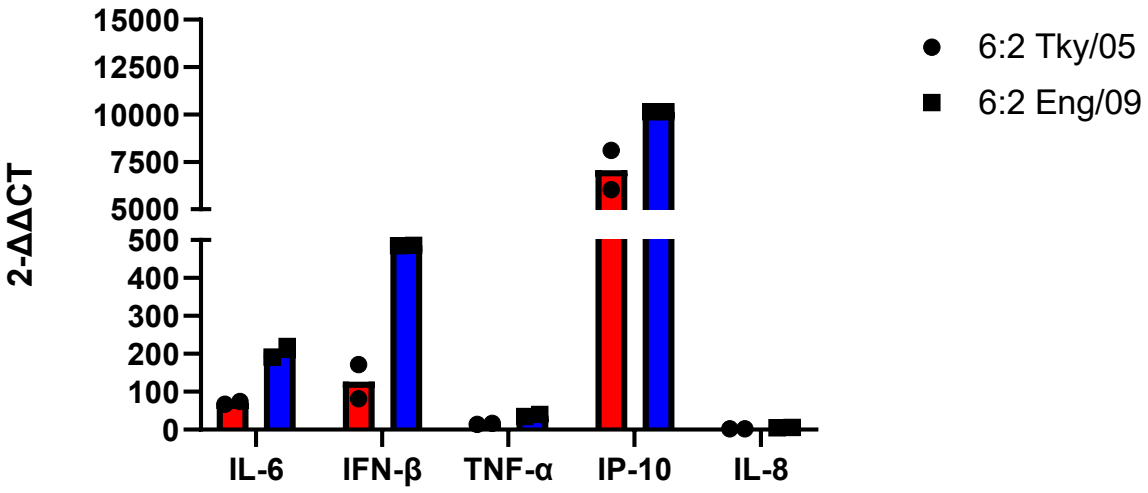

Figure 3.9. Cytokine expression following infection of hMDMs with 6:2 Tky/05 and 6:2 Eng/09 viruses. hMDMs were infected with 6:2 Eng/09 and 6:2 Tky/05 at an MOI of 1 and at 6 h.p.i, total RNA was extracted. RNA was DNAse I on-column treated, and concentration measured by spectrophotometry. Equal amounts of RNA (50 ng) were used to generate cDNA using Quantiscript reverse transcriptase and primer. qRT-PCR performed using Fast SYBR green master mix and primers targeting GAPDH and Il-6, IFN-β, TNF-α, IP-10 and IL-8. Relative expression was calculated by the 2 -ΔΔ CT method normalised to the GAPDH housekeeping gene and shown as fold increase over the mock infected cells. Statistical analysis was not performed due to small sample size

(n = 2 biological replicates). RNA extractions and qPCR analysis were performed by Miss Ziyun Zhang. The data from this figure was used for Figure 1 in (Zhang et al., 2022).

3.3 Discussion

This chapter has demonstrated that both 6:2 Tky/05 and 6:2 Eng/09 viruses can replicate vRNA to a similar extent in macrophages and dendritic cells. We also observe that the 6:2 Tky/05 and 6:2 Eng/09 virus show a similar induction of both IL-6 and TNF-α in the murine BMDMs but that IFN-α secretion was only detected following infection with the 6:2 Tky/05 virus. Infections performed in the hMDMs also demonstrate similar M gene copy numbers for 6:2 Tky/05 and 6:2 Eng/09 with the latter virus inducing higher cytokine gene expression early post infection. Table 3.1 summarises the results obtained in this Chapter for comparative infections using the 6:2 Tky/05 and 6:2 Eng/09 virus.

Figure	Cell Type		6:2 Tky/05	6:2 Eng/09
3.1	A549	NA vRNA	=*	=*
		IFN-β mRNA	=*	=*
3.4	Murine GM-DC	NA vRNA	=†	=†
	Murine BMDM	NA vRNA	=†	=†
3.5	Murine BMDM	NA vRNA	=*†	=*†
3.7	Murine BMDM	IL-6 mRNA	=*	=*
		TNF-α mRNA	=*	=*
		IFN-α protein	>*	<*
3.8	Human MDM	M gene copies	=¶	=¶
3.9		IL-6 mRNA	<¶	>¶
		TNF-α mRNA	<¶	>¶
		IFN-β mRNA	<¶	>¶

Table 3.1. Collective results comparing both vRNA replication and cytokine induction in the cell types infected with 6:2 Tky/05 and 6:2 Eng/09. = represents results were not different between the two viruses, > and < represents a difference, * denotes 24 h.p.i, † denotes 8 h.p.i and ¶ denotes 6 h.p.i.

Our initial observation that the 6:2 Tky/05 and 6:2 Eng/09 virus both replicate their viral RNA to similar levels in lung epithelial cells (Figure 3.1B) is consistent with previous work from our laboratory (Li et al., 2018), as well as with other studies comparing H5N1 strains with seasonal

strains (Chan et al., 2005; Yu et al., 2011). Conversely, the similarity in viral replication between the 6:2 Tky/05 and 6:2 Eng/09 virus in the murine GM-DCs (Figure 3.4A) was a rather surprising outcome as contradicts the findings in Li et al. (2018). However, it should be noted that the primers and house-keeping gene used in this series of experiments differed to those used in Li et al. (2018), and therefore could have impacted on the results obtained. Indeed, house-keeping gene stability is integral for accurate expression levels and previous studies have shown that the choice of house-keeping gene greatly affects the biological conclusions drawn in murine bone marrow cells (Tanaka et al., 2017). Furthermore, there may have been differences in the propagation of the virus stocks used in their studies compared to ours, which may have altered the genome copy: PFU ratio which could potentially affect replication.

In the murine BMDMs we saw a similar pattern to those obtained for the GM-DCs, namely that the 6:2 Tky/05 and 6:2 Eng/09 virus had similar vRNA replication kinetics (Figure 3.5A). These findings suggest that viruses containing the internal genes of a HPAIV virus and those containing internal genes of a more mammalian adaptive virus are equally able to replicate within macrophages and dendritic cells. This agrees with previous studies; levels of M gene copies have been shown to be similar between the HPAIV H5N1 and a seasonal H1N1 strain in human alveolar macrophages (Yu et al., 2011), in human MDMs comparing H5N1 with seasonal H1N1 (Hui et al., 2009) and in murine BMDMs comparing H5N1 strains with a seasonal H1N1 (Chan et al., 2012) at numerous time points.

Abortive replication was observed in the hMDMs infected with both the 6:2 Tky/05 and 6:2 Eng/09 virus (Figure 3.8B). Although many studies suggest that H5N1 can replicate productively in macrophages, this has mainly been attributed to the H5 HA. By creating recombinant seasonal viruses that express the H5 HA, Cline et al. (2013), were able to demonstrate that the HA protein was responsible for efficient productive replication. This is further supported by Westenius et al. (2018), who highlighted the importance of the H5 HA multi-basic cleavage site for productive replication. They showed that efficient cleavage of HA0 into HA1 and HA2 in the absence of trypsin and an increased ability to spread and produce infectious progeny in human macrophages was unique to HPAIV H5N1 viruses. Therefore, it is not entirely surprising that we observe no difference in abortive vs productive replication; both the viruses used in these experiments replicate abortively due to expressing the PR8 HA.

All influenza viruses analysed were able to induce cytokine responses regardless of whether murine or human macrophages were infected (Figures 3.7A, B and Figure 3.9). In the murine BMDMs, there was no noticeable difference in mRNA expression for both IL-6 and TNF-α between the 6:2 Eng/09 and 6:2 Tky/05 virus, but this was vastly increased for those infected with the 7:1 Tky/05 LOW virus (Figure 3.7A-B). There were significant differences for IFN-α secretion; only the viruses with Tky/05 internal genes induced detectable protein levels at 24 h.p.i, with the 7:1 Tky/05 virus inducing significantly higher levels than the 6:2 Tky/05 virus (Figure 3.7C). The higher expression of IL-6, TNF-α and IFN-α by the 7:1 Tky/05 LOW compared to the 6:2 Tky/05 virus is intriguing and warrants further investigation. Although the NA segments differ and could potentially be responsible for this difference in cytokine induction, the current literature does not support this. Mok et al. (2009) demonstrated that the HA, NA and PB1 genes from a HPAIV H5N1 upon a WSN or PR8 background were inefficient at restoring a high cytokine induction phenotype in hMDMs. Similarly, previous work in our laboratory showed that the Tky05 HA and NA on a PR8 background did not induce high IFN-α in GM-DCs (Li et al., 2018). An alternative explanation is that the 6:2 Tky/05 and 7:1 Tky/05 LOW differ in amounts of an RNA replication product generated, increasing the amount of PAMP to trigger pro-inflammatory cytokine and IFN-α production. We saw a strong band for a PCR product that was between 450-500nt derived from the PB1 segment that was most likely a DVG in the 7:1 Tky/05 LOW infected BMDMs (Figure 3.6). Therefore, the quality of the viral stock (including levels of immunostimulatory DVGs) could potentially affect the magnitude of the cytokine response. This will be explored further in Chapters 4 and 5.

We showed higher IFN-α protein secretion in the 6:2 Tky/05 infected BMDMs over those infected with the 6:2 Eng/09 virus (Figure 3.7C). Whilst this was observed previously by Li et al. (2018), this was attributed to higher replication by the 6:2 Tky/05 virus, we cannot draw the same conclusion. Interestingly, Sakabe et al. (2013), also showed no significant difference in viral replication in hMDMs between high and low cytokine inducing H5N1 viruses but rather mapped the high cytokine phenotype to the PA gene. Whilst the underlying mechanism for how the PA subunit orchestrates higher cytokine production is unknown, PA has been shown previously to directly interact with components of innate immune signalling by binding to IRF3 and inhibiting IFN-β transcription. However, IRF3 binding was attributed to amino acid position 108; both H1N1pdm09 and H5N1 strains have an aspartic acid at this position, and

both were able to inhibit IFN-β expression to similar levels (Yi et al., 2017). Many of the internal segments of IAV are known to encode proteins that can interact with IFN signalling such as PA-X, PB1-F2 and NS1 (Elshina & Te Velthuis, 2021; Nogales et al., 2018) and some studies show strain specific differences in how such proteins can modulate innate immune responses (Conenello et al., 2007; Dankar et al., 2011; McAuley et al., 2010). Li et al. (2018) tried to explore which polymerase segment was responsible for high IFN-α secretion in GM-DCs by creating a panel of recombinant viruses with polymerase genes swapped between Tky/05 and Eng/09 but could not attribute this phenotype to a particular segment. Similarly, a recombinant Eng/09 virus that contained the Tky/05 NS segment did not lead to high IFN-α production (Li et al., 2018). Therefore, the mechanism for how the internal genes of the Tky/05 virus confer higher IFN-α expression still needs to be elucidated but our results in BMDMs indicate it is not due to enhanced viral replication. It would be interesting to introduce more mammalian adapted substitutions into the Tky/05 polymerase segments and see how these may alter IFN-α production in the BMDMs; this will be explored briefly in Chapter 6.

In the hMDMs, 6:2 Eng/09 infections resulted in greater pro-inflammatory cytokine mRNA expression (Figure 3.9). This is in direct contrast to numerous studies where they show that the H5N1 virus elicits a greater inflammatory response in hMDMs (Hui et al., 2009; Lee et al., 2009a; Woo et al., 2010). However, in agreement with our findings, Sakabe et al. (2011), showed that not all H5N1 strains induced higher cytokines than a seasonal H1N1. Similarly, Friesenhagen et al. (2012), demonstrated higher levels of IFN-β and TNF-α mRNA at both 5 and 24 h.p.i for PR8 H1N1 infected hMDMs compared to HPAIV H5N1 infected hMDMs. Further experiments established a lack of M2 protein expression in the H5N1 infected hMDMs resulting in an inability to activate the NRLP3 inflammasome and subsequent IL-1β processing (Friesenhagen et al., 2012). Unfortunately, we did not assess IL-1β protein levels so therefore cannot establish whether inflammasome activation is likewise impaired by the 6:2 Tky/05 virus. However, the amount of viral RNA recovered from the cell lysate at 0 hours was 2 logs higher from the 6:2 Eng/09 infection compared to the 6:2 Tky/05 infected cells (Figure 3.8), suggesting that unintentionally a higher MOI of the 6:2 Eng/09 inoculum was used, which could have induced higher cytokine expression.

The difference in cytokine expression for both viruses between the murine BMDMs and hMDMs is intriguing as both are model systems used to investigate macrophage responses to IAV infection. However, it is difficult to justify making a direct comparison. Differences between the culture conditions used, tissue origin, species of host and state of activation and/or polarity have all been shown to affect experimental outcome. For example, cytokine responses were markedly different between human macrophages derived from monocytes in the blood and those isolated from the BAL fluid following H5N1 infection (van Riel et al., 2011). Likewise, murine dendritic cells were shown to be less permissive to infection with IAV than human dendritic cells (Hartmann et al., 2013), and even the source of M-CSF used for differentiation of BMDMs can alter the cytokine response to stimuli (Heap et al., 2021).

We also used different viral doses and analysed different time points for cytokine mRNA expression for the murine BMDM and hMDM infections. An MOI of 1 was used for infections in the hMDMs due to comparing cytokine responses between influenza and SARS CoV-2; the latter virus stock had a low viral titre, prohibiting using an MOI of 10 (Zhang et al., 2022). Similarly, we would have analysed the 24- hour time point for the hMDM infections but unfortunately the RNA yield was too low for qRT-PCR analysis. We did observe strong CPE in the infected hMDMs at 24 h.p.i, and this high cell death could have attributed to the loss of cellular RNA. Indeed, Osterlund et al. (2010), cited this reason for omitting qRT-PCR data in their study analysing immune responses in human dendritic cells. Previous work has shown that cytokine expression is dependent on the time point analysed as cytokine kinetics can differ between strains (Westenius et al., 2014). One major limitation with the hMDM infection is that all cells were derived from one donor. For a more comprehensive analysis, experiments would ideally be performed in multiple donors as there can be considerable variation in responsiveness between donors (Stoddart et al., 2012).

Whether pro-inflammatory cytokines require active viral replication for their induction was not directly addressed in this study. However past studies have attempted to answer this question by treating viruses to render them replication-incompetent prior to infection. Most studies demonstrate a clear requirement for viral replication; β-propiolactone (BPL) inactivated H5N1 did not induce higher levels of cytokines over mock infected hMDMs in direct contrast to untreated H5N1 (Sakabe et al., 2011). Additionally, a panel of UV-inactivated viruses did not result in IFN-α production in murine GM-DCs (Li et al., 2018).

Interestingly, some studies indicate that viral replication is not needed to produce all cytokines. Sandbulte et al. (2008), demonstrated that BPL inactivated H5N1 virus resulted in human pDCs unable to secrete IFN-α but had no effect on TNF-α or IP-10 secretion. Similarly, UV-inactivated PR8 virus showed no detectable levels of TNF-α or IFN-α but still produced IP-10 in human alveolar macrophages (Wang et al., 2012). This indicates that distinct virus-cell interactions occur resulting in cytokine expression within the same cell. Indeed, viral activation of innate immune cells is believed to be initiated through TLR, RLR, CLR and NLRs, some of which do not require a functional viral genome (Malmgaard et al., 2004; Marongiu et al., 2021). This could perhaps explain why the 6:2 Tky/05 virus resulted in greater IFN-α secretion in the BMDMs than the 6:2 Eng/09 but did not lead to an increase in IL-6 or TNF-α mRNA (Figure 3.6). The role of specific PRRs could be elucidated through utilising cells that have a PRR (or adaptor molecule in signalling pathway) knocked out and observing which (if any) cytokines are reduced. This approach was used by Li et al; they demonstrated that GM-DCs derived from *Mavs*$^{-/-}$ mice did not result in IFN-α expression, suggesting that RIG-I was the PRR responsible for triggering this response (Li et al., 2018). There is also the added complexity that some chemokines (such as IP-10) are ISGs and therefore could be primarily produced by uninfected cells through paracrine signalling (Tokunaga et al., 2018). In this study, we analysed bulk cellular RNA so therefore cannot distinguish between the contribution of directly infected and uninfected cells; scRNA sequencing would perhaps be better suited to address this.

Overall, these findings clearly demonstrate that IAV generates vRNA within murine BMDMs, GM-DCs and hMDMs inducing a pro-inflammatory cytokine response. However, further work is still needed to fully explore differences in the host innate immune response following infections with HPAIV and more mammalian adapted IAV strains within these immune cells. Understanding the exact contribution of macrophages and dendritic cells to the HPAIV cytokine storm in mammalian infections and elucidating the molecular mechanisms driving this are fundamental in guiding therapeutic options in the event of an outbreak.

Chapter 4 Elucidating the role of DVGs in modulating innate immune responses in vitro

4.1 Introduction

An interesting observation from Chapter 3 was that a virus stock containing higher levels of DVGs (7:1 Tky/05 LOW) resulted in increased pro-inflammatory cytokine induction and type I IFN response following infection in murine BMDMs. This is not entirely unsurprising as DVGs have been associated with immune activation in numerous viral infections (Genoyer & Lopez, 2019; Killip et al., 2013; Tapia et al., 2013). For many paramyxoviruses which primarily generate copyback DVGs, the interferon cascade is only initiated once these have accumulated to sufficient levels (Killip et al., 2013; Sun et al., 2015). Indeed, the PRR RIG-I has shown to only bind to copyback DVGs and not the full genome of Sendai virus (Baum & Garcia-Sastre, 2011). In the case of IAV, the higher immune activation has been mainly attributed to the preference for RIG-I to bind to shorter IAV segments and DVGs presumably due to their reduced length compared to WT (Baum et al., 2010; Rehwinkel et al., 2010). Numerous studies have demonstrated that IAV stocks abundant in DVGs initiate a strong type I IFN response, more so than stocks that contain low or minimal levels of DVGs (Liu et al., 2019; Xue et al., 2016). As type I IFN production results in signalling events that also lead to the production of pro-inflammatory cytokines, these are often elevated once DVGs have been detected (Tapia et al., 2013).

As DVGs are preferentially replicated due to their shorter size they can accumulate to high levels within cells (Laske et al., 2016; Mendes & Russell, 2021). Here they compete for viral polymerase and NP for encapsidation of the genome. Due to IAV DVGs maintaining packaging signals, it was commonly accepted that they were also preferentially packaged into virions (Duhaut & McCauley, 1996), but this has recently been disputed (Alnaji et al., 2021). It is however apparent that DVG generation can interfere with standard viral replication, reducing infectious particle production, resulting in decreased viral titres *in vitro* (Frensing et al., 2013; Kupke et al., 2020). This property of DVGs coupled with promoting IFN induction can therefore impact viral kinetics and infection outcome.

RIG-I is not the only PRR that has been demonstrated to bind to DVGs; ZBP1 has also been implicated (Thapa et al., 2016; Zhang et al., 2020). Upon nucleic acid binding, ZBP1 induces

various cell death pathways as well as inflammasome activation and production of pro-inflammatory cytokines (Mo & Han, 2021). Engagement of ZBP1 with the NLRP3 inflammasome has been shown to induce pyroptosis in IAV infected macrophages (Kuriakose et al., 2016). A study by Wang et al. (2019), demonstrated necroptosis occurring in both lung epithelial and infiltrating immune cells following IAV infection in mice. Zhang et al. (2020), also demonstrated a role for ZBP1-mediated necroptosis in IAV infection. They showed that necroptosis was caused by ZBP1 binding to Z-RNAs which were produced by replicating IAV. Interestingly, they observed increased cell death in MEF cells infected with a high DVG stock of PR8 when compared to a PR8 stock containing lower levels of DVGs. Necroptosis as an inflammatory form of cell death has been implicated in the pathogenesis of ARDS (Faust & Mangalmurti, 2020). As severe IAV infections often culminate in ARDS, understanding the role that DVGs have in the activation of ZBP1 would be insightful.

The aim of this chapter is to contribute to understanding how IAV DVGs modulate the innate immune response *in vitro*. We will compare stocks of IAV containing the H5N1 internal genes that differ in their abundance of non-infectious particles and subsequently characterise the polymerase DVGs present. Infections were performed in various cell types, DVG accumulation tracked and type I IFN and pro-inflammatory cytokine induction quantified. DVGs identified will be cloned and used in vRNP reconstitution assays to directly measure immunostimulatory properties. We will also measure ZBP1 mediated cell death and determine whether this varies by genome copy number/ml to PFU/ml ratio.

4.2 Results

4.2.1 The 7:1 Tky/05 stock contains high levels of non-infectious particles

To investigate the DVG content of our virus stocks, we firstly performed plaque assays to measure the number of infectious particles. This was followed by a RT-qPCR to measure M gene copy numbers used to quantify the number of total particles. The ratio of M gene copy numbers/ml to PFU/ml was calculated (Figure 4.1). The 6:2 Tky/05 and the 6:2 Eng/09 virus displayed very similar ratios (6:2 Tky/05 = 28:1, 6:2 Eng/09 = 22:1) whereas the ratio for the 7:1 Tky/05 virus was much higher (813:1), indicating that there were more non-infectious particles present in this virus stock.

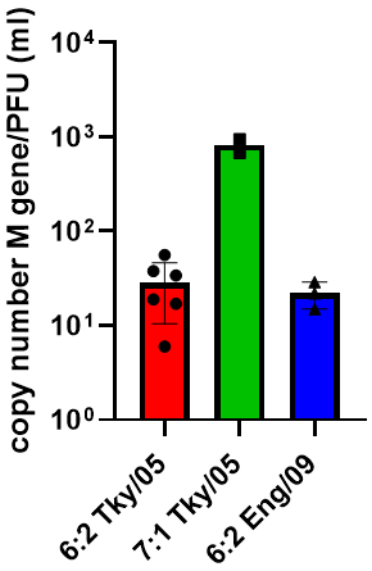

Figure 4.1. Copy number: PFU ratio for virus stocks. Mean PFU/ml was determined for each virus stock (n =3) and this used to calculate the ratio. RNA was extracted from viral stocks and a one-step RT-qPCR performed using primers and probe for M gene in order to calculate M gene copy number/ml. Data points show ratio calculated using RNA obtained from at least two independent extractions.

4.2.2 DVGs present in the virus stocks accumulate over the course of infection in A549 cells

As DVGs are known to be replicated alongside the full length viral genome (Vignuzzi & Lopez, 2019), we wished to track their amplification during an infection in a human lung epithelial cell line. A549 cells were infected at an MOI of 1 with the 6:2 Tky/05, 7:1 Tky/05 or 6:2 Eng/09 virus stocks or mock infected and total RNA was harvested at 2, 6 and 24 hours. As previously described in Chapter 3, cDNA synthesis was performed using the Uni12 primer and PCR using primers that bind to the 3' and 5' termini of the polymerase segments (Hoffman primers). We also performed an additonal PCR using primers that bind to an internal region of the polymerase segments. These internal primers should only amplify full genome due to their target being absent in DVGs as they contain a large central deletion. All viruses showed successful amplification of all polymerase segments (Figure 4.2, full genome panels). All the infections resulted in 300-800nt long PCR products detected using the terminal primers that accumulated over time indicating these were DVGs (Figure 4.2, DVG panels). However there were also faint bands present in the mock infected cells using the PB1 and PB2 Hoffman primers suggesting that there may have been some non specific products being generated

(blue boxes). Interestingly, DVGs were either absent or faint at 2 h.p.i for the 6:2 Tky/05 and 6:2 Eng/09 infections, but were strongly detected at 2 h.p.i following infection with the 7:1 Tky/05 virus.

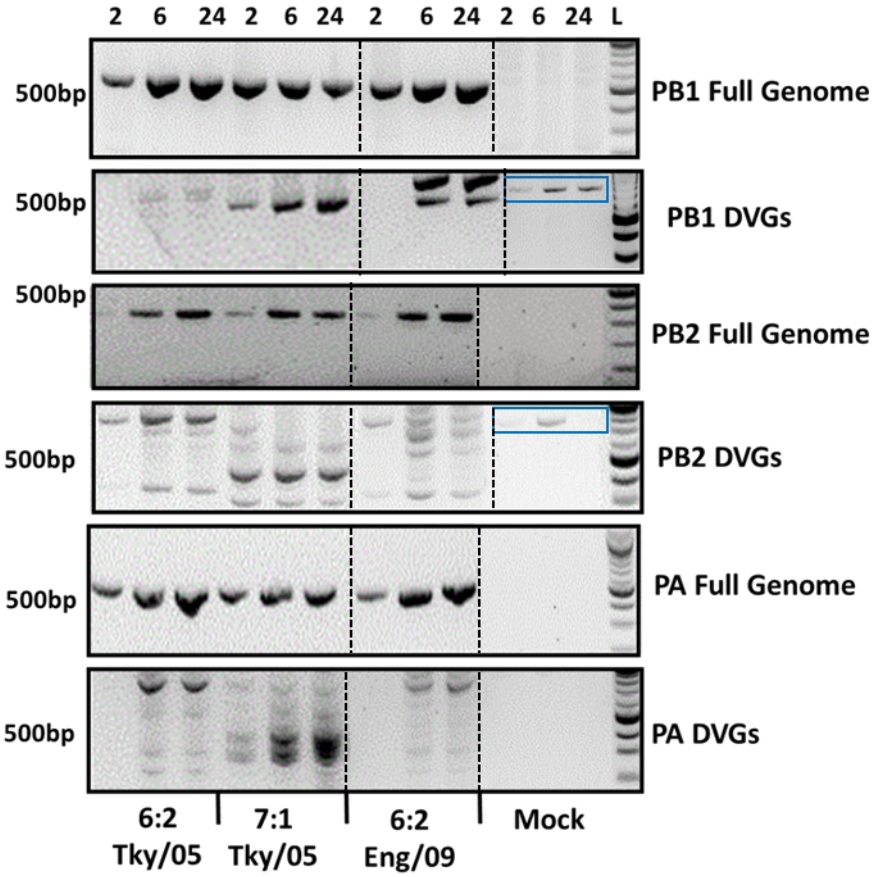

Figure 4.2. Influenza polymerase DVG accumulation in A549 cells. A549 cells were infected using 6:2 Tky/05, 7:1 Tky/05 and 6:2 Eng/09 virus at an MOI of 1 or mock infected. At 2, 6 and 24 h.p.i., total RNA was extracted, DNAse I on-column treated, and concentration measured by spectrophotometry. 200ng of RNA was used for cDNA synthesis with Superscript IV RT and Uni12 primer that targets the 3' end of vRNA. PCR was performed using KOD polymerase and either Hoffman primers targeting the conserved 3' and 5' termini of vRNA for detection of full genome and DVGs, or an internal primer set for detection of full genome only. PCR products were ran on a 1.5% agarose gel with GelRed. (n =2). Gels show one representative well at each time point. Lanes on gels were rearranged for conformity and boundaries are indicated with dotted lines.

4.2.3 The 7:1 Tky/05 virus stock induces high type I IFN early post infection

To test whether the 7:1 Tky/05 virus would be able to induce higher levels of type I IFN early post infection, we conducted RT-qPCR on the RNA extracted from the A549 cells infected previously and assessed IFN-β mRNA levels at the 2 h.p.i time point (Figure 4.3). The 6:2

Tky/05 and 6:2 Eng/09 only induced marginal IFN-β mRNA, whereas this was greatly increased following infection with the 7:1 Tky/05 virus.

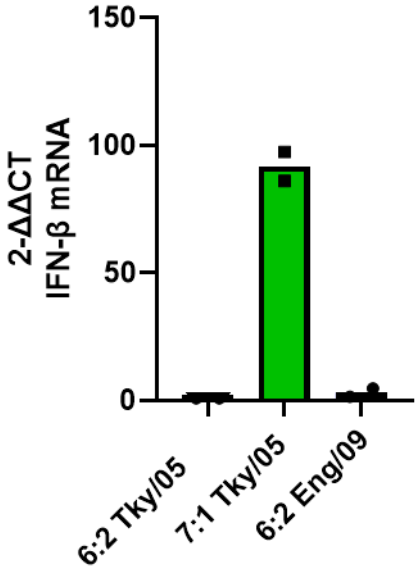

Figure 4.3. The 7:1 Tky/05 virus stock induces high IFN-β gene expression in A549 cells early post infection. A549 cells were infected as in Figure 4.2. RNA was extracted at 2 h.p.i , DNAse I on-column treated, and concentration measured by spectrophotometry. Equal amounts of RNA (200 ng) were used to generate cDNA using RevertAid reverse transcriptase and primer for Oligo(dT). qRT-PCR was performed using Fast SYBR green master mix and primers targeting GAPDH and IFN-β. Relative expression was calculated by the 2 -ΔΔ CT method normalised to the GAPDH housekeeping gene and shown as fold increase over the mock infected cells. qRT-PCR was performed using primers for IFN-β. Data represents mean from 2 technical replicates for each biological replicate. Statistics were not performed due to small sample size.

4.2.4 Virus stocks grown at different MOIs contain different amounts of infectious viral particles

In order to explore the relationship between the level of DVGs and IFN induction further, additional stocks of the 7:1 Ty/05 virus were propagated at different MOIs in order to vary the levels of DVGs present. The 7:1 Tky/05 virus was passaged at a low MOI (0.0001) or a higher MOI of 0.01 to generate the virus stocks 7:1 Tky/05 LOW and 7:1 Tky/05 HIGH (Figure 4.4). We hypothesised that the virus stock grown at the low MOI (7:1 Tky/05 LOW) would show a reduction in the amont of DVGs and non-infectious particles present compared to the 7:1 Tky/05 stock, whereas the 7:1 Tky/05 HIGH would contain more DVGs and non-infectious particles.

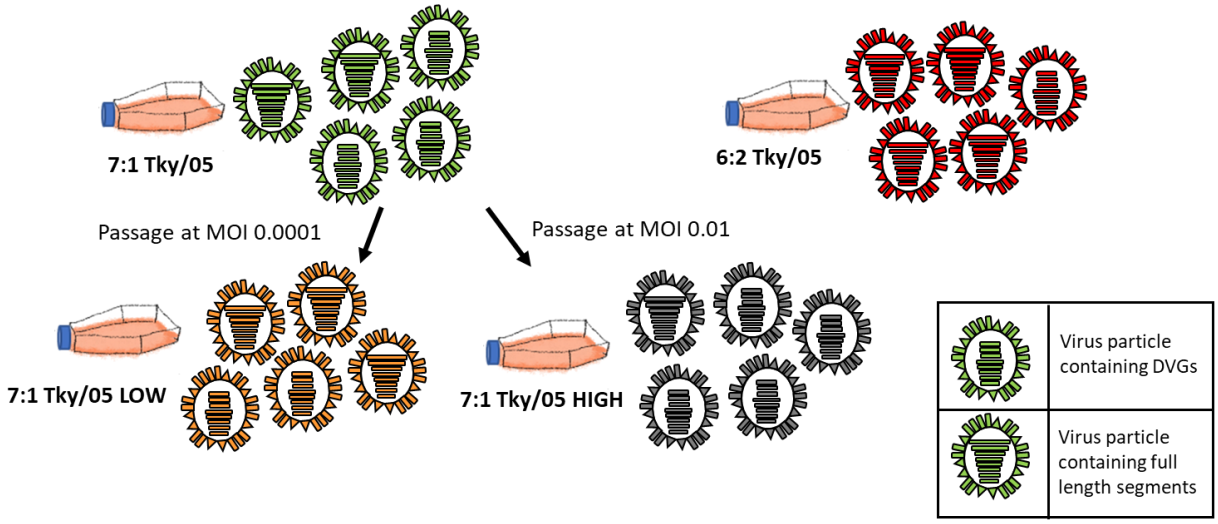

Figure 4.4. Schematic of generation of virus stocks and theoretical particle content. This figure forms part of Figure 1 in (Penn et al., 2022).

We then calculated the M gene copy number/ml to PFU/ml ratio as previously described for the 7:1 Tky/05 LOW and 7:1 Tky/05 HIGH virus stocks (Figure 4.5). The 7:1 Tky/05 HIGH stock had a significantly elevated ratio (18,781:1) when compared to the predessesor virus (7:1 Tky/05), whereas the 7:1 Tky/05 LOW was much lower (40:1) and was more similar to the ratio obtained for the 6:2 Tky/05 virus which was grown at the same MOI. As an alternative means to measure the total number of particles, we also performed an HA assay on all the virus stocks and used this to calculate the infectivity to total titre (I/T) as described in (Xue et al., 2016). We found that the I/T ratios were reduced for the 7:1 Tky/05 HIGH (150) and 7:1 Tky/05 virus (977) when compared to the 7:1 Tky/05 LOW (20,019) and the 6:2 Tky/05 virus (41,016). Overall, these findings strongly indicate that the 7:1 Tky/05 and 7:1 Tky/05 HIGH viruses have high numbers of non-infectious particles.

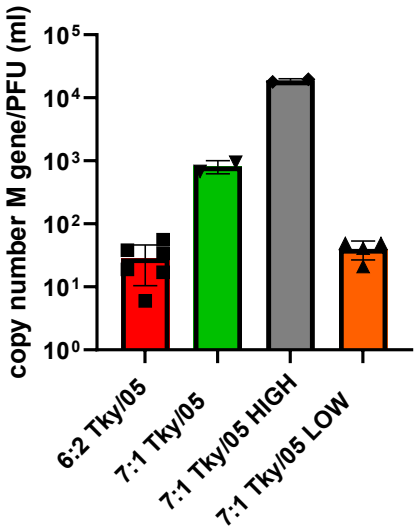

Figure 4.5. Stocks grown at different MOIs contain different amounts of non-infectious particles. Copy number M gene/ml to PFU/ml ratio. Mean PFU/ml was determined for each virus stock (n =3) and this used to calculate the ratio. RNA was extracted from viral stocks and a one-step RT-qPCR performed using primers and probe for M gene in order to calculate M gene copy number/ml. Data points show ratio calculated using RNA obtained from at least two independent extractions. (Data for 6:2 Tky/05 and 7:1 Tky/05 is same as in Figure 4.1).

Virus stock	Infectivity titre (I): PFU/25µl	Total titre (T): HA/25µl	I/T	M gene copy number/ PFU
6:2 Tky/05	5250000	128	41016	28
7:1 Tky/05	500000	512	977	813
7:1 Tky/05 HIGH	77000	512	150	18,781
7:1 Tky/05 LOW	5125000	256	20019	40

Table 4.1. Infectivity to total (I/T) particle ratios in virus stocks. (n = 3). M gene copy number/PFU from Figure 4.5 is also shown. Data in this figure forms part of Figure 1 in (Penn et al., 2022).

4.2.5 Characterisation of polymerase DVGs in the viral stocks

To correlate the high amount of non-infectious particles with a high abundance of DVGs, we characterised the DVGs generated from the polymerase segments for our virus stocks. We performed a RT-PCR using terminal primers and visualised PCR products on an agarose gel, using RNA extracted from the virus supernatants (Figure 4.6). As the Hoffman primers used for amplifying the terminal regions generated non-specific bands previously (Figure 4.2), we

designed Tky/05 specific terminal primers to increase specificity which were successful as they did not result in non-specific bands in mock infected samples in a subsequent experiment (Figure 4.9). We observed small products (approx 350-800nt) derived from the three polymerase segments for all the virus stocks. However, the bands for the 7:1 Tky/05, 7:1 Tky/05 HIGH and also the 7:1 Tky/05 LOW stocks were strongest. In comparison there were fewer and weaker small bands seen for the 6:2 Tky/05 virus stock. There was also poor amplification of the full-length segments for the 7:1 Tky/05 and 7:1 Tky/05 HIGH stocks, indicative of a high DVG content.

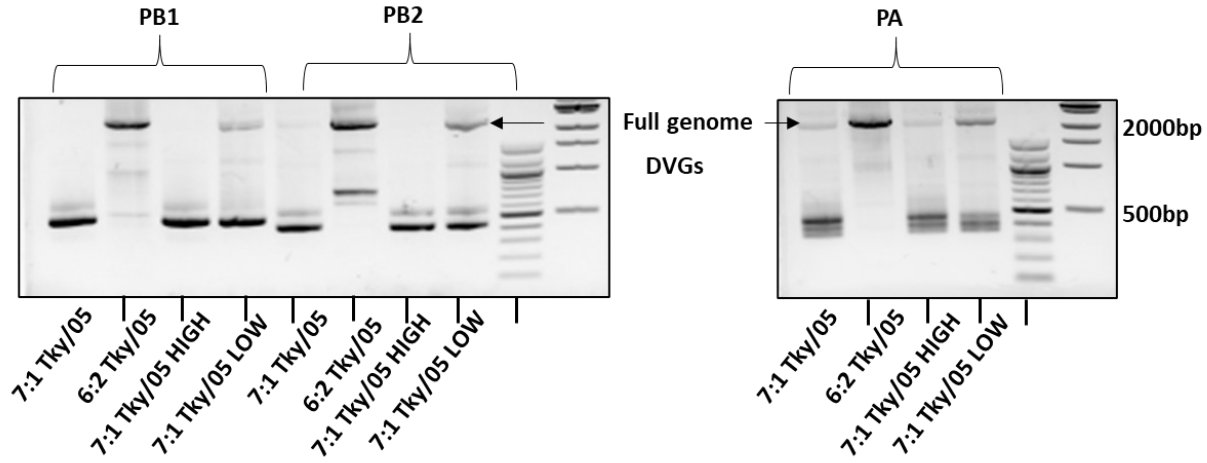

Figure 4.6. Polymerase DVGs present in the virus stocks. RNA was extracted from the virus supernatants and equal volumes of RNA was used for cDNA synthesis with Superscript IV RT and Uni12 primer that targets the 3' end of vRNA. PCR was performed using KOD polymerase and Tky/05 specific terminal primers for both full genome and DVGs for the PB1, PB2 and PA segment. PCR products were ran on a 1.5% agarose gel with GelRed. Arrows indicate the size of the full genome, whereas any bands below this indicate potential DVGs. This figure forms part of Figure 2 in (Penn et al., 2022).

To confirm that these smaller bands amplified by RT-PCR were genuine DVGs, we extracted all the small products amplified from the 6:2 Tky/05 and 7:1 Tky/05 LOW stock. We next cloned these into the TOPO vector, followed by Sanger sequencing to determine their genetic composition. Most of the small bands we could define as DVGs due to retaining both the 3' and 5' ends but containing a large internal deletion with unique junctions (Figure 4.7A and 4.7B). As all of the DVGs arising from the 7:1 Tky/05 LOW stock were identical in size to those

from the 7:1 Tky/05 and 7:1 Tky/05 HIGH stock (Figure 4.6), we assumed that all of these virus populations would contain identical DVGs as all originated from the same stock (7:1 Tky/05). To confirm this, we additionally cloned and sequenced 1 DVG derived from each polymerase segment from the 7:1 Tky/05 and 7:1 Tky/05 HIGH stock. All of these were indeed identical in sequence to the same size DVG isolated from the 7:1 Tky/05 LOW virus. All DVGs cloned and sequenced from the independently rescued 6:2 Tky/05 virus were genetically distinct. Analysis of the sequences flanking the junction sites tended to show the presence of direct short repeats, although this was not universally observed (Figure 4.7B). For example, the 6:2 Tky/05 PA DVG has AAAA in the deleted part of the sequence immediately after the junction which is repeated in the DVG sequence on the other side of the junction. Unfortunately, if a DVG contains these direct repeats, it does make it impossible to precisely determine the true breakpoint. However, it should be emphasised that the exact sequence of the DVG remains unchanged. For consistency, we mapped the breakpoint start positions to the nucleotide preceding the direct repeat on the 5' side of the deletion.

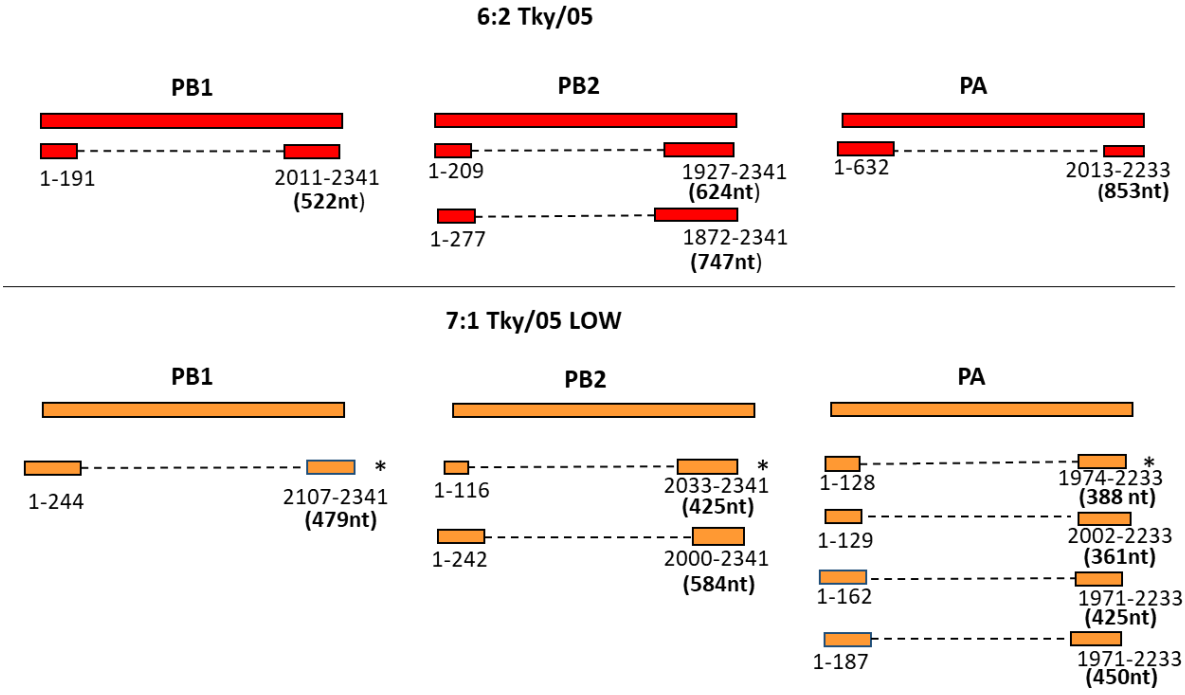

Figure 4.7 Genetic characterisation of polymerase DVGs from viral stocks. All PCR bands not corresponding to the full length genome (presumed to be DVGs) from the 6:2 Tky/05 and 7:1 Tky/05 LOW stock were gel extracted, cloned into TOPO vectors and Sanger sequenced. Sequences were mapped to the full-length segments using Geneious and junctions calculated. Coloured rectangles represent the 5' and 3' ends of the

DVGs and dotted connecting lines represent the large internal deletion. The junction positions are shown and all are depicted in the positive sense. One PCR product from each polymerase segment (PB1 =band size of 479nt, PB2 = band size of 425nt and PA = band size 388nt) were also cloned and sequenced from the 7:1 Tky/05 and 7:1 Tky/05 HIGH virus stocks and were identical in sequence to those present in the 7:1 Tky/05 LOW stock (marked as asterisks). This figure forms part of Figure 2 in (Penn et al., 2022).

Virus	Segment	Deletion junction	Junction sites	Length of DVG (nts)
6:2 Tky/05	PB1	191/2011	TGGAC/aaaa aact/ACGCA	522
6:2 Tky/05	PB2	209/1927	GACAA/gaga gttt/TCTTC	624
6:2 Tky/05	PB2	277/1872	TGATG/ctgg agat/AATAAA	747
6:2 Tky/05	PA	632/2013	GAAGA/aaaa caag/AAAAT	853
7:1 Tky/05	PB1	244/2107	ACTAC/gtca caat/CTATT	479
7:1 Tky/05	PB2	116/2033	GCCAT/aatc cttg/GAAAG	425
7:1 Tky/05	PB2	242/2000	AATGA/acaa aact/ACAA	584
7:1 Tky/05	PA	128/1974	AAATT/tgct tata/TGCA	388
7:1 Tky/05	PA	129/2002	AATTT/gctg ttca/GCTGA	361
7:1 Tky/05	PA	162/1971	GTTTC/agtg gctt/ATATG	425
7:1 Tky/05	PA	187/1971	TATTG/atga gctt/ATATG	450

Table 4.2. Table of DVGs showing detailed information on junction sites. Uppercase text represents sequence of the junction sites whereas lowercase text corresponds to the sequence which is deleted adjacent to the junction site and is therefore absent in the DVG. Underlined text indicates junction sites where the deleted nucleotides are identical to those located on the opposite side of the junction.

4.2.6 The 7:1 Tky/05 HIGH virus replicates poorly in both MDCK and A549 cells

We next investigated how the growth kinetics of the viruses were affected by their DVG content. We performed viral infections in both MDCK and A549 cells using the 6:2 Tky/05, 7:1 Tky/05 HIGH and 7:1 Tky/05 LOW. At 12, 24, 48 and 72 h.p.i supernatants were harvested and the amount of virus released was quantified by plaque assay (Figure 4.8). All viruses replicated faster and to higher titres in MDCK cells. In both cell lines, the 6:2 Tky/05 and 7:1 Tky/05 LOW virus showed similar replication kinetics and were not statistically different from each other. In contrast, the 7:1 Tky/05 HIGH replicated to lower titres over the course of the infection in both MDCK and A549 cells.

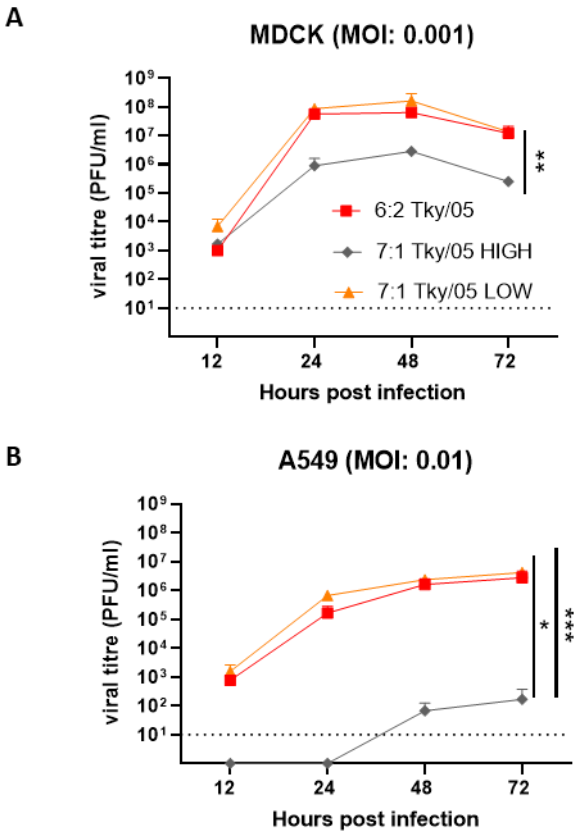

Figure 4.8. Growth kinetics in MDCK and A549 cells. A) MDCK and B) A549 cells were infected with the indicated MOI of 7:1 Tky/05, 7:1 Tky/05 HIGH and 7:1 Tky/05 LOW virus. At the indicated time points, the virus supernatant was harvested and plaque assays performed to quantify the amount of released infectious viral particles. Data shown as mean ± SD (n=3). Area under the curve (AUC) was calculated for each virus and differences were analysed by one-way ANOVA with Bonferroni's post hoc test for multiple comparisons. * P<0.05, ** P<0.01, *** P<0.001. Dotted line represents limit of detection. This figure forms part of Figure 3 in (Penn et al., 2022).

4.2.7 Intracellular DVGs accumulate early post infection and trigger type I IFN in A549 cells

Similar to earlier in this chapter, we infected A549 cells with an MOI of 1 of the 6:2 Tky/05, 7:1 Tky/05 HIGH and 7:1 Tky/05 LOW viruses and tracked the amplification of intracellular DVGs over time (Figure 4.9). By RT-PCR analysis, DVGs with band sizes correlating with those present in the original viral stocks were detected (Figure 4.6). Following infection with the 7:1 Tky/05 HIGH virus, there were strong bands for DVGs at 2 h.p.i, which were either largely absent or markedly reduced folowing infection with the 6:2 Tky/05 and 7:1 Tky/05 LOW virus. By 6 and 24 h.p.i, both the 6:2 Tky/05 and 7:1 Tky/05 LOW virus had accumulated high levels

of DVGs suggesting these were amplified over the 24 hour time course; this was particularly noticeable for the PB2 segment where we also observed less signal for the full genome.

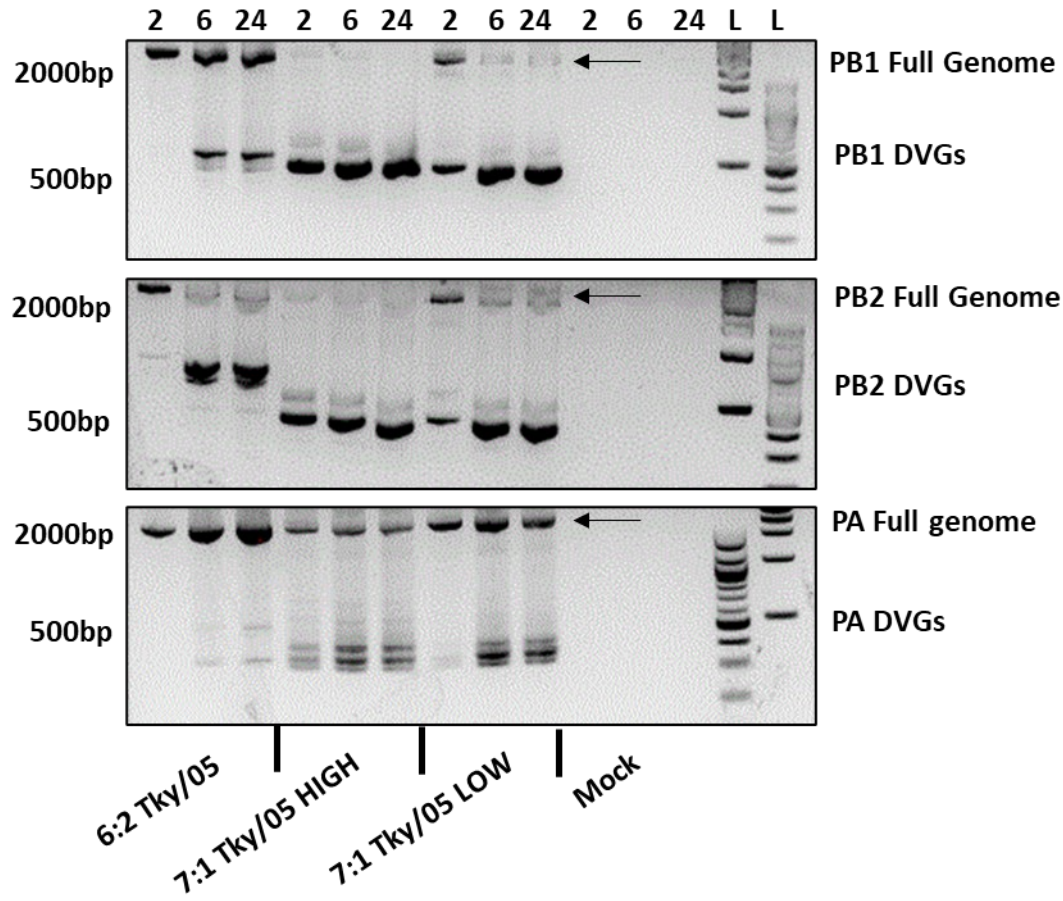

Figure 4.9 Influenza polymerase DVG accumulation in A549 cells from viruses differing in non-infectious particle content. A549 cells were infected using 6:2 Tky/05, 7:1 Tky/05 HIGH and 7:1 Tky/05 LOW virus at an MOI of 1 or mock infected. At 2, 6 and 24 h.p.i., total RNA was extracted, DNAse I on-column treated, and concentration measured by spectrophotometry. 500ng of RNA was used for cDNA synthesis with Superscript IV RT and Uni12 primer that targets the 3' end of vRNA. PCR was performed using KOD polymerase and Tky/05 terminal primers for detection of full genome and DVGs. PCR products were ran on a 1.5% agarose gel with GelRed. (n =3). Gels show one representative well. Arrows indicate the size of the full genome. This figure forms part of Figure 3 in (Penn et al., 2022).

Based on our previous findings that the 7:1 Tky/05 virus induced high IFN-β expression early post infection, we assessed whether this was also the case for the 7:1 Tky/05 HIGH virus by determing the IFN-β mRNA expression by qRT-PCR using total RNA from the same experiment. In addition, we quantified secreted IFN-β protein in the supernatants by ELISA.

At both 2 and 6 h.p.i., the IFN-β mRNA levels were highest for the 7:1 Tky05/HIGH virus (Figure 4.10A). Additionally, IFN-β protein was only detected in the supernatants harvested from cells infected with the 7:1 Tky/05 HIGH virus at 24 h.p.i., all other time points were below the limit of detection of 7.9pg/ml (Figure 4.10B).

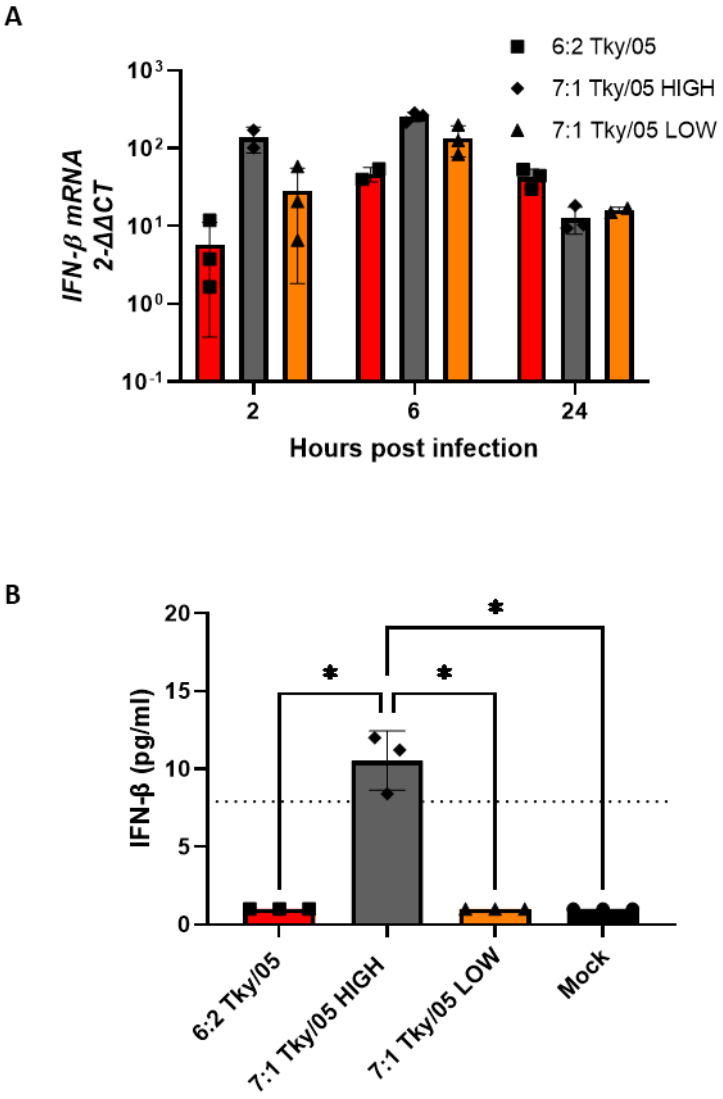

Figure 4.10. Differing IFN-β expression in A549 cells. A) RNA from A549 cells infected in Figure 4.9 was extracted at 2, 6 and 24 h.p.i ,DNAse I on-column treated, and concentration measured by spectrophotometry. Equal amounts of RNA (500 ng) were used to generate cDNA using RevertAid reverse transcriptase and primer for Oligo(dT). qRT-PCR performed using Fast SYBR green master mix and primers targeting GAPDH and IFN-β. Relative expression was calculated by the 2 -ΔΔ CT method normalised to the GAPDH housekeeping gene and shown as fold increase over the mock infected cells. (n =2/3 due to some data points missing). Statistical analysis was not perfomed due to low sample number due to missing data points. B) IFN-β levels in cell supernatants harvested at 24 h.p.i determined by ELISA. Bar represents mean (n = 3). Variance among groups

was calculated by a Kruskal-Wallis test with Dunn test for multiple comparisons. * P<0.05. Dotted line represents limit of detection. This figure forms part of Figure 3 in (Penn et al., 2022).

As another means of assessing induction of IFN-β, we performed infections in the A549 IFN-β luc reporter cell line which contain a stable copy of the firefly luciferase gene driven by the IFN-β promoter. We infected the A549 IFN-β luc cells at an MOI of 1 and at 2, 6 and 24 h.p.i, measured the luciferase signal (Figure 4.11). At 2 h.p.i., only the 7:1 Tky/05 HIGH stock induced a detectable increase of IFN-β promoter activity over mock. Indeed, the 7:1 Tky/05 HIGH virus induced the highest levels of IFN-β promoter activity at all time points analysed. By 24 h.p.i., the 7:1 Tky/05 LOW also showed statistically significantly higer levels than the 6:2 Tky/05 virus. Overall these findings suggest that the level of DVGs in the initial virus stock can modulate the type I IFN response in lung epithelial cells *in vitro.*

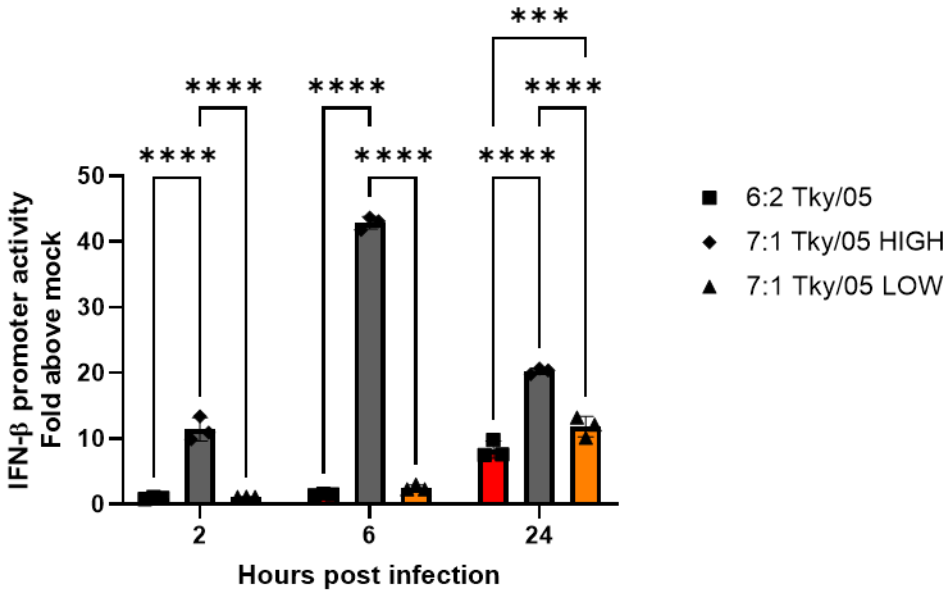

Figure 4.11. IFN-β promoter activity in A549 IFN-β luc cells. A549 IFN-β luc cells were infected with 6:2 Tky/05, 7:1 Tky/05 HIGH and 7:1 Tky/05 HIGH virus at an MOI of 1 or mock infected and at 2, 6 and 24 h.p.i., cells were lysed, and luciferase activity measured. Data is expressed as fold increase over mock and bars represent mean ± SD (n=3). Variance among groups was calculated by a two-way ANOVA with Tukey post hoc test for multiple comparisons. *** P<0.001, **** P<0.0001. This figure forms part of Figure 3 in (Penn et al., 2022).

4.2.8 Intracellular DVGs accumulate in both murine BMDMs and GM-DCs and trigger pro-inflammatory cytokine expression

In Chapter 3 we showed that the 6:2 Tky/05, 7:1 Tky/05 LOW and 6:2 Eng/09 replicated within murine BMDMs and induced IFN-α as well as other pro-inflammatory cytokines. Additonally, we observed an increase in the levels of IL-6 and TNF-α mRNA expression in the 7:1 Tky/05 LOW infected BMDMs, as well as elevated IFN-α protein levels, leading to the hypothesis that higher levels of DVGs could be responsible for this outcome. We therefore explored this further by infecting both murine GM-DCs and BMDMs with the 6:2 Tky/05, 7:1 Tky/05 HIGH and 7:1 Tky/05 LOW viruses and assessing intracellular DVG accumulation and pro-inflammatory cytokine induction over the course of the infection. We infected both GM-DCs and BMDMs with an MOI of 1 and at 6 and 24 h.p.i. (GM-DCs) or 2, 6 and 24 h.p.i. (BMDMs), harvested total RNA and conducted RT-PCR using terminal primers to amplify both full length polymerase segments and any DVGs derived from these (Figure 4.12). Similar to the A549 cells, we detected small bands that were a similar size to the DVGs in the virus stock (Figure 4.7). We also observed strong bands for all DVGs at 2 h.p.i. with the 7:1 Tky/05 HIGH in BMDMs.

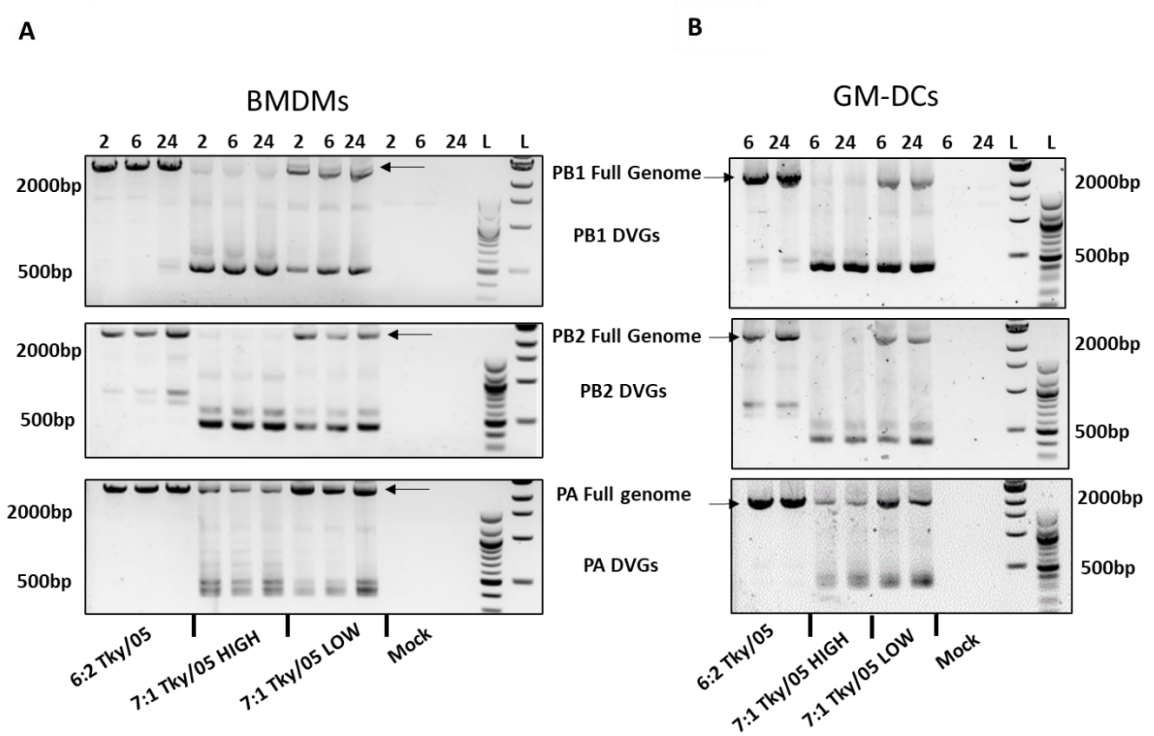

Figure 4.12. Polymerase DVGs detected in BMDM and GM-DCs. A) BMDMs and B) GM-DCs were infected using 6:2 Tky/05, 7:1 Tky/05 HIGH and 7:1 Tky/05 LOW virus at an MOI of 1 or mock infected. At 2, 6 and 24 h.p.i.,

total RNA was extracted, DNAse I on-column treated, and concentration measured by spectrophotometry. 100ng of RNA was used for cDNA synthesis with Superscript IV RT and Uni12 primer that targets the 3' end of vRNA. PCR was performed using KOD polymerase and Tky/05 terminal primers for detection of full genome and DVGs. PCR products were run on a 1.5% agarose gel with GelRed. (n =3). Gels show one representative well. Arrows indicate the size of the full genome. A forms part of Figure 4 in (Penn et al., 2022).

Total RNA extracted at 2, 6 and 24 h.p.i was then used to perform RT-qPCR for the mRNA gene expression of both IL-6 and TNF-α in BMDMs and at 6 and 24 h.p.i in GM-DCs (Figure 4.13). At all time points analysed there was higher IL-6 mRNA expression in both the BMDMs and GM-DCs infected with the 7:1 Tky/05 HIGH virus which by 24 h.p.i reached statistical significance. Similarly, by 24 h.p.i we also observed statistically higher TNF-α mRNA expression in both the 7:1 Tky/05 HIGH infected BMDMs and GM-DCs. These results demonstrate that the stock containing the highest DVG levels (7:1 Tky/05 HIGH) is able to induce higher amounts of pro-inflammatory cytokines.

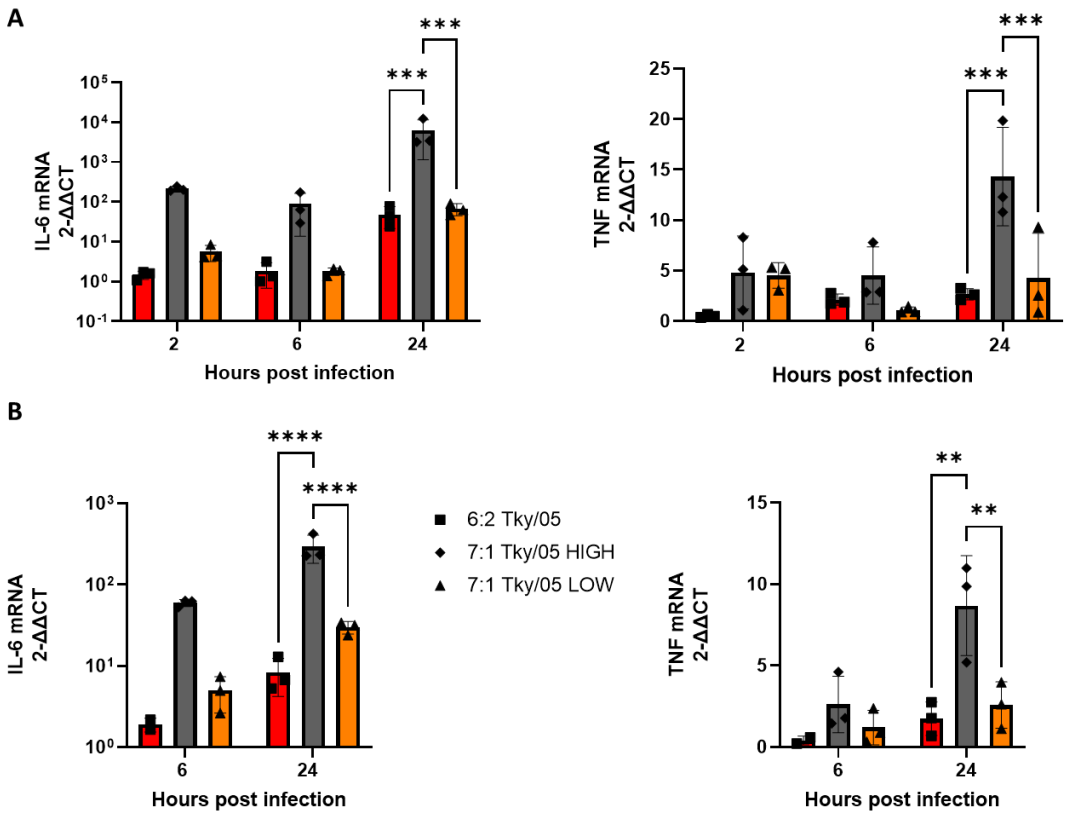

Figure 4.13. Cytokine expression in BMDMs and GM-DCs. A) BMDMs and B) GM-DCs were infected with an MOI of 1 or mock infected as in Figure 4.13. Total RNA was isolated at indicated time points and DNAse I on-column treated, and concentration measured by spectrophotometry. Equal amounts of RNA (200 ng) were

used to generate cDNA using RevertAid reverse transcriptase and primer for Oligo(dT). qRT-PCR performed using Fast SYBR green master mix and primers targeting GAPDH, IL-6 or TNF-α. Relative expression was calculated by the 2 -ΔΔ CT method normalised to the GAPDH housekeeping gene and shown as fold increase over the mock infected cells. Data represents mean ± SD (n=3). Variance among groups was calculated by a two-way ANOVA with Tukey post hoc test for multiple comparisons. **** P<0.0001, *** P<0.001, **P<0.01. A forms part of Figure 4 in (Penn et al., 2022).

4.2.9 DVGs cloned from the 7:1 Tky/05 virus are immunostimulatory

Our results so far indicate that if virus stocks contain high levels of DVGs (such as 7:1 Tky/05 HIGH), they trigger a strong early innate immune response including the expression of interferons and pro-inflammatory cytokines. The magnitude of this response is much greater when compared to stocks that do not contain as many DVGs (7:1 Tky/05 LOW or 6:2 Tky/05). In order to show that the DVGs present in the 7:1 Tky/05 stocks are immunostimulatory, we subcloned them into pPolI plasmids. We took plasmid DNA isolated from TOPO vectors containing the following DVGs: DVG 1 PB1 (479nt), DVG 2 PB2 (425nt), DVG 3 PB2 (584nt), DVG 4 PA (361nt), DVG 5 PA (388nt) and performed PCR using primers to introduce BsmBI sites (PB1 and PA DVGs) or BsaI sites (PB2 DVGs). Following digestion with the relevant restriction enzyme, the DVGs were ligated into the pPolI plasmid so that the DVG sequence was flanked at the 5' end by the human pol I promoter and 3' end by the mouse terminator (shown schematically in Figure 4.14). Correct construction of these pPolI plasmids was verified by Sanger sequencing.

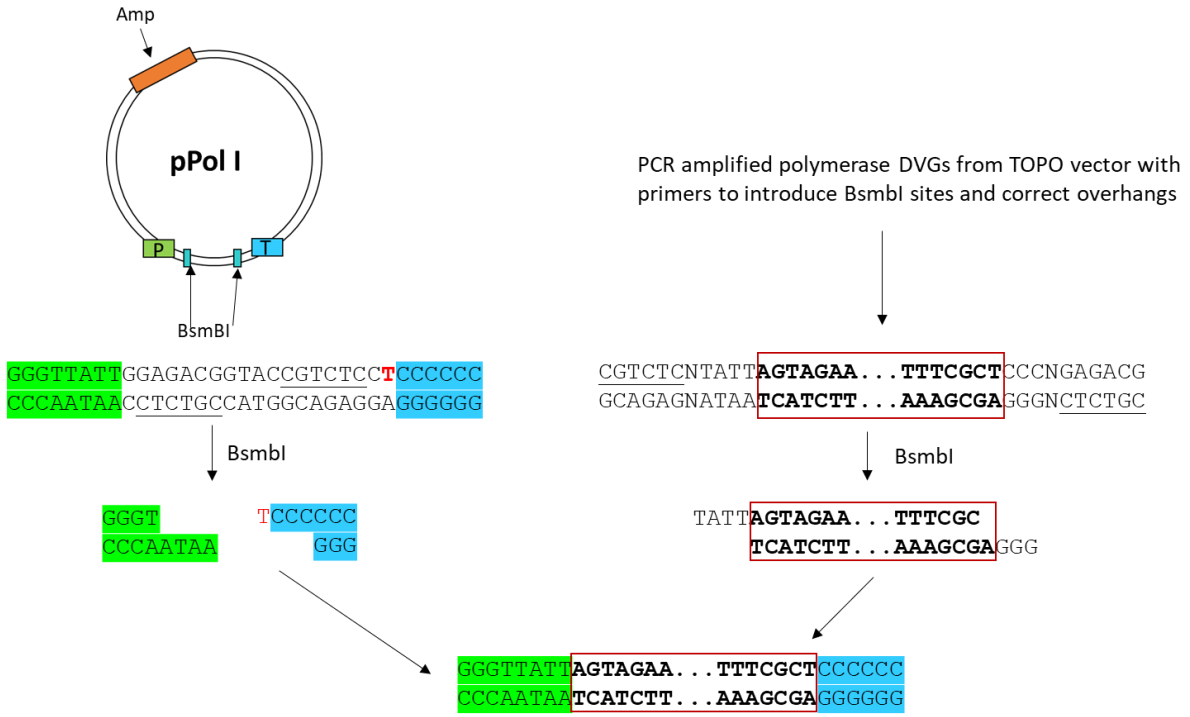

Figure 4.14. Generation of pPol plasmids containing DVGs. DNA from TOPO clones containing DVGs were amplified by PCR and restriction sites added with correct overhangs. PCR products were digested with BsmBI and cloned into pPolI plasmid. BsmBI restriction sites are underlined. The human pol I promoter is highlighted in green and the mouse terminator in blue. The thymidine nucleotide upstream of the terminator sequence (T) is shown in red and represents the 3' end of the DVG. All DVG sequences are shown in bold and outlined with a red box. BsaI was used to digest DVGs derived from the PB2 segment due to these containing an internal restriction site for BsmBI. Figure is adapted from (Neumann et al., 1999) with publisher's permission. Copyright (1999) National Academy of Sciences, U.S.A.

We next performed a vRNP reconstitution assay (schematically shown in Figure 4.15). As the human pol I can synthesise influenza viral-like RNA (Zobel et al., 1993), we used pPolI plasmids to either express the DVGs or full-length (FL) polymerase segment RNA alongside plasmids expressing the viral polymerase and NP in HEK293T cells as well as a *IFNB* and *Renilla* reporter plasmid. We could thus quantify luciferase signal as a means to measure the IFN-β promoter activity induced by their replication in the absence of any other viral products.

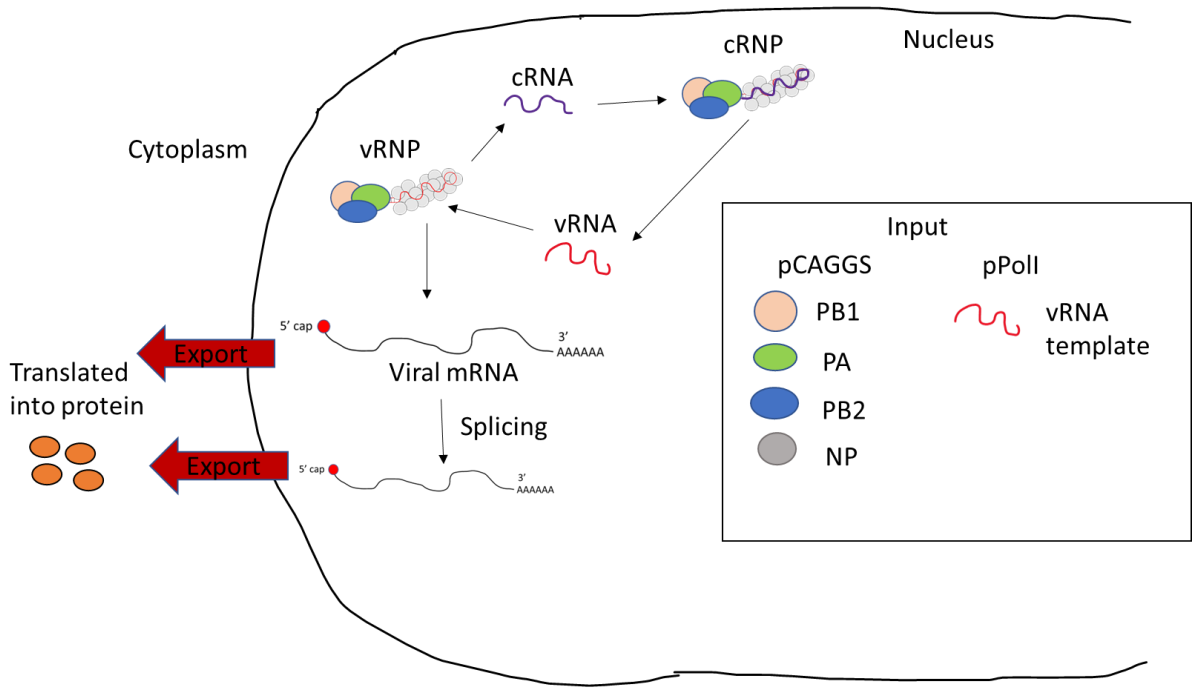

Figure 4.15. The vRNP reconstitution assay. The pCAGGS polymerase plasmids are transcribed by host RNA polymerase II generating mRNAs that are 5' capped and 3' polyadenlyated leading to the translation of the proteins that form the vRNP complex. The pPolI plasmid is transcribed by the host RNA polymerase I, generating a vRNA. The 3' and 5' UTRs of this vRNA act as a promotor for the reconstituted influenza polymerase to initiate both replication and transcription, mimicking an influenza infection. Only 1 vRNA segment is expressed rather than all 8 segments so there is no production of infectious virus. Adapted from (Sanchez et al., 2014).

To firstly confirm that there was successful replication of the DVGs and FL segments, we extracted RNA 24 hours post transfection and performed a RT-PCR (Figure 4.16B). To ensure there was no amplification of residual plasmid DNA, we used a tagged Uni12 primer for cDNA synthesis followed by PCR using the tag sequence in the forward primer. The PCR primers would therefore only amplify cDNA that had incorporated the tag (Figure 4.16A). As an additonal control we also performed an identical PCR reaction but omitted adding any reverse transcriptase (RT) (Figure 4.16C). All DVGs were sucessfully amplifed as strong bands were observed at the expected corresponding sizes. Simialrly, both the PB2 and PA FL segments were also successfully amplified, whereas amplification of the PB1 FL segment resulted in a weaker band which ran slightly higher than the expected size of 2341nt and an additional extra band at approx. 1000nt. Sanger sequencing of this plasmid revealed a large 700nt bacterial insert that could not be eliminated even when cloned at lower temperatures, which

has been previously reported for expression plasmids containing avian polymerase segments (Bhat et al., 2020). There were no bands present when the RT was omitted from the cDNA synthesis step confirming that the PCR products were not amplified directly from the incoming plasmid DNA.

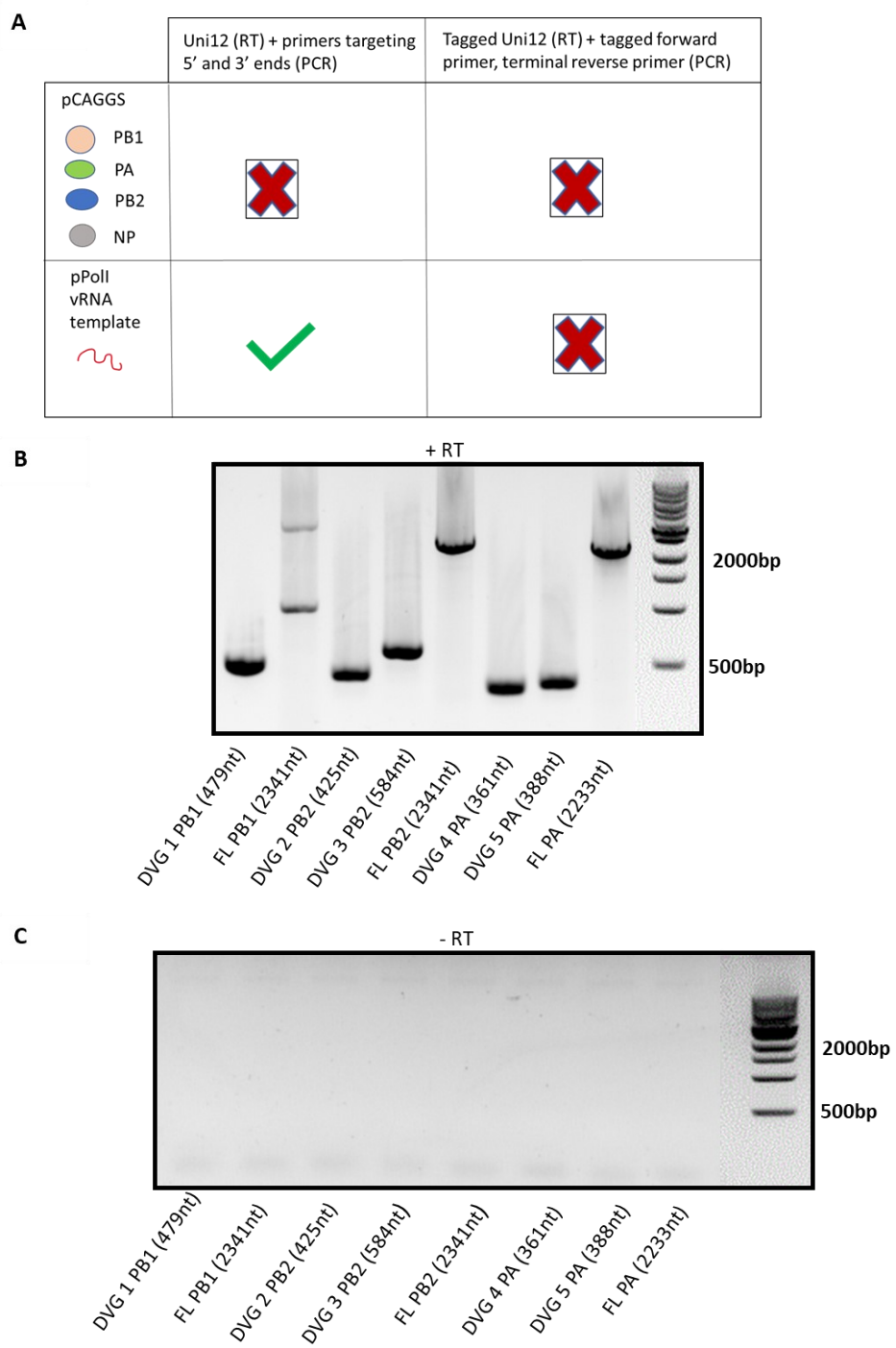

Figure 4.16 Confirmation of amplification of DVGs and FL segments from vRNP reconstitution assay. A) Schematic illustrating the rationale for using a tagged Uni12 primer in RT-PCR analysis. The pCAGGS plasmids do not contain the 5' and 3' UTRs of the influenza segments so the Uni12 (either tagged or untagged) and

terminal primers for PCR cannot amplify any residual plasmid DNA. In contrast the pPolI vRNA plasmid does contain both 5' and 3' NCRs so any residual DNA originating from the plasmid would be amplified using the Uni12 primer. The tagged Uni12 primer contains a tag at the 5' end generating cDNA that incorporates this tag, When this cDNA is used in RT-PCR, a forward primer targeting the tag ensures specificity. B-C) RNA was extracted 24 hours post transfection from HEK293T cells transfected with 3P and NP expression plasmids, alongside reporter plasmids and DVG or FL pPolI plasmids. cDNA synthesis was performed using equal amounts of RNA with B) reverse transcriptase present or C) reverse transcriptase omitted using tagged Uni12 primer. PCR was performed using KOD polymerase with tagged forward primer and relevant terminal primer. PCR products were ran on a 1.5% agarose gel with GelRed (n=3). One representative well is shown and the gel was spliced to remove empty wells for clarity as indicated by dotted line. B forms part of Figure 8 in (Penn et al., 2022).

All DVGs and FL segments activated the IFN-β promoter *in situ* (Figure 4.17). The PA DVGs induced the highest IFN-β activity and were even more immunostimulatory than their cognate FL segment. All other DVGs either resulted in a similar level of IFN-β promoter activity to FL or in the case of PB2 DVG 3 (584nt), significantly less activity. These results demonstrate that all DVGs were immunostimualtory but that not all DVGs trigger type I IFN equally.

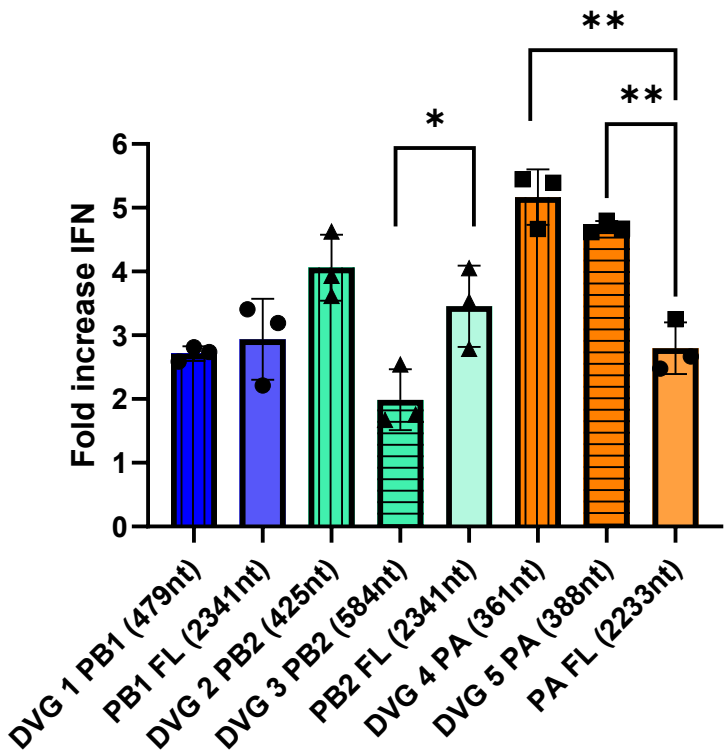

Figure 4.17. IFN-β promoter activation induced by the replication of either FL segment or DVG. HEK293T cells were transfected with 3P and NP expression plasmids, alongside reporter plasmids and DVG or FL pPolI

plasmids. Transfections were also performed where the PB2 pCAGGS plasmid was omittied (2P) and empty pCAGGS transfected instead. Cells were lysed 24 hours post transfection and luciferase measured. Values were normalised to Renilla and expressed as fold increase over 2P. Data represents mean ± SD (n=3). Differences between each DVG and the full-length segment it has been derived from was calculated by a two-sided unpaired t-test. * P<0.05, ** P<0.01. This figure forms part of Figure 8 in (Penn et al., 2022).

4.2.10 Virus stocks with high levels of DVGs initiate more ZBP1 induced cell death

We investigated whether an increase in cell death in MEF cells following infection with the high DVG stocks and could be attributed to activation of ZBP1. In an initial experiment we used stocks of viruses that all had similar genome to PFU ratios (Figure 4.18A). The viruses had either mammalian (6:2 Eng/09) or avian adapted (6:2 Tky/05 v2, 5:3 50-92 627E, 5:3 50-92 627K) internal genes. This was to elucidate whether there were differences in ZBP1-mediated cell death between diverse influenza strains. Due to depleted stocks, the 6:2 Tky/05 v2 was a new stock passaged at a low MOI (0.0001) from the same rescue as the 6:2 Tky/05 virus. The 5:3 50-92 virus is from another H5N1 isolate that has the HA, NA and M gene derived from PR8. This virus naturally has the avian signature glutamic acid at position 627 in the PB2 segment (627E). We also included an identical virus that only differed by having the mammalian adapted lysine (K) at this position. We infected MEF cells that lacked expression of ZBP1 (ZBP1 -/-), alongside ZBP1-/- cells reconstituted with WT ZBP1 (MEF ZBP1 +/+) and measured cell survival (Figure 4.18B). There was a slight decrease in cell survival observed for the 6:2 Tky/05 v2 infected ZBP1+/+ MEFs when compared to the ZBP1-/- MEFs although this was not statistically significant. There was no significant difference in cell survival between the MEF ZBP1 -/- and the MEF ZBP1 +/+ lines for any of the viruses analysed. Interestingly, there was greater cell death measured in both cell lines for the Eng/09 virus. These findings suggest that ZBP1 mediated cell death does not readily occur in IAV infections using standard virus stocks and may not vary between different IAV strains.

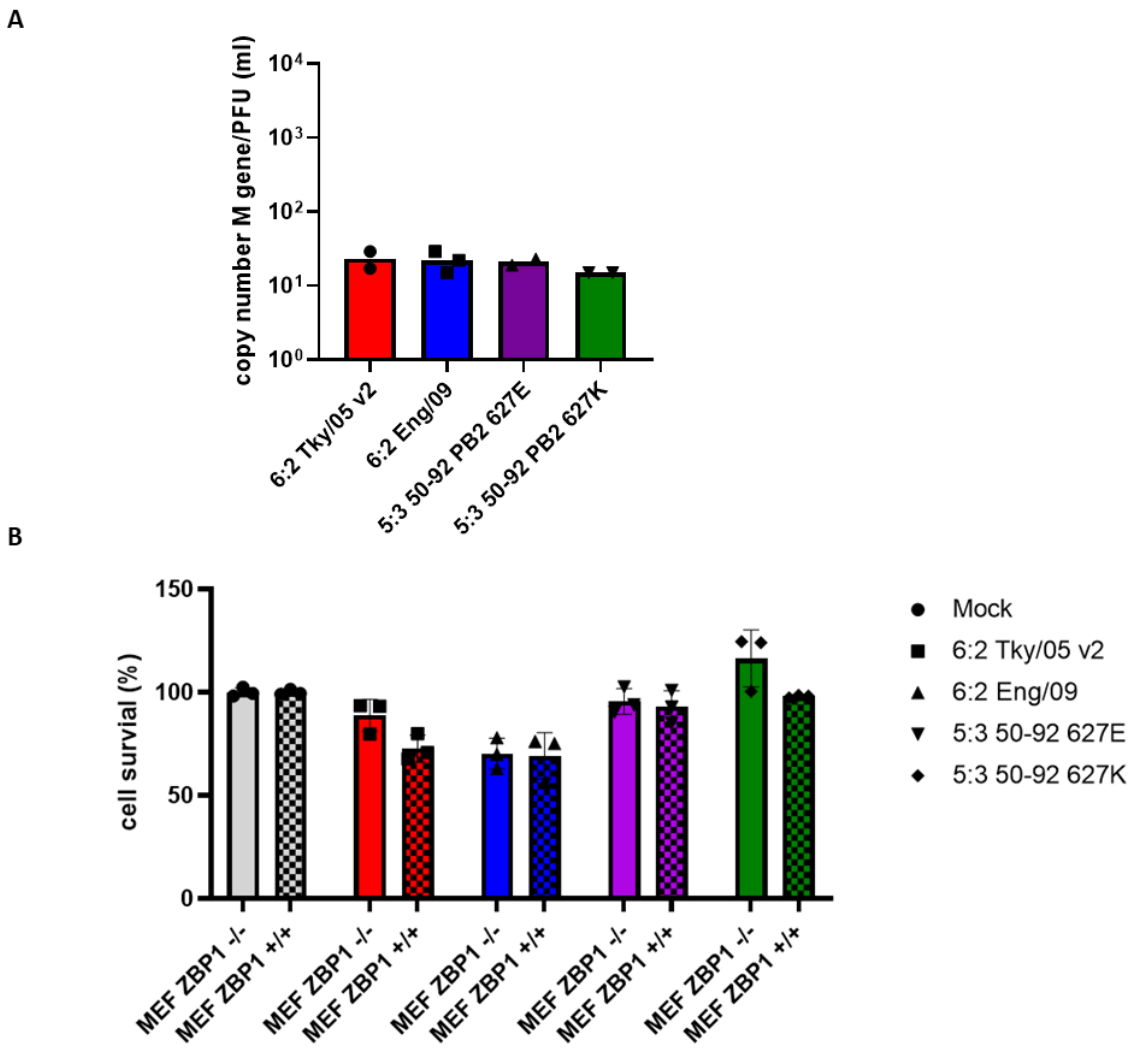

Figure 4.18. ZBP1 mediated cell death is not strain dependent. A) Copy number M gene/ml to PFU/ml ratio. Mean PFU/ml was determined for each virus stock (n =3) and this used to calculate the ratio. RNA was extracted from viral stocks and a one-step RT-qPCR performed using primers and probe for M gene in order to calculate M gene copy number/ml. Data points show ratio calculated using RNA obtained from at least two independent RNA extractions. B) ZBP1 -/- MEFs or ZBP1 +/+ MEFs were infected at an MOI of 1 with 6:2 Tky/05 v2, 6:2 Eng/09, 5:3 50-92 PB2 627E or 627K or mock infected. 24 hours later cells were lysed using cell titre glo and luciferase signal measured. Cell survival was calculated as the percentage normalised to the equivalent mock infected which was expressed as 100%. Data represents mean ± SD (n=3). Variance between ZBP1-/- and ZBP1+/+ cells for each virus was calculated by multiple two-sided unpaired t-tests but showed no statistical difference.

We next used a different panel of viruses to infect the MEF cells which differed in their genome to PFU/ml ratio (Fig 4.19A). Due to depleted stocks, new preparations of the 7:1

Tky/05 and 7:1 Tky/05 HIGH were generated (7:1 Tky/05 v2 and 7:1 Tky/05 HIGH v2). In addition to performing infections in MEFs that varied in expression of ZBP1, we also used MEFs that were reconstituted with a ZBP1 protein that was unable to bind to nucleic acids (Zα1α2^{mut}) due to altered key binding residues (Maelfait et al., 2017). Following influenza infection at the same MOI as used previously (MOI = 1), we saw significantly decreased cell survival in the ZBP1 +/+ MEFs when compared to both the ZBP1-/- MEFs and ZBP1 Zα1α2mut MEFs (Figure 4.19B). There was also a noticeable trend for cell survival to be higher in the ZBP1 +/+ MEFs when the copy number to PFU ratio was lower. Therefore our findings demonstrate that the Z-RNA binding domain is essential for ZBP1 mediated cell death and this pathway is activated when there are high levels of DVGs present in the virus stock.

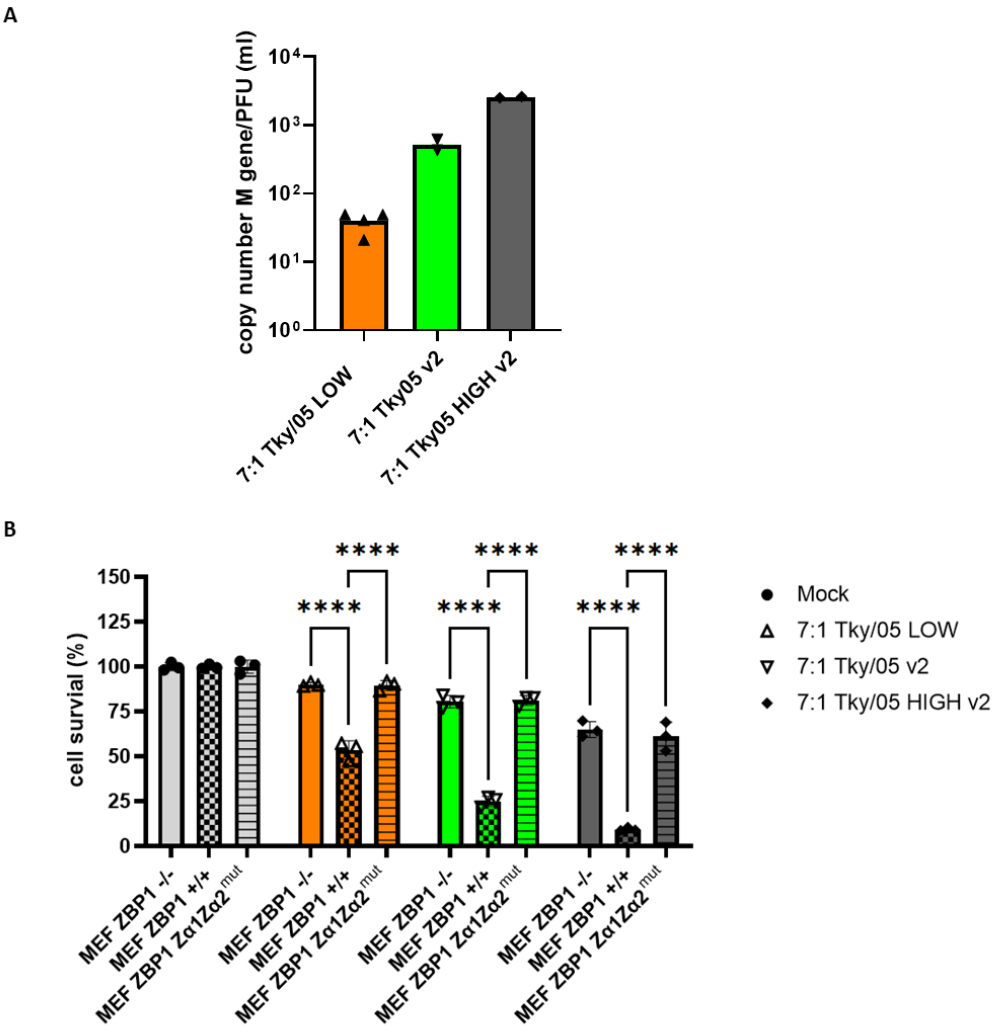

Figure 4.19. ZBP1 mediated cell death is impacted by DVG levels. A) Copy number M gene/ml to PFU/ml ratio. Mean PFU/ml was determined for each virus stock (n =3) and this used to calculate the ratio. RNA was extracted from viral stocks and a one-step RT-qPCR performed using primers and probe for M gene in order

to calculate M gene copy number/ml. Data points show ratio calculated using RNA obtained from at least two independent extractions. B) ZBP1 -/- MEFs, ZBP1 +/+ MEFs or ZBP1 Zα1α2mut MEFs were infected at an MOI of 1 with 7:1 Tky/05 LOW, 7:1 Tky/05 v2, or 7:1 Tky/05 HIGH v2 or mock infected. 24 hours later, cells were lysed using cell titre glo and luciferase signal measured. Cell survival was calculated as the pecentage normalised to the equivalent mock infected which was expressed as 100%. Data represents mean ± SD (n =3). Variance among groups was calculated by a one-way ANOVA with Tukeys post hoc test for multiple comparisons. ****P<0.0001.

4.3 Discussion

The results presented in this chapter demonstrate that DVGs can modulate innate immune responses within both epithelial and immune cells which is in agreement with the literature (Genoyer & Lopez, 2019; López, 2014; Vignuzzi & Lopez, 2019). By using virus stocks grown at various MOIs, thus containing different levels of DVGs, we demonstrate that the levels and kinetics of type I IFN and pro-inflammatory cytokines are vastly divergent following IAV infection. We also show that ZBP1-mediated cell death is affected by DVG content in the virus inocula.

We observed that viruses grown at low MOIs (0.0001) all had comparable genome to PFU ratios; these were much lower than those that had been passaged at higher MOI (Figure 4.1 and Figure 4.5A). This aligns with other studies where propogation at high MOI leads to increased numbers of DVGs and non-infectious particles (Xue et al., 2016). It should be noted that we used RNA as a proxy for total particles; theoretically only 1 copy of M gene should be packaged into a virion although this is often higher for most RNA viruses (Bhat et al., 2022). As another means to measure total particles, we also used an HA assay. When we measured the ratio of infectious to total particles we saw the expected inverse relationship; higher values were obtained for those grown at low MOI (Figure 4.5B). Although these results indicate there are high levels of non-infectious particles in the viruses grown at high MOI, these may not all represent particles containing DVGs (DIPs). IAV infections also readily generate semi-infectious (SI) particles which fail to express all 8 genome segments and thus like DVGs require complementation for infectivity (Brooke, 2014).

We confirmed that the viruses containing higher ratios of non-infectious to infectious particles do indeed contain DVGs (Figures 4.6 and Figure 4.7). We restricted our analysis to the polymerase segments as numerous studies demonstrate a higher propensity for DVGs to be derived from them (Alnaji et al., 2019; Boussier et al., 2020). The poor amplification of the full length polymerase segments for the 7:1 Tky/05 and 7:1 Tky/05 HIGH stocks is not surprising as smaller products are preferentially amplified in PCR and these stocks showed strong bands for shortened products (presumably DVGs) (Figure 4.6). Although not a quantitative assay, visualing DVGs on agarose gels following RT-PCR is a simple method to establish whether DVGs are present and is still routinely used (Huo et al., 2020; Swieton et al., 2020; Vasilijevic et al., 2017; Xue et al., 2016). Indeed RT-PCR has the added advantage of not needing to know the exact sequence of the junction site; terminal primers can still be used due to size differences between the full length segment and DVGs. We could have adopted the approach by Schwartz and Lowen (2016) where they semi-quantifed DVGs by qRT-PCR still using terminal primers. Here they used terminal primers in parallel with a second set of primers that amplified an internal region of the genome and compared the Δ-CT ratios.

The polymerase DVGs characterised in our virus stocks range from 361-853nt in length with an overall mean average length of 566nt (Figures 4.6 and 4.7), similar to other studies (Pelz et al., 2021; Saira et al., 2013). This indicates that there may be an optimal length for DVGs. Indeed Mendes and Russell (2021), elegantly demonstrated that there is a trade-off between influenza replication and packaging with the former process favouring smaller length sequences and the latter favouring longer length sequences. This resulted in the enrichment of DVGs centering around 400nt in length and could explain why DVGs averaging this length are more readily detected following IAV infection. By cloning DVGs into TOPO vectors and Sanger sequencing, we were able to determine the full sequence and map the break point and rejoin regions (Figure 4.7). In nearly half of all DVGs analysed, there were at least 2 nucleotides that were repeated adjacent to junctions. Repeated sequences have also been observed by others and supports the model that DVG formation is caused by viral polymerase slippage (Boussier et al., 2020; Lui et al., 2019; Saira et al., 2013). However direct repeats were not observed for all the DVGs identified, which has also been reported (Alnaji et al., 2019).

Therefore the exact mechanism governing their formation is unlikely to be solely caused by repetitive sequences.

Our results demonstrate that preparation of completely DVG free viral stocks is challenging. We observed DVG generation by all rescued viruses; the 6:2 Tky/05 virus contained DVGs even after one passage directly following the original rescue. Although the 7:1 Tky/05 virus had a noticeably reduced genome copy number to PFU ratio compared with the original 7:1 Tky/05 stock (813: 1 to 40:1), this virus still contained strong DVG bands when visualised by RT-PCR. This is consistent with findings reported by other groups; DVG content could be reduced by passaging high DVG stocks at low MOI, but they were still detectable either by RT-PCR or NGS (Alnaji et al., 2019; Frensing et al., 2013; Frensing et al., 2014).

Infections in different cell types with the virus stocks led to amplification of the DVGs. This was particularly evident in the A549 cells where PCR bands corresponding to the DVGs present in virus stocks were much more prominent by 6 and 24 h.p.i, especially for the 6:2 Tky/05 and 7:1 Tky/05 LOW virus (Figure 4.9). Although not as pronounced, presumably due to being less permissive to infection, we also observed similar for infections in BMDMs and GM-DCs (Figure 4.12). We did however observe some differences; no PA DVGs were amplified in BMDMs and GM-DCs following infection with the 6:2 Tky/05 virus whereas in the A549 cells faint DVG bands were observed at 6 and 24 h.p.i. However, the sizes of these PCR products did not correspond with those detected in the viral stocks and could therefore represent *de novo* DVG generation. Interestingly, Wang et al. (2020), also observed DVGs that were not detected in all infected cell types following high MOI infection of PR8. Huo et al. (2020), showed that DVGs were more readily amplified early post infection with H1N1 virus in the immune cell line HMC-1 than A549 cells. They contributed this to HMC-1 cells highly expressing AGO-2 which is a critical component of the RNA silencing machinary. By knocking down AGO-2, they showed a reduction in abundance of DVGs only in the HMC-1 cells. It therefore seems that specific host factors differentially expressed by cell types could account for differences in overall DVG abundance and perhaps also selection of individual DVG species.

As expected, the replication of the 7:1 Tky/05 HIGH virus was attenuated in both MDCK and A549 cells (Figure 4.8). There was a slight difference in growth kinetics between the two cell types for all of the virus stocks tested, with the A549 cells showing overall reduced infectious virus particles at all time points, even though these cells were infected with a 10-fold higher MOI. This is not surprising as A549 cells are reported to be less permissive to IAV infection compared to MDCKs (Zhai et al., 2012). Although by RT-PCR analysis, the 7:1 Tky/05 LOW virus stock contains stronger bands for DVGs and a greater amount of DVGs were idenitified when compared to the 6: 2 Tky/05 virus stock (Figure 4.6), the growth kinetics are similar. This may seem rather surprising if DVGs in the context of DIPs reduce infectious virus titres. However, the M gene copy number/ml to PFU/ml ratio of the two viruses are not vastly different. Moveover, modelling studies suggest that in order to substantially inhibit standard virus replication, DIPs must be present at high doses. Rudiger et al. (2021), proposed that in the suspension MDCK cell line, DIPs needed to be present at a ratio of 10,000 to 1 infectious viral particle in order to reduce infectious virus titres by four orders of magnitude.

By measuring type I IFN induced by infection with the different virus stocks we show that the DVG content can impact on the timing and breadth of this cruicial antiviral response. In A549 cells we observed a stronger upregulation of IFN-β mRNA at 2 h.p.i with the 7:1 Tky/05 HIGH virus which manifested as high protein levels at 24 p.i (Figure 4.10). This was further supported by the higher activity of the IFN-β promoter at all time points analysed (Figure 4.11). As these infections were performed at an MOI of 1 based on PFU, one could argue that the increased vRNA in the inoulum of the 7:1 Tky/05 HIGH virus leads to more PAMP in the cell, elevating the type I IFN levels induced. However this seems unlikely; incoming IAV vRNA in the form of vRNPs are poor activators of the type I IFN cascade (Killip et al., 2014), whereas incoming IAV DVGs are known to associate with RIG-I and cause phosphorylation of IRF3, an essential transcription factor required for type I IFN production (Liu et al., 2019).

We also observed significantly higher mRNA levels of the pro-inflammatory cytokines IL-6 and TNF in murine BMDMs and GM-DCs at 24 h.p.i folllowing infection with the 7:1 Tky/05 HIGH stock (Figure 4.13). Intrestingly, there was no obvious difference observed between the 6:2 Tky/05 and 7:1 Tky/05 LOW stocks in the BMDMs; this is in direct contrast to a previous infection in these cells where the 7:1 Tky/05 LOW stock induced higher mRNA expression

(Chapter 3,Figure 3.7A-B). This discrepancy is likely due to the different MOIs used for infection; an MOI of 1 was used in these experiments whereas an MOI of 10 was previously used. The high MOI infection would increase the likelihood of co-infection in cells with infectious particles and DIPs, resulting in the preferential replication of DVGs and generation of more DIPs over time (Thompson & Yin, 2010). Although the 6:2 Tky/05 infections at an MOI of 10 did result in a slight increase in mRNA expression compared to the lower MOI infection, this increase was not as elevated as those seen for the 7:1 Tky/05 LOW virus.

To directly confirm that the DVGs we identified are indeed responsible for triggering type I IFN, we cloned them and used in a vRNP reconstitution assay to assess the induction of IFNB promoter activity induced by their replication (Figure 4.17). Although all DVGs and FL segments were immunostimulatory, the signal was rather low. However this is reflective of findings in similar studies where HEK293T cells are used (French et al., 2022; Te Velthuis et al., 2018) and is most likely due to these cells expressing low levels of transcripts for key genes involved in innate immunity (Rausell et al., 2016). To enhance sensitivity, we could have co-transfected a plasmid expressing nuclear RIG-I such as adopted by Liu et al. (2018). We observed that not all DVGs were able to elicit a greater increase in IFN-β promoter activity over their FL genome. This was also recently observed by Mendes and Russell (2021), who demonstrated that by comparing the type I IFN response between two distinct PB1 DVGs, only one of these DVGs resulted in an increase over the FL PB1 segment. Furthermore, they showed that interferon induction was not a function of the length of the DVG. This suggests that the sequence of the DVG is a crucial factor in stimulating innate immunity. In support of these findings, French et al. (2022), showed that only mvRNAs that generated specific transient t-loop structures triggered IFN-β promoter activity. As large deletions result in sequences that do not normally reside next to each in the FL segment, being bought in close proximity to each other, this would presumably lead to an altered secondary structure. Interestingly, reduction of influenza NP expression has also been shown to enhance both DVG and mvRNA generation resulting in activation of the antiviral response (Nilsson-Payant et al., 2021). Indeed, DVGs may not be properly encapsidated, leaving parts of the RNA exposed (Dadonaite et al., 2019). Perhaps different DVG species vary in their level of NP encapsidation resulting in differences in host innate immune recognition. This will be investigated further in Chapter 6.

It has been speculated that IAV DVGs could potentially generate mRNAs that will be translated as they typically maintain parts of the ORF from the FL segment. In a combined scRNA-seq and bulk RNA-seq study of IAV infection, Kupke et al. (2020), clearly captured DVG mRNAs which were direct transcriptional descendants of DVG vRNAs as they contained identical junction sites. These could theorectically be translated into short polypeptides. Indeed, Boergeling et al. (2015), identified such a H5N1 PB1 DVG encoded truncated protein which they directly showed was responsible for triggering the IFN response; this property did not lie with the RNA. Whilst we did not investigate whether any of the DVGs were expressed as protein (such as by western blot), translation of the DVG sequences identified could potentially result in truncated proteins. It is therefore plausible that we may have observed higher IFN induction if we had tested the interferon inducing capability of any DVG encoded protein rather then the RNA. However this is unlikely considering transcription and translation of the viral gene products would occur in the vRNP reconstitution assay.

Another RNA sensor that has been implicated in the recognition of IAV DVGs is ZBP1. Our results show that when virus stocks contain low levels of DVGs (and therefore DIPs), there was minimal ZBP1 mediated cell death (Figure 4.18). Furthermore, a range of different viruses were tested, all displaying the same phenotype which suggests that this is universal amongst different strains. This lack of ZBP1-mediated cell death does not agree with previous studies which instead demonstrate that IAV triggers cell death in a ZBP1 dependant manner (Kesavardhana et al., 2017; Thapa et al., 2016; Zhang et al., 2020). However, all of these studies performed infections at a higher MOI than we employed here, ranging from an MOI of 2-10. Additionally, the quality of the virus stocks with regards to DVGs was not reported. Our results do show a decrease in cell survival in ZBP1 +/+ MEFs compared to ZBP1 -/- MEFs when high DVG stocks were used (Figure 4.19). This is in agreement with Zhang et al. (2020), who not only showed earlier ZBP1-mediated cell death following infection with a high DVG PR8 stock compared to a low DVG stock, but also direct binding of ZBP1 with PA DVGs ranging from 350-500nt in size. Thapa et al. (2016), also found that ZBP1 had a similar IAV vRNA binding profile to RIG-I, with specific enrichment of the 5’ and 3’ ends of the polymerase segments and importantly all association was lost when the binding domain was mutated. This agrees with our findings; when we perfomed infections in the Zα1α2mut MEFs we

observed no difference in cell survival when compared to the ZBP1-/- MEFs (Figure 4.18B). As ZBP1 senses nucleic acids in the Z conformation only, it is likely that DVGs via a currently unknown mechanism, adopt this conformation. Indeed, Zhang et al. (2020), using immunofluorescence microscopy, clearly demonstrated that IAV infections produce Z-RNA and that at 6 h.p.i these were only observed in the high DVG stock, correlating with onset of cell death. We did attempt to perform Z-RNA staining using the method by Zhang et al. (2020), but observed clear staining in the mock infected cells which was not consistent with the results obtained by the authors (data not shown). Due to time constraints, this was not further pursued but with more optimisation could have helped to strengthen the evidence that DVGs are a dominant source of Z-RNAs. It would be interesting to elucidate specifically what type of cell death we were measuring in our MEF cell lines as ZBP1 can mediate multiple death pathways. Specific components of each cell death signalling pathway could be measured (i.e. MLKL phosphorylation for necroptosis), or alternatively blocked by selective inhibitors (i.e. those targeting gasdermin proteins to prevent pyroptosis) to establish the exact cell death type.

Overall, this chapter adds to the existing literature and shows that the amount of DVGs present in the virus stock can influence the early innate immune response to IAV infection. However, these studies cannot define whether such a response would be beneficial or detrimental to the host; this can only be adequately assessed *in vivo*. Therefore Chapter 5 aims to answer this fundamental question by utilising the BALB/c mouse model.

Chapter 5 Investigating the role of DVGs in determining the outcome of infection in a mouse model

5.1 Introduction

Numerous research findings in animal models demonstrate that virus stocks from a diverse range of virus families containing high levels of DVGs reduce viral virulence (Rabinowitz & Huprikar, 1979; Swieton et al., 2020; Tapia et al., 2013; Vasilijevic et al., 2017). Moreover, purified defective particles administered prior to infection can protect the host from lethal viral challenge (Chaturvedi et al., 2021; Dimmock et al., 2012; Hein et al., 2021a; Hein et al., 2021b; Scott et al., 2011; Welch et al., 2020). Like experiments in cell culture, this reduced virulence has been largely attributed to DVGs triggering a strong antiviral response and resulting in a reduction of virus replication and ultimately resulting in promoting survival of the host *in vivo*.

Studies focusing on influenza infection in the mouse model typically use laboratory strains such as WSN or PR8 as these are able to robustly infect mice (Kamal et al., 2014). However, infections with these strains may not adequately reflect the same outcome as an HPAIV mammalian infection. Indeed, some studies assessing aberrant replication products in HPAIV infections have demonstrated a link between their presence and a more severe infection. Te Velthuis et al. (2018) demonstrated that high levels of mvRNAs were detected in the lungs of ferrets infected the 1918 pandemic H1N1 strain, correlating with increased cell death and pro-inflammatory cytokine expression. Similarly, Boergeling et al. (2015), showed that a H5N1 virus that contained a PB2 DVG led to a more severe infection in mice when compared to an identical stock that did not contain this same DVG. In direct contrast, a study by Huo et al. (2020), demonstrated that when a high DVG H5N1 stock was used for infections in mice, they lost less weight and had higher survival rates than infections performed using the equivalent low DVG stock.

The aim of this chapter is to therefore determine whether the recombinant virus stocks containing the internal genes of Tky/05 characterised in Chapter 4, which differ in their DVG content, can impact on the pathogenicity of infection in mice. Although we demonstrated that the high DVG stocks *in vitro* resulted in early type I IFN production and would probably translate in a mild infection *in vivo*, type I IFN has been implicated in exacerbating disease

progression (Davidson et al., 2014; Davidson et al., 2016; Major et al., 2020). As HPAIV mammalian infections are associated with hypercytokinemia, there is the valid concern that DVGs could tip the host immunity from a protective response to a more pathological one. By performing experiments in mice with equivalent infectious doses of the recombinant Tky/05 viruses and observing weight loss and survival rates alongside analysing DVG amplification, virus replication and cytokine induction, we hope to gain a better understanding into how DVGs contribute to the cytokine storm and ultimately how they can modulate severity in the mouse model.

5.2 Results

5.2.1 The 7:1 Tky/05 virus infection led to increased pathogenicity in the mouse model

We carried out a preliminary experiment to assess the pathogenicity of the 6:2 Tky/05, 7:1 Tky/05 and 6:2 Eng/09 viruses. We infected BALB/c mice intranasally with 10^5 PFU of each virus and monitored weight loss daily over 7 days. All infected mice lost weight, but this was most rapid in mice infected with the 7:1 Tky/05 virus and resulted in significantly decreased body weight by days 2 and 3 when compared to the other infected mice (Figure 5.1A). Any mouse losing ≥ 20% original body weight was culled in accordance with Home Office guidelines and survival curves were plotted (Figure 5.1B). By day 4, 1/5 mice infected with the 7:1 Tky/05 virus was culled, followed by another mouse on day 5. In the 6:2 Tky/05 infected group, 1/5 mice had reached the severity limit by day 6 but by the end of the experiment (day 7), this had increased to 3/5 mice. In contrast, by day 7, all mice (5/5) infected with the 6:2 Eng/09 virus maintained their body weight to above 80% of their original weight.

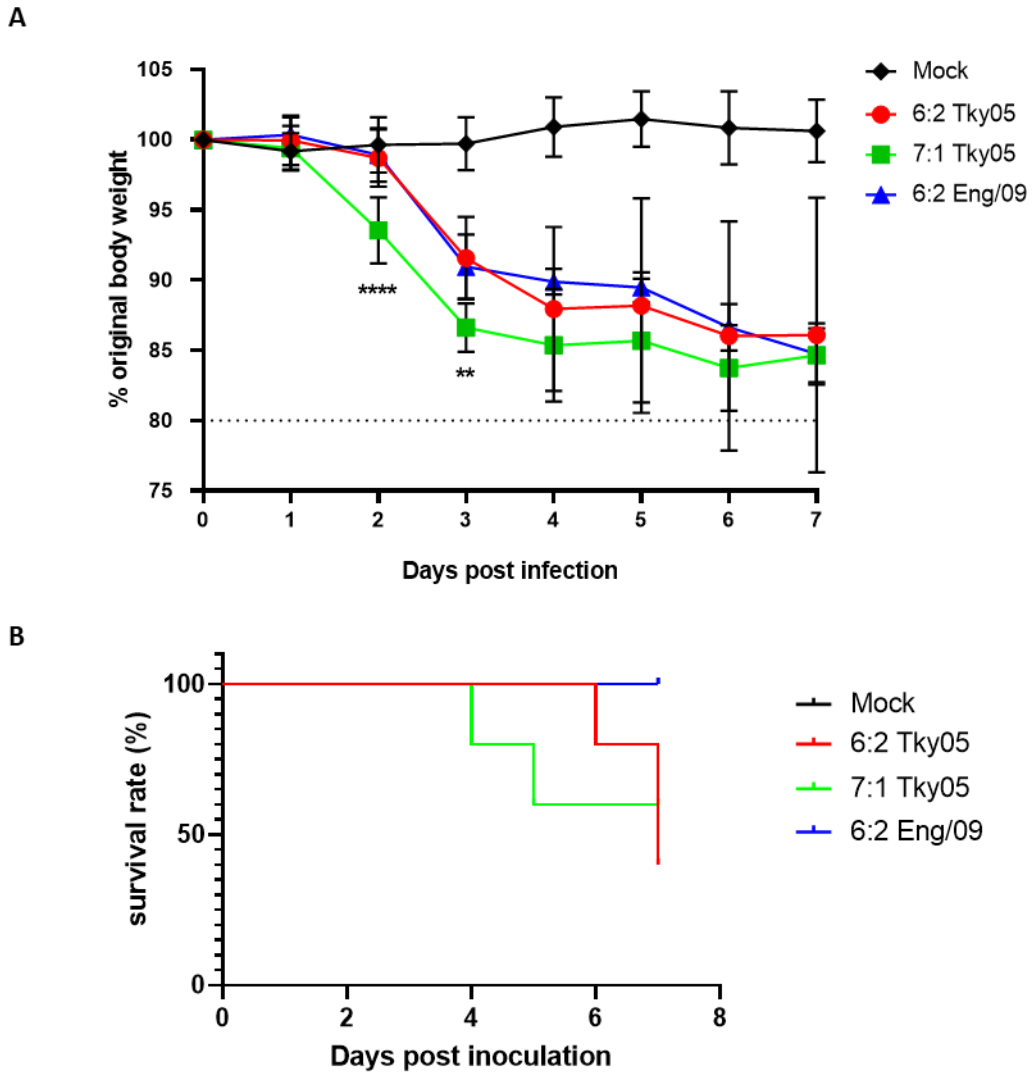

Figure 5.1. Pathogenicity of the recombinant viruses. A) Six to eight week old female BALB/c mice (15 per group) were mock infected (PBS) or infected intranasally with 10^5 PFU of 6:2 Tky/05, 7:1 Tky/05 or 6:2 Eng/09 virus in 25µl volumes. 5 mice per group were culled at 48 hrs, 72 hrs and 7 days post infection. Weight loss was monitored daily. Dotted line represents the severity limit. Variance among groups was calculated by a two-way ANOVA with Tukey post hoc test for multiple comparisons. ** P<0.001, **** P<0.0001. B) Survival curve of infected mice. All mice were culled when they lost ≥20% of original body weight (day 0). *In vivo* mouse work was performed alongside Mrs Rebecca Frise and Ms Laury Baillon. The data in this figure was used for part of Figure 5 in (Penn et al., 2022).

We next ascertained whether an increase in viral load in the lungs could be contributing to the increased pathogenicity in the 7:1 Tky/05 infected mice. We therefore performed plaque assays on lung homogenates harvested on day 2, 3 and 7 post infection to determine viral titres (Figure 5.2). We recovered virus in all lung homogenates at day 2 and 3 days from the infected mice. Interestingly, higher viral titres were obtained from the lungs of mice infected

with the 6:2 Eng/09 virus and viral titres from the 7:1 Tky/05 infected mice were statistically lower. By day 7, the remaining mice in the 7:1 Tky/05 infected group had cleared the virus and only 1/2 surviving mice in the 6:2 Tky/05 infected group had infectious virus remaining in the lung. In contrast 0/5 mice in the group infected with the 6:2 Eng/09 virus had cleared the infection; lung viral titres ranged from 1.5 x 10^4 PFU/gm to 6.8 x 10^4 PFU/gm. These results therefore demonstrate that the increased pathogenicity observed by the 7:1 Tky/05 virus was not caused by higher viral loads in the lung.

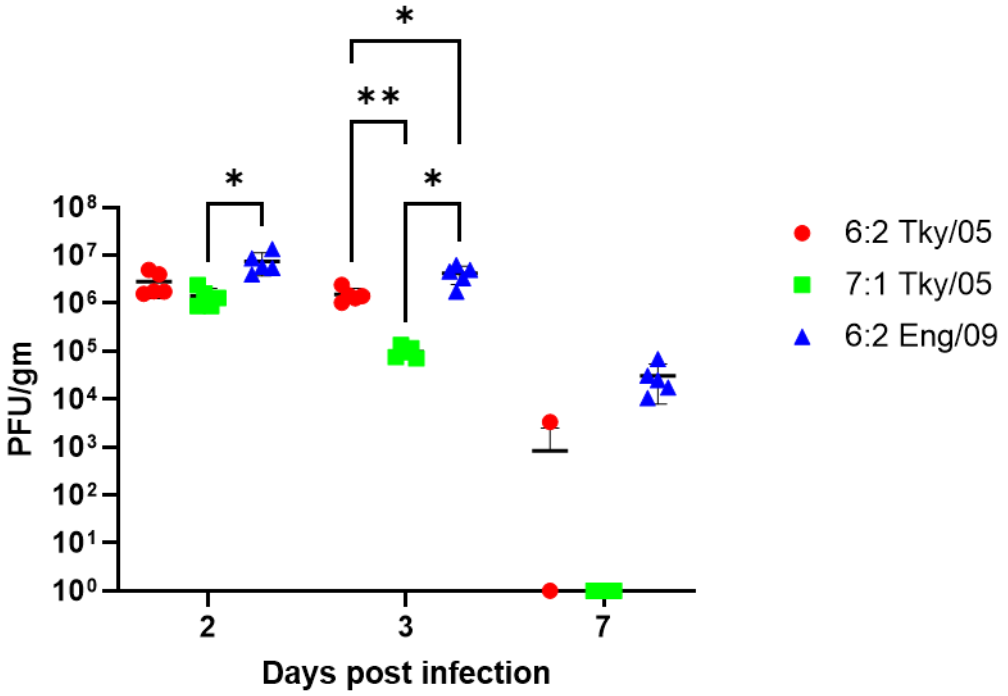

Figure 5.2. Virus titres in the homogenised lung tissues. Mice were infected as in Figure 5.1 and lungs were harvested at days 2, 3 and 7 days post infection, homogenised and weighed. Plaque assays were performed to determine viral titre and calculated as PFU/gm. Data is expressed as mean ± SD (n =5). Variance among groups was calculated by a two-way ANOVA with Tukey post hoc test for multiple comparisons. * P<0.05, ** P<0.001. The data in this figure was used for part of Figure 5 in (Penn et al., 2022).

In chapter 4, we showed that the higher DVG content of the 7:1 Tky/05 virus induced an early type I IFN response in lung epithelial cells (Chapter 4, Figure 4.3). We therefore wished to assess the secretion of IFN-α in the lungs at both 48 and 72 h.p.i (Figure 5.3). All virus infections led to the secretion of IFN-α whereas the mice that were mock infected did not. At both time points analysed, the highest amount of IFN-α was measured in the 6:2 Tky/05

infected lung homogenates. Interestingly, there was no statistical difference in the amount secreted between the 6:2 Eng/09 infected mice or the 7:1 Tky/05 infected mice.

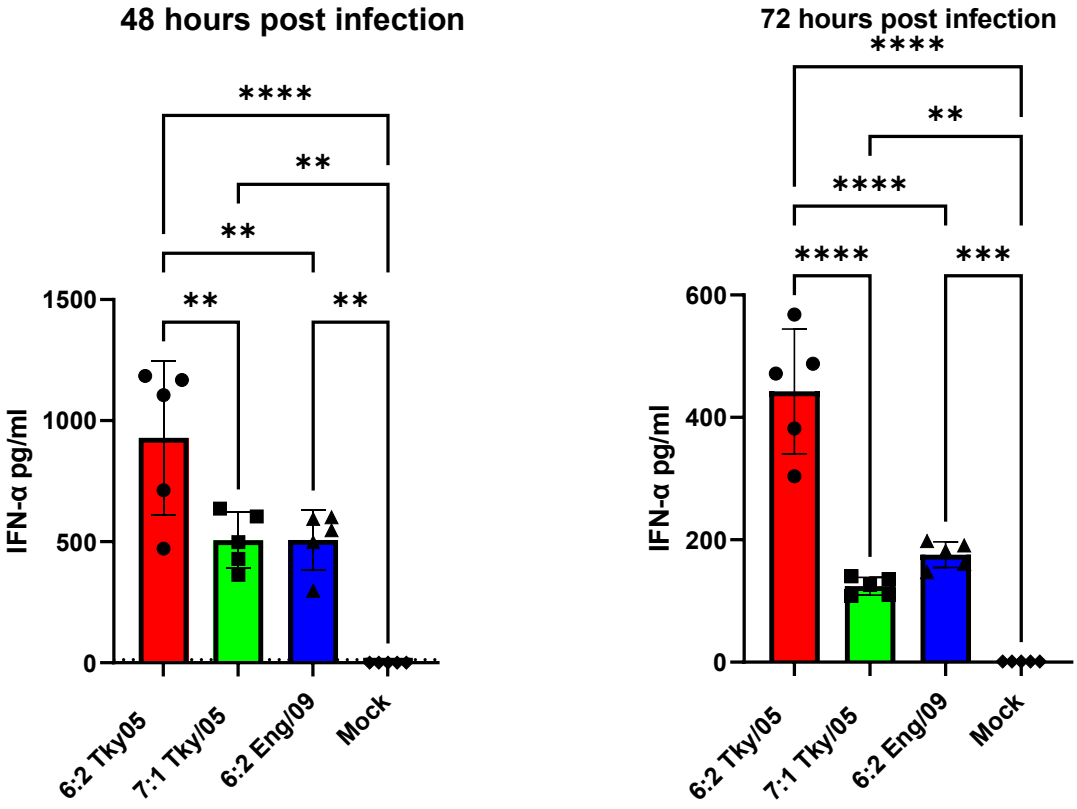

Figure 5.3. IFN-α levels in the homogenised lung tissues. Mice were infected as in Figure 5.1 and lungs were harvested at 48 and 72 hours post infection. IFN-α levels were assessed by ELISA (limit of detection= 12.5pg/ml). Bars represent mean ± SD (n=5). Variance among groups was calculated by a two-way ANOVA with Tukey post hoc test for multiple comparisons. * P<0.05, ** P<0.001.

5.2.2 The amount of DVGs in the inoculum impacts infection outcome *in vivo*

As the 7:1 Tky/05 virus led to more rapid weight loss, we wished to determine whether the levels of DVGs in the inoculum influence disease severity. We therefore performed another infection in the BALB/c mice using the viruses propagated and characterised for DVGs in Chapter 4 (6:2 Tky/05, 7:1 Tky/05 HIGH and 7:1 Tky/05 LOW) with the aim to explore differences in viral load, cytokine induction and pathogenesis. BALB/c mice were infected intranasally with 10^5 PFU of the virus stocks and weight loss monitored (Figure 5.4A). The 6:2 Tky/05 and 7:1 Tky/05 LOW infected mice lost significantly more weight compared to the healthy mock infected control group. However, the 7:1 Tky/05 LOW infected mice displayed

more rapid weight loss and by day 5, 4/5 mice had reached the severity limit and all mice were culled (Figure 5.4B). Conversely, the 7:1 Tky/05 HIGH virus caused no significant weight loss when compared to the mock infected group over the whole experimental time course (14 days).

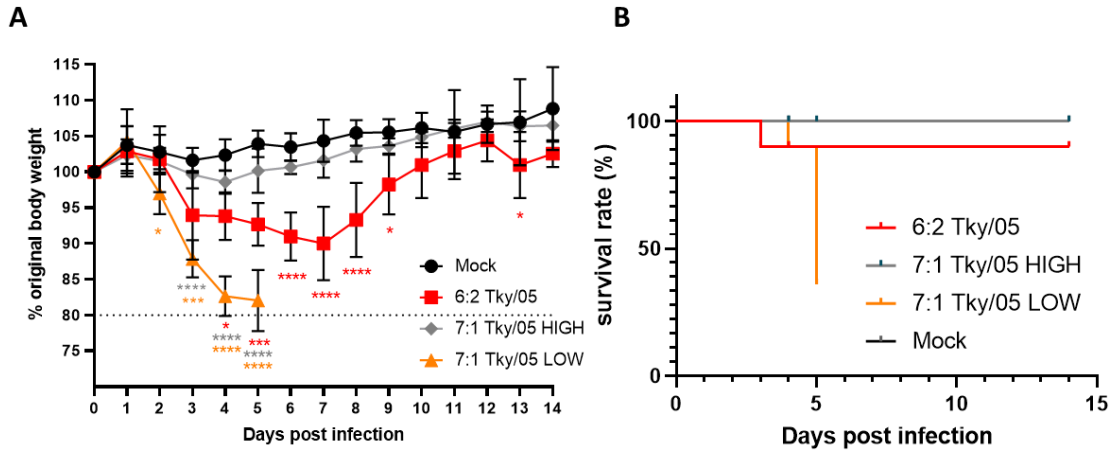

Figure 5.4. Levels of DVGs in the virus inoculum impact on pathogenesis. A) Six to eight week old female BALB/c mice (25 per group) were mock infected (PBS) or infected intranasally with 10^5 PFU of 6:2 Tky/05, 7:1 Tky/05 HIGH or 7:1 Tky/05 LOW virus in 35µl volumes. 5 mice per group were culled at 6 hrs, 24 hours, 48 hrs and 96 hrs post infection. Weight loss was monitored daily. Dotted line represents the severity limit. Orange asterisks indicate statistical significance between 6:2 Tky/05 and 7:1 Tky/05 LOW, grey asterisks indicate statistical significance between 7:1 Tky/05 HIGH and 7:1 Tky/05 LOW, red asterisks indicate stastical significance between 7:1 Tky/05 HIGH and 6:2 Tky/05. Variance among groups was calculated by a two-way ANOVA with Tukey post hoc test for multiple comparisons. * P<0.05, ** P<0.01, *** P<0.001 **** P<0.0001. B) Survival curve of infected mice. All mice were culled when they lost ≥20% of original body weight (day 0). *In vivo* mouse work was performed alongside Mrs Rebecca Frise and Ms Laury Baillon. This figure forms part of Figure 5 in (Penn et al., 2022).

Lung homogenate viral load measured by PFU showed significantly lower PFU/gm in lungs from mice infected with 7:1 Tky/05 HIGH and higher PFU/gm in the 7:1 Tky/05 LOW infected lungs at all time points (Figure 5.5A). We also measured the M gene copy number/gm in the lungs. At 6 h.p.i, the 7:1 Tky/05 HIGH infected mice had the highest M gene copy numbers/gm but by 24 h.p.i., this was significantly higher for the 7:1 Tky/05 LOW group (Figure 5.5B).

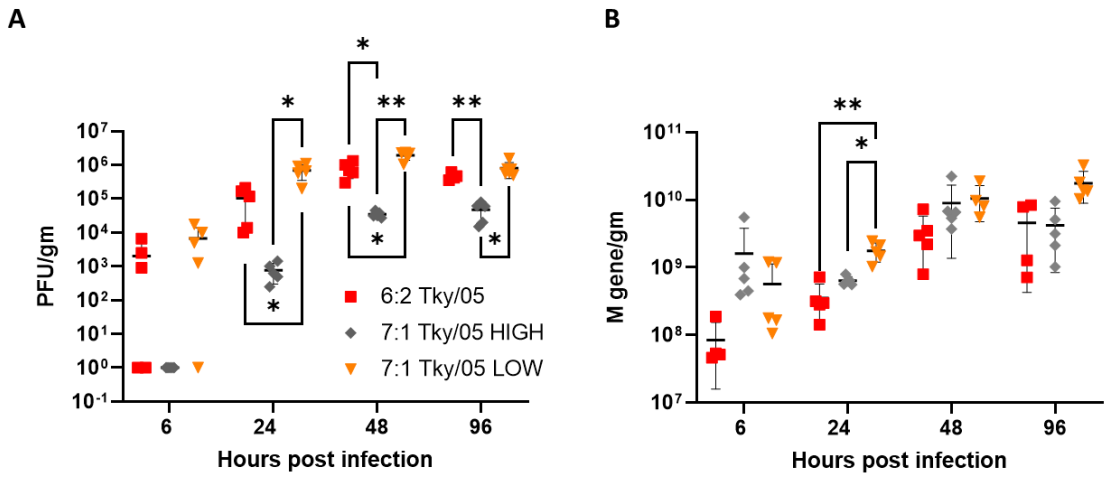

Figure 5.5. Virus titres in the homogenised lung tissues. Lungs were harvested at 6, 24, 48 and 96 hours post infection, homogenised and weighed. A) Plaque assays were performed to determine viral titre and calculated as PFU/gm. Data is expressed as mean ± SD (n =5 per group). B) RNA was extracted from the homogenised lungs and one-step qRT-PCR performed using primers and probe for M gene (n = 5 per group). Variance among groups was calculated by a two-way ANOVA with Tukey post hoc test for multiple comparisons. * P<0.05, ** P<0.001. This figure forms part of Figure 5 in (Penn et al., 2022).

As the influx of immune cells into the lung indicates inflammation, we decided to quantify the total number of cells in the BAL fluid (Figure 5.6). By 24 h.p.i., we observed that only the 7:1 Tky/05 LOW infected BAL fluid had a stastically higher number of cells than the mock infected. However, by 48 h.p.i, all virus infected BAL fluid contained significantly higher cell counts than the mock infected.

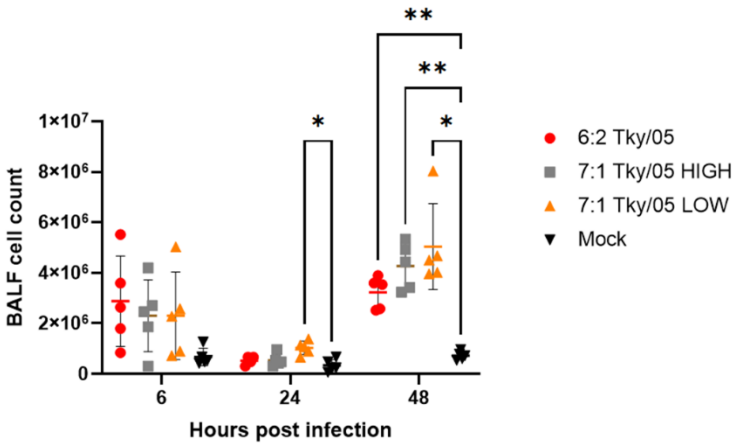

Figure 5.6. Cellular infiltration in BAL fluid. BAL fluid was taken at 6, 24 and 48 h.p.i. and cell counts calculated (n = 5 per group). Variance among groups was calculated by a two-way ANOVA with Tukey post hoc test for

multiple comparisons. * P<0.05, ** P<0.01. BAL fluid taken and analysis performed by Dr John Tregoning. This figure forms part of Figure 5 in (Penn et al., 2022).

We next investigated the kinetics of the cytokine/chemokine response induced by infection with these viruses. We firstly measured the mRNA levels by RT-qPCR in the homogenised lungs for both IFN-α5 and the ISG ZBP1 (Figure 5.7A and B). IFN-α5 mRNA peaked at 6 h.p.i. following infection with the 7:1 Tky/05 HIGH virus, whereas IFN-α5 mRNA expression peaked at 48 hours following infection with either 6:2 Tky/05 or 7:1 Tky/05 LOW (Figure 5.7A). We also observed an earlier induction of ZBP1 mRNA following infection with the 7:1 Tky/05 HIGH virus peaking at 24 h.p.i., in direct contrast to the 6:2 Tky/05 or 7:1 Tky/05 LOW infected lungs where peak mRNA expression was at 48 h.p.i. (Figure 5.7B). IFN-α and pro-inflammatory cytokine protein levels were also analysed in the lung homogenates by ELISA (Figure 5.7C-E). IFN-α as measured by ELISA also showed a similar trend to the RT-qPCR results; infection with the 7:1 Tky/05 HIGH virus resulted in earlier IFN-α protein in the lungs peaking at 24 h.p.i., whereas the 7:1 Tky/05 LOW virus resulted in highest protein levels at 48 h.p.i. and this reached statistical significance (Figure 5.7D). IL-1β protein levels were more variable within the groups; typically, only 1 or 2 murine lungs per group contained detectable levels. However, there was a trend for early measurable IL-1β protein in the 7:1 Tky/05 HIGH group (24 h.p.i. only), whereas IL-1β was only detected at later time points for 7:1 Tky/05 LOW (24 and 48 h.p.i.) and 6:2 Tky/05 (48 and 96 h.p.i.) (Figure 5.7E). Interestingly, TNF-α was only measured in the 7:1 Tky/05 LOW lung homogenates and only at 48 h.p.i.(Figure 5.7C).

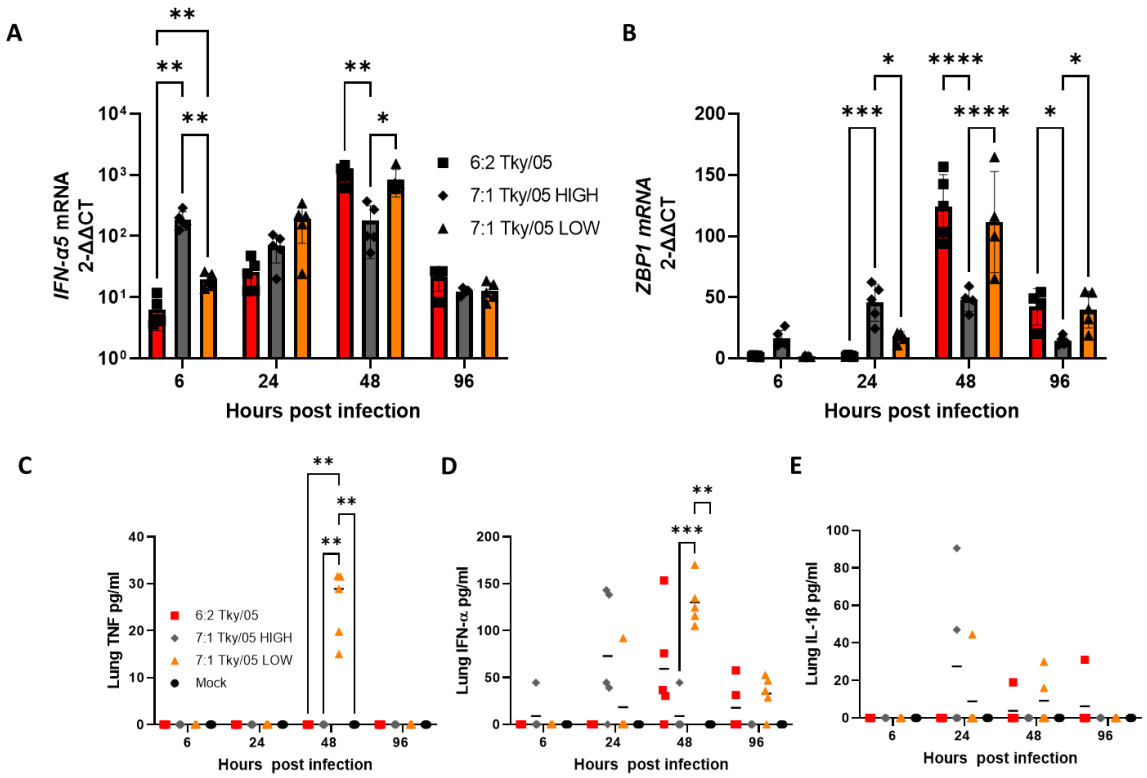

Figure 5.7. Cytokine levels in the homogenised mouse lungs. Murine lungs were harvested at 6, 24, 48, 96 h.p.i. and homogenised. A-B) Total RNA was extracted, Dnase I column treated and concentration measured by spectrophotometry. cDNA was synthesised by the high-capacity cDNA reverse transcription kit using 500ng total RNA. qRT-PCR was performed using either A) Taqman expression murine IFN-α5 assay and Taqman expression murine GAPDH assay or B) Fast SYBR green master mix and primers targeting GAPDH and ZBP1 (n = 5 per group and bars represent mean ± SD). C-E) Lung homogenates were used in ELISA for detection of C) TNF-α, D) IFN-α and E) IL-1β. (n = 5 per group and line represents mean). Variance among groups was calculated by a two-way ANOVA with Tukey *post hoc* test for multiple comparisons. * P<0.05, ** P<0.01, ***P<0.001, ****P<0.0001. A, C-E form part of Figure 6 in (Penn et al., 2022).

Cytokine/chemokines were also measured at 48 h.p.i in the BAL fluid by a multiplex ELISA (MSD) (Figure 5.8). Strikingly, infection with the 7:1 Tky/05 LOW virus resulted in high protein levels of the pro-inflammmatory cytokines TNF-α and IL-6 as well as the chemokines MCP-1, IP-10 and MIP-1β. In contrast IFN-γ, was detected at marginally higher levels in the BAL fluid of the 7:1 Tky/05 LOW infected mice but this was not statisticaly significant over the mock infected mice. For all cytokines/chemokines analysed, the lowest values measured were in the 7:1 Tky/05 HIGH infected group but these were not significantly different when compared to the 6:2 Tky/05 infected group.

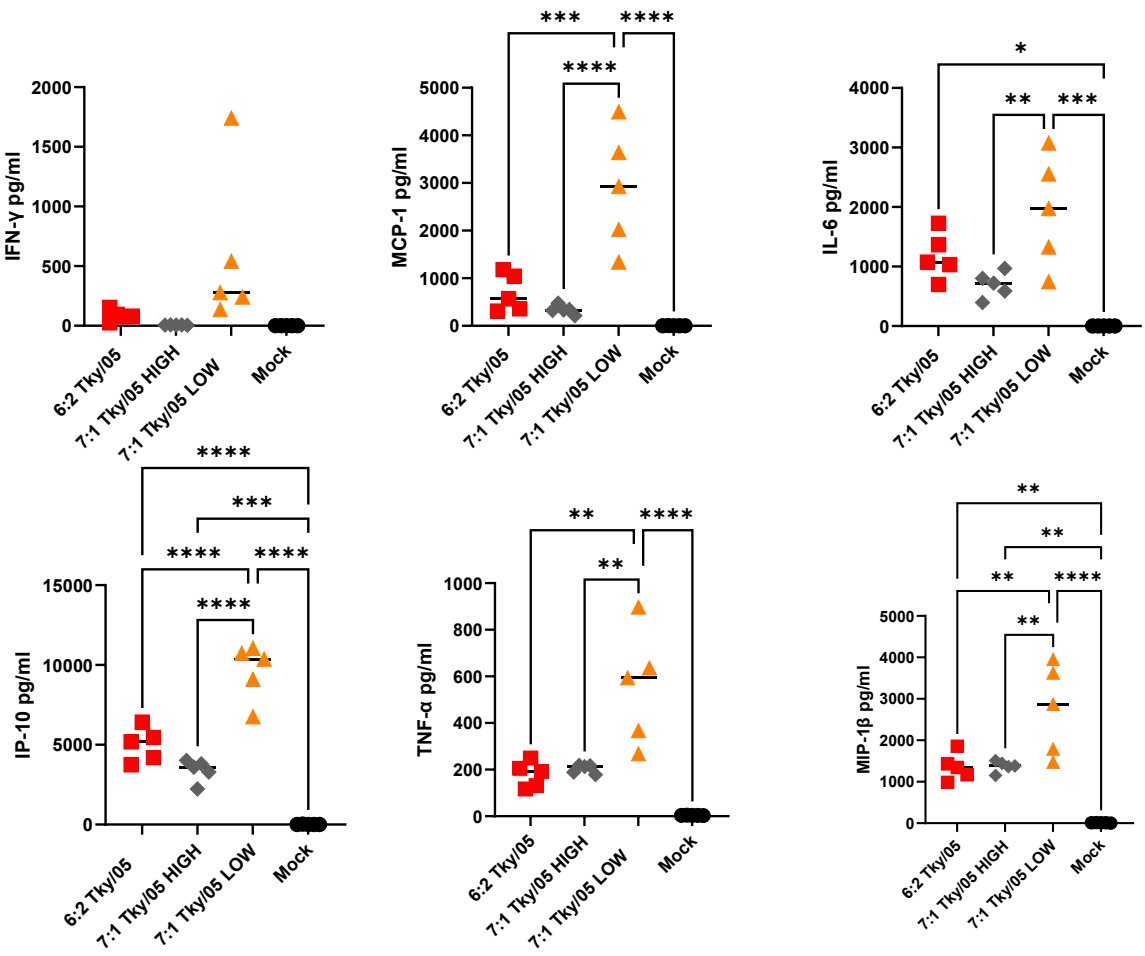

Figure 5.8. Cytokine/chemokine detection in BAL fluid. BAL fluid was harvested at 48 h.p.i. and analysed by multiplex ELISA (MSD (n = 5 per group). Variance among groups was calculated by a one-way ANOVA with Tukey post hoc test for multiple comparisons. * P<0.05, ** P<0.01, ***P<0.001, ****P<0.0001. BAL fluid taken by Dr John Tregoning and analysis performed by Ms Katie Flight. This figure forms part of Figure 6 in (Penn et al., 2022).

5.2.3 DVGs are detected *in vivo*

To confirm that DVGs can be detected *in vivo*, we conducted RT-PCR using the RNA extracted from the murine lung homogenates. By using internal and terminal primers we amplified both PB2 segment and PB2 DVGs arising early post infection (Figure 5.9). By 6-24 h.p.i., PB2 DVGs can be observed in some of the lungs from the 7:1 Tky/05 HIGH and 7:1 Tky/05 LOW infected mice. The short PCR bands observed are the same length as those observed in the virus stock

(Chapter 4, Figure 4.6). This is in direct contrast to the lungs harvested from the 6:2 Tky/05 infected mice where no DVGs were detected at these early time points. However, later in the infection (48-96 h.p.i.), faint small bands can be detected in the 6:2 Tky/05 infected murine lung homogenates and their sizes do not correlate with DVGs already identified in the viral stock, suggesting *de novo* generation. Conversley, at these later time points, PB2 DVGs were still present in some of the 7:1 Tky/05 HIGH and 7:1 Tky/05 LOW infected murine lungs but the length of these bands were identical to those observed earlier in the infection and in the virus stock. We observed very strong PCR bands for an internal portion of the FL PB2 segment in many 7:1 Tky/05 LOW infected mice lungs at all time points analysed. This is not observed for the other two viral infections; the 7:1 Tky/05 HIGH mouse lungs display highly variable bands at all time points analysed whereas the 6:2 Tky/05 infected group show weak bands in some of the murine lungs at 6 h.p.i., but by 96 h.p.i., all 5 murine lungs contained strong bands for the PB2 segment. There were no bands present in the mock infected murine lung analysed for either an internal portion of the FL PB2 segment or PB2 DVGs.

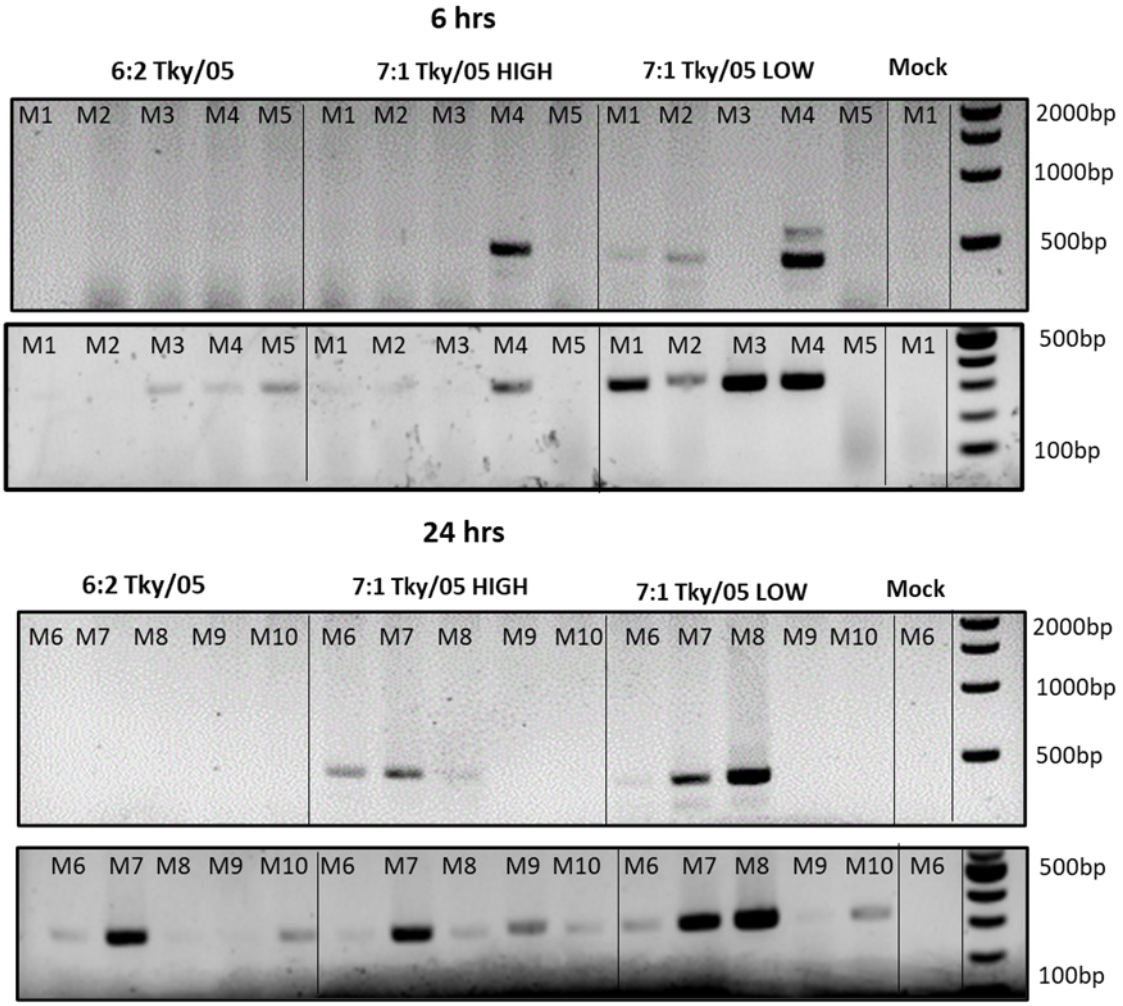

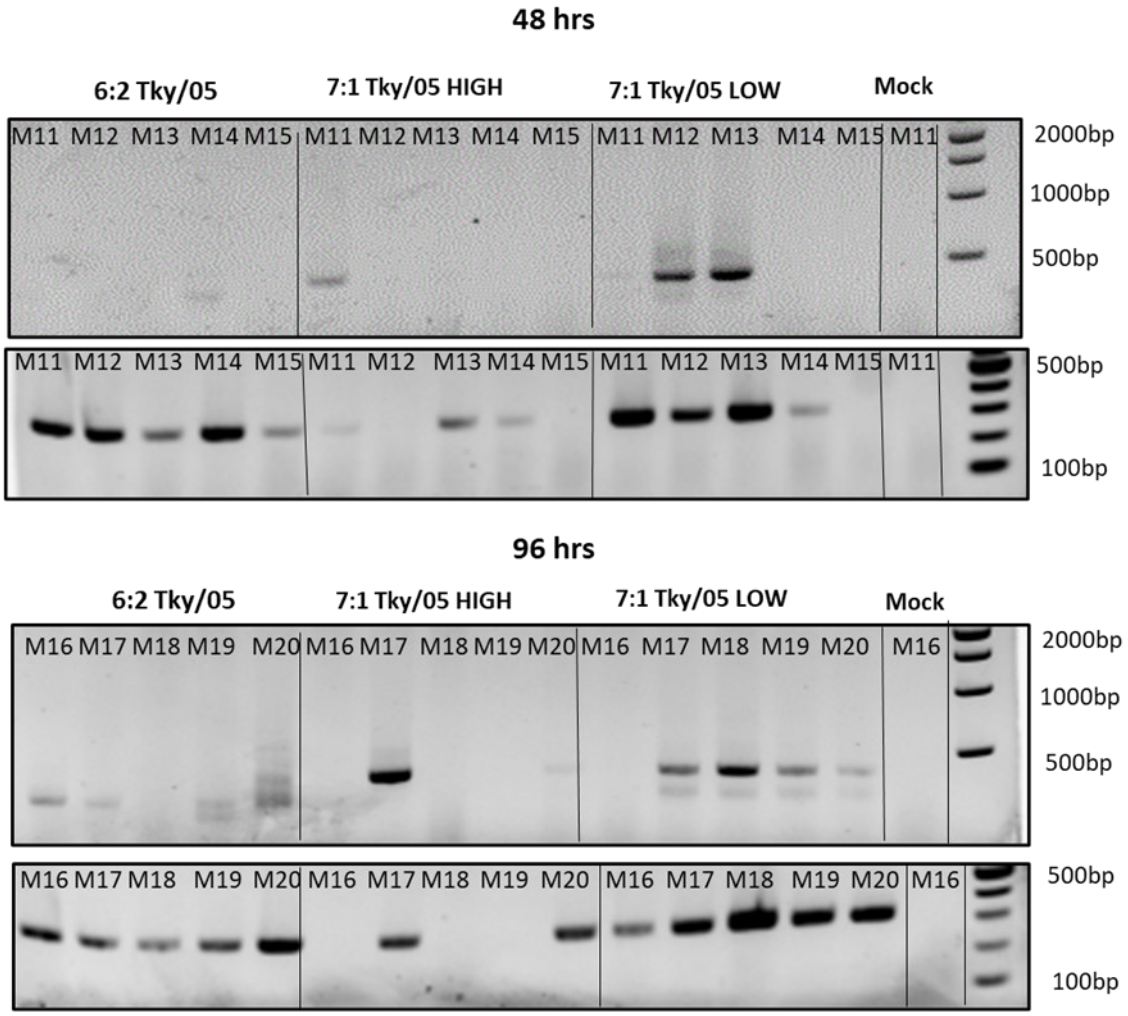

Figure 5.9. PB2 DVGs are detected in the lung homogenates of infected mice. Murine lungs were harvested at 6, 24, 48 and 96 h.p.i and homogenised. Total RNA was extracted, DNase I on-column treated, and concentration measured by spectrophotometry. 2µg RNA was used for cDNA synthesis using the Uni12 primer and superscript IV. RT-PCR was performed using Tky/05 PB2 terminal primers (upper panels) or Tky/05 PB2 internal primers (lower panels). M1-M20 correspond to the lungs harvested from each mouse per group (n =5 per virus at each time point). Only 1 murine lung from the mock group was analysed at each time point. PCR products were visualised on 1.5% agarose gels with GelRed.

We next extracted, cloned and sequenced the small bands present in the lung homogenates harvested at 96 h.p.i. from the 6:2 Tky/05 infected mice (Figure 5.9) to confirm these were DVGs and to identify the junctions. As expected, these were DVGs and contained different junction sites to those previously identified in the virus stock (Figure 5.10). We observed a DVG 324nt in length containing identical junction sites in 3/4 murine lungs.

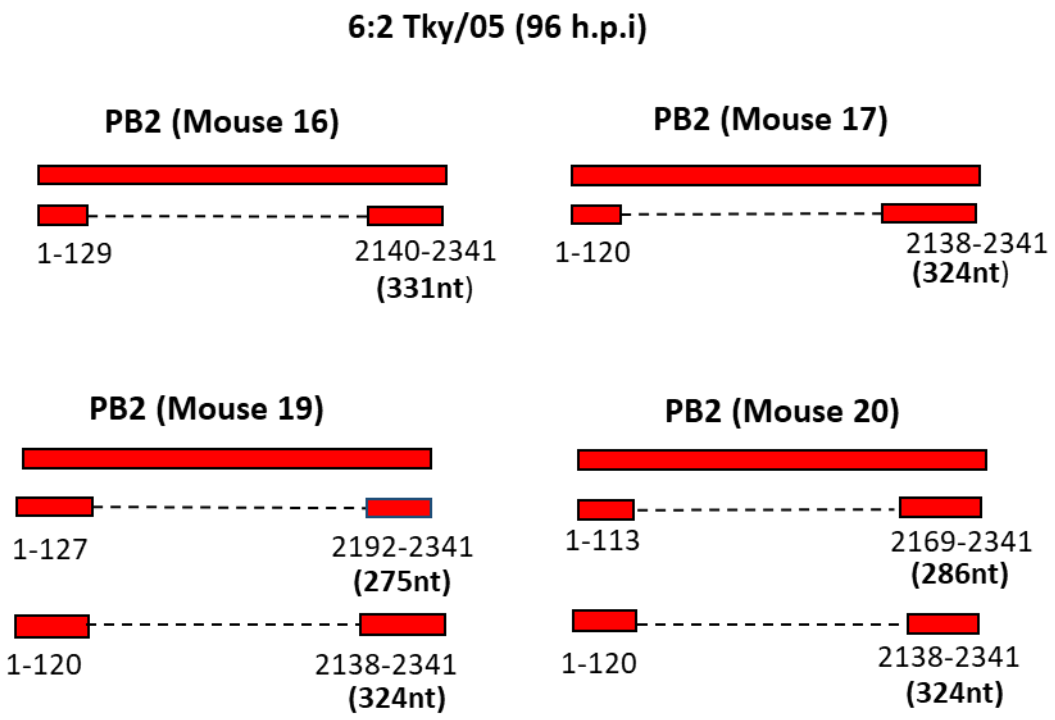

Figure 5.10 Genetic characterisation of PB2 DVGs from the 6:2 Tky/05 infected murine lungs. All small PCR bands that were amplified using PB2 Terminal primers using RNA extracted from murine lungs harvested at 96 h.p.i., were gel extracted, cloned into TOPO vectors and Sanger sequenced. Coloured rectangles represent the 5' and 3' ends of the DVGs and dotted connecting lines represent the large internal deletion. The junction positions are shown underneath, and all are depicted in the positive sense.

To gain a more thorough and robust analysis of DVG content throughout these *in vivo* infections, we also characterised DVGs in the lung homogenates using NGS and ViReMa which has previously been used to detect influenza deletion DVGs (Alnaji et al., 2019). This NGS approach involves PCR amplifying all eight vRNA segments followed by sequencing using the illumina MISeq platform. The algorithm ViReMa is used to identify viral recombination junction locations thereby allowing precise mapping of breakpoints (Routh & Johnson, 2014). We analysed 2 murine lungs at each time point (6, 24, 48 and 96 h.p.i.) per virus apart from the 6:2 Tky/05 group where at 48 and 96 h.p.i, only 1 murine lung was analysed. This was due to technical difficulties during library construction, resulting in insufficient yield for sequencing. Table 5.1 summarises the DVGs detected in the murine lungs by ViReMa (a more comprehensive summary can be found in the Appendix). As expected, some of the DVGs detected in the lungs by NGS were those previously cloned and Sanger sequenced from the viral stock (Chapter 4, Figure 4.6). We also identified the same 324nt long DVG (break points:

120 and 2138) in the 6:2 Tky05 infected mouse lung (M17) at 96 h.p.i. that we had characterised through cloning and sequencing from the same murine lung (Figure 5.10). Additionally, we obtained reads for the 331nt long DVG (break points: 129 and 2140) at 96 h.p.i., that we had previously identified in the lung of mouse 16 via cloning and sequencing (Figure 5.10), in the lung of mouse 17 by NGS. There were also many DVGs identified that we hadn't previously detected in the virus stocks which likely represent newly synthesised DVGs. We observed that at the later time points analysed (48 and 96 h.p.i.), all mice from the 7:1 Tky/05 LOW and 6:2 Tky/05 groups showed an increase in the diversity of the DVGs detected derived from all of the polymerase segments. This was not mirrored in the 7:1 Tky/05 HIGH group where the numbers of individual DVGs were relatively high at 6 h.p.i., and were not so drastically different to those detected at later time points. Interestingly, no PB1 DVGs were supported by >30 reads from the 6:2 Tky/05 infected mice at any of the observed time points. The PB2 segment generated the most diversity for all infected mice. We also observed few DVGs that mapped to non-polymerase segments; only an NP and HA DVG were identified. Interestingly, the NP DVG was observed in all infected mice at various time points, even from the mice infected with the independently rescued 6:2 Tky/05 virus.

Virus	Time point	PB1 DVGs	PB2 DVGs	PA DVGs	NP DVGs	HA DVGs
6:2 Tky/05	6 hrs		**277-1872**			
6:2 Tky/05	24 hrs		**277-1872, 209-1927**		243-919	
6:2 Tky/05*	48 hrs		**209-1927, 277-1872,** 162-2138	295-1812		
6:2 Tky/05*	96 hrs		120-2138, 162-2097, **277-1872**, 165-2138, 190-2039, 129-2140, 217-2031	138-1958	243-919	
7:1 Tky/05 HIGH	6 hrs	**244-2107,** 210-2308, 361-2040	**116-2033, 242-2000,** 149-2068, 158-2114, 110-2130, 243-2121	**129-2002, 128-1974, 162-1971**		91-1510
7:1 Tky/05 HIGH	24 hrs	**244-2107**	**116-2033, 242-2000**, 149-2068, 158-2114, 110-2130	**129-2002, 128-1974**	243-919	
7:1 Tky/05 HIGH	48 hrs	**244-2107**, 210-2038, 361-2040	**116-2033, 242-2000,** 149-2068, 158-2114, 110-2130, 244-2027, 243-2121, 215-2003	**128-1974 , 129-2002, 187-1971**		
7:1 Tky/05 HIGH	96 hrs	**244-2107**	**116-2033, 242-2000,** 149-2068, 190-2039, 158-2114, 110-2130, 243-2121, 215-2019, 215-2003	**129-2002, 128-1974, 187-1971**	243-919	
7:1 Tky/05 LOW	6 hrs	**244-2107**	**116-2033, 242-2000,** 149-2068	**128-1974, 129-2002**	243-919	
7:1 Tky/05 LOW	24 hrs	**244-2107,** 231-2097, 210-2038	**116-2003, 242-2000,** 149-2068, 175-2099, 158-2114, 110-2130, 120-2118	**129-2002, 128-1974, 187-1971, 162-1971**	243-919	
7:1 Tky/05 LOW	48 hrs	**244-2107,** 210-2038, 231-2097	**116-2033,** 149-2068, **242-2000,** 158-2114, 243-2121, 175-2099, 110-2130	**129-2002, 128-1974, 187-1971, 162-1971**		
7:1 Tky/05 LOW	96 hrs	**244-2107,** 210-2308, 231-2097, 190-2092	**116-2033, 242-2000,** 149-2068, 158-2114, 175-2046, 110-2130, 243-2121, 120-2118 , 120-2138, 175-2099, 169-2121, 155-2067, 119-2147	**128-1974, 129-2002,** 134-1973, **187-1971, 162-1971,** 204-1973, 164-1885		

Table 5.1. Summary of NGS data compiled from murine lung following ViReMa analysis. All the DVGs detected are those supported by >30 reads and the deletion junctions are shown. Those in bold and underlined have the same deletion junctions as those identified in the corresponding viral stock. DVGs in red

are those that were only observed in 1/2 mice, whereas those in black were detected in both murine lungs. * only 1 murine lung was sequenced.

To compare the levels of DVGs across all samples even though the total number of viral reads differed considerably, we divided the total number of junction reads (detected by ViReMa), by the total number of mapped viral reads (Figure 5.11). This approach will not accurately quantify absolute levels of DVGs due to both uneven genome coverage and PCR bias but allows relative comparison between samples. As expected, at 6 h.p.i., we saw a higher level of all the polymerase DVGs for the mice infected with the 7:1 Tky/05 HIGH stock. However, this changed over time and by 96 h.p.i., there were higher numbers of DVGs detected in the 7:1 Tky/05 LOW infected murine lungs for all 3 polymerase segments. The PB2 segment gave rise to the highest levels of DVGs for all mice across all time points. Of note, the most abundant DVGs detected for both the PB1 and PB2 segments for all viruses were those found in the virus stocks and this was not dependent on the time point analysed (see Appendix for reads per DVG). This was also true for the PA DVGs found in the 7:1 Tky/05 HIGH and LOW murine lungs but not for those infected with 6:2 Tky/05; the PA DVGs arising at 48 and 96 h.p.i. were not detected in the virus stock (Table 5.1).

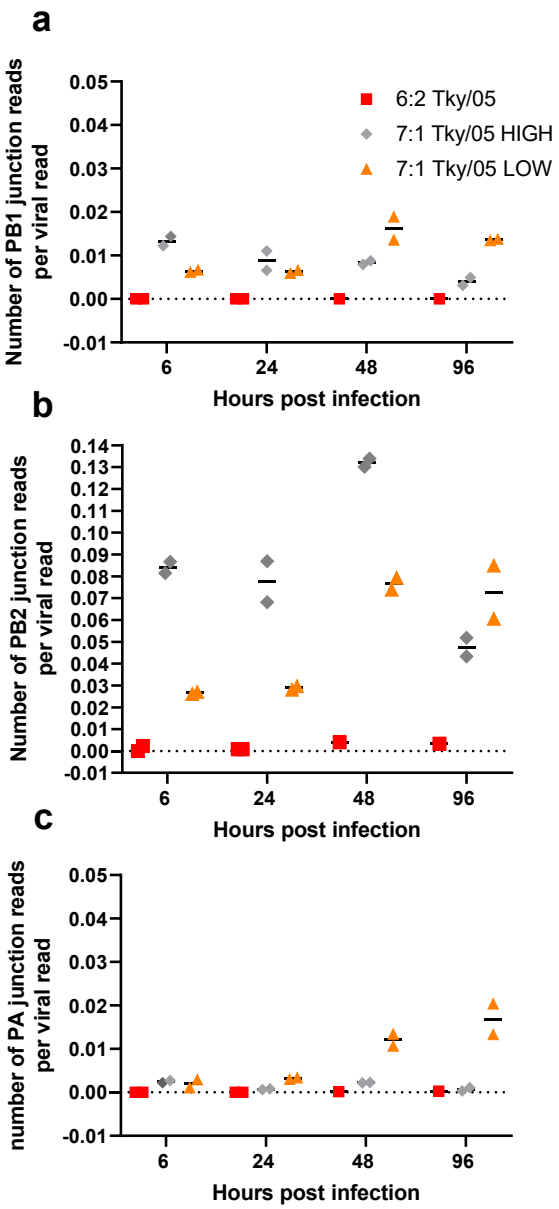

Figure 5.11. Number of DVG junction reads per viral read in infected murine lungs. RNA was extracted from the lungs of the infected mice, NGS performed and analysed by ViReMa. The total number of junction reads per segment were divided by the total number of viral reads per sample. Each data point represents 1 mouse (n = 2 apart from 6:2 Tky/05 48 and 96 h.p.i where only 1 murine lung was analysed). This figure forms Figure 7 in (Penn et al., 2022).

5.3 Discussion

In this chapter, we utilised a virus containing the internal genes of an HPAIV H5N1 subtype and demonstrate that the amount of DVGs present in the starting inoculum can influence disease progression in a BALB/c mouse model. By analysing the kinetics of cytokine expression, viral replication and DVG amplification we showed that these differed remarkably following infection with these viruses and ultimately dictated the outcome.

Our preliminary mouse experiment demonstrated that the 6:2 Tky/05 and 6:2 Eng/09 virus induced similar weight loss curves (Figure 5.1A) but displayed different survival curves (Figure 5.1B). This similarity in weight loss was somewhat surprising as previous work in our laboratory has shown a stark difference between these two viruses (Li et al., 2018). However, infection with the 7:1 Tky/05 virus resulted in a more rapid decrease in body weight and mice reaching the severity limit earlier but could not be correlated to a higher lung load (Figure 5.2). We also could not associate this difference in pathogenicity to the amount of IFN-α secreted in the lungs at day 2 or 3; this was not significantly elevated or decreased when compared to the 6:2 Eng/09 virus (Figure 5.3). As we saw very early type I IFN mRNA expression elevated following infection with the 7:1 Tky/05 virus in A549 cells (Chapter 4, Figure 4.3), we propose that a day 2 time point may have been too late to capture peak IFN-α production in the lung following infection in mice with this virus. Interestingly, we did observe a statistically higher level of IFN-α in the 6:2 Tky/05 infected lungs when compared to the 6:2 Eng/09 virus which agreed with previous findings (Li et al., 2018).

As no RNA was extracted from the lungs of the first mouse experiment, we were limited on the number of cytokines analysed and could not directly probe for DVGs. Therefore, another mouse experiment was performed, using the 6:2 Tky/05, 7:1 Tky/05 HIGH and 7:1 Tky/05 LOW viruses. We also decided to harvest lungs at earlier time points to ensure a more robust assessment of viral replication, DVG and cytokine kinetics. We found that the stock with high DVGs (7:1 Tky/05 HIGH) led to a very mild infection. In contrast, infection with a virus stock with lower starting DVG content but identical genetic background (7:1 Tky/05 LOW) resulted in greater severity. The genetically similar 6:2 Tky/05 virus that contained low levels of DVGs was also pathogenic in mice but did not result in as drastic weight loss as that observed for the 7:1 Tky/05 LOW virus (Figure 5.4).

The extremely mild infection caused by the 7:1 Tky/05 HIGH virus agrees with numerous studies: high levels of DVGs attenuate infection (Genoyer & Lopez, 2019; Swieton et al., 2020; Vasilijevic et al., 2017). We had previously demonstrated that this virus replicated poorly in both A549 and MDCK cells when assessed by plaque assay (Chapter 4, Figure 4.8). This finding was reflected in the murine lungs; viral load as measured by plaque assay was significantly lower than that measured in the 6:2 Tky/05 and 7:1 Tky/05 LOW virus infected lungs (Figure 5.5). We also observed early (6-24 h.p.i.) induction of type I IFN (Figures 5.7A and 5.7D), which has been shown in mice to be beneficial during infections with H5N1 (Szretter et al., 2009). Additionally, we demonstrated earlier IL-1β release in the 7:1 Tky/05 HIGH infected lungs, although this was variable and not statistically significantly higher than the other virus infected lungs or even mock infected (Figure 5.7E). IL-1β in its mature form is dependent on inflammasome activation and mediates the inflammatory response (Lopez-Castejon & Brough, 2011). Interestingly, early NLRP3 inflammasome activation has been shown previously to play a protective role in severe IAV infection (Tate et al., 2016; Thomas et al., 2009). In support of our assessment of the DVG content of these viruses (Chapter 4, Figures 4.5 and 4.6), we observed high levels of polymerase DVGs at 6 h.p.i. by both RT-PCR and NGS in the 7:1 Tky/05 HIGH infected lung homogenates (Figures 5.9 and 5.11, Table 5.1). We therefore propose that the abundance of DVGs in this stock most probably reduced the amplification of infectious virus by directly competing with replication of the standard full genome and for viral resources and packaging (Laske et al., 2016). Furthermore, the activation of a robust early type I IFN response would also inhibit viral replication mediated by expression of ISGs. Indeed, the ISG ZBP1 is significantly upregulated at 24 h.p.i., in the 7:1 Tky/05 HIGH infected murine lungs (Figure 5.7B). Overall, we did not find any indication that this high DVG stock led to immunopathology.

Infection with the 7:1 Tky/05 LOW virus led to the most severe infection (Figure 5.4). This was coupled with higher viral replication in the murine lungs (Figure 5.5), an increase in infiltrating immune cells in the BAL fluid and significantly higher pro-inflammatory expression in both the BAL fluid and lungs (Figures 5.6-5.8). The kinetics of IFN-α were also different. Although type I IFN is crucial for an antiviral response, elevated and sustained type I IFN can amplify pro-inflammatory responses and exacerbate pathology (Makris et al., 2017). Interestingly, by 96 h.p.i., IFN-α protein was not detected in the 7:1 Tky/05 HIGH murine lungs but was found in

some of the 7:1 Tky/05 LOW and 6:2 Tky/05 infected lungs. Peak IFN-α expression in the Tky/05 LOW infected lungs was also delayed when compared to the 7:1 Tky/05 HIGH virus, with both mRNA and protein levels peaking 1 day later (Figure 5.7). This delay was likewise observed for the 6:2 Tky/05 infection. It is therefore no surprise that viral load measured by PFU was higher for both these viruses when compared to the 7:1 Tky/05 HIGH virus; there was however, a modest but significant increase at 48 h.p.i in the lungs of the 7:1 Tky/05 LOW infected mice when compared to the 6:2 Tky/05 (Figure 5.5). Although severe disease caused by HPAIVs can be associated with high viral load, it is more closely correlated with hypercytokinemia and immunopathology (Peiris et al., 2010; Perrone et al., 2008). This agrees with our results; the pro-inflammatory cytokines TNF-α and IL-6, along with the chemokines MCP-1, IP-10 and MIP-1β were all significantly elevated only in the 7:1 Tky/05 LOW virus infected murine lungs (Figure 5.8). As the emergence of DVGs in viral infections coincides with the production of cytokines (Sun et al., 2015; Tapia et al., 2013), it seems likely that it is the disparity in DVG content of these viruses that underlies the difference in their cytokine levels. The 7:1 Tky/05 LOW had more abundant DVGs in the initial viral stock when characterised by RT-PCR than the 6:2 Tky/05 virus (Chapter 4, Figure 4.6), as well as higher levels of DVGs at all time points in the murine lungs determined by NGS (Figure 5.11). Importantly, the high pro-inflammatory cytokine signature observed by the 7:1 Tky/05 LOW virus is in keeping with other studies examining cytokine induction in severe influenza infections and highlights the role of hypercytokinemia in H5N1 pathogenesis (Belser & Tumpey, 2013; de Jong et al., 2006).

We cannot ignore the fact that the differences in severity between the 6:2 Tky/05 and 7:1 Tky/05 LOW could simply be attributed to the different NA. The H5N1 NA has previously been shown to enhance virulence in mice due to its short stalk length (Matsuoka et al., 2009; Zhou et al., 2009). However, in both studies the H5N1 NA was paired with its matched H5 HA. As HA receptor affinity and NA sialidase activity needs to be carefully balanced, it is unclear to what extent the mismatch of the HA/NA pairing in our study would impact the infection dynamics. Indeed, previous work has showed that when the short stalk Tky/05 NA was paired with the H1N1pdm09 A/Eng/195/2009 HA, this virus showed a reduced ability to initiate an infection in the presence of mucus when directly compared to an identical virus with its cognate NA or a long stalk NA (Blumenkrantz et al., 2013). It should also be noted that we have observed a similar weight loss curve to the 7:1 Tky/05 LOW presented in this study when

using a different preparation of the 6:2 Tky/05 virus (Li et al., 2018). Therefore, differences in pathogenicity are more likely to reflect the starting levels of DVGs in the inocula.

A study examining copy-back DVG (cbDVG) accumulation in both nasal wash and nasopharyngeal swab samples from humans infected with RSV demonstrated a clear link between the timing of DVG generation and severity (Felt et al., 2021). DVGs detected early in infection correlated with a mild outcome whereas DVGs generated later or that were sustained were associated with more severe disease. This is somewhat similar to our results; we observed higher DVG levels early (6 h.p.i.) in the lungs of the mice infected with the 7:1 Tky/05 HIGH virus that caused minimal weight loss, whereas at 96 h.p.i, DVGs were the most abundant in the 7:1 Tky/05 LOW infected murine lungs and this infection resulted in severe weight loss (Figure 5.10). This could be explained by the following scenario: at the early stages of infection (6-24 h.p.i.), DVG levels in the 7:1 Tky/05 LOW infected mice were too low to trigger the innate immune response, leading to unchecked viral replication. At later time points (24-48 h.p.i.) when DVGs had accumulated to sufficient levels for activation of the immune system, this was presumably too late to be protective, as viral loads were already high. This is akin to starting IFN-α treatment in mice during an active influenza infection where it exacerbates immunopathology (Davidson et al., 2016). Therefore, the timing of DVG generation and amplification most likely contributes to the differences in severity we observed.

One major caveat of the work presented in this chapter is that like any animal model, infections in mice may not necessarily reflect the same findings as a human infection due to fundamental immunological differences (Mestas & Hughes, 2004). Perhaps the most notable, is the lack of a functional Mx protein which renders most inbred mouse strains (including BALB/c), highly susceptible to influenza infections (Staeheli et al., 1988). This lack of Mx is particularly important when assessing infection outcomes as Mx is an ISG and is believed to be important for the antiviral response, especially since avian strains have been shown to be more susceptible to Mx restriction than human adapted isolates (Deeg et al., 2017). Interestingly, Hein et al. (2021a), demonstrate the importance of a functional Mx protein in the mouse model when assessing the antiviral activity of the well-characterised PR8 DIP DI244. Here they show stark differences in survival rates between two mouse strains. When mice had no functional Mx protein (D2-Mx1$^{-/-}$), administration of DI244 alongside PR8 virus

resulted in no difference in weight loss when compared to virus alone and all mice succumbed to infection by day 7. Strikingly, when the same experiment was performed in mice that contained the human Mx1 gene (D2-Mx1$^{r/r}$), co-treatment with the DI244 DIP reduced body weight loss and resulted in 100% survival. This is in direct contrast to our results, as the BALB/c mice used in our *in vivo* infections are Mx deficient, yet we still observed a great difference in weight loss between the 7:1 Tky/05 HIGH and the 7:1 Tky/05 LOW/6:2 Tky/05 infected mice. This suggests that diminished viral replication in the 7:1 Tky/05 HIGH virus infection is largely due to DVG interference with standard viral replication and not the interferon response, although we cannot rule out that other ISGs (and not Mx) are mediating this antiviral effect.

Another limitation is that although the NGS approach we used for detection of DVGs in the infected murine lungs has been shown to accurately map the junctions for influenza DVGs, it is RT-PCR based (Alnaji et al., 2019). This means that accurate quantification of the DVGs in the viral population cannot be determined due to both bias for shorter lengths and uneven genome coverage. Indeed, one study comparing RT-seq with RT-PCR seq for DVG detection indicates that although RT-PCR seq was more sensitive it resulted in overestimation of the frequency of DVGs and this bias was both length and sequence dependent (Boussier et al., 2020). Interestingly, they observed that a 424-nt long PB2 DVG was detected at a much higher frequency than a 425-nt long PB1 DVG when their actual frequencies were identical. This could explain why we detected more abundant DVGs derived from the PB2 segment than from the PB1 and PA segment (Figure 5.11). Ideally, if time allowed, we would have also explored a direct RNA-seq approach to accurately quantify DVGs, rather than comparing the relative number of junctions reads per viral read for our samples.

Overall, this chapter expands on the results observed in Chapter 4; DVGs can modulate the innate immune response and impact on viral replication. Here we show that this can influence the outcome of infection when using virus stocks that contain the internal genes of the HPAIV H5N1; crucially the timing of both DVG amplification and pro-inflammatory cytokine production impact disease outcome and our results show that not all DVG generation reduces viral virulence in the BALB/c mouse model.

Chapter 6 Investigating the viral factors that impact the generation of aberrant RNA replication products and activation of innate immunity by the HPAIV polymerase

6.1 Introduction

Erroneous replication of the influenza viral genome can result in aberrant RNA replication products such as DVGs and mvRNAs that can play a role in innate immune activation (Elshina & Te Velthuis, 2021). Numerous studies have linked the presence of DVGs during viral infection with an increased type I IFN response (Tapia et al., 2013; Wang et al., 2020; Xue et al., 2016). Although certainly physiologically relevant, the use of virus makes the analysis of *de novo* generation more difficult; many virus stocks already contain DVGs and their amplification during infection hinders efforts to identify ones that are newly synthesised. This is a universal feature of virus propagation; influenza DVGs have been reported to be present in both egg and cell propagated virus stocks as well as in the live attenuated influenza vaccine (LAIV) (Gould et al., 2017; Xue et al., 2016). Indeed, the recombinant virus stocks used throughout this thesis contain DVGs even when passaged at low MOI. In the first part of this chapter, we will therefore use vRNP reconstitution assays for assessing *de novo* production as this enables the assessment of any polymerase-driven RNA products in the absence of virus. Such assays have been routinely used in similar studies demonstrating their suitability (Te Velthuis et al., 2018). Of note, this is not a concern for mvRNAs as these can be made independently of NP and are believed not to form canonical vRNPs and therefore are not subsequently packaged into virions (Turrell et al., 2013).

Factors orchestrating the formation of aberrant RNA replication products are still poorly understood but a role for NP levels and specific polymerase amino acid residues have been implicated. Nilsson-Payant et al. (2021), using vRNP reconstitution assays demonstrated that when levels of NP were insufficient to support full genome replication, mvRNAs were synthesised leading to activation of the IFN-β promoter. They also showed that in infections using an influenza virus engineered to be compromised in its ability to express NP protein, more DVGs were produced resulting in higher levels of IFN induction. Liu et al. (2019), also found that when NP was omitted from vRNP reconstitution assays, aberrant RIG-I activating RNAs were generated. Te Velthuis et al. (2018) observed that when NP and polymerase levels

were imbalanced, more mvRNAs were synthesised. Furthermore, they also demonstrated that mvRNAs were more readily detected from HPAIV infections in mammalian cells when directly compared to infections using a mammalian adapted strain. Moreover, specific avian-associated mutations in the PB2 gene conferred this phenotype. Interestingly, mutations in other viral genes that affect DVG formation have been identified such as in the PA gene (Fodor et al., 2003).

In this chapter we wish to examine the extent to which Tky/05 polymerase can generate aberrant RNA replication products *de novo* and to test whether these are immunostimulatory. We will also examine the impact on both aberrant replication and IFN induction when NP is limited. Furthermore, we will analyse the effect of mammalian adaptive amino acids in the PB2 protein. Using vRNP reconstitution assays we will determine whether any of these substitutions alter mvRNA production and IFN induction compared to the WT Tky/05 PB2. Additionally, we will also rescue viruses incorporating these mutations and analyse growth kinetics as well as investigating replication and cytokine induction in BMDMs. Finally, we will determine pathogenicity in the mouse model.

6.2 Results

6.2.1 The HPAIV Tky/05 polymerase generates immunostimulatory aberrant replication products

To investigate whether the HPAIV Tky/05 polymerase generates aberrant replication products *de novo*, we utilised the vRNP reconstitution assay as previously described in Chapter 4 (Figure 4.15). The Tky/05 viral polymerase (PB1, PB2 and PA) and NP pCAGGS plasmids as well as a vRNA segment (pPolI plasmid) were reconstituted by transfection into HEK293T cells (schematic of methods outlined in Figure 6.1).

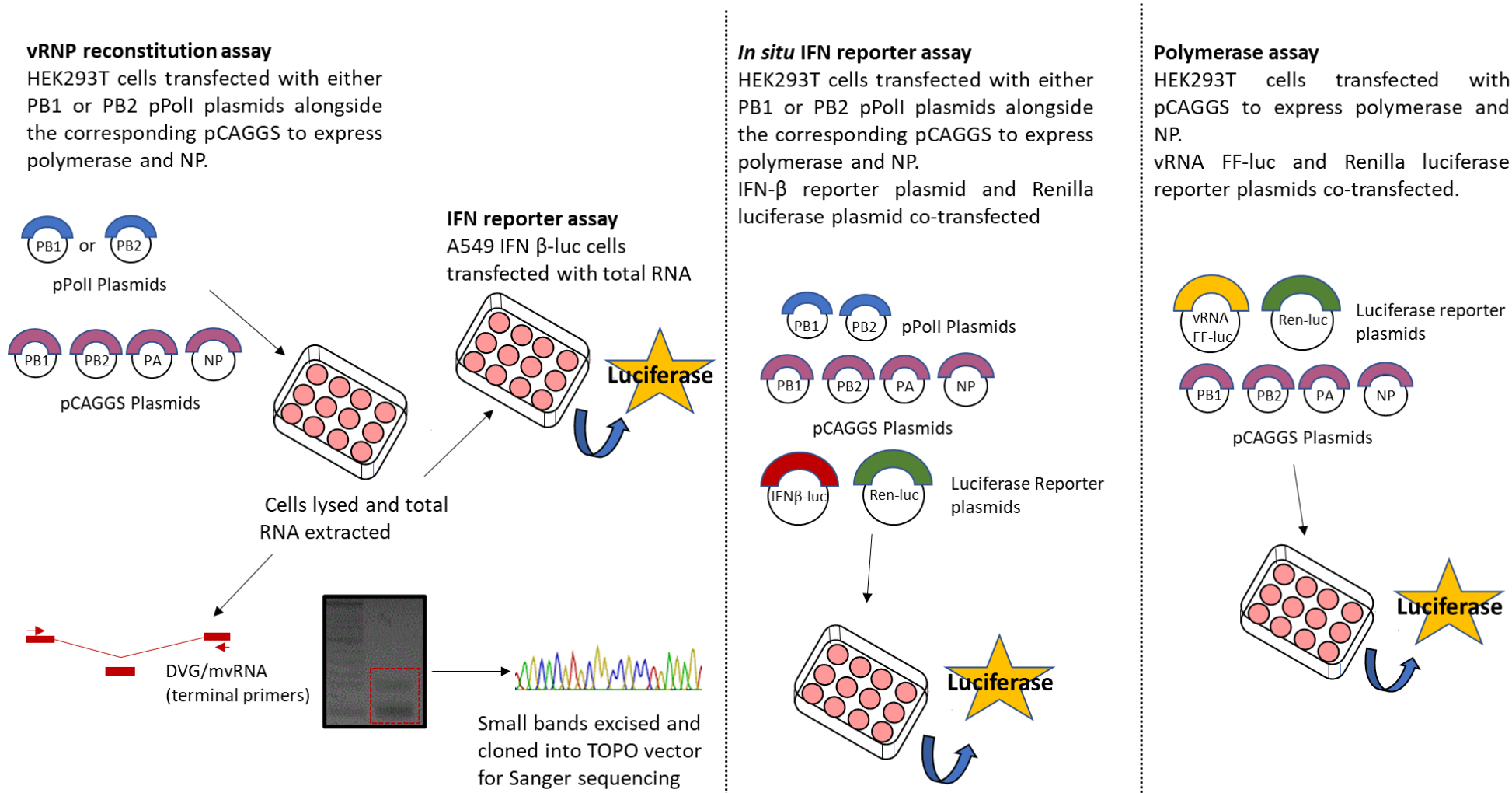

Figure 6.1. Schematic of techniques used throughout Chapter 6

The pPolI plasmid encoding the PB1 segment was initially chosen to provide the vRNA template as DVGs and mvRNAs derived from PB1 have been seen previously (Saira et al., 2013; Te Velthuis et al., 2018). By extracting total RNA, followed by RT-PCR using (Uni12 and Hoffman) PB1 primers that bind to the terminal ends, we were able to detect small PCR products, likely representing aberrant RNAs (Figure 6.2A). Importantly, when a plasmid encoding a subunit of the polymerase was omitted from the transfection (2P), no small bands were detected. This demonstrates that these replication products were only generated when the whole trimeric polymerase was present. To establish these small bands were not simply artefacts of PCR, we analysed their sequences. Gel isolation followed by TOPO cloning and Sanger sequencing revealed that the small PCR bands were mvRNAs/DVGs ranging from 74-193nt in length (Figure 6.2B). In parallel, as a control for functional polymerase activity, the pPolI PB1 plasmid was replaced with a pPolI luciferase reporter plasmid and normalized to Renilla luciferase activity. As expected, we observed polymerase activity when the trimeric polymerase and NP were transfected but this was abolished when only 2P was transfected (Figure 6.2C).

A

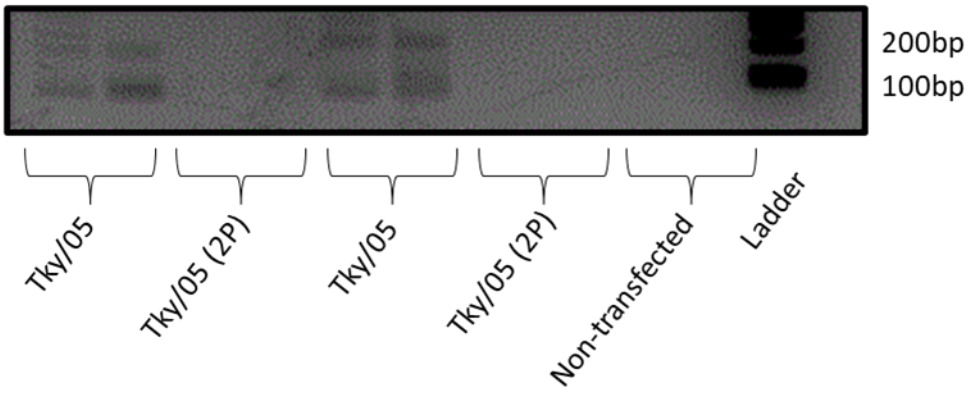

B

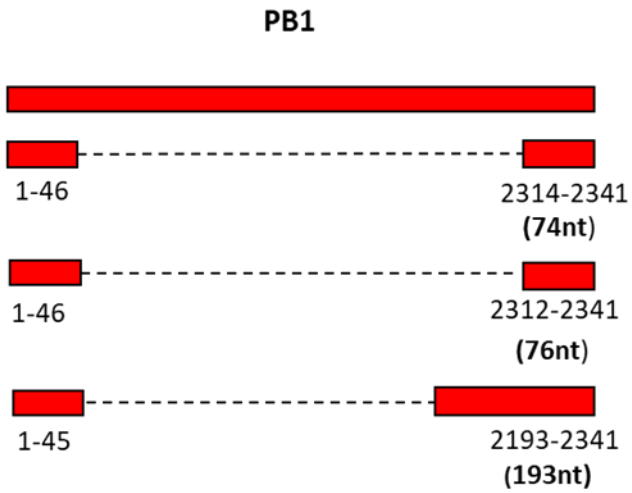

C

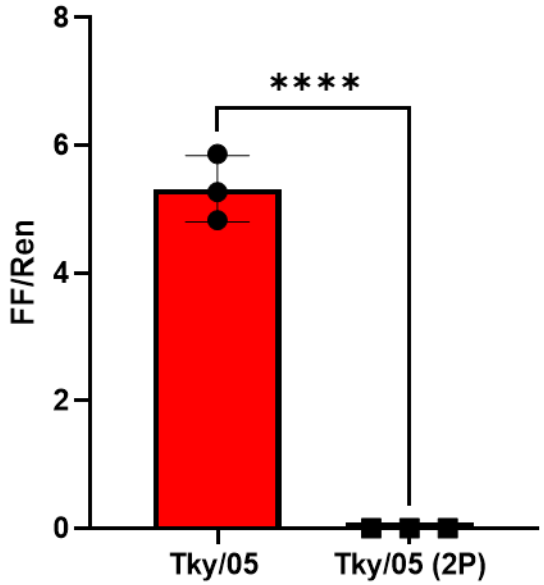

Figure 6.2. The Tky/05 polymerase generates aberrant RNA replication products. A) vRNP reconstitution assays were performed in HEK293T cells. pCAGGS expression plasmids encoding the viral polymerase (3P-PB1,

PB2, PA) and NP from H5N1 Tky/05 were co-transfected with a pPolI plasmid encoding the Tky/05 PB1 vRNA in a 2:2:1:4:2 ratio. Transfections were also performed where empty pCAGGS plasmid was used instead of PB1 pCAGGS plasmid (2P). Total RNA was extracted 24 hours post transfection and cDNA synthesised using Uni12 primer. RT-PCR was used using PB1 Hoffman primers that bind to the 3' and 5' termini and a short extension time of 10 seconds. PCR products were ran on a 2% agarose gel with GelRed by electrophoresis. B) PCR products were gel excised and ligated into TOPO vectors and plasmid DNA was Sanger sequenced. Sequences were mapped to the full-length Tky/05 PB1 segment using Geneious and junctions calculated. Coloured rectangles represent the 5' and 3' ends of the DVGs and dotted connecting lines represent the large internal deletion. The junction positions are shown underneath, and all are depicted in the positive sense. Length of mvRNA/DVG is shown in brackets. C) vRNP reconstitution assay performed as described for A) but a pPolI-firefly luciferase minigenome reporter plasmid was used instead of the PB1 pPolI plasmid. A Renilla pol II plasmid was also transfected (FF: Ren is 2: 0.25) and data is shown as firefly activity normalised to Renilla, plotted as mean ± SD from triplicate samples. The difference between the Tky/05 and Tky/05 (2P) groups was calculated by a two-tailed unpaired t-test **** P<0.0001.

To determine whether other segments give rise to aberrant RNA replication products, we performed a further vRNP reconstitution assay where we replaced the pPolI plasmid encoding the PB1 vRNA template with one encoding PB2. We observed bands smaller than 300bp (Figure 6.3A). Sanger sequencing revealed that the upper band from the Tky/05 transfection was a DVG with a length of 272nt (Figure 6.3B) Sequencing analysis of the lower band from the Tky/05 transfection were of poor quality so unfortunately this could not be confirmed as a mvRNA. To establish whether the replication products were immunostimulatory, we took the total RNA from the vRNP reconstitution assays and transfected these directly into the A549 IFN-β luc reporter cells to assess IFN-β promoter activity (Figure 6.3C). Poly I:C was also transfected as a positive control as this is a potent RIG-I agonist. The transfected RNA from the Tky/05 vRNP reconstitution assays induced type I IFN activity, similar to that induced by transfected Poly I:C. Importantly, RNA isolated from cells expressing a non-functional viral polymerase (2P), nor RNA extracted from non-transfected HEK293T cells did not induce reporter activity. Therefore, the Tky/05 polymerase reconstitution results in RNA that is immunostimulatory.

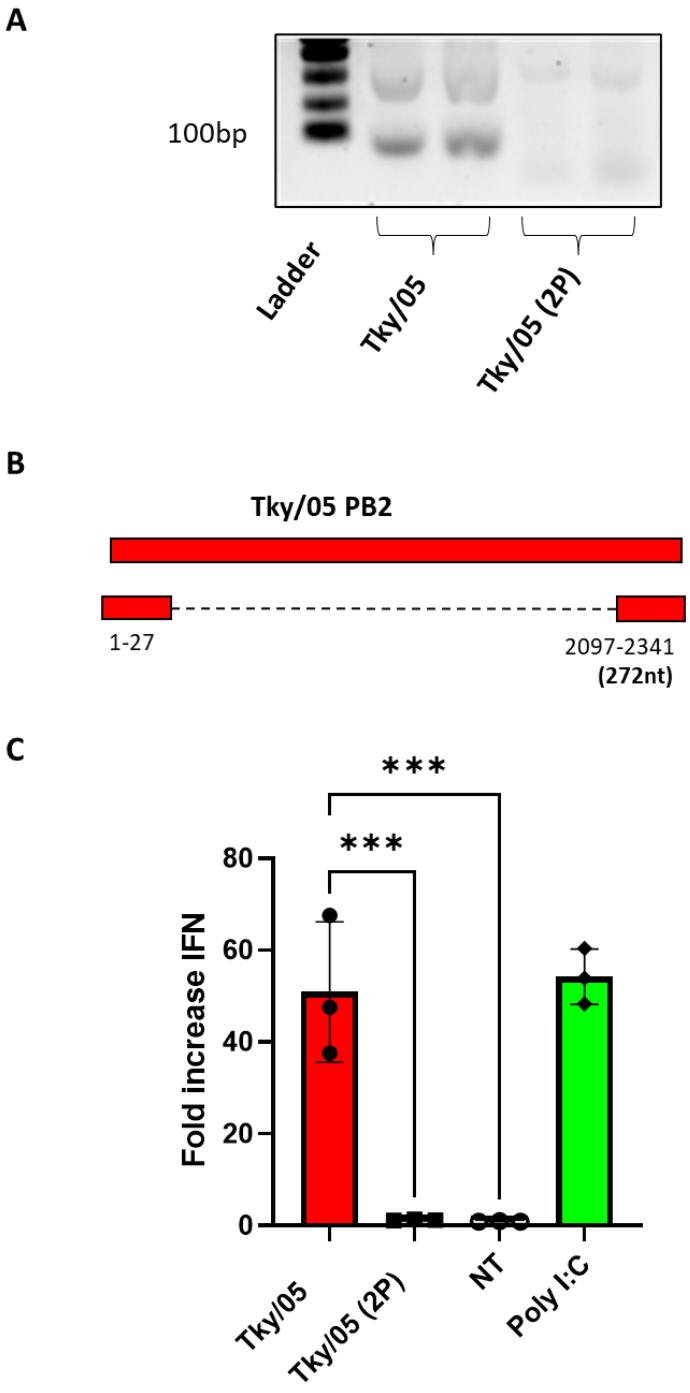

Figure 6.3 Aberrant RNAs derived from the PB2 segment are generated by the Tky/05 polymerase. A) RNP reconstitution assays were performed in HEK293T cells in duplicate. pCAGGS expression plasmids encoding the viral polymerase (3P-PB1, PB2, PA) and NP from H5N1 Tky/05 were co-transfected with a pPolI plasmid encoding the Tky/05 PB2 vRNA in a 2:2:1:4:2 ratio. Transfections were also performed where empty pCAGGS plasmid was used instead of PB1 pCAGGS plasmid (2P). Total RNA was extracted 24 hours post transfection and cDNA synthesised using Uni12 primer. RT-PCR was used using PB2 Hoffman primers that bind to the 3' and 5' termini and a short extension time of 10 seconds. PCR products were analysed on a 2% agarose gel with GelRed by electrophoresis. B) PCR products were gel excised and ligated into TOPO vectors and plasmid DNA

was Sanger sequenced. Sequences were mapped to the full-length Tky/05 PB2 segment using Geneious and junctions calculated. Coloured rectangles represent the 5' and 3' ends of the DVGs and dotted connecting lines represent the large internal deletion. The junction positions are shown underneath, and all are depicted in the positive sense. Length of mvRNA/DVG is shown in brackets. C) 350ng of total RNA extracted from the vRNP reconstitution assay in Figure 6.3A were directly used for transfections in the A549 IFN-β luc reporter cell line. Only 1/2 RNAs was used for transfections. 24 hours later, cells were lysed and luciferase activity measured. Data is expressed as fold increase over mock transfected cells and bars represent mean ± SD from triplicate samples. Variance among the groups was analysed by a students unpaired, two-tailed t-test, *** P<0.001.

6.2.2 Immunostimulatory activity is abolished by CIP treatment of extracted RNA

RIG-I is a key PRR for type I IFN induction in IAV infections (Loo et al., 2008). We therefore explored whether treatment with calf intestinal phosphate (CIP) would abolish the immunostimulatory activity of the RNA extracted from the vRNP reconstitution assays. As it has been shown that RIG-I sensing is dependent on a 5' di or tri-phosphate moiety (Goubau et al., 2014; Hornung et al., 2006), CIP treatment which removes any 5' phosphates would allow us to confirm that RIG-I is responsible for IFN induction. Total RNA from the vRNP reconstitution assays where PB2 vRNA was provided as template (seen in Figure 6.3C) were treated with CIP (+CIP) or not (-CIP). This ensured that only the incubation with the enzyme was responsible for any differences observed and not any of the other conditions during the treatment. We then transfected equal amounts of the treated -/+ CIP RNAs into the A549 IFN-β luc reporter cells alongside untreated Poly I:C as a positive control. RNAs treated with CIP lost all immunostimulatory activity, but not if the enzyme was absent (Figure 6.4). This strongly suggests that the IFN-β promoter activity we observed was mediated through sensing by RIG-I.

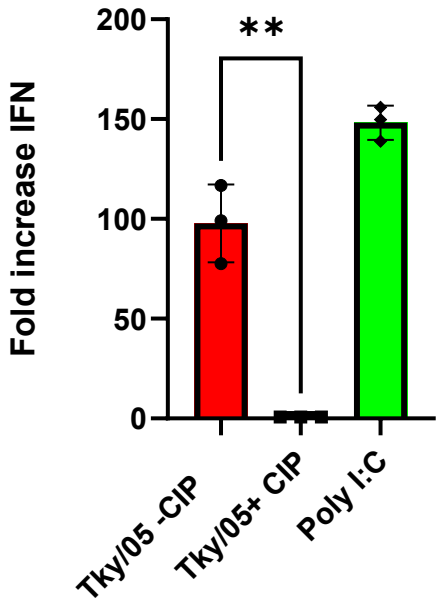

Figure 6.4. Immunostimulatory activity is abolished by CIP treatment of RNA. 1µg of total RNA extracted from the vRNP reconstitution assay in Figure 6.3A where PB2 vRNA was expressed were treated with (+ CIP) or without CIP (-CIP) according to manufacturer's instructions and RNA recovered by Trizol/choloroform extraction and clean up on Zymo RNA clean and concentrator columns. 350ng of +/-CIP treated RNA was directly used for transfections in the A549 IFN-β luc reporter cell line. 1/2 RNAs was used for transfection. 24 hours later, cells were lysed and luciferase activity measured. Data is expressed as fold increase over mock transfected cells and bars represent mean ± SD from triplicate samples. Differences between the +CIP and -CIP RNA were analysed by a students unpaired two-tailed t-test **P<0.01.

6.2.3 Limiting NP increases IFN induction

We performed Tky/05 vRNP reconstitution assays using PB2 as template where the amount of NP transfected was decreased from the standard amount (200ng). RT-PCR analysis using PB2 terminal primers showed that less full-length (FL) PB2 was generated when 50ng was transfected but there was an increased intensity of FL bands when higher amounts of NP were expressed (Figure 6.5A). Conversely, a small PCR band <100nt in length was more abundant when 50ng NP was transfected than for higher NP levels. Additionally, we also performed *in situ* IFN assays which include co-transfecting the *IFN-β* and *Renilla* reporter plasmids alongside the reconstituted vRNP, thus allowing for IFN-β promoter activity to be measured *in situ.* Here, we observed a clear increase in IFN induction when 50ng NP was transfected compared to higher levels (Figure 6.5B). Conversely, we saw less polymerase activity at 50ng

NP when compared to higher amounts of NP (Figure 6.5C). These results suggest that when NP levels are limited in the cell then there is a greater tendency for the formation of aberrant RNA replication products which also correlates with an increase in IFN activity.

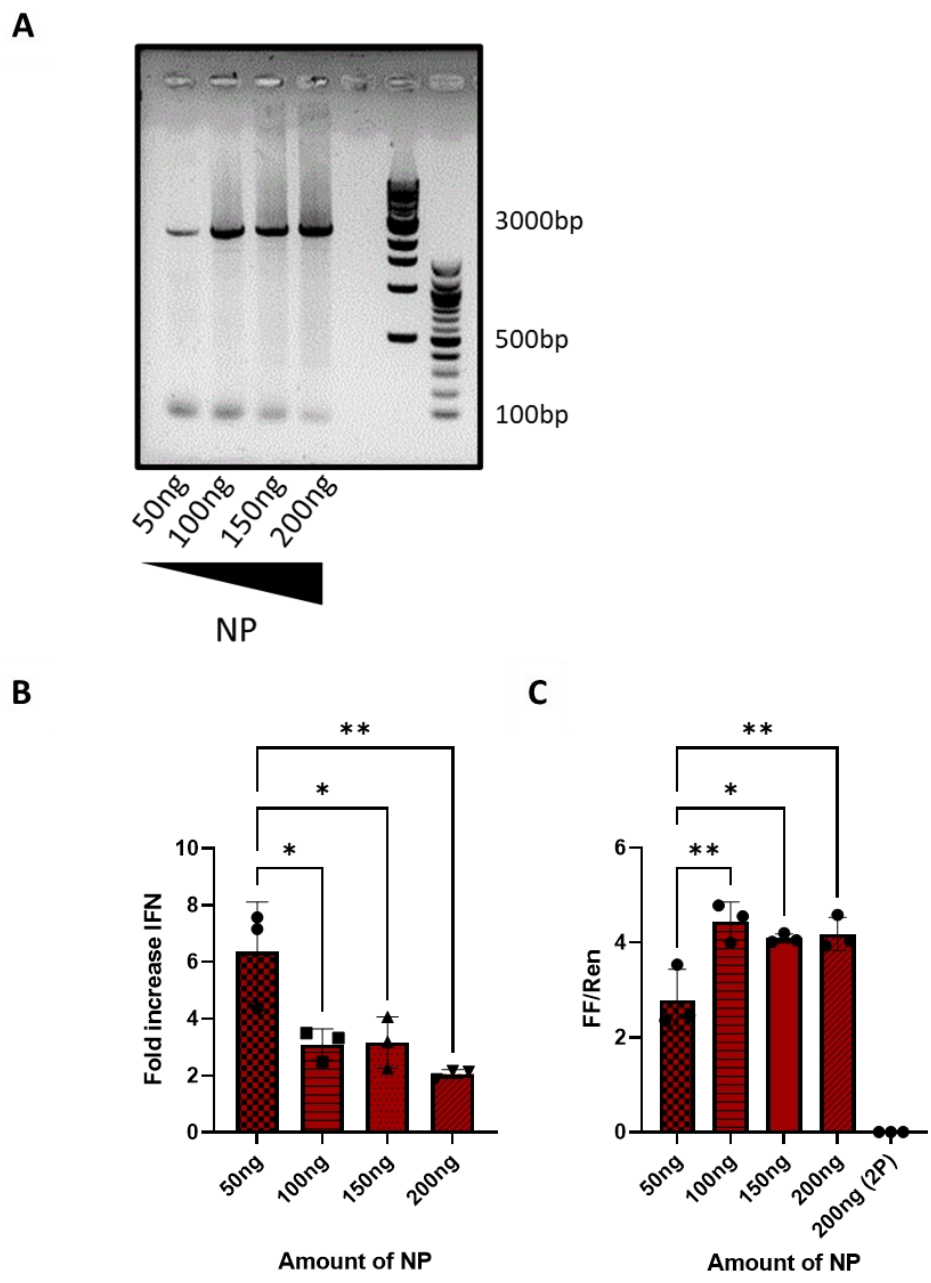

Figure 6.5 Limiting NP expression promotes the production of aberrant replication products and increases IFN-β promoter activity. A) HEK293T cells were transfected with Tky/05 3P and NP expression plasmids, alongside reporter plasmids and PB2 pPolI plasmid. All plasmid ratios were as previously described except for the NP plasmid where the amount of NP transfected is shown. Transfections were also performed where the PB2 pCAGGS plasmid was omitted (2P). To balance the total amount of DNA transfected, an empty pCAGGS plasmid was used. A total of 4 wells per condition were transfected. A) Total RNA was extracted from one

well, 24 hours post transfection and cDNA synthesised using the tagged Uni12 primer. RT-PCR was performed using PB2 Tky/05 terminal primers that bind to the 3' and 5' termini and products were ran on a 2% agarose gel with GelRed by electrophoresis. B) Cells were lysed from the remaining 3 wells at 24 hours post transfection and luciferase measured. Values were normalised to Renilla and expressed as fold increase over 2P. Data represents mean ± SD from triplicate samples and variance among the groups was determined by one-way ANOVA ** P<0.01, * P<0.05 C) RNP reconstitution assay performed as described for A) but a PpolI-firefly luciferase minigenome reporter plasmid was used instead of the PB2 PpolI plasmid. A Renilla pol II plasmid was also transfected (FF: Ren is 1: 0.25) and data is shown as firefly activity normalised to Renilla, plotted as mean ± SD from triplicate samples. Variance among the groups was analysed by a one-way ANOVA with Tukey post hoc test for multiple comparisons, **P<0.01, *P<0.05.

To further strengthen our findings, we performed additional *in situ* IFN assays using either the PB2 or PB1 PolI plasmid to provide the vRNA template and used an intermediate level of NP. When 75ng of NP was transfected (~2.6-fold lower than the standard amount), this induced significantly higher IFN than in transfections where either no NP (0ng) was added or when the standard amount of 200ng was provided (Figure 6.6). This was not dependent on the segment as this phenotype was observed when either the PB1 or PB2 pPolI plasmids were used. Interestingly, there was no difference in IFN-β promoter activity between conditions when the standard amount of NP was transfected or when NP was absent.

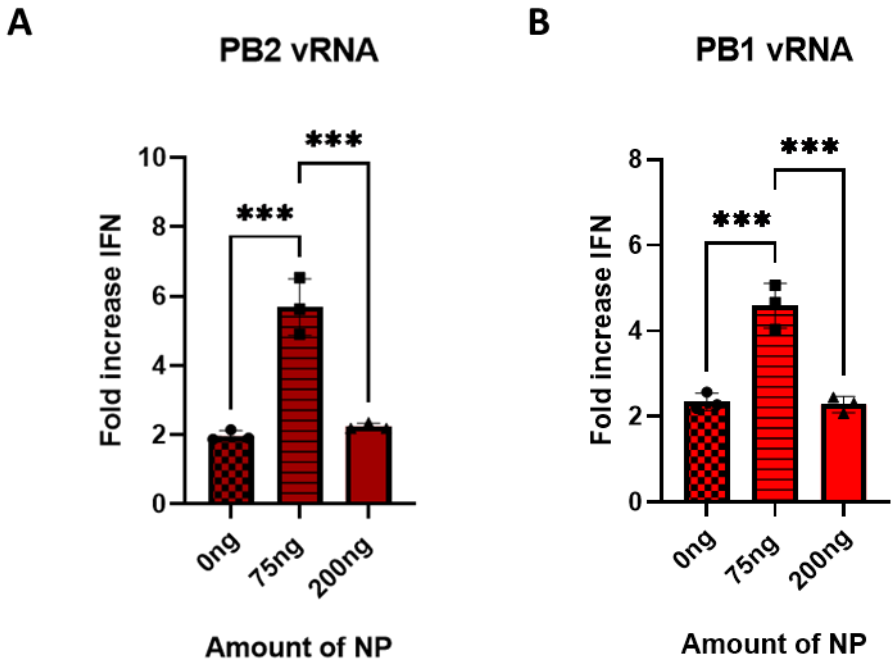

Figure 6.6. Intermediate amounts of NP leads to higher IFN-β promoter activity in vRNP reconstitution assays. HEK293T cells were transfected with Tky/05 3P and NP expression plasmids, alongside reporter plasmids and a PB2 pPolI plasmid (A) or PB1 pPolI plasmid (B). All plasmid ratios were as previously described except for the NP plasmid where the amount of NP transfected is shown. The IFN-β reporter plasmid and Renilla pol II plasmid were transfected at a ratio 2:0.25. Transfections were also performed where the PB2 pCAGGS plasmid was omittied (2P). To balance the total amount of DNA transfected an empty pCAGGS plasmid was used. Cells were lysed 24 hours post transfection and luciferase measured. Values were normalised to Renilla and expressed as fold increase over 2P. Data represents mean ± SD from triplicate samples. Variance among the groups was analysed by a one-way ANOVA with Tukey post hoc test for multiple comparisons, * P<0.05, ** P<0.01.

6.2.4 The introduction of mammalian adaptive mutations into the Tky/05 PB2 segment impact on the type I IFN response but did not alter levels of aberrant RNA replication products in vRNP reconstitution assays

We next focused on two mammalian adaptive residues, position 9 and position 81, due to both previously being associated with affecting type I IFN responses. Position 9 is a key "signature" change associated with adaption to human hosts and has been shown to alter the intracellular localisation of PB2. Over 99% of human IAVs contain an asparagine or threonine at this position in PB2 conferring localisation to both the nucleus and the mitochondria (Long

& Fodor, 2016). Avian isolates predominantly contain an aspartic acid at this position and the PB2 subunits of these strains only localise to the nucleus (Miotto et al., 2008). Mitochondrial localisation of PB2 has been proposed to contribute to IFN control. Previous work has shown that by introducing the mitochondrial localising N into a H5N1 PB2 segment, virulence is increased in a mouse model (Kim et al., 2010). A study by Graef et al. (2010), showed that a non-mitochondrial PB2 caused reduced virulence in mice and a higher induction of IFN-β expression in cell culture. Moreover, Te Velthuis et al. (2018) showed that this residue affected mvRNA production; by introducing the avian associated D into a human adapted PB2 segment that naturally has an N, mvRNA levels were increased. Interestingly, this position resides near to the template exit channel on the trimeric polymerase complex, as does position 81 (monomeric structure shown in Figure 6.7A and dimer structures formed during viral replication are shown in Appendix). By mutating both positions from human adapted to avian adapted residues, they could increase both mvRNA levels and IFN induction, with the double mutant conferring the highest increase (Te Velthuis et al., 2018). We therefore introduced the human adapted mutations (D9N and T81M) alone or together into both the Tky/05 pPolI PB2 and pCAGGS PB2 plasmid as well as creating 6:2 recombinant viruses with these substitutions by reverse genetics. All mutations were verified by Sanger sequencing (Figure 6.7B).

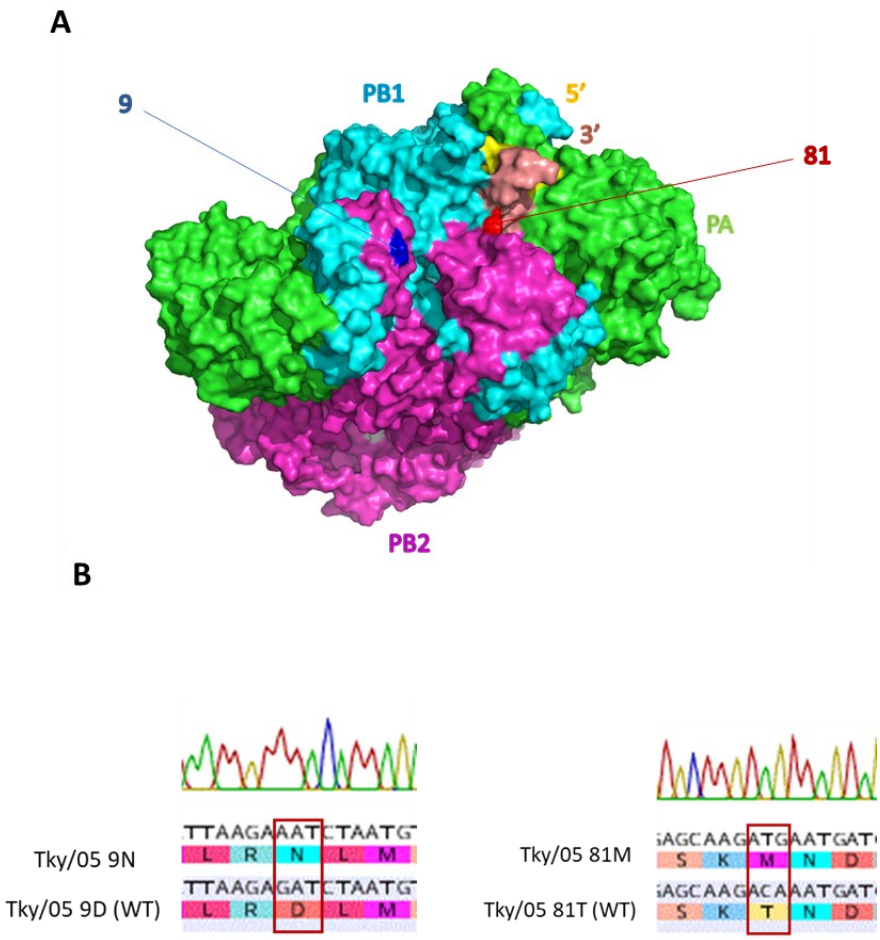

Figure 6.7. Localisation of PB2 amino acid residues of interest and subsequent verification of desired mutations. A) Structure of the monomeric influenza polymerase complex (PB1 subunit highlighted in cyan, PB2 in magenta and PA in green) bound to vRNA promoter (yellow and pink) with PB2 amino acid residues 9 (dark blue) and 81 (red) highlighted. Figure made in Pymol using protein databank reference: 6RR7-A/NT/60/1968, H3N2. B) Sanger sequencing verification of the D9N and T81M substitutions (red box) from rescued recombinant viruses. Only the single mutations are shown but a double mutant was also generated. Both the mutated pPolI and pCAGGS plasmids were verified to contain the desired mutations by Sanger sequencing prior to virus rescue (data not shown). Sequence analysis was performed in Geneious.

We assessed aberrant RNA replication products generated by the Tky/05 polymerases with the different PB2 mutations by using either the WT, 9N, 81M or 9N + 81M (referred to as double mutant; DM) PB2 pCAGGS plasmid in a vRNP reconstitution assay alongside the Tky/05 pPol PB2 plasmid to generate the vRNA template. Total RNA extracted from the vRNP reconstitution was used for the RT-PCR analysis using Tky/05 PB2 terminal primers. As expected, all vRNP reconstitutions resulted in the amplification of FL PB2 indicated by strong PCR bands at the correct size of 2341nt (Figure 6.8A). Additionally, we observed a weak band corresponding to FL PB2 when only 2P was transfected. No small PCR bands were detected

when any of the PB2 pCAGGS were used in vRNP reconstitutions indicating that no aberrant RNA replication products were generated. This was unexpected as even when WT Tky/05 PB2 was used, there were no small RNAs, directly conflicting with prior results (Figure 6.3A). To test to see whether these RNA products were immunostimulatory, equal amounts of RNA were transfected into the A549 IFN-β luc cells. IFN-β promoter activity was significantly increased when the 9N, 81M and DM pCAGGS plasmids were used when compared to transfections using the Tky/05 WT PB2 pCAGGS (Figure 6.8B).

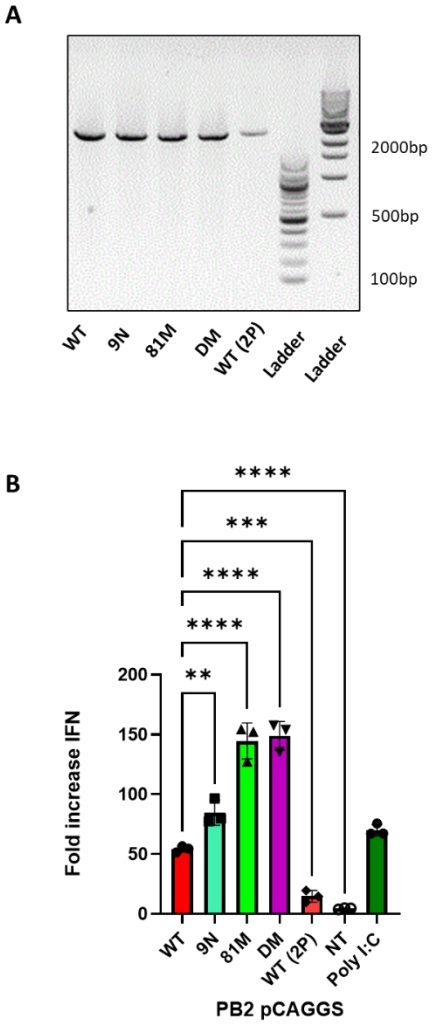

Figure 6.8. The human-adapted substitutions T81M, D9N and D9N + 81M in the Tky/05 PB2 subunit do not increase aberrant RNAs but are immunostimulatory. A) Standard vRNP reconstitution assay was performed in HEK293T cells where Tky/05 WT, 9N, 81M, or DM pCAGGS PB2 plasmids were used. Total RNA was extracted 24 hours post transfection, and cDNA synthesis was performed using 200ng of RNA using Superscript IV and tagged Uni12 primer. PCR was performed using KOD polymerase with tagged forward primer and terminal PB2 primer. PCR products were analysed on a 1.5% agarose gel with GelRed. B) 350ng of RNA from vRNP reconstitution assay was directly used for transfections in the A549 IFN-β luc reporter cell line. 24 hours later,

cells were lysed and luciferase activity measured. Data is expressed as fold increase over mock transfected cells and bars represent mean ± SD from triplicate samples. NT represents RNA extracted from non-transfected HEK293T cells in the vRNP reconstitution assay. Variance among the groups was analysed by a one-way ANOVA with Dunnett's post hoc test for multiple comparisons, **** P<0.0001, *** P<0.001, ** P<0.01.

We also analysed the effect on polymerase activity that introduction of the mammalian adapted substitutions had compared to the WT. We performed *in vitro* polymerase assays using either the WT PB2 pCAGGS plasmid or the 9N, 81M or DM, with the cognate PB1, PA and NP pCAGGS plasmids, together with the pPolI-firefly luciferase and pPolI-renilla luciferase reporter plasmids. We found that all the introduced mutations had similar polymerase activity to the WT, apart from the single 81M change that resulted in a slight increase (<1.5-fold) in polymerase activity (Figure 6.9A).

Additionally, an *in situ* vRNP IFN assay was performed using the IFN-β reporter plasmid (Figure 6.9B). Similar to when the total RNA from the vRNP reconstitution assays was transfected, IFN-β promoter activity was significantly increased when the 81M or DM PB2 pCAGGS plasmid was used, compared to transfections using the Tky/05 WT PB2 pCAGGS. The single D9N substitution only increased IFN-β promoter activity over WT when the RNA was extracted and used to transfect the reporter cells (Figure 6.8B), not when tested *in situ* (Figure 6.9B).

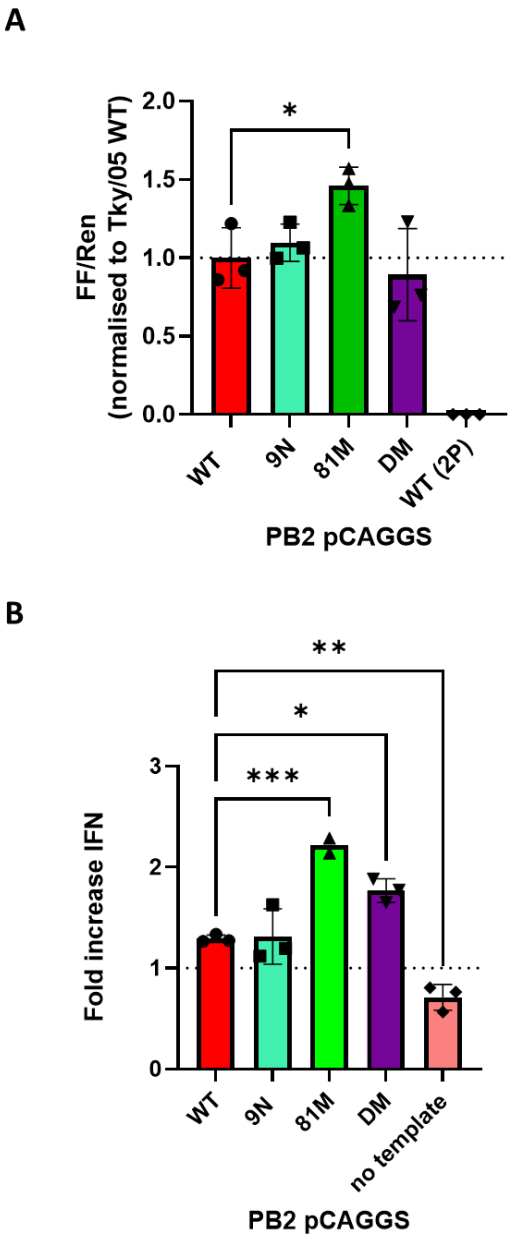

Figure 6.9. The human-adapted substitutions T81M and D9N + T81M in the Tky/05 PB2 subunit increase IFN-β promoter activity. A) The polymerase complex (3P) and NP PCAGGS expression plasmids, alongside the mini-genome firefly reporter plasmid pPolI-Fifrefly were transfected into HEK293T cells. A Renilla pol II plasmid was also transfected (FF: Ren is 1: 0.25) as well as a parallel transfection were the PB2 pCAGGS plasmid was omitted (2P). Cells were lysed 24 hours post transfection and data is shown as firefly activity/Renilla normalised to the Tky/05 WT (set at 1) and plotted as mean ± SD from triplicate samples. Variance among the groups was analysed by a one-way ANOVA. *P<0.05. B) HEK293T cells were transfected with Tky/05 3P and NP expression plasmids, alongside reporter plasmids and PB2 pPolI plasmid. Transfections were also performed where the PB2 pCAGGS plasmid was omittied (2P), or the pPolI plasmid was omitted (no template). To balance the total amount of DNA transfected an empty pCAGGS plasmid was used. Cells were lysed 24 hours post transfection and luciferase measured. Values were normalised to Renilla and expressed as fold

increase over 2P. Data represents mean ± SD from triplicate samples and variance among the groups was analysed by a one-way ANOVA with Dunnett's post hoc test for multiple comparisons,* P<0.001, ** P<0.01, * P<0.05**

6.2.5 Viral growth kinetics of PB2 mutants

After rescuing viruses containing these PB2 mutations, we generated virus stocks by passaging in MDCK cells at an MOI of 0.0001. We performed both qRT-PCR and plaque assays to obtain M gene copy number/ml: PFU/ml ratios. All the viruses displayed similar ratios, suggesting that the number of non-infectious to infectious particles in these stocks were not vastly different (Figure 6.10A). We next examined growth kinetics in MDCK cells to determine whether any of the mutations conferred a growth advantage or grew significantly worse when compared to the Tky/05 WT, by performing multi-cycle assays using low MOI. We found that there were no significant differences in growth at any of the time point measured (Figure 6.10B).

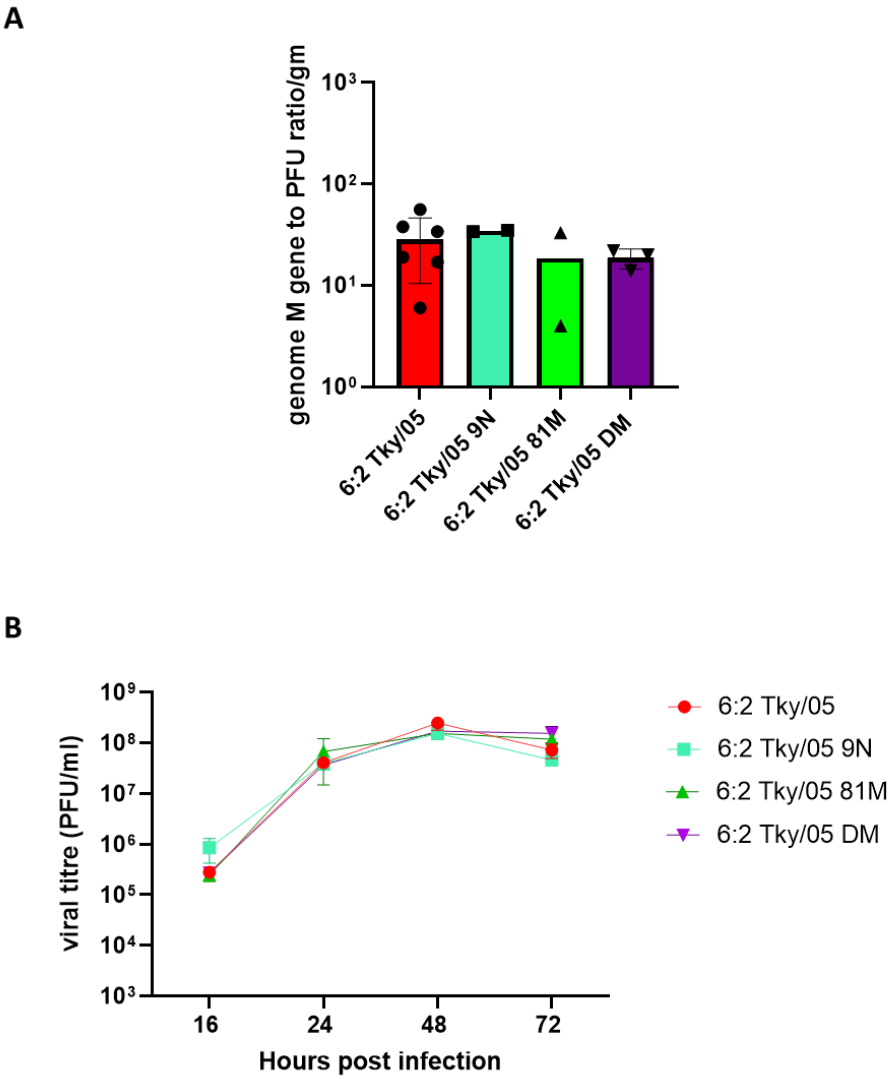

Figure 6.10. Effect of PB2 mutations on copy number/ml to PFU/ml ratio and viral growth kinetics. A) Copy number M gene/ml to PFU/ml ratio. Mean PFU/ml was determined for each virus stock (n=3) and this used to calculate the ratio.RNA was extracted from viral stocks and a one-step RT-qPCR was performed using primers and probe for M gene in order to calculate M gene copy number/ml. Data points show ratio calculated using RNA obtained from at least two independent extractions. B) MDCK cells were infected at an MOI of 0.001 with 6:2 Tky/05, 6:2 Tky/05 9N, 6:2 Tky/05 81M and 6:2 Tky/05 DM virus. At the indicated time points, the virus supernatant was harvested, and plaque assays performed to quantify the amount of released infectious viral particles. Data shown as mean ± SD (n =3). A two-way ANOVA was performed with Dunnets test for multiple comparisons, but no statistical differences were seen at any time point.

We also analysed the polymerase segment derived DVGs by performing a RT-PCR using terminal primers and visualising the PCR products on an agarose gel, using RNA extracted from the virus supernatants (Figure 6.11A). The 6:2 Tky/05 DM virus yielded small PCR

products derived from the PB1 and PB2 segments, the 6:2 Tky/05 9N virus yielded one truncated PCR product from the PA segment and the 6:2 Tky/05 81M virus one from the PB2 segment. We also observed a strong band corresponding to the size of a previously identified PB2 DVG from the 6:2 Tky/05 WT virus (red box). We next extracted, cloned and sequenced the small bands present from the 6:2 Tky/05 DM PB1 RT-PCR (purple box) to confirm these were DVGs and to identify the junctions (Figure 6.11B).

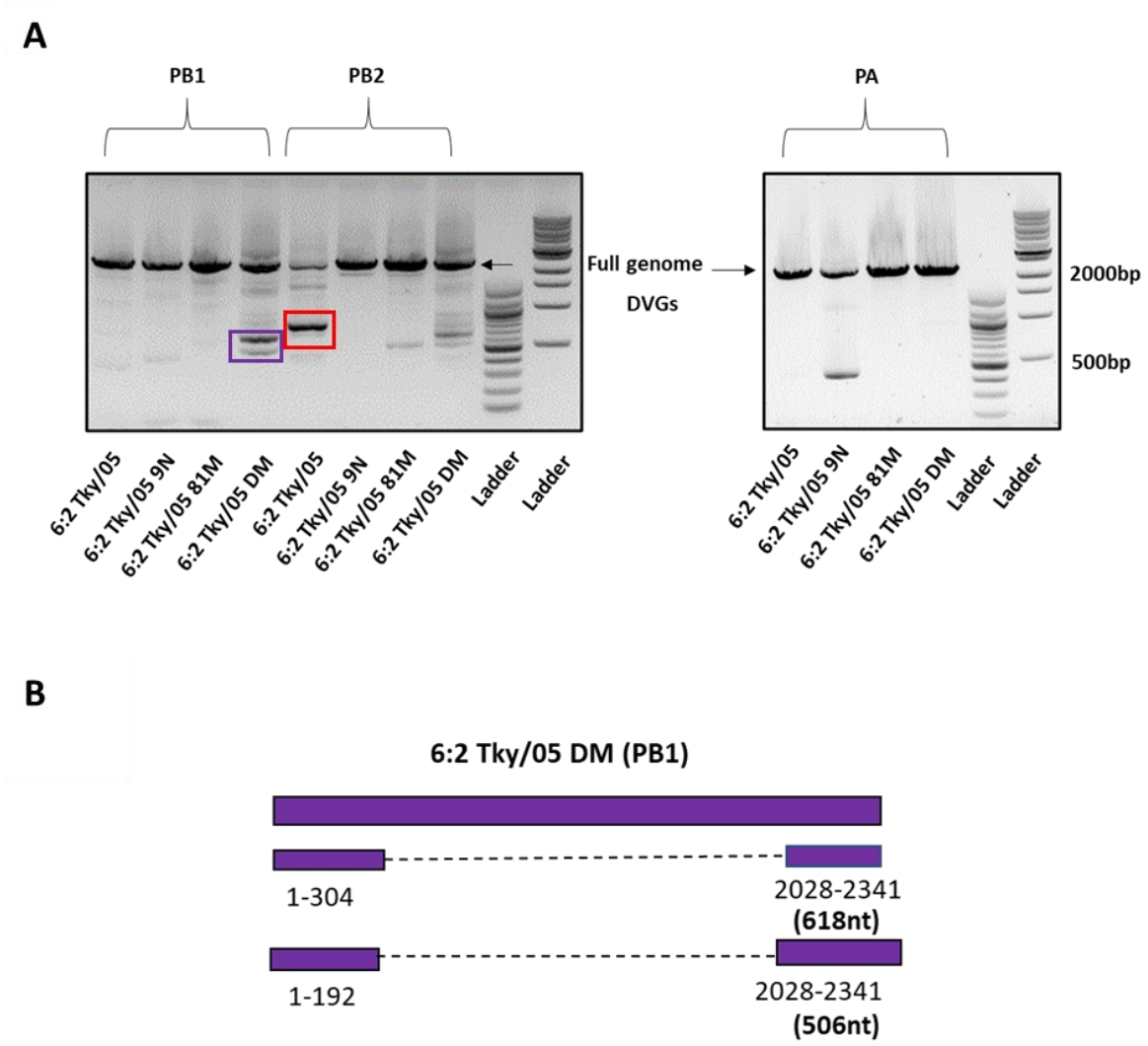

Figure 6.11. Polymerase DVGs present in the virus stocks. RNA was extracted from the virus supernatants and equal volumes of RNA were used for cDNA synthesis with Superscript IV RT and Uni12 primer that targets the 3' end of vRNA. PCR was performed using KOD polymerase and Tky/05 specific terminal primers for both full genome and DVGs for the PB1, PB2 and PA segment. A) PCR products were analysed on a 1.5% agarose gel with GelRed. Arrows indicate the size of the full genome, whereas any bands below this indicate potential DVGs. The red box indicates a PB2 DVG previously identified from the 6:2 Tky/05 stock (Chapter 4, Figures 4.6 and 4.7A) and the purple box indicates those selected for further characterisation. B) PCR bands (purple box) were extracted, cloned into TOPO vectors and Sanger sequenced. Sequences were mapped to the full-length

segments using Geneious and junctions calculated. Coloured rectangles represent the 5' and 3' ends of the DVGs and dotted connecting lines represent the large internal deletion. The junction positions are shown underneath, and all are depicted in the positive sense.

6.2.6 The 6:2 Tky/05 DM virus increases innate immune responses in BMDMs

We chose the 6:2 Tky/05 DM virus for use in further experiments as these mutations led to increased IFN-β promoter activity but had similar polymerase activity to the WT 6:2 Tky/05. We therefore used this virus to infect murine BMDMs[2] along with the 6:2 Tky/05 virus to establish whether there were differences in pro-inflammatory cytokine and IFN production. These viruses replicated similarly in the BMDMs (Figure 6.12A and B), but both IL-6 and TNF-α mRNA was increased by 24 h.p.i for the DM when compared to the WT 6:2 Tky/05 virus (Figure 6.12C and 6.12D). Similarly, IFN-α protein levels were also significantly higher for the 6:2 Tky/05 DM virus (Figure 6.12E). We also found stronger bands for PB1 derived DVGs in the 6:2 Tky/05 DM infected BMDMs when compared to the WT infected BMDMs (Figure 6.12E).

[2] The data shown for the Tky/05 infected BMDMs is the same as that shown in Chapter 3, Figures 3.5 and 3.7

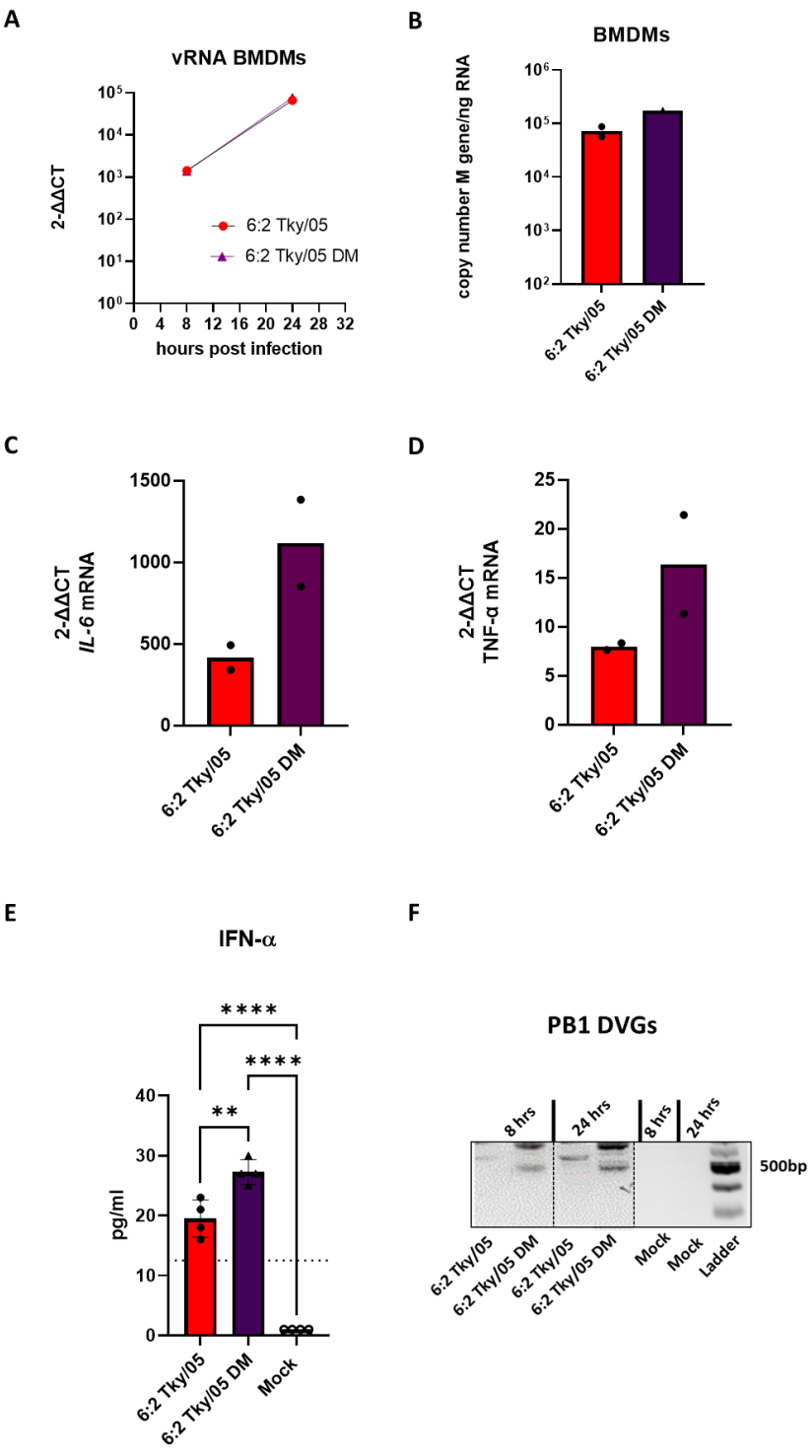

Figure 6.12. Introduction of PB2 mutations has no effect on replication in BMDMs but does increase innate immune responses.BMDMs were infected with 6:2 Tky/05 and 6:2 Tky/05 DM at an MOI of 10, or mock infected in quadruplicate. Total RNA was extracted at 8 and 24 h.p.i, DNAse I on-column treated, and concentration measured by spectrophotometry. RNA was pooled from two wells to ensure sufficient yields for RT-qPCR. A) Equal amounts of RNA (100 ng) were used to generate cDNA using RevertAid reverse transcriptase and tagged primers against NA vRNA or Oligo(dT). qPCR was performed using Fast SYBR green master mix and primers to amplify NA vRNA or GAPDH. Relative expression was calculated by the 2 -ΔΔ CT

method normalised to the GAPDH housekeeping gene and shown as fold increase over the mock infected cells. Data represents mean (n=2 biological replicates) performed in technical duplicates. B) RNA extracted at 8 h.p.i was used in a one-step qRT-PCR using primers and probe for M gene and calculated as M gene copy number/ng of RNA. Statistical analysis was not performed due to small sample size. C and D) Equal amounts of RNA (100 ng) were used to generate cDNA using RevertAid reverse transcriptase and primer for Oligo(dT). qRT-PCR performed using Fast SYBR green master mix and primers targeting GAPDH and (C) Il-6 (D) TNF-α. Relative expression was calculated by the 2 -ΔΔ CT method normalised to the GAPDH housekeeping gene and shown as fold increase over the mock infected cells. E) IFN-α levels in cell supernatants harvested at 24 h.p.i determined by ELISA. Variance among groups was calculated by one-way ANOVA with Tukey post hoc test for multiple comparisons (** p<0.0001, **, p<0.01, ns= unlabelled indicates no significant difference. Statistical analysis on A-D was not performed due to small sample size (n=2). Error bars depict mean + SD. F) PB1 DVGs detected in the BMDMs. 100ng of RNA was used for cDNA synthesis with Superscript IV RT and Uni12 primer that targets the 3' end of vRNA. PCR was then performed using KOD polymerase and Hoffman primers that target the conserved 3' and 5' termini of PB1 vRNA and products analysed on a 1.5% agarose gel with GelRed. For clarity, wells not corresponding to the data presented here were removed and lanes rearranged accordingly (indicated by dotted line).**

6.2.7 The 6:2 Tky/05 DM virus did not affect weight loss in mice or IFN-α production in the lungs

We next performed intranasal infections in BALB/C mice using 10^5 PFU/25µl of the 6:2 Tky/05 or 6:2 Tky/05 DM virus, alongside a group given PBS as a mock-infection[3]. Mice infected with both viruses lost weight when compared to the mock infected mice and the weight loss curves were similar (Figure 6.13A). By day 7, 3/5 mice in the 6:2 Tky/05 infected group had reached the severity limit, whereas all those in the group that were infected with the 6:2 Tky/05 DM virus remained above the severity threshold (Figure 6.13B). These viruses also replicated to similar levels in the lungs as measured by PFU (Figure 6.13C). An ELISA performed on the lung homogenates harvested 72 h.p.i, showed that the IFN-α protein levels were not statistically different from one another (Figure 6.13D).

[3] The data shown for the Tky/05 infected mice is the same as that shown in Chapter 5, Figures 5.1-5.3.

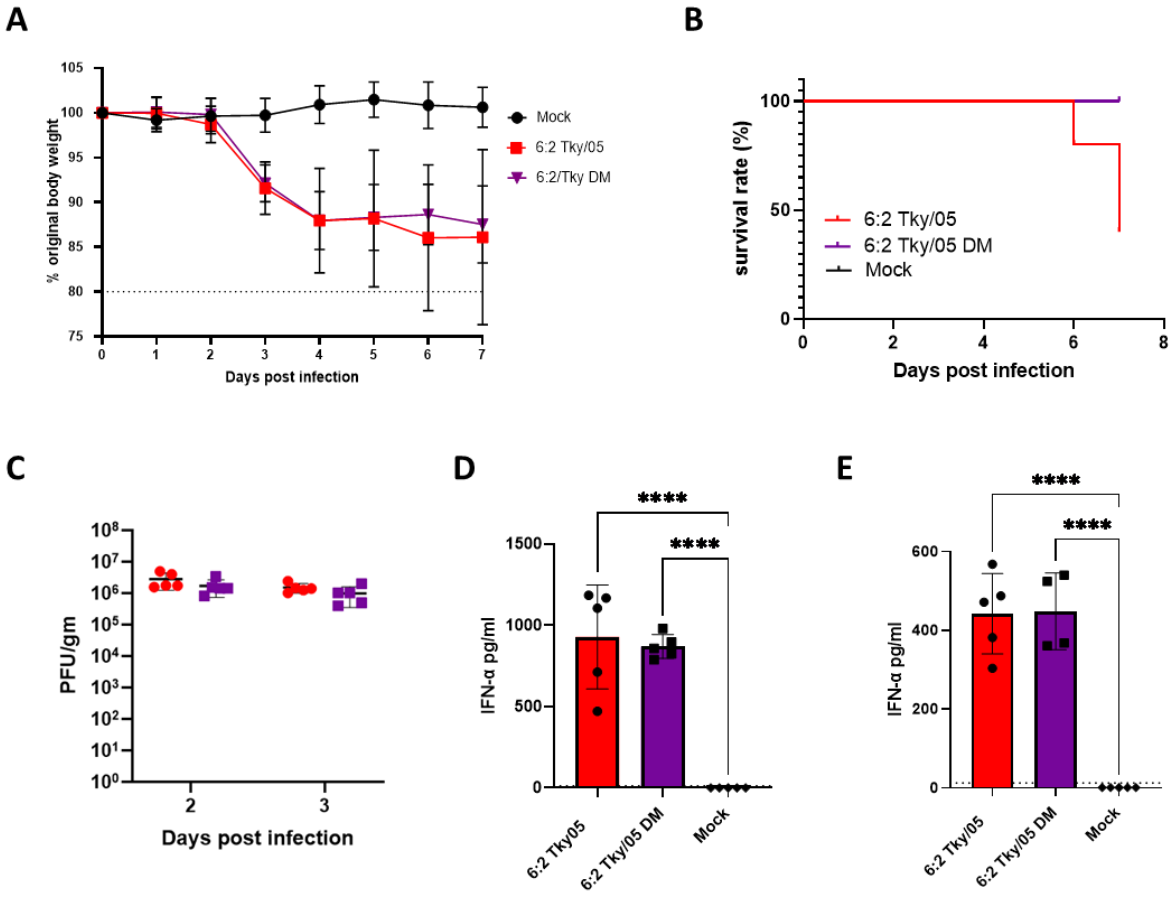

Figure 6.13. *In vivo* analysis of the 6:2 Tky/05 DM virus. A) Six to eight week old female BALB/c mice (15 per group) were mock infected (PBS) or infected intranasally with 10^5 PFU of 6:2 Tky/05 or 6:2 Tky/05 DM virus in 25µl volumes. 5 mice per group were culled at 2, 3 and 7 days post infection. Weight loss was monitored daily. Dotted line represents the severity limitB) Survival curve of infected mice. All mice were culled when they lost ≥20% of original body weight (day 0) C) Virus titres in the homogenised lung tissues. Lungs were harvested at days 2 and 3 days post infection, homogenised and weighed. Plaque assays were performed to determine viral titre and calculated as PFU/gm. Data is expressed as mean ± SD (n = 5). D-E) IFN-α levels in the homogenised lung tissues. Lungs were harvested at days 2 and 3 post infection. IFN-α levels were assessed by ELISA (limit of detection= 12.5pg/ml). Bars represent mean ± SD (n=4-5). Variance among groups was calculated by a two-way ANOVA with Tukey post hoc test for multiple comparisons. ****P<0.0001. No significant difference was observed between the two viruses for weight loss (A) or PFU/gm (C) at any time points analysed. *In vivo* mouse work was performed alongside Mrs Rebecca Frise and Ms Laury Baillon.

6.3 Discussion

By using vRNP reconstitution assays, we found that the Tky/05 polymerase synthesises short aberrant RNAs (Figures 6.2A and 6.3A). Although vRNP reconstitution assays have been used previously to demonstrate the synthesis of aberrant RNAs, few have provided the full-length

vRNA segment (pPolI) as template. Instead, pPolI plasmids expressing a shorter vRNA have been used such as a 246nt long vRNA derived from the NP segment (Te Velthuis et al., 2018), or a 200nt long vRNA derived from the NA segment (Nilsson-Payant et al., 2021). Liu et al. (2019), used FL segments in vRNP reconstitution assays for analysis of type I IFN induction; for detection of aberrant RNAs following vRNP reconstitution, they used a pPolI luciferase reporter that contained the 5' and 3' UTRs of the NP segment. The reasons for not providing the FL segment are unknown but could simply ensure efficient replication as shorter templates are more rapidly amplified and would therefore enhance the detection of any aberrant RNAs generated. However, by using a pPolI plasmid that encodes the FL segment in our experiments, we are mimicking the vRNA template that would be replicated in a cell following authentic influenza infection and showing such products are generated d*e novo*.

Our results suggest that aberrant RNAs are synthesised regardless of the vRNA segment provided; transfection with either Tky/05 PB1 or PB2 pPolI plasmids resulted in their detection (Figures 6.2A and 6.3A). The finding that aberrant products were detected from multiple segments agrees with other studies; mvRNAs were most abundantly derived from the HA, NP, NA and PB1 segment following WSN infection but were also observed at lower levels from all 8 segments (Te Velthuis et al., 2018). A later study analysing mvRNA levels in both BM/18 (HPAIV H1N1) infected ferret lungs and WSN infected A549 cells showed these were most abundant from the PB2, HA, NP, M and NS segments but again were observed arising from all (French et al., 2022). We only focused on the longest polymerase segments PB1 and PB2, but if time had allowed it would be interesting to see whether such aberrant RNAs would also be generated from others.

IFN induction was assessed by two methods, either extracting the total RNA from vRNP reconstitution assays and using equal amounts for transfections into the A549 IFN-β luc reporter cells, or by co-transfecting an IFN-β reporter plasmid alongside plasmids needed for vRNP reconstitution to directly assess IFN induction *in situ.* For the former assay, our results agree with those of Rehwinkel et al. (2010), namely that RNA extracted from the vRNP reconstitutions were more immunostimulatory than RNA from non-transfected cells or those that did not express a functional polymerase (2P) (Figures 6.3C and 6.9B). It should also be noted that total RNA is extracted from the vRNP reconstitution assays and therefore does not just constitute the viral RNA. Furthermore, the full length vRNA cannot be distinguished from

any smaller aberrant RNAs present. A more specific method to analyse the contribution of immunostimulatory RNAs would be to fractionate the RNA according to size and use these for transfections into the A549 IFN-β luc cells, such as performed in Te Velthuis et al. (2018).

It is not wholly unsurprising that the RNA extracted from the vRNP reconstitution assays were immunostimulatory. The process of RNA extraction would strip away the polymerase and NP proteins resulting in a "naked" RNA containing a 5' triphosphate moiety that is a well-recognised motif for RIG-I binding. We confirmed that RIG-I was indeed required for IFN-β promoter activity as CIP treatment completely abolished this (Figure 6.4), which agrees with other studies (Baum et al., 2010; Pichlmair et al., 2006; Rehwinkel et al., 2010). In direct contrast, a recent study demonstrated that RNAs generated from IAV infected cells still retained immunostimulatory capabilities even after CIP treatment (Steinberg et al., 2021). They showed that the viral genome was not solely responsible for IFN induction, a cleaved host cellular RNA termed endogenous RIG-I ligand (eRL) also contributed. This eRL was only found in IAV infected cells and IFN induction was dependent on a 2'3' cyclic phosphate which was unaffected by CIP treatment (Steinberg et al., 2021). Whilst our results do not support a role for eRL contributing to immune activation, it should be noted that the total RNA extracted in our experiments is from vRNP reconstitutions rather than IAV infections.

Naked RNAs are not believed to be generated in IAV infections as during viral replication newly synthesised RNAs are encapsidated by NP and polymerase. Current models suggest that an encapsidating polymerase forms a dimer with the replicating polymerase and as the 5' end of the nascent RNA emerges from the active site, NP is recruited to the RNA to form vRNP/cRNP complexes (Te Velthuis et al., 2021). Therefore, assays where IFN induction is measured *in situ* (as previously used in Chapter 4) are perhaps more physiologically relevant as vRNA would be sensed in the context of vRNPs.

Our results support the existing literature; limiting NP promotes IFN induction (Nilsson-Payant et al., 2021; Te Velthuis et al., 2018). By decreasing the amount of NP transfected, we enhanced IFN induction (Figures 6.5B and 6.6). Furthermore, increased IFN-β promoter activity correlated with less polymerase activity (Figure 6.5C), a reduction in FL genome (Figure 6.6A upper band) and an increase in small aberrant products (Figure 6.6A lower band). It is widely recognised that NP is an elongation factor for vRNA and cRNA synthesis, thereby promoting the processivity of the polymerase (Honda et al., 1988; Turrell et al., 2013). It is

therefore hardly surprising that by reducing the amount of NP, we reduce the amount of FL genome and polymerase activity. Interestingly, it was only when 50ng of NP was transfected that we observed a decrease in polymerase activity and FL genome; transfecting 100ng, 150ng and 200ng of NP did not yield any significant differences. However, this could be attributed to NP levels at 100ng being already saturated, and addition of NP beyond this amount is not necessary. Western blots could have been performed to confirm expression levels of NP, alongside a titration series of NP to determine the exact levels that reduce full length genome elongation.

We observed that when NP was omitted from the vRNP reconstitution assays, we saw similar levels of IFN induction to when the standard (200ng) amount of NP was transfected (Figure 6.6). Te Velthuis et al. (2018), observed a similar result; only a low induction of IFN was reported when 3P alone or 3P and NP were (along with vRNA), expressed in vRNP reconstitution assays but this was significantly increased when 3P was expressed prior to viral infection. Furthermore, Nilsson-Payant et al. (2021), also observed very low IFN-β induction when NP was absent or when added at high concentrations in vRNP reconstitution assays. Both studies nicely illustrate that when NP is limited, IFN induction increases, coinciding with the generation of mvRNAs. Our RT-PCR results also support this; small PCR products were amplified by the Tky/05 terminal primers; these were more pronounced when NP levels were lower (Figure 6.5A). Although we cannot confirm the exact identity of these bands as we did not clone and sequence these, it is likely these would be mvRNAs as would contain both the 3' and 5' termini as well as being <100nt in length. Interestingly, we did not observe any larger DVGs.

The mechanism by which reduced levels of NP leads to the generation of aberrant products and higher immune activation is still not fully understood. French et al. (2022), demonstrated that some mvRNAs form t-loops through hybridization of the 3' terminus of the template to a further upstream site, causing the polymerase to stall and lose processivity, allowing binding to RIG-I. The authors proposed that this most likely occurs on partially formed RNPs, due to an increase in exposed secondary structure which would be enriched when NP levels are low. Nakano et al. (2021), using both high-speed atomic force and cryoelectron microscopy showed that alongside the expected helical vRNP structure, a deformed vRNP was also formed during i*n vitro* RNA synthesis. This deformed vRNP associated with looped RNA that

was mostly double stranded as opposed to single-stranded folded RNA associated with the canonical helical vRNP. They only observed dsRNA in a very small percentage of Vero cells following infection with PR8, whereas higher deformed vRNAs were seen *in vitro*. However, the *in vitro* methods employed do not represent infection conditions due to the absence of cellular host factors and NP. It was therefore proposed that this looped RNA may represent an aberrant RNA replication product, likely comprising both nascent RNA and template vRNA. This is further supported by findings from (Liu et al., 2019) where when performing NP-free vRNP reconstitution assays, they observed small aberrant replication products incapable of stimulating IFN-β promoter activity if extracted total RNA was assessed but were able to induce IFN when *in situ* assays were performed. Therefore, the aberrant replication products produced are also likely to represent an intermolecular duplex formed by the complementarity between itself and corresponding template RNA. NP depletion would also abolish interaction with UAP56 which is a host cellular RNA helicase and this may explain why the formation of dsRNA is not prevented (Wisskirchen et al., 2011). Therefore, different RIG-I activating aberrant RNAs might be generated depending on the exact levels of available NP.

It is important to remember that although valuable, vRNP reconstitution assays are not reflective of an influenza infection. Transfection of only one expression plasmid for vRNA was performed in these experiments so not all viral proteins would be generated such as NS1, an important virally expressed IFN antagonist. Single cell sequencing of IFN producing cells following IAV infection showed that the lack of NS was the most predominant defect although by no means the only one (Russell et al., 2019). Interestingly, a recent pre-print highlighted a crucial role for NEP/NS2 in promoting IFN-induction possibly by mediating export of viral RNAs to the cytoplasm for sensing. This study demonstrated that some inactivating mutations in the NS segment were less immunostimulatory than those inactivating the NS1 protein alone, due to the concurrent loss of NEP (Vicary et al., 2022).

In this chapter we also explored the effect of mutating the amino acid residues at positions 9 and 81 in the Tky/05 PB2 segment to those associated with human adapted viruses. vRNP reconstitution assays showed that the introduced PB2 mutations did not alter polymerase activity significantly from the WT, apart from the single 81M mutation which conferred a slight increase (Figure 6.9A). However, it should be noted that western blots were not performed to confirm PB2 expression. We also showed that both the individual mutations

and DM increased IFN-β promoter activity when compared to the WT Tky/05. We performed both an *in situ* IFN reporter assay (Figure 6.9B) or following vRNP reconstitution we used the RNA to directly transfect the A549 IFN-β luc reporter cells (Figure 6.8B). There was general agreement between the two assays; the T81M substitution and DM led to an increase in IFN-β promoter activity in both assays. However, this was not observed for the D9N substitution; there was only an increase over WT when RNA was directly used to activate IFN-β promoter activity (Figure 6.8B). However as previously discussed, we feel that the *in situ* IFN reporter assay is more representative of an influenza infection. It would have been interesting to see whether infections in the A549 IFN-β luc reporter cells using the 6:2 Tky/05 9N virus would yield higher luciferase activity. Graef et al. (2010), showed that the N9D avian-like substitution in WSN PB2 increased IFN-β mRNA levels in A549 cells. This is consistent with Te Velthuis et al. (2018), who when using vRNP reconstitution assays where the IFN-β reporter plasmid was also transfected, demonstrated a modest increase in IFN for the N9D substitution. They also observed an increase in IFN-β promoter activity when the avian associated 81T was introduced into the WSN PB2, and the virus containing both mutations induced the highest increase in IFN (Te Velthuis et al., 2018). This is therefore in direct contrast to our results as our observations suggested the opposite, switching these amino acids from typically avian to human adapted mutations increased IFN. Perhaps by introducing different amino acids from those typically found at these sites, we imbalance the host type I IFN response, regardless of the genetic background of the virus.

How these mutations affect the type I IFN response is still not clear. It could be that the mitochondrial localisation of PB2 9N affects MAVS function through direct binding. However, Graef et al. (2010), observed that the non-mitochondrial PB2 9D bound to MAVS *in vitro* and another study demonstrated that the human-adapted PB2 9N shows a mitochondrial localisation in both MAVS deficient and competent cells (Long & Fodor, 2016). Furthermore, this study demonstrated that the PB2 9N was imported directly into the mitochondrial matrix and therefore is unlikely to directly bind to MAVs. Instead, the authors proposed that interference with the function of MAVS was most likely explained by changes in the mitochondrial membrane potential (MMP) (Long & Fodor, 2016). Maintenance of MMP is integral to IFN production through signalling via MAVS (Koshiba et al., 2011). It is therefore

unsurprising that other virally encoded proteins that are known to modulate the IFN response such as PB1-F2, can also localise to the mitochondria and dissipate MMP (Cheung et al., 2020).

Alternatively, the generation of more immunostimulatory mvRNAs by the non-mitochondrial localising 9D was suggested to be the mechanism for increased IFN by Te Velthuis et al. (2018). Structurally, both residues 9 and 81 are located near the putative template exit channel of the polymerase complex. The 81 residue resides in the 80-90 loop which has been shown to undergo a conformational change during the elongation process during viral transcription (Wandzik et al., 2020). As elongation is believed to occur in a similar manner for viral replication (Te Velthuis & Fodor, 2016), perhaps mutations at this position detrimentally affect the ability to synthesise full-length vRNA or cRNA, resulting in the generation of aberrant RNA replication products. Our results do not support a role for these amino acid residues in the Tky/05 PB2 affecting mvRNA generation (Figure 6.8A). By using a vRNP reconstitution assay and subsequent RT-PCR, we did not detect any mvRNAs generated by any of the polymerases tested, not even for the Tky/05 WT polymerase which we have previously shown can make aberrant RNAs when provided with the same vRNA template (Figures 6.3A and 6.5A). This discrepancy in results may be reflective of the stochastic nature of aberrant RNA formation or simply that the methods used here lack sensitivity. Further experiments are therefore required to fully examine the contribution of these amino acids to mvRNA formation. Interestingly, when assessing the DVG content of the 9N, 81T and DM viruses by RT-PCR, we observed a noticeable increase in the abundance of distinct PB1 and PB2 DVGs for the 6:2 Tky/05 DM virus when compared to the 6:2 Tky/05 WT virus (Figure 6.11). However, the copy number M gene/ml to PFU/ml ratios for all the viruses were similar (Figure 6.10A). This indicates that although there may be more individual DVGs characterised from the 6:2 Tky/05 DM virus, these were not at such high levels that they increased the overall quantity of non-infectious particles in the virus stock.

We were able to successfully rescue the PB2 mutant viruses which had similar growth kinetics to the 6:2 Tky/05 WT virus in a multi-cyclic growth curve performed in MDCKs (Figure 6.10B). Past studies have shown no growth defects in A549 cells when 9D was introduced into the WSN virus (Graef et al., 2010) but when performed in MEFs, this virus replicated to lower titres than the wildtype (9N) (Long & Fodor, 2016). Interestingly, a study mapping the adaptation of the avian PB2 segment to humans using a deep mutational scanning approach,

showed that the substitution that offered the greatest increase in both replication and polymerase activity in A549 cells was actually a D9K substitution although D9N was also selected for (Soh et al., 2019). However, a lysine at this position is not found in natural influenza isolates. This is probably due to being evolutionary inaccessible as two nucleotide substitutions are required to evolve from the avian associated aspartic acid to a lysine.

The 6:2 Tky/05 DM virus resulted in an increase in pro-inflammatory cytokines and IFN-α in murine BMDMs compared to the 6:2 Tky/05 WT virus but did not result in an increase in replication (Figure 6.12A-E). This is similar to what was reported in Chapter 3; the internal genes of the 6:2 Tky/05 virus induced higher IFN-α than the 6:2 Eng/09 strain but this was not correlated with increased replication (Chapter 3, Figure 3.7C). We also observed DVGs present in the BMDMs at both 8 and 24 hrs post infection (Figure 6.12F), which is in keeping with our previous findings (Figure 3.6). We analysed the PB1 segment, and the sizes of the PCR bands correlated with those observed in the viral stocks for the 6:2 Tky/05 DM virus, whereas there was a visible PCR band at approx. 600nt in length in the 6:2 Tky/05 infected BMDMs that was not present in the virus stocks (Figure 6.12F). This could be a *de novo* produced DVG, one that is present at low levels in the viral stock, or simply a non-specific band as the Hoffman primers (used here), were previously shown to generate these (Chapter 4, Figure 4.2). Reflective of the viral stock, there were stronger PCR bands observed for the PB1 DVGs derived from the 6:2 Tky/05 DM virus infections in the BMDMs and this could explain the slightly increased IFN-α protein levels and IL-6 and TNF-α mRNA levels observed.

When these recombinant viruses were used for mouse infections, we saw similar pathogenicity in terms of weight loss with both the 6:2 Tky/05 and 6:2 Tky/05 DM viruses causing a decrease in weight compared to mock infected mice from day 3 (Figure 6.13A). The survival curve indicates that the 6:2 Tky/05 virus was more virulent as by the end of the study only 2/5 mice remained at ≥80% of their original body weight, whereas no mice infected with the 6:2 Tky/05 DM virus were culled (Figure 6.13B). This slight increase in virulence was not caused by an increased viral lung load as at all time points measured there was no statistical difference between the viruses (Figure 6.13C). Similarly, this could not be explained by differences in the level of IFN-α in the lung homogenates at day 2 or 3 post infection (Figure 6.13D). However, there was high variability in weight loss between mice in the 6:2 Tky/05 infected group, more so than in the DM infected group. We had observed less variability in

weights when the 6:2 Tky/05 virus was used to infect mice in an additional experiment (Chapter 5, Figure 5.4B) and a greater proportion of mice survived until the end of infection.

It would have been interesting to explore the contribution that other PB2 residues have in influencing the innate immune response or pathogenicity in the mouse model. Fan et al. (2014), identified position 588 in the PB2 protein of a H5N1 virus as contributing to virulence in BALB/c mice; substituting this from an asparagine to a threonine reduced the MLD_{50} by over a log. They also demonstrated that 588T in combination with 147T and 337T reduced this even further. H5N1 viruses that belong to the Qinghai Lake lineage, like Tky/05, already contain PB2 147T and 337T and additionally have a lysine at position 627. In the same study, Fan et al. (2014), observed that the addition of 627K to the three mutations identified (147T, 337T and 588T) was the most pathogenic in the mouse model and a H5N1 virus bearing all these mutations has been isolated from a fatal human case (Wan et al., 2011). A valine at PB2 588 has been associated with increased virulence in other avian subtypes such as H7N9, H9N2 and H10N8 (Xiao et al., 2016). Furthermore, both studies demonstrated that PB2 588T/V increased polymerase activity in mammalian cells (Fan et al., 2014; Xiao et al., 2016). Position 588 in the PB2 protein therefore seems to be important for determining virulence in the mouse model. A recent review highlighted that many immunomodulatory mutations in PB2 have been linked to the mid-link domain which encompasses residues 247-320 and 482-538 (Elshina & Te Velthuis, 2021). H9N2 isolates that have a valine at residue 292 rather than the typical avian associated isoleucine, have increased polymerase activity in mammalian cells, a decreased type I IFN response and are more pathogenic in a mouse model (Gao et al., 2019). In structural studies, some residues of this mid-link domain face each other in the asymmetric dimer which forms during v-cRNA synthesis between a replicating polymerase and an encapsidating polymerase, bridged by the pro-viral host factor ANP32 (Carrique et al., 2020). This mid-link domain of PB2 could therefore be important for the recruitment of NP and/or encapsidation as proposed by Elshina and Te Velthuis (2021). Interestingly, Wang et al. (2022), recently demonstrated that the C-terminal low-complexity acidic region (LCAR) of ANP32 is required for the recruitment of NP to nascent viral RNA. Future work could therefore examine whether mid-link PB2 mutations affect interactions between ANP32 and NP. It therefore seems reasonable to assume that PB2 mutations associated with mammalian adaption may

promote more favourable interactions between PB2 and mammalian host factors in response to IAV infection.

Overall, the results presented in this chapter demonstrate that the Tky/05 polymerase generates aberrant RNA replication products. Our results show that the vRNP reconstitutions generate immunostimulatory RNAs, although the methods employed here were unable to confer this specifically to aberrant RNAs. In agreement with recent findings, we observe that limiting the expression of NP enhances type I IFN, coinciding with the presence of small RNA replication products although further work is required to fully elucidate the mechanisms involved. Our observations also suggest that there is an increase in IFN-ß promoter activity *in vitro* when mammalian adapting mutations at position 9 and 81 are introduced into the Tky/05 PB2 protein. Additionally, there was an increase in pro-inflammatory cytokines and IFN induction in BMDMs conferred by these two mutations. However*, in vivo*; mean weight loss, viral lung load and IFN-α in the lung homogenates were unaffected by the PB2 9N and 81M substitution.

Chapter 7 Final Discussion

Pandemic influenza is a constant threat to the human population with the potential to kill millions due to poor prior existing immunity. HPAIV H5N1 viruses are of particular concern due to their high lethality and the fact that only few mutations are needed to cause respiratory droplet transmission in mammals (Herfst et al., 2012; Imai et al., 2013). The exaggerated inflammatory response to HPAIV of the H5N1 subtype in mammalian models is well documented (Belser & Tumpey, 2013; de Jong et al., 2006; Xu et al., 2006). One key feature is the elevated levels of pro-inflammatory cytokines and chemokines observed at the site of infection and in the circulation (Liem et al., 2009; Yuen et al., 1998). This is not unique to HPAIV H5N1, hypercytokinemia was also observed for SARS CoV-2 patients admitted to intensive care units (ICU) early in the COVID-19 pandemic (Huang et al., 2020), and has been implicated in other medical conditions (Fajgenbaum & June, 2020).

The underlying mechanism for the formation of a cytokine storm following HPAIV infection is still poorly understood. Figure 7.1 summarises some of the factors that have been identified as contributing to this. In this thesis, we investigated the role that aberrant replication has in the activation of a cytokine storm. We explored whether high replication in macrophages by a virus containing the internal genes of H5N1 (6:2 Tky/05) was associated with hypercytokinemia (Chapter 3) or whether instead this could be associated with the production or transmission of aberrant RNAs such as DVGs (Chapters 4 and 5). We also explored mvRNA and DVG generation by the H5N1 polymerase and identified factors that could influence their formation (Chapter 6).

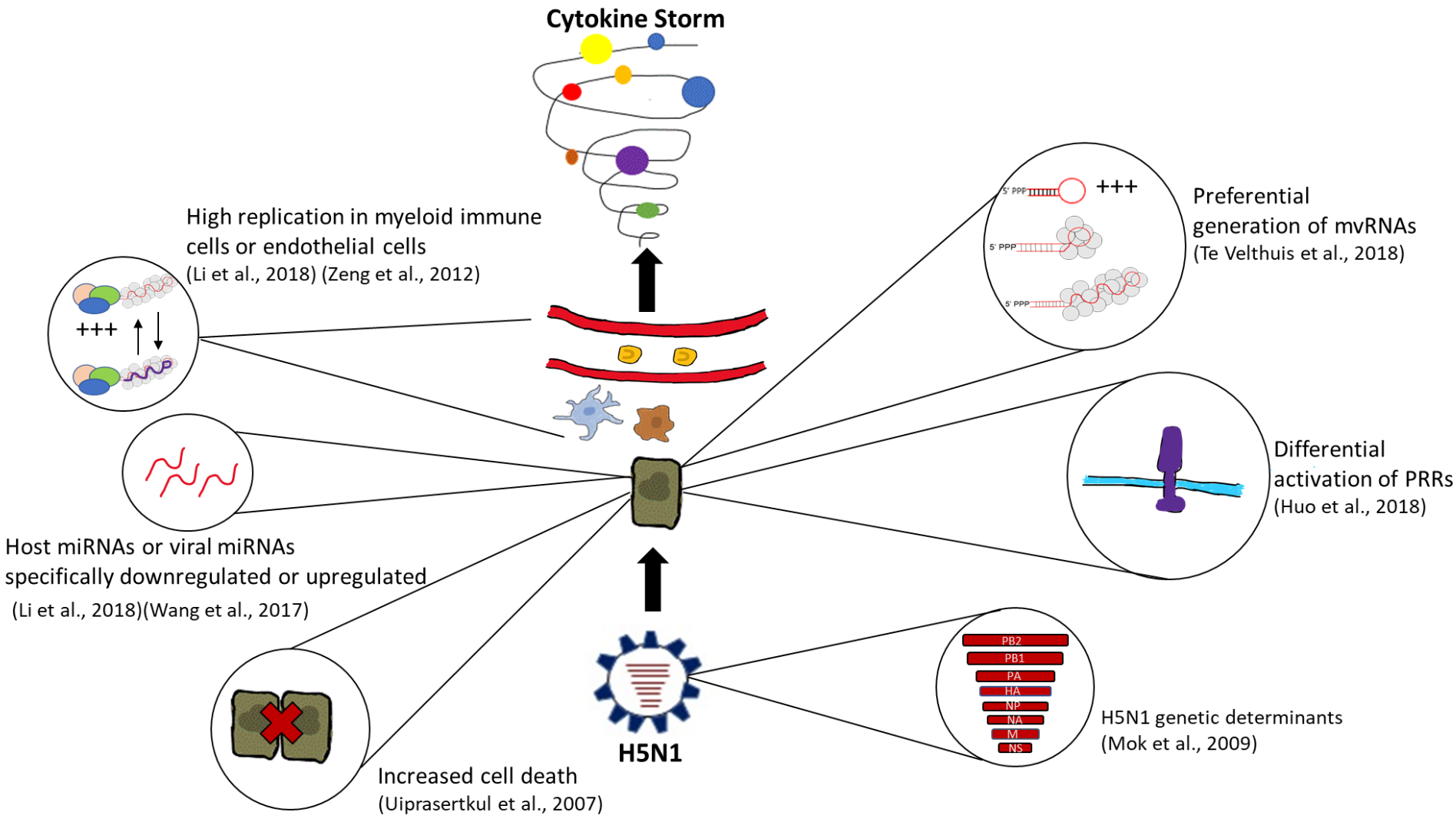

Figure 7.1. Factors that have been implicated in the pathogenesis of H5N1.

7.1 The role of viral replication in macrophages

Viral replication within cells of the innate immune system has previously been linked to the cytokine storm as these cells are major contributors to the pro-inflammatory cytokine milleu. A prior study in the Barclay laboratory found an association between high viral replication in myeloid immune cells and severe outcomes following infection with the 6:2 Tky/05 virus (Li et al., 2018). Our results In Chapter 3 did not confirm these findings but we did observe a significant increase in the amount of secreted IFN-α determined by ELISA in the 6:2 Tky/05 infected murine BMDMs when compared to those infected with the 6:2 Eng/09 virus (Figure 3.7). We had hoped that a potential application for performing influenza infections in the murine BMDMs was that they could be used as an alternative to *in vivo* mouse studies. We hypothesised that high IFN-α production in these cells could be indicative of a poor outcome in mice. However, this did not appear to be as promising when we compared the pathogenicity in 6:2 Tky/05 and 6:2 Eng/09 infected mice as overall weight loss was similar (Chapter 5, Figure 5.1). Similarly, in Chapter 6, the 6:2 Tky/05 DM virus induced higher IFN-α in BMDMs but did not exhibit greater weight loss in mice (Figures 6.12E and 6.13A). This was disappointing as a cell-based assay predictive of pathogenicity would alleviate the requirement for experiments in mice, thus conforming with the NC3Rs. However, we did find that infections with the 7:1 Tky/05 LOW virus induced rapid weight loss in mice as well as high IFN-α secretion in murine BMDMs (Chapter 5, Figure 5.4 and Chapter 3, Figure 3.7). By performing further experiments in both murine BMDMs and mice with a panel of viruses that vary in their pathogenicity, we may gain more insight into the appropriateness of this assay as a predictor for mammalian severity. Interestingly, a recent mathematical modelling study showed that the dominant factor for driving strain-specific immune responses was the production rate of type I IFN; this was 2-3 times faster in H5N1 infected mice compared to H1N1 infected mice, correlating with disease severity (Ackerman et al., 2022).

In human MDMs, we showed that there was a stronger pro-inflammatory and IFN-β response when 6:2 Eng/09 was used for infection compared to the 6:2 Tky/05 virus (Figure 3.9). However, possible differences in the amount of inoculum added could have accounted for this (Figure 3.8). If time allowed, quantification of pro-inflammatory cytokine proteins could have been undertaken as it may be that there are differences at the transcriptional and protein level which has been reported previously (Shebl et al., 2010). Interestingly, IFN-α

protein quantified by ELISA, was only detected in one of two wells of hMDMs infected with the 6:2 Tky/05 virus at 24 hours post infection; all the 6:2 Eng/09 infected hMDMs were below the limit of detection. Therefore, like observed for the murine BMDMs, IFN-α protein was only secreted by those infected with the 6:2 Tky/05 virus, although further experiments would be required to confirm this. It should be noted that not all the same measurements were made so it is difficult to compare the hMDMs and murine BMDMs directly.

Interestingly, the cytokine profile between HPAIVs and pathogenic coronaviruses such as SARS CoV-2 are strikingly different although both can cause a cytokine storm in mammalian models. A delayed type I IFN and pro-inflammatory cytokine response by SARS CoV-2 compared to other respiratory viruses is well documented (Blanco-Melo et al., 2020; Galani et al., 2021). Work conducted with Ms Ziyun Zhang confirmed these findings: SARS CoV-2 infection in hMDMs only resulted in low levels of pro-inflammatory cytokines and type I IFN. We also demonstrated that macrophages were refractory to infection with SARS CoV-2 (Zhang et al., 2022), which has been confirmed by other studies (Niles et al., 2021; Thorne et al., 2021; Zankharia et al., 2022). This suggests there are fundamental differences in the mechanisms that contribute to the cytokine storm for different viruses such as the magnitude and kinetics of type I IFNs/pro-inflammatory cytokines induced and the specific cell types that secrete them.

One major caveat to any research performed in these primary immune cells is that *in vitro* experiments fail to reproduce the complex interactions between different cell types and cytokines and therefore cannot recapitulate the lung microenvironment. This is highlighted by studies showing alterations in the levels of cytokines secreted by primary immune cells if these are exposed to conditioned media or pre-treated with other cytokines (Thorne et al., 2021; Zhang et al., 2022). An attractive approach would be to use co-cultures or even precision cut lung slices/lung-on chip models as interactions between different cell types could be captured (Saygili et al., 2021; Viana et al., 2022).

7.2 Levels of DVGs in virus stocks impact the infection outcome

A finding reported throughout this thesis, was that DVGs could modulate the early innate immune response and influence the outcome of infection. This work culminated in a

publication in the Journal of Virology in 2022 (Penn et al., 2022). In Chapter 3, we demonstrated that the 7:1 Tky/05 LOW stock induced significantly higher pro-inflammatory cytokines and IFN-α than the 6:2 Tky/05 stock in murine BMDMs (Figure 5.6). Further characterisation of this virus stock was performed in Chapter 4, alongside other Tky/05 virus stocks generated to contain different levels of DVGs. Here we showed that polymerase DVGs could be amplified during infections in both epithelial (A549) and murine immune cells (Figures 4.9 and 4.12) and that the virus stock containing the highest levels of DVGs (7:1 Tky/05 HIGH) induced more type I IFN and pro-inflammatory cytokines (Figures 4.10, 4.11 and 4.13). Furthermore, after cloning a set of these DVGs into pPolI plasmids, we were able to directly demonstrate they could activate the IFN-β promoter during an *in situ* IFN-β reporter vRNP reconstitution assay (Figure 4.16). These results reaffirm findings from existing studies; influenza DVGs trigger innate immunity (Baum & Garcia-Sastre, 2011; Tapia et al., 2013).

By performing infections in mice, we showed that the stocks containing different levels of DVGs varied in their severity (Chapter 5, Figures 5.1 and 5.4). The 7:1 Tky/05 HIGH virus caused minimal weight loss and all mice survived the infection (Figure 5.4), which agrees with the longstanding view that high levels of DVGs at the onset of infection lead to attenuation (Swieton et al., 2020; Vasilijevic et al., 2017). The 7:1 Tky/05 LOW stock led to the most severe infection associating with both high viral load (Figure 5.5) and elevated cytokines (Figures 5.7 and 5.8). Interestingly, analysis of the relative levels of polymerase DVGs in the lungs of infected mice, showed that those infected with the 7:1 Tky/05 LOW mice accumulated DVGs to the highest levels by 96 h.p.i (Figure 5.11). One interpretation is that DVGs replicated later in infection are unable to lessen viral load, but instead contribute to immunopathology. This is supported by the 6:2 Tky/05 mouse infection as comparative lung DVG levels were lower at all time points analysed and this virus caused less morbidity in the mice (Figure 5. 10). However, due to these viruses containing different NA segments, we cannot disregard this influencing severity. Ideally, the *in vivo* mouse study would be repeated using genetically identical viruses that only differed in their DVG content to mitigate any concerns with the mismatched NA segment. It is therefore encouraging that Felt et al. (2021), demonstrated findings correlating with ours. They showed that the timing of precisely when RSV DVGs were detected in human clinical samples had a vast impact on clinical outcome; those detected later were associated with a more severe infection. This study and our data therefore seek to

challenge the belief that all DVG generation is beneficial to the host; rather the kinetics of DVG amplification needs to be considered, those generated early in infection or introduced in the inoculum may be protective to the host whereas those arising later may contribute to pathogenicity. Further work is needed to address whether this is a common feature for all influenza subtypes or indeed other viral infections. Interestingly, a recent preprint investigating DVG generation in SARS CoV-2 infection found that DVGs were more abundant in symptomatic individuals than asymptomatic individuals. Furthermore, they also found prolonged DVG generation in an immunocompromised patient (Zhou et al., 2022). As past studies have generally focused on the presence of DVGs and do not address when they arise and how levels change, future studies where DVGs are sampled throughout an active infection, combined with analysis of cytokine levels, infectious viral load and severity would be informative.

Our studies emphasise that when generating virus stocks, care should be taken to ensure minimal levels of DVGs. This is particularly important if comparisons between different viruses are to be made regarding host immune responses. However, even by using low MOIs and short incubation times, generating a completely free DVG stock is difficult. It is therefore imperative that both infectious and non-infectious particles are taken into consideration when comparative experiments are designed. This could be achieved by ensuring viral stocks have similar genome/PFU ratios or by normalizing input by assays that quantify total particles instead of just infectious particles. Furthermore, this isn't just required for studies on influenza but should be adopted for all virology research. A study that elegantly demonstrates this is one focusing on Ebola virus disease, where the authors show that preparations of a genetically identical Ebola virus varied in their disease progression in cynomolgus macaques due to different particle: PFU ratios (Alfson et al., 2015). Promisingly, several SARS CoV-2 publications have reported the genome: PFU ratios of the virus stocks used (Liu et al., 2021; Shiliaev et al., 2021).

7.3 Are DVGs transmitted in natural infections?

Many studies have identified a relatively tight transmission bottleneck for influenza virus, some suggesting less than 10 virions are required to establish an infection (McCrone et al., 2018; Varble et al., 2014). This severely reduces the probability of co-infection at the onset of

infection occurring. However, for direct contact in ferrets, looser bottlenecks have been described (Frise et al., 2016). Interestingly one study analysing DVGs from the URT of H1N1 infected individuals found genetically identical DVGs in two students who attended the same university (Saira et al., 2013). This is intriguing as either DVGs were transmitted or the same DVG arose independently in different individuals. As most human infections with H5N1 are associated with direct contact with infected birds (Van Kerkhove et al., 2011), there is a possibility that DIPs could be transmitted alongside infectious particles. To our knowledge, no studies have identified DVGs in human H5N1 samples, but they have been detected in clinical samples from H7N9-infected patients, although no correlation to clinical severity was identified (Lui et al., 2019). However, this study did highlight that the expression of DVGs was lower in comparative samples from H3N2 infected individuals.

7.4 *De novo* aberrant RNA replication products

In Chapter 5, we were able to identify DVGs in the infected murine lungs by both RT-PCR followed by Sanger sequencing (Figures 5.9-5.10) and NGS (Table 5.1) that were not detected in the initial viral stocks or indeed at early time points, indicating that these may have arisen *de novo*. In Chapter 6 we therefore assessed aberrant replication RNAs made *de novo* by the Tky/05 polymerase. We confirmed that the Tky/05 polymerase generated mvRNAs and DVGs by utilizing vRNP reconstitution assays. We detected both DVGs and mvRNAs when the Tky05 FL PB1 or PB2 vRNA template was provided (Figures 6.2A, 6.2B, 6.3A and 6.3B). mvRNAs have been previously shown to be preferentially generated by HPAIV polymerases (Te Velthuis et al., 2018). However, a subsequent study highlighted that not all mvRNAs were equal in activating the IFN-B promoter and abundance was not correlated with greater immune activation (French et al, 2022). Instead, mvRNAs that were poorly replicated and formed specific t-loop structures, were in fact more immunostimulatory. This suggests that the sequence of the aberrant RNA is the determining factor in activating type I IFN. Work by Mendes and Russell (2021), supports this; they showed that type I IFN induction by IAV DVGs was length independent. Therefore, future work could address the role of introducing both synonymous and non-synonymous mutations into the pPolI plasmid that provides the vRNA template to ascertain whether this alters mvRNA generation and type I IFN induction. Further

in vivo studies could be performed using viruses containing these genetic differences to compare infection outcomes.

We also introduced two mammalian adaptive mutations into the Tky/05 PB2 protein. The rationale behind this was to see whether by making this subunit of the polymerase more adapted to mammalian cells we could reduce the formation of aberrant replication products. Our results indicated that substitution of two residues at the N-terminus (D9N and T81M) in the Tky/05 PB2 protein did not result in any aberrant product formation (Figure 6.8). However, in the same assay we were unable to demonstrate DVGs or mvRNAs formed from the 6:2 Tky/05 WT polymerase so these results are difficult to interpret. We did however clearly demonstrate an association with limiting NP and the formation of mvRNAs (Figure 6.5A) which is in accordance with other studies (Nilsson-Payant et al., 2021; Te Velthuis et al., 2018). This is most likely due to these mvRNAs retaining the ability to be replicated independently of NP whereas FL vRNA isn't (Turrell et al., 2013). Therefore, it may be beneficial in future experiments to limit the amount of NP used in vRNP reconstitution assays, to maximise the chance of detecting aberrant RNAs. Additionally, as our analysis relied solely on RT-PCR, future work could utilise more sensitive approaches such as NGS to capture the full repertoire of aberrant RNAs generated.

Attempts to analyse the immunostimulatory potential of the aberrant RNA products generated by the vRNP reconstitution assays were less informative as in both methods used (RNAs transfected into A549 IFN-β luc cells and *in situ* IFN-β reporter assays), both FL vRNA and aberrant RNAs would be present. scRNAseq is an elegant alternative, as it would allow resolution at the single cell level. This has been successfully employed to distinguish between cells enriched in DVGs and those enriched in FL transcripts and the associated interferon response (Wang et al., 2020). This therefore allows better definition of the contribution of each RNA species to activating type I IFN.

7.5 Mammalian adapting mutations in the Tky/05 PB2 protein

In contrast to our vRNP reconstitution assays, when assessing virus stocks, we detected more polymerase DVGs formed by the 6:2 Tky/05 DM virus than the WT 6:2 Tky/05 virus (Figure 6.11). However, we only rescued virus once and it is unclear as to whether we would have the

same outcome if performed again. This raises a valid question; how many replicates are required to be confident that certain mutations are responsible for aberrant RNA replication product formation? In the study by Vasilijevic et al. (2017), two independent virus stocks were generated from both mild and fatal URT swabs from IAV H1N1 infected individuals. They were able to demonstrate that both mild virus stocks contained greater numbers of PB2 DVGs by RT-PCR than both the stocks cultured from the fatal swab. Of note, the band sizes of the DVGs detected from the two independent mild stocks differed, suggesting that different DVG species were generated in these stocks.

The 9N and 81M PB2 mutations could modestly increase the pro-inflammatory and type I IFN response *in vitro* (Figures 6.9 and 6.12C-E). This was not unsurprising as past research has showed these positions were important for modulating type I IFN induction (Graef et al., 2010; Long & Fodor, 2016; Te Velthuis et al., 2018). Surprisingly, we observed no change in weight loss *in vivo*, nor a difference in IFN-α protein in the murine lung homogenates between the 6:2 Tky/05 and 6:2 Tky/05 DM virus (Figure 6.13). This is in stark contrast to the significant difference in pathogenicity observed between the 7:1 Tky/05 LOW and the 6:2 Tky/05 virus (Chapter 5, Figure 5.4). This demonstrates that the effects of these substitutions are not able to alter the outcome of infection whereas increased polymerase DVG content or a differing NA segment could. Ideally, we would have generated viruses containing other mammalian adaptive substitutions in PB2 and analysed these *in vivo*. Furthermore, extending mutagenesis to other polymerase segments might have resulted in enhanced pathogenicity *in vivo* as numerous mammalian adaptive mutations in PB1 and PA in avian strains have also been shown to increase pathogenicity (Xu et al., 2012; Yamaji et al., 2015a).

7.6 The emerging role of ZBP1 in pathogenesis

A high level of cell death is a common feature of mammalian H5N1 infection (Korteweg & Gu, 2008). An exciting result in Chapter 4 was that the levels of polymerase DVGs in the virus stocks modulated the amount of ZBP1-induced cell death (Figure 4.19). Whilst prior studies have confirmed ZBP1 binds to Z-RNAs (Jiao et al., 2020; Zhang et al., 2020), how influenza RNAs (FL, DVGs, mvRNAs) adopt this Z-confirmation and whether aberrant RNAs are more likely to form this confirmation is still unclear and future studies should address this.

If time allowed, we could have conducted *in vivo* studies in ZBP1-/- mice. The literature to date shows inconclusive results with some studies suggesting ZBP1 is protective *in vivo* (Momota et al., 2020; Thapa et al., 2016) and others demonstrating a detrimental role (Kuriakose et al., 2016). Interestingly, (Momota et al., 2020), reported that if IAV was given intranasally then the ZBP1-/- mice succumbed to infection but if administered via the trachea, the mice had an increased survival rate. As mammalian infections with HPAIVs are associated with replication in the LRT rather than the URT, and are associated with increased cell death, mortality may well be higher in mice expressing ZBP1 following a H5N1 infection. However, our *in vitro* data only showed a slight but non-significant increase in ZBP1-mediated cell death following infection with the 6:2 Tky/05 virus when compared to a more mammalian adaptive strain (Figure 4.17). To our knowledge, comparisons between HPAIVs and seasonal influenza viruses in ZBP1-/- mice have not yet been performed. We therefore could firstly determine whether there are differences regarding pathogenicity in the ZBP1-/- mice between viruses containing HPAIV or seasonal internal genes that have similar levels of DVGs, and then explore whether levels of DVGs in the virus stocks also impact mortality.

In humans, there have been recent studies suggesting a link between ZBP1 and severe infection with SARS CoV-2. For example, ZBP1 mRNA has been shown to be upregulated in immune cells to a greater extent in individuals requiring critical care than those who had only mild infections (Arefinia et al., 2022; Karki et al., 2022). In Chapter 5, (Figure 5.7), we also saw that ZBP1 mRNA levels in the lungs were significantly higher at 48 h.p.i in mice from the 7:1 Tky/05 LOW and 6:2 Tky/05 infected groups than those infected with the 7:1 Tky/05 HIGH virus, echoing the SARS-CoV-2 findings; increased upregulation of ZBP1 expression is associated with higher pathogenicity. Furthermore, Karki et al. (2022), showed that IFN-β treatment after β-coronavirus infection (mouse hepatitis virus; MHV) increased mortality, whereas ablation of ZBP1 or its Zα domain, led to increased survival. As ZBP1 is an ISG, this study highlights the need for careful evaluation of IFN-β as a treatment, as its use to treat COVID-19 could potentially lead to a worse outcome.

7.7 Treatment options for managing respiratory virus induced cytokine storms

Treating cytokine storms induced by respiratory viruses remains challenging. Hospitalised patients may require critical care due to hypoxic respiratory failure, resulting in invasive mechanical ventilation (IMV). This was sadly particularly prevalent during the first wave of the COVID-19 pandemic (Richardson et al., 2020). The corticosteroid dexamethasone, which possesses anti-inflammatory properties due to decreasing the transcription of genes encoding for pro-inflammatory cytokines and chemokines (Rhen & Cidlowski, 2005), demonstrated a clear benefit for treating severe COVID-19 (The RECOVERY Collaborative Group, 2020). However, this benefit was not observed for those patients with less severe COVID-19 who did not require any respiratory support, and in fact there was a slight increase in mortality.

Although, corticosteroids including dexamethasone have also been used to treat severe influenza infections (Brun-Buisson et al., 2011; Cao et al., 2016), the benefit is still inconclusive with studies suggesting early treatment with corticosteroids could increase mortality (Brun-Buisson et al., 2011). This is further supported by Lee et al. (2009b), where the early use of corticosteroids in patients hospitalized with seasonal A/H1N1 resulted in increased viral titres and prolonged viral shedding when compared to non-corticosteroid-treated patients.

The effects of dexamethasone to treat H5N1 has not been shown to be beneficial in BALB/c mice (Xu et al., 2009), nor in humans (Carter, 2007). However, the use of antivirals in combination with corticosteroids or other treatments that modulate the immune system, have proved to be more successful. Mice treated with the neuraminidase inhibitor zanamivir in combination with the immunomodulators celecoxib and mesalazine, had significantly improved survival rates following challenge with a high dose of H5N1 virus over individual or no treatment (Zheng et al., 2008). Interestingly, mice treated with zanamivir alone showed reduced viral replication but had similar levels of cytokines and chemokines in their lungs to untreated mice. This emphasises the requirement for a two-pronged approach; early antivirals are clearly needed to reduce viral replication but by the time symptoms develop, viral load is often high and may have already triggered immunopathology which cannot be dampened by further suppression of viral replication. At this stage immunomodulators may be effective. Therefore, the timing of treatment administration is critical which can only be

effectively applied through an understanding of viral kinetics and pathogenesis. Importantly, clinical trials evaluating the effectiveness of both antivirals and immune modulators for hospitalised patients following seasonal influenza infection are currently taking place in the UK (National Institute for Health and Care Research, 2022).

7.8 DVGs as therapies

An alternative treatment option would be to harness the antiviral properties of DVGs and use defective interfering particles (DIPs). One very attractive feature of IAV DIPs is that the chance of resistance to interference is extremely low since both FL segments and DIPs share a promoter sequence. Therefore, any escape mutants would need to have changes in the promoter region of all genome segments to ensure specificity for FL segments only, as well as a compensatory mutation in the viral polymerase to enable their replication. DIPs have either been isolated from viral infections, such as the well characterised DI/244 from A/PR/8/34 (Easton et al., 2011) or instead synthesised (Tilston-Lunel et al., 2021; Yao et al., 2021). The use of DIPs prophylactically has been shown to offer protection to the host in numerous animal studies, even with severe pathogenic viruses. Indeed, when administered prophylactically, H5N1 DIPs increased the survival rates of mice against lethal H5N1 challenge (Huo et al., 2020). This is not just limited to HPAIV IAV, DIPs developed from the Nipah virus genome with strong antiviral activity *in vitro*, also increased survival of hamsters from a lethal Nipah challenge (Welch et al., 2022). Similarly, those developed from SARS-CoV-2 have also proved effective against a homologous challenge in hamsters (Chaturvedi et al., 2021).

Major challenges associated with the use of DIPs as therapy is the questions of dosage and timing of administration. Welch et al. (2022), were able to demonstrate that a 100:1 DIP:virus ratio was still able to mediate protection, whereas Dimmock et al. (2008), reported a 2-log increase of DI/244 was required to restrict the spread of infection, and has been verified by modelling studies (Rudiger et al., 2021). As previously mentioned, human infections can be initiated by only a few infectious particles so by extrapolating these findings, a similar level of DIPs could potentially be administered intranasally, although to date no experiments in humans have been performed. The timings of when DIPs should be given is of the utmost importance. Many studies show very strong protection when given prophylactically but when administered after infection there is a short therapeutic window. For example, Xiao et al.

(2021), using an engineered poliovirus type 1 derived DVG to generate therapeutic interfering particles (eTIP1s), demonstrated that these could protect from infection by SARS CoV-2 and PR8 if given 24 h.p.i, but this was lost if administered at 48 h.p.i. Studies using DI/244 showed 80-100% survival if administered 24 h.p.i but at 48 h.p.i there was only partial protection with 33% mice surviving the infection (Dimmock et al., 2008).

Whilst not an aim of this thesis, it would have been interesting to determine whether the polymerase DVGs characterised from the 7:1 Tky.05 virus stocks could have provided protection if used as a treatment. This is traditionally achieved by either UV-irradiating the standard "helper" virus in the virus stock (Duhaut & Dimmock, 1998) or coinfecting cells with standard virus and cloned DVGs and then UV-irradiating the standard virus (Dimmock et al., 2012). More recently, DI/244 was successfully generated through co-expression of FL segments 2-8, DI/244 and a cell line expressing the missing viral protein (PB2/segment 1) for in trans delivery (Bdeir et al., 2019). This is particularly attractive as different DIPs could be generated with no possibility of contamination from the standard virus. Our findings in both Chapter 4 and 5 would suggest that some of the polymerase DVGs characterised could be effective if given as a prophylaxis. The 7:1 Tky/05 HIGH virus stock contained a high ratio of non-infectious to infectious particles (Figure 4.5) and displayed reduced viral titres in cell culture, (Figure 4.8) suggesting that the DVGs present at these high levels can interfere with standard viral replication. Furthermore, infection with this virus in the mouse model resulted in minimal clinical symptoms and weight loss (Figure 5.4). By producing individual cloned DIPs and administering these at the time of infection we could elucidate specifically which DVG conferred the best antiviral activity in vivo. Conversely, the 7:1 Tky/05 LOW virus stock was highly pathogenic in our mouse model (Figure 5.4) although the stock contained identical DVGs to the 7:1 Tky/05 HIGH virus albeit at lower amounts (Figures 4.5 and 4.6). This therefore emphasises the importance of ensuring the correct dosage of DIPs. The high pathogenicity of the 7:1 Tky/05 LOW stock (Figures 5.4), also suggests that these DIPs could potentially worsen disease if administered therapeutically as DVGs increased between 6-96 hours following infection when determined by NGS (Figure 5.11). Therefore, although a promising therapy for viral infections which warrants further investigation, our findings highlight the need for a thorough assessment of DIPs *in vivo* if they are to be used as a non-

prophylactic antiviral treatment, to ensure that they do not unintentionally exacerbate disease progression.

7.9 Concluding Remarks

In summary, we have characterised aberrant RNAs produced by a HPAIV H5N1 polymerase in both viral infections and vRNP reconstitution assays as well as exploring viral replication in macrophages. We showed that increased IFN-alpha secretion from 6:2 Tky/05 infected murine macrophages was not dependent on high vRNA levels, moreover the internal genes of H5N1 conferred this phenotype. We also demonstrated that the levels of non-infectious particles, including DIPs, had a profound impact on the severity of infection in mice. Additionally, we showed that although mammalian associated substitutions in the N-terminal region of the H5N1 PB2 could affect type I IFN induction *in vitro,* this was not observed *in vivo.* Finally, we demonstrated that reduced levels of IAV NP increased aberrant RNAs and type I IFN induction. Altogether, this study has shown that aberrant RNAs stimulate innate immunity and whether these responses are protective or detrimental to the host are likely influenced by their amplification kinetics. By furthering our understanding of the molecular mechanisms and subsequent pathology of viral-induced cytokine storms, we increase the chances of developing effective future treatment strategies.

References

Abdel-Ghafar, A., Chotpitayasunondh, T., Gao, Z., Hayden, F., Nguyen, D., de Jong, M., Naghdaliyev, A., Peiris, J., Shindo, N., & Soeroso, S. (2008). Writing Committee of the Second World Health Organization Consultation On Clinical Aspects of Human Infection with Avian Influenza A(H5N1) Virus. Update on Avian Influenza A (H5N1) Virus Infection in Humans. *New England Journal of Medicine*, *358*(3), 261-273.

Ackerman, E. E., Weaver, J. J., & Shoemaker, J. E. (2022). Mathematical Modeling Finds Disparate Interferon Production Rates Drive Strain-Specific Immunodynamics During Deadly Influenza Infection. *Viruses*, *14*(5), 906.

Adalja, A., & Inglesby, T. (2022). A Novel International Monkeypox Outbreak. *Annals of Internal Medicine 175*(8), 1175-1176.

Addetia, A., Phung, Q., Bradley, B. T., Lin, M. J., Zhu, H., Xie, H., Huang, M.-L., & Greninger, A. L. (2021). In Vivo Generation of BK and JC Polyomavirus Defective Viral Genomes in Human Urine Samples Associated With Higher Viral Loads. *Journal of Virology*, *95*(12), e00250-00221.

Aldridge Jr, J. R., Moseley, C. E., Boltz, D. A., Negovetich, N. J., Reynolds, C., Franks, J., Brown, S. A., Doherty, P. C., Webster, R. G., & Thomas, P. G. (2009). TNF/iNOS-Producing Dendritic Cells Are The Necessary Evil of Lethal Influenza Virus Infection. *Proceedings of the National Academy of Sciences*, *106*(13), 5306-5311.

Alfson, K. J., Avena, L. E., Beadles, M. W., Staples, H., Nunneley, J. W., Ticer, A., Dick Jr, E. J., Owston, M. A., Reed, C., & Patterson, J. L. (2015). Particle-to-Pfu Ratio of Ebola Virus Influences Disease Course And Survival In Cynomolgus Macaques. *Journal of Virology*, *89*(13), 6773-6781.

Ali, S., Mann-Nüttel, R., Schulze, A., Richter, L., Alferink, J., & Scheu, S. (2019). Sources of Type I Interferons in Infectious Immunity: Plasmacytoid Dendritic Cells Not Always In the Driver's Seat. *Frontiers in Immunology*, *10*, 778.

Alnaji, F. G., Holmes, J. R., Rendon, G., Vera, J. C., Fields, C. J., Martin, B. E., & Brooke, C. B. (2019). Sequencing Framework for the Sensitive Detection and Precise Mapping of Defective Interfering Particle-Associated Deletions across Influenza A and B Viruses. *Journal of Virology*, *93*(11). https://doi.org/10.1128/JVI.00354-19

Alnaji, F. G., Reiser, W. K., Rivera-Cardona, J., Te Velthuis, A. J., & Brooke, C. B. (2021). Influenza A Virus Defective Viral Genomes Are Inefficiently Packaged into Virions Relative to Wild-Type Genomic RNAs. *mBio*, *12*(6), e02959-02921.

Arefinia, N., Ramezani, A., Farokhnia, M., Zadeh, A. M. A., Yaghobi, R., & Sarvari, J. (2022). Association Between Expression of ZBP1, AIM2, and MDA5 Genes and Severity of Covid-19. *EXCLI journal*, *21*, 1171-1183.

Banchereau, J., Briere, F., Caux, C., Davoust, J., Lebecque, S., Liu, Y.-J., Pulendran, B., & Palucka, K. (2000). Immunobiology of Dendritic Cells. *Annual Review of Immunology*, *18*(1), 767-811. https://doi.org/10.1146/annurev.immunol.18.1.767

Bancroft, C. T., & Parslow, T. G. (2002). Evidence for Segment-Nonspecific Packaging of the Influenza A Virus Genome. *Journal of Virology*, *76*(14), 7133-7139.

Barbezange, C., Jones, L., Blanc, H., Isakov, O., Celniker, G., Enouf, V., Shomron, N., Vignuzzi, M., & Van der Werf, S. (2018). Seasonal Genetic Drift of Human Influenza A Virus Quasispecies Revealed by Deep Sequencing. *Frontiers in Microbiology*, *9*, 2596.

Baskin, C. R., Bielefeldt-Ohmann, H., Tumpey, T. M., Sabourin, P. J., Long, J. P., García-Sastre, A., Tolnay, A.-E., Albrecht, R., Pyles, J. A., & Olson, P. H. (2009). Early and Sustained Innate Immune Response Defines Pathology and Death in Nonhuman Primates Infected by Highly Pathogenic Influenza Virus. *Proceedings of the National Academy of Sciences*, *106*(9), 3455-3460.

Basler, C. F., Reid, A. H., Dybing, J. K., Janczewski, T. A., Fanning, T. G., Zheng, H., Salvatore, M., Perdue, M. L., Swayne, D. E., & Garcia-Sastre, A. (2001). Sequence of the 1918 Pandemic Influenza Virus Nonstructural Gene (NS) Segment and Characterization of Recombinant Viruses Bearing the 1918 NS Genes. *Proceedings of the National Academy of Sciences*, *98*(5), 2746-2751.

Baum, A., & Garcia-Sastre, A. (2011). Differential Recognition of Viral RNA by RIG-I. *Virulence*, *2*(2), 166-169. https://doi.org/10.4161/viru.2.2.15481

Baum, A., Sachidanandam, R., & Garcia-Sastre, A. (2010). Preference of RIG-I for Short Viral RNA Molecules in Infected Cells Revealed by Next-Generation Sequencing. *Proceedings of the National Academy of Sciences of the United States of America*, *107*(37), 16303-16308. https://doi.org/10.1073/pnas.1005077107

Baum, S. G. (2008). Zoonoses-with Friends Like This, Who Needs Enemies? *Transactions of the American Clinical and Climatological Association*, *119*, 39.

Bdeir, N., Arora, P., Gärtner, S., Hoffmann, M., Reichl, U., Pöhlmann, S., & Winkler, M. (2019). A System for Production of Defective Interfering Particles in the Absence of Infectious Influenza A Virus. *PloS One*, *14*(3), e0212757.

Beare, A., Schild, G., & Craig, J. (1975). Trials in Man with Live Recombinants Made from A/PR/8/34 (H0N1) and Wild H3N2 Influenza Viruses. *The Lancet*, *306*(7938), 729-732.

Behrens, E. M., Gadue, P., Gong, S. y., Garrett, S., Stein, P. L., & Cohen, P. L. (2003). The Mer Receptor Tyrosine Kinase: Expression and Function Suggest a Role in Innate Immunity. *European Journal of Immunology*, *33*(8), 2160-2167.

Belser, J. A., Katz, J. M., & Tumpey, T. M. (2011). The Ferret as a Model Organism to Study Influenza a Virus Infection. *Disease Models & Mechanisms*, *4*(5), 575-579.

Belser, J. A., & Tumpey, T. M. (2013). H5N1 Pathogenesis Studies in Mammalian Models. *Virus Research*, *178*(1), 168-185. https://doi.org/10.1016/j.virusres.2013.02.003

Bhat, S., Bialy, D., Sealy, J. E., Sadeyen, J.-R., Chang, P., & Iqbal, M. (2020). A Ligation and Restriction Enzyme Independent Cloning Technique: An Alternative to Conventional Methods for Cloning Hard-to-Clone Gene Segments in the Influenza Reverse Genetics System. *Virology Journal*, *17*(1), 1-9.

Bhat, T., Cao, A., & Yin, J. (2022). Virus-Like Particles: Measures and Biological Functions. *Viruses*, *14*(2). https://doi.org/10.3390/v14020383

Bhatia, M., & Moochhala, S. (2004). Role of Inflammatory Mediators in the Pathophysiology of Acute Respiratory Distress Syndrome. *Journal of Pathology*, *202*(2), 145-156. https://doi.org/10.1002/path.1491

Billiau, A., & Matthys, P. (2009). Interferon-Γ: A Historical Perspective. *Cytokine and Growth Factor Reviews*, *20*(2), 97-113.

Blanco-Melo, D., Nilsson-Payant, B. E., Liu, W.-C., Uhl, S., Hoagland, D., Møller, R., Jordan, T. X., Oishi, K., Panis, M., & Sachs, D. (2020). Imbalanced Host Response to SARS-Cov-2 Drives Development of Covid-19. *Cell*, *181*(5), 1036-1045. e1039.

Blumenkrantz, D., Roberts, K. L., Shelton, H., Lycett, S., & Barclay, W. S. (2013). The Short Stalk Length of Highly Pathogenic Avian Influenza H5N1 Virus Neuraminidase Limits Transmission of Pandemic H1N1 Virus in Ferrets. *Journal of Virology*, *87*(19), 10539-10551. https://doi.org/10.1128/JVI.00967-13

Boergeling, Y., Rozhdestvensky, T. S., Schmolke, M., Resa-Infante, P., Robeck, T., Randau, G., Wolff, T., Gabriel, G., Brosius, J., & Ludwig, S. (2015). Evidence for a Novel Mechanism of Influenza Virus-Induced Type I Interferon Expression by a Defective RNA-Encoded Protein. *PLoS Pathogens*, *11*(5), e1004924.

Boussier, J., Munier, S., Achouri, E., Meyer, B., Crescenzo-Chaigne, B., Behillil, S., Enouf, V., Vignuzzi, M., van der Werf, S., & Naffakh, N. (2020). RNA-Seq Accuracy and Reproducibility for the Mapping and Quantification of Influenza Defective Viral Genomes. *RNA*, *26*(12), 1905-1918.

Brooke, C. B. (2014). Biological Activities of 'Noninfectious' Influenza A Virus Particles. *Future Virology*, *9*(1), 41-51. https://doi.org/10.2217/fvl.13.118

Brun-Buisson, C., Richard, J.-C. M., Mercat, A., Thiébaut, A. C., & Brochard, L. (2011). Early Corticosteroids in Severe Influenza a/H1N1 Pneumonia and Acute Respiratory Distress Syndrome. *American Journal of Respiratory and Critical Care Medicine*, *183*(9), 1200-1206.

Cameron, C. M., Cameron, M. J., Bermejo-Martin, J. F., Ran, L., Xu, L., Turner, P. V., Ran, R., Danesh, A., Fang, Y., & Chan, P.-K. M. (2008). Gene Expression Analysis of Host Innate Immune Responses During Lethal H5N1 Infection in Ferrets. *Journal of Virology*, *82*(22), 11308-11317.

Cao, B., Gao, H., Zhou, B., Deng, X., Hu, C., Deng, C., Lu, H., Li, Y., Gan, J., & Liu, J. (2016). Adjuvant Corticosteroid Treatment in Adults with Influenza a (H7N9) Viral Pneumonia. *Critical Care Medicine*, *44*(6), e318-e328.

Cao, W., Taylor, A. K., Biber, R. E., Davis, W. G., Kim, J. H., Reber, A. J., Chirkova, T., Juan, A., Pandey, A., & Ranjan, P. (2012). Rapid Differentiation of Monocytes into Type I IFN-Producing Myeloid Dendritic Cells as an Antiviral Strategy against Influenza Virus Infection. *The Journal of Immunology*, *189*(5), 2257-2265.

Carrat, F., & Flahault, A. (2007). Influenza Vaccine: The Challenge of Antigenic Drift. *Vaccine*, *25*(39-40), 6852-6862.

Carrique, L., Fan, H., Walker, A. P., Keown, J. R., Sharps, J., Staller, E., Barclay, W. S., Fodor, E., & Grimes, J. M. (2020). Host ANP32A Mediates the Assembly of the Influenza Virus Replicase. *Nature*, *587*(7835), 638-643.

Carter, M. J. (2007). A Rationale for Using Steroids in the Treatment of Severe Cases of H5N1 Avian Influenza. *Journal of Medical Microbiology*, *56*(7), 875-883.

Cascella, M., Rajnik, M., Aleem, A., Dulebohn, S. C., & Di Napoli, R. (2022). *Features, Evaluation, and Treatment of Coronavirus (Covid-19)* (Vol. Treasure Island (FL). In *StatPearls*. StatPearls Publishing LLC.

Chan, L. L., Nicholls, J. M., Peiris, J., Lau, Y. L., Chan, M. C., & Chan, R. W. (2020). Host DNA Released by Netosis in Neutrophils Exposed to Seasonal H1N1 and Highly Pathogenic H5N1 Influenza Viruses. *Respiratory Research*, *21*(1), 1-10.

Chan, M. C., Cheung, C. Y., Chui, W. H., Tsao, S. W., Nicholls, J. M., Chan, Y. O., Chan, R. W., Long, H. T., Poon, L. L., Guan, Y., & Peiris, J. S. (2005). Proinflammatory Cytokine Responses Induced by Influenza a (H5N1) Viruses in Primary Human Alveolar and Bronchial Epithelial Cells. *Respiratory Research*, *6*, 135. https://doi.org/10.1186/1465-9921-6-135

Chan, R. W., Leung, C. Y., Nicholls, J. M., Peiris, J. S., & Chan, M. C. (2012). Proinflammatory Cytokine Response and Viral Replication in Mouse Bone Marrow Derived Macrophages Infected with Influenza H1N1 and H5N1 Viruses. *PloS One*, *7*(11), e51057. https://doi.org/10.1371/journal.pone.0051057

Chaturvedi, S., Vasen, G., Pablo, M., Chen, X., Beutler, N., Kumar, A., Tanner, E., Illouz, S., Rahgoshay, D., & Burnett, J. (2021). Identification of a Therapeutic Interfering Particle—a Single-Dose SARS-Cov-2 Antiviral Intervention with a High Barrier to Resistance. *Cell*, *184*(25), 6022-6036. e6018.

Cheung, C., Poon, L., Lau, A., Luk, W., Lau, Y., Shortridge, K., Gordon, S., Guan, Y., & Peiris, J. (2002). Induction of Proinflammatory Cytokines in Human Macrophages by Influenza a (H5N1) Viruses: A Mechanism for the Unusual Severity of Human Disease? *The Lancet*, *360*(9348), 1831-1837.

Cheung, P. H. H., Lee, T. W. T., Chan, C. P., & Jin, D. Y. (2020). Influenza a Virus PB1-F2 Protein: An Ambivalent Innate Immune Modulator and Virulence Factor. *Journal of Leukocyte Biology*, *107*(5), 763-771.

Cline, T. D., Karlsson, E. A., Seufzer, B. J., & Schultz-Cherry, S. (2013). The Hemagglutinin Protein of Highly Pathogenic H5N1 Influenza Viruses Overcomes an Early Block in the Replication Cycle to Promote Productive Replication in Macrophages. *Journal of Virology*, *87*(3), 1411-1419. https://doi.org/10.1128/JVI.02682-12

Cohen, M., Zhang, X.-Q., Senaati, H. P., Chen, H.-W., Varki, N. M., Schooley, R. T., & Gagneux, P. (2013). Influenza A Penetrates Host Mucus by Cleaving Sialic Acids with Neuraminidase. *Virology Journal*, *10*(1), 1-13.

Conenello, G. M., Zamarin, D., Perrone, L. A., Tumpey, T., & Palese, P. (2007). A Single Mutation in the PB1-F2 of H5N1 (HK/97) and 1918 Influenza A Viruses Contributes to Increased Virulence. *PLoS Pathogens*, *3*(10), e141.

Connor, R. J., Kawaoka, Y., Webster, R. G., & Paulson, J. C. (1994). Receptor Specificity in Human, Avian, and Equine H2 and H3 Influenza Virus Isolates. *Virology*, *205*(1), 17-23.

Cox, R. (2013). Correlates of Protection to Influenza Virus, Where Do We Go from Here? *Human Vaccines & Immunotherapeutics*, *9*(2), 405-408.

Cromer, D., Van Hoek, A. J., Jit, M., Edmunds, W. J., Fleming, D., & Miller, E. (2014). The Burden of Influenza in England by Age and Clinical Risk Group: A Statistical Analysis to Inform Vaccine Policy. *Journal of Infection*, *68*(4), 363-371.

Crotta, S., Davidson, S., Mahlakoiv, T., Desmet, C. J., Buckwalter, M. R., Albert, M. L., Staeheli, P., & Wack, A. (2013). Type I and Type Iii Interferons Drive Redundant Amplification Loops to Induce a Transcriptional Signature in Influenza-Infected Airway Epithelia. *PLoS Pathogens*, *9*(11), e1003773.

Cui, P., Shi, J., Wang, C., Zhang, Y., Xing, X., Kong, H., Yan, C., Zeng, X., Liu, L., & Tian, G. (2022). Global Dissemination of H5N1 Influenza Viruses Bearing the Clade 2.3. 4.4 B HA Gene and Biologic Analysis of the Ones Detected in China. *Emerging Microbes & Infections*, *11*(1), 1693-1704.

Dadonaite, B., Gilbertson, B., Knight, M. L., Trifkovic, S., Rockman, S., Laederach, A., Brown, L. E., Fodor, E., & Bauer, D. L. (2019). The Structure of the Influenza A Virus Genome. *Nature Microbiology*, *4*(11), 1781-1789.

Dadonaite, B., Vijayakrishnan, S., Fodor, E., Bhella, D., & Hutchinson, E. C. (2016). Filamentous Influenza Viruses. *The Journal of General Virology*, *97*(8), 1755.

Dankar, S. K., Wang, S., Ping, J., Forbes, N. E., Keleta, L., Li, Y., & Brown, E. G. (2011). Influenza A Virus NS1 Gene Mutations F103l and M106I Increase Replication and Virulence. *Virology Journal*, *8*, 13. https://doi.org/10.1186/1743-422X-8-13

Davidson, S., Crotta, S., McCabe, T. M., & Wack, A. (2014). Pathogenic Potential of Interferon Alphabeta in Acute Influenza Infection. *Nature Communications*, *5*, 3864. https://doi.org/10.1038/ncomms4864

Davidson, S., McCabe, T. M., Crotta, S., Gad, H. H., Hessel, E. M., Beinke, S., Hartmann, R., & Wack, A. (2016). IFN Λ Is a Potent Anti-Influenza Therapeutic without the Inflammatory Side Effects of IFN A Treatment. *EMBO Molecular Medicine*, *8*(9), 1099-1112.

de Jong, M. D., Simmons, C. P., Thanh, T. T., Hien, V. M., Smith, G. J., Chau, T. N., Hoang, D. M., Chau, N. V., Khanh, T. H., Dong, V. C., Qui, P. T., Cam, B. V., Ha do, Q., Guan, Y., Peiris, J. S., Chinh, N. T., Hien, T. T., & Farrar, J. (2006). Fatal Outcome of Human Influenza a (H5N1) Is Associated with High Viral Load and Hypercytokinemia. *Nature Medicine*, *12*(10), 1203-1207. https://doi.org/10.1038/nm1477

de Marcken, M., Dhaliwal, K., Danielsen, A. C., Gautron, A. S., & Dominguez-Villar, M. (2019). TLR7 and TLR8 Activate Distinct Pathways in Monocytes During RNA Virus Infection. *Science Signaling*, *12*(605), eaaw1347.

De Veer, M. J., Holko, M., Frevel, M., Walker, E., Der, S., Paranjape, J. M., Silverman, R. H., & Williams, B. R. (2001). Functional Classification of Interferon-Stimulated Genes Identified Using Microarrays. *Journal of Leukocyte Biology*, *69*(6), 912-920.

Deeg, C. M., Hassan, E., Mutz, P., Rheinemann, L., Götz, V., Magar, L., Schilling, M., Kallfass, C., Nürnberger, C., & Soubies, S. (2017). In Vivo Evasion of MXA by Avian Influenza Viruses Requires Human Signature in the Viral Nucleoprotein. *Journal of Experimental Medicine*, *214*(5), 1239-1248.

Deng, T., Vreede, F. T., & Brownlee, G. G. (2006). Different De Novo Initiation Strategies Are Used by Influenza Virus RNA Polymerase on Its CRNA and Viral RNA Promoters During Viral RNA Replication. *Journal of Virology*, *80*(5), 2337-2348.

Desai, T. M., Marin, M., Chin, C. R., Savidis, G., Brass, A. L., & Melikyan, G. B. (2014). IFITM3 Restricts Influenza A Virus Entry by Blocking the Formation of Fusion Pores Following Virus-Endosome Hemifusion. *PLoS Pathogens*, *10*(4), e1004048.

Dias, A., Bouvier, D., Crépin, T., McCarthy, A. A., Hart, D. J., Baudin, F., Cusack, S., & Ruigrok, R. W. (2009). The Cap-Snatching Endonuclease of Influenza Virus Polymerase Resides in the PA Subunit. *Nature*, *458*(7240), 914-918.

Dimmock, N. J., Dove, B. K., Scott, P. D., Meng, B., Taylor, I., Cheung, L., Hallis, B., Marriott, A. C., Carroll, M. W., & Easton, A. J. (2012). Cloned Defective Interfering Influenza Virus Protects Ferrets from Pandemic 2009 Influenza a Virus and Allows Protective Immunity to Be Established. *PloS One*, *7*(12), e49394.

Dimmock, N. J., Rainsford, E. W., Scott, P. D., & Marriott, A. C. (2008). Influenza Virus Protecting RNA: An Effective Prophylactic and Therapeutic Antiviral. *Journal of Virology*, *82*(17), 8570-8578.

Diskin, E. R., Friedman, K., Krauss, S., Nolting, J. M., Poulson, R. L., Slemons, R. D., Stallknecht, D. E., Webster, R. G., & Bowman, A. S. (2020). Subtype Diversity of Influenza A Virus in North American Waterfowl: A Multidecade Study. *Journal of Virology*, *94*(11), e02022-02019.

Dou, D., Revol, R., Östbye, H., Wang, H., & Daniels, R. (2018). Influenza A Virus Cell Entry, Replication, Virion Assembly and Movement. *Frontiers in Immunology*, 1581.

Drake, J. W. (1993). Rates of Spontaneous Mutation among RNA Viruses. *Proceedings of the National Academy of Sciences*, *90*(9), 4171-4175.

DuBois, R. M., Zaraket, H., Reddivari, M., Heath, R. J., White, S. W., & Russell, C. J. (2011). Acid Stability of the Hemagglutinin Protein Regulates H5N1 Influenza Virus Pathogenicity. *PLoS Pathogens*, *7*(12), e1002398.

Duhaut, S., & McCauley, J. (1996). Defective RNAs Inhibit the Assembly of Influenza Virus Genome Segments in a Segment-Specific Manner. *Virology*, *216*(2), 326-337.

Duhaut, S. D., & Dimmock, N. J. (1998). Heterologous Protection of Mice from a Lethal Human H1N1 Influenza A Virus Infection by H3N8 Equine Defective Interfering Virus: Comparison of Defective RNA Sequences Isolated from the DI Inoculum and Mouse Lung. *Virology*, *248*(2), 241-253.

Easton, A. J., Scott, P. D., Edworthy, N. L., Meng, B., Marriott, A. C., & Dimmock, N. J. (2011). A Novel Broad-Spectrum Treatment for Respiratory Virus Infections: Influenza-Based Defective Interfering Virus Provides Protection against Pneumovirus Infection in Vivo. *Vaccine*, *29*(15), 2777-2784. https://doi.org/10.1016/j.vaccine.2011.01.102

Eisfeld, A. J., Kawakami, E., Watanabe, T., Neumann, G., & Kawaoka, Y. (2011). Rab11A Is Essential for Transport of the Influenza Virus Genome to the Plasma Membrane. *Journal of Virology*, *85*(13), 6117-6126.

Eisfeld, A. J., Neumann, G., & Kawaoka, Y. (2015). At the Centre: Influenza A Virus Ribonucleoproteins. *Nature Reviews Microbiology*, *13*(1), 28-41.

Elshina, E., & Te Velthuis, A. J. (2021). The Influenza Virus RNA Polymerase as an Innate Immune Agonist and Antagonist. *Cellular and Molecular Life Sciences*, *78*(23), 7237-7256.

Engelhardt, O. G., Smith, M., & Fodor, E. (2005). Association of the Influenza A Virus RNA-Dependent RNA Polymerase with Cellular RNA Polymerase II. *Journal of Virology*, *79*(9), 5812-5818.

Englen, M., Valdez, Y., Lehnert, N., & Lehnert, B. (1995). Granulocyte/Macrophage Colony-Stimulating Factor Is Expressed and Secreted in Cultures of Murine L929 Cells. *Journal of Immunological Methods*, *2*(184), 281-283.

Erlich, Z., Shlomovitz, I., Edry-Botzer, L., Cohen, H., Frank, D., Wang, H., Lew, A. M., Lawlor, K. E., Zhan, Y., Vince, J. E., & Gerlic, M. (2019). Macrophages, Rather Than DCs, Are Responsible

for Inflammasome Activity in the GM-CSF BMDC Model. *Nature Immunology*, *20*(4), 397-406. https://doi.org/10.1038/s41590-019-0313-5

Etienne, L., Bibollet-Ruche, F., Sudmant, P. H., Wu, L. I., Hahn, B. H., & Emerman, M. (2015). The Role of the Antiviral APOBEC3 Gene Family in Protecting Chimpanzees against Lentiviruses from Monkeys. *PLoS Pathogens*, *11*(9), e1005149.

Fajgenbaum, D. C., & June, C. H. (2020). Cytokine Storm. *New England Journal of Medicine*, *383*(23), 2255-2273.

Fan, H., Walker, A. P., Carrique, L., Keown, J. R., Serna Martin, I., Karia, D., Sharps, J., Hengrung, N., Pardon, E., & Steyaert, J. (2019). Structures of Influenza A Virus RNA Polymerase Offer Insight into Viral Genome Replication. *Nature*, *573*(7773), 287-290.

Fan, S., Hatta, M., Kim, J. H., Halfmann, P., Imai, M., Macken, C. A., Le, M. Q., Nguyen, T., Neumann, G., & Kawaoka, Y. (2014). Novel Residues in Avian Influenza Virus PB2 Protein Affect Virulence in Mammalian Hosts. *Nature Communications*, *5*(1), 1-12.

Faust, H., & Mangalmurti, N. S. (2020). Collateral Damage: Necroptosis in the Development of Lung Injury. *American Journal of Physiology-Lung Cellular and Molecular Physiology*, *318*(2), L215-L225.

Felt, S. A., Sun, Y., Jozwik, A., Paras, A., Habibi, M. S., Nickle, D., Anderson, L., Achouri, E., Feemster, K. A., Cardenas, A. M., Turi, K. N., Chang, M., Hartert, T. V., Sengupta, S., Chiu, C., & Lopez, C. B. (2021). Detection of Respiratory Syncytial Virus Defective Genomes in Nasal Secretions Is Associated with Distinct Clinical Outcomes. *Nature Microbiol*ogy,6, 672-681 https://doi.org/10.1038/s41564-021-00882-3

Feng, X., Wang, Z., Shi, J., Deng, G., Kong, H., Tao, S., Li, C., Liu, L., Guan, Y., & Chen, H. (2016). Glycine at Position 622 in PB1 Contributes to the Virulence of H5N1 Avian Influenza Virus in Mice. *Journal of Virology*, *90*(4), 1872-1879. https://doi.org/10.1128/JVI.02387-15

Fenner, F., & Woodroofe, G. M. (1965). Changes in the Virulence and Antigenic Structure of Strains of Myxoma Virus Recovered from Australian Wild Rabbits between 1950 and 1964. *Australian Journal of Experimental Biology and Medical Science*, *43*, 359-370.

Fitzgerald, K. A., & Kagan, J. C. (2020). Toll-Like Receptors and the Control of Immunity. *Cell*, *180*(6), 1044-1066.

Flick, R., & Hobom, G. (1999). Interaction of Influenza Virus Polymerase with Viral RNA in the 'Corkscrew'Conformation. *Journal of General Virology*, *80*(10), 2565-2572.

Fodor, E., Mingay, L. J., Crow, M., Deng, T., & Brownlee, G. G. (2003). A Single Amino Acid Mutation in the PA Subunit of the Influenza Virus RNA Polymerase Promotes the Generation of Defective Interfering RNAs. *Journal of Virology*, *77*(8), 5017-5020.

Fodor, E., Pritlove, D. C., & Brownlee, G. G. (1994). The Influenza Virus Panhandle Is Involved in the Initiation of Transcription. *Journal of Virology*, *68*(6), 4092-4096.

Fodor, E., Pritlove, D. C., & Brownlee, G. G. (1995). Characterization of the RNA-Fork Model of Virion RNA in the Initiation of Transcription in Influenza A Virus. *Journal of Virology*, *69*(7), 4012-4019.

Fong, C. H.-Y., Lu, L., Chen, L.-L., Yeung, M.-L., Zhang, A. J., Zhao, H., Yuen, K.-Y., & To, K. K.-W. (2022). Interferon-Gamma Inhibits Influenza A Virus Cellular Attachment by Reducing Sialic Acid Cluster Size. *Iscience*, *25*(4), 104037.

Fornek, J. L., Gillim-Ross, L., Santos, C., Carter, V., Ward, J. M., Cheng, L. I., Proll, S., Katze, M. G., & Subbarao, K. (2009). A Single-Amino-Acid Substitution in a Polymerase Protein of an H5N1 Influenza Virus Is Associated with Systemic Infection and Impaired T-Cell Activation in Mice. *Journal of Virology*, *83*(21), 11102-11115.

Franca, M., Stallknecht, D., & Howerth, E. (2013). Expression and Distribution of Sialic Acid Influenza Virus Receptors in Wild Birds. *Avian Pathology*, *42*(1), 60-71.

French, H., Pitré, E., Oade, M. S., Elshina, E., Bisht, K., Jahun, A., King, A., Bauer, D. L. V., & Te Velthuis, A. J. W. (2022). Transient RNA Structures Cause Aberrant Infuenza Virus Replication

and Innate Immune Activation. *Science Advances, 8(36)*, eabp8655. https://doi.org/10.1126/sciadv.abp8655

Frensing, T., Heldt, F. S., Pflugmacher, A., Behrendt, I., Jordan, I., Flockerzi, D., Genzel, Y., & Reichl, U. (2013). Continuous Influenza Virus Production in Cell Culture Shows a Periodic Accumulation of Defective Interfering Particles. *PloS One*, *8*(9), e72288. https://doi.org/10.1371/journal.pone.0072288

Frensing, T., Pflugmacher, A., Bachmann, M., Peschel, B., & Reichl, U. (2014). Impact of Defective Interfering Particles on Virus Replication and Antiviral Host Response in Cell Culture-Based Influenza Vaccine Production. *Applied Microbiology and Biotechnology*, *98*(21), 8999-9008. https://doi.org/10.1007/s00253-014-5933-y

Friesenhagen, J., Boergeling, Y., Hrincius, E., Ludwig, S., Roth, J., & Viemann, D. (2012). Highly Pathogenic Avian Influenza Viruses Inhibit Effective Immune Responses of Human Blood-Derived Macrophages. *Journal of Leukocyte Biology*, *92*(1), 11-20. https://doi.org/10.1189/jlb.0911479

Frise, R., Bradley, K., Van Doremalen, N., Galiano, M., Elderfield, R. A., Stilwell, P., Ashcroft, J. W., Fernandez-Alonso, M., Miah, S., & Lackenby, A. (2016). Contact Transmission of Influenza Virus between Ferrets Imposes a Looser Bottleneck Than Respiratory Droplet Transmission Allowing Propagation of Antiviral Resistance. *Scientific Reports*, *6*(1), 1-14.

Gabriel, G., Klingel, K., Otte, A., Thiele, S., Hudjetz, B., Arman-Kalcek, G., Sauter, M., Shmidt, T., Rother, F., & Baumgarte, S. (2011). Differential Use of Importin-A Isoforms Governs Cell Tropism and Host Adaptation of Influenza Virus. *Nature Communications*, *2*(1), 1-7.

Gack, M. U., Shin, Y. C., Joo, C.-H., Urano, T., Liang, C., Sun, L., Takeuchi, O., Akira, S., Chen, Z., & Inoue, S. (2007). TRIM25 Ring-Finger E3 Ubiquitin Ligase Is Essential for RIG-I-Mediated Antiviral Activity. *Nature*, *446*(7138), 916-920.

Galani, I.-E., Rovina, N., Lampropoulou, V., Triantafyllia, V., Manioudaki, M., Pavlos, E., Koukaki, E., Fragkou, P. C., Panou, V., & Rapti, V. (2021). Untuned Antiviral Immunity in Covid-19 Revealed by Temporal Type I/III Interferon Patterns and Flu Comparison. *Nature Immunology*, *22*(1), 32-40.

Galani, I. E., Triantafyllia, V., Eleminiadou, E.-E., Koltsida, O., Stavropoulos, A., Manioudaki, M., Thanos, D., Doyle, S. E., Kotenko, S. V., & Thanopoulou, K. (2017). Interferon-Λ Mediates Non-Redundant Front-Line Antiviral Protection against Influenza Virus Infection without Compromising Host Fitness. *Immunity*, *46*(5), 875-890. e876.

Gamblin, S. J., & Skehel, J. J. (2010). Influenza Hemagglutinin and Neuraminidase Membrane Glycoproteins. *Journal of Biological Chemistry*, *285*(37), 28403-28409.

Gao, R., Sheng, Z., Sreenivasan, C. C., Wang, D., & Li, F. (2020). Influenza a Virus Antibodies with Antibody-Dependent Cellular Cytotoxicity Function. *Viruses*, *12*(3), 276.

Gao, W., Zu, Z., Liu, J., Song, J., Wang, X., Wang, C., Liu, L., Tong, Q., Wang, M., & Sun, H. (2019). Prevailing I292V PB2 Mutation in Avian Influenza H9N2 Virus Increases Viral Polymerase Function and Attenuates IFN-B Induction in Human Cells. *The Journal of General Virology*, *100*(9), 1273.

Garten, W., & Klenk, H.-D. (2008). Cleavage Activation of the Influenza Virus Hemagglutinin and Its Role in Pathogenesis. In *Avian Influenza* (Vol. 27, pp. 156-167). Karger Publishers.

Gautier, E. L., Shay, T., Miller, J., Greter, M., Jakubzick, C., Ivanov, S., Helft, J., Chow, A., Elpek, K. G., Gordonov, S., Mazloom, A. R., Ma'ayan, A., Chua, W. J., Hansen, T. H., Turley, S. J., Merad, M., Randolph, G. J., & Immunological Genome, C. (2012). Gene-Expression Profiles and Transcriptional Regulatory Pathways That Underlie the Identity and Diversity of Mouse Tissue Macrophages. *Nature Immunology*, *13*(11), 1118-1128. https://doi.org/10.1038/ni.2419

Gavazzi, C., Yver, M., Isel, C., Smyth, R. P., Rosa-Calatrava, M., Lina, B., Moulès, V., & Marquet, R. (2013). A Functional Sequence-Specific Interaction between Influenza a Virus Genomic RNA Segments. *Proceedings of the National Academy of Sciences*, *110*(41), 16604-16609.

Genoyer, E., & Lopez, C. B. (2019). The Impact of Defective Viruses on Infection and Immunity. *Annual Review of Virology*, *6*(1), 547-566. https://doi.org/10.1146/annurev-virology-092818-015652

Goubau, D., Schlee, M., Deddouche, S., Pruijssers, A. J., Zillinger, T., Goldeck, M., Schuberth, C., Van der Veen, A. G., Fujimura, T., & Rehwinkel, J. (2014). Antiviral Immunity Via RIG-I-Mediated Recognition of RNA Bearing 5'-Diphosphates. *Nature*, *514*(7522), 372-375.

Graef, K. M., Vreede, F. T., Lau, Y.-F., McCall, A. W., Carr, S. M., Subbarao, K., & Fodor, E. (2010). The PB2 Subunit of the Influenza Virus RNA Polymerase Affects Virulence by Interacting with the Mitochondrial Antiviral Signaling Protein and Inhibiting Expression of Beta Interferon. *Journal of Virology*, *84*(17), 8433-8445.

Gu, J., Xie, Z., Gao, Z., Liu, J., Korteweg, C., Ye, J., Lau, L. T., Lu, J., Gao, Z., & Zhang, B. (2007). H5N1 Infection of the Respiratory Tract and Beyond: A Molecular Pathology Study. *The Lancet*, *370*(9593), 1137-1145.

Guilligay, D., Tarendeau, F., Resa-Infante, P., Coloma, R., Crepin, T., Sehr, P., Lewis, J., Ruigrok, R. W., Ortin, J., & Hart, D. J. (2008). The Structural Basis for Cap Binding by Influenza Virus Polymerase Subunit PB2. *Nature Structural & Molecular Biology*, *15*(5), 500-506.

Guillot, L., Le Goffic, R., Bloch, S., Escriou, N., Akira, S., Chignard, M., & Si-Tahar, M. (2005). Involvement of Toll-Like Receptor 3 in the Immune Response of Lung Epithelial Cells to Double-Stranded RNA and Influenza A Virus. *Journal of Biological Chemistry*, *280*(7), 5571-5580.

Hamilton, B. S., Whittaker, G. R., & Daniel, S. (2012). Influenza Virus-Mediated Membrane Fusion: Determinants of Hemagglutinin Fusogenic Activity and Experimental Approaches for Assessing Virus Fusion. *Viruses*, *4*(7), 1144-1168.

Han, Y., Bo, Z.-j., Xu, M.-y., Sun, N., & Liu, D.-h. (2014). The Protective Role of TLR3 and TLR9 Ligands in Human Pharyngeal Epithelial Cells Infected with Influenza A Virus. *The Korean Journal of Physiology & Pharmacology: Official Journal of the Korean Physiological Society and the Korean Society of Pharmacology*, *18*(3), 225.

Hartmann, B. M., Li, W., Jia, J., Patil, S., Marjanovic, N., Martinez-Romero, C., Albrecht, R. A., Hayot, F., Garcia-Sastre, A., Wetmur, J. G., Moran, T. M., & Sealfon, S. C. (2013). Mouse Dendritic Cell (DC) Influenza Virus Infectivity Is Much Lower Than That for Human DCs and Is Hemagglutinin Subtype Dependent. *Journal of Virology*, *87*(3), 1916-1918. https://doi.org/10.1128/JVI.02980-12

Hayden, F. G., Fritz, R., Lobo, M. C., Alvord, W., Strober, W., & Straus, S. E. (1998). Local and Systemic Cytokine Responses During Experimental Human Influenza a Virus Infection. Relation to Symptom Formation and Host Defense. *The Journal of Clinical Investigation*, *101*(3), 643-649.

Hayman, A., Comely, S., Lackenby, A., Hartgroves, L., Goodbourn, S., McCauley, J., & Barclay, W. (2007). NS1 Proteins of Avian Influenza A Viruses Can Act as Antagonists of the Human Alpha/Beta Interferon Response. *Journal of Virology*, *81*(5), 2318-2327.

Hayman, A., Comely, S., Lackenby, A., Murphy, S., McCauley, J., Goodbourn, S., & Barclay, W. (2006). Variation in the Ability of Human Influenza A Viruses to Induce and Inhibit the IFN-B Pathway. *Virology*, *347*(1), 52-64.

Hayman, T. J., Hsu, A. C., Kolesnik, T. B., Dagley, L. F., Willemsen, J., Tate, M. D., Baker, P. J., Kershaw, N. J., Kedzierski, L., & Webb, A. I. (2019). Riplet, and Not TRIM25, Is Required for Endogenous RIG-I-Dependent Antiviral Responses. *Immunology and Cell Biology*, *97*(9), 840-852.

Heap, R. E., Marin-Rubio, J. L., Peltier, J., Heunis, T., Dannoura, A., Moore, A., & Trost, M. (2021). Proteomics Characterisation of the L929 Cell Supernatant and Its Role in BMDM Differentiation. *Life Science Alliance*, *4*(6). https://doi.org/10.26508/lsa.202000957

Hein, M. D., Arora, P., Marichal-Gallardo, P., Winkler, M., Genzel, Y., Pohlmann, S., Schughart, K., Kupke, S. Y., & Reichl, U. (2021a). Cell Culture-Based Production and in Vivo Characterization

of Purely Clonal Defective Interfering Influenza Virus Particles. *BMC Biology*, *19*(1), 91. https://doi.org/10.1186/s12915-021-01020-5

Hein, M. D., Kollmus, H., Marichal-Gallardo, P., Puttker, S., Benndorf, D., Genzel, Y., Schughart, K., Kupke, S. Y., & Reichl, U. (2021b). OP7, a Novel Influenza a Virus Defective Interfering Particle: Production, Purification, and Animal Experiments Demonstrating Antiviral Potential. *Applied Microbiology and Biotechnology*, *105*(1), 129-146. https://doi.org/10.1007/s00253-020-11029-5

Helft, J., Bottcher, J., Chakravarty, P., Zelenay, S., Huotari, J., Schraml, B. U., Goubau, D., & Reis e Sousa, C. (2015). GM-CSF Mouse Bone Marrow Cultures Comprise a Heterogeneous Population of CD11c(+)MHCII (+) Macrophages and Dendritic Cells. *Immunity*, *42*(6), 1197-1211. https://doi.org/10.1016/j.immuni.2015.05.018

Herfst, S., Schrauwen, E. J., Linster, M., Chutinimitkul, S., de Wit, E., Munster, V. J., Sorrell, E. M., Bestebroer, T. M., Burke, D. F., & Smith, D. J. (2012). Airborne Transmission of Influenza A/H5N1 Virus between Ferrets. *Science*, *336*(6088), 1534-1541.

Herold, S., Steinmueller, M., von Wulffen, W., Cakarova, L., Pinto, R., Pleschka, S., Mack, M., Kuziel, W. A., Corazza, N., & Brunner, T. (2008). Lung Epithelial Apoptosis in Influenza Virus Pneumonia: The Role of Macrophage-Expressed TNF-Related Apoptosis-Inducing Ligand. *The Journal of Experimental Medicine*, *205*(13), 3065-3077.

Honda, A., Ueda, K., Nagata, K., & Ishihama, A. (1988). RNA Polymerase of Influenza Virus: Role of NP in RNA Chain Elongation. *The Journal of Biochemistry*, *104*(6), 1021-1026.

Horimoto, T., Nakayama, K., Smeekens, S. P., & Kawaoka, Y. (1994). Proprotein-Processing Endoproteases PC6 and Furin Both Activate Hemagglutinin of Virulent Avian Influenza Viruses. *Journal of Virology*, *68*(9), 6074-6078.

Hornung, V., Ellegast, J., Kim, S., Brzózka, K., Jung, A., Kato, H., Poeck, H., Akira, S., Conzelmann, K.-K., & Schlee, M. (2006). 5'-Triphosphate RNA Is the Ligand for RIG-I. *Science*, *314*(5801), 994-997.

Hsiang, T.-Y., Zhao, C., & Krug, R. M. (2009). Interferon-Induced ISG15 Conjugation Inhibits Influenza A Virus Gene Expression and Replication in Human Cells. *Journal of Virology*, *83*(12), 5971-5977.

Huang, C., Wang, Y., Li, X., Ren, L., Zhao, J., Hu, Y., Zhang, L., Fan, G., Xu, J., & Gu, X. (2020). Clinical Features of Patients Infected with 2019 Novel Coronavirus in Wuhan, China. *The Lancet*, *395*(10223), 497-506.

Huang, Y., Xu, W., & Zhou, R. (2021). NLRP3 Inflammasome Activation and Cell Death. *Cellular & Molecular Immunology*, *18*(9), 2114-2127.

Hui, K. P., Lee, S. M., Cheung, C. Y., Ng, I. H., Poon, L. L., Guan, Y., Ip, N. Y., Lau, A. S., & Peiris, J. S. (2009). Induction of Proinflammatory Cytokines in Primary Human Macrophages by Influenza A Virus (H5N1) Is Selectively Regulated by IFN Regulatory Factor 3 and P38 MAPK. *Journal of Immunology*, *182*(2), 1088-1098. https://doi.org/10.4049/jimmunol.182.2.1088

Huo, C., Cheng, J., Xiao, J., Chen, M., Zou, S., Tian, H., Wang, M., Sun, L., Hao, Z., & Hu, Y. (2020). Defective Viral Particles Produced in Mast Cells Can Effectively Fight against Lethal Influenza A Virus. *Frontiers in Microbiology*, *11*, 553274. https://doi.org/10.3389/fmicb.2020.553274

Huo, C., Jin, Y., Zou, S., Qi, P., Xiao, J., Tian, H., Wang, M., & Hu, Y. (2018). Lethal influenza A virus preferentially activates TLR3 and triggers a severe inflammatory response. *Virus Research, 257,* 102-112. https://doi.org/10.1016/j.virusres.2018.09.012

Hussain, Z. (2022). Ghana Declares Its First Outbreak of Marburg Virus Disease after Two Deaths. *British Medical Journal (Clinical Research Ed.),* 378, o1797. https://doi.org/10.1136/bmj.o1797

Hutchinson, E. C., Charles, P. D., Hester, S. S., Thomas, B., Trudgian, D., Martínez-Alonso, M., & Fodor, E. (2014). Conserved and Host-Specific Features of Influenza Virion Architecture. *Nature Communications*, *5*(1), 1-11.

Hutchinson, E. C., von Kirchbach, J. C., Gog, J. R., & Digard, P. (2010). Genome Packaging in Influenza A Virus. *Journal of General Virology*, *91*(2), 313-328.

Ichinose, T., Pang, I. K.-s., & Iwasaki, A. (2010). Influenza Virus Activates Inflammasomes through Intracellular M2 Channel. *Nature Immunology,* 11(5), 404–410. https://doi.org/10.1038/ni.1861

Imai, M., Herfst, S., Sorrell, E., Schrauwen, E., Linster, M., De Graaf, M., Fouchier, R., & Kawaoka, Y. (2013). Transmission of Influenza A/H5N1 Viruses in Mammals. *Virus Research*, *178*(1), 15-20.

Ioannidis, L. J., Verity, E. E., Crawford, S., Rockman, S. P., & Brown, L. E. (2012). Abortive Replication of Influenza Virus in Mouse Dendritic Cells. *Journal of Virology*, *86*(10), 5922-5925.

Isaacs, A., & Lindenmann, J. (1957). Virus Interference. I. The Interferon. *Proceedings of the Royal Society of London. Series B-Biological Sciences*, *147*(927), 258-267.

Ito, T., Wang, Y.-H., & Liu, Y.-J. (2005). Plasmacytoid Dendritic Cell Precursors/Type I Interferon-Producing Cells Sense Viral Infection by Toll-Like Receptor (TLR) 7 and TLR9. *Springer Seminars in Immunopathology*, 26(3), 221–229. https://doi.org/10.1007/s00281-004-0180-4

Iwasaki, A., & Pillai, P. S. (2014). Innate Immunity to Influenza Virus Infection. *Nature Reviews: Immunology*, *14*(5), 315-328. https://doi.org/10.1038/nri3665

Jagger, B., Wise, H., Kash, J., Walters, K.-A., Wills, N., Xiao, Y.-L., Dunfee, R., Schwartzman, L., Ozinsky, A., & Bell, G. (2012). An Overlapping Protein-Coding Region in Influenza A Virus Segment 3 Modulates the Host Response. *Science*, *337*(6091), 199-204.

Jennings, P. A., Finch, J. T., Winter, G., & Robertson, J. S. (1983). Does the Higher Order Structure of the Influenza Virus Ribonucleoprotein Guide Sequence Rearrangements in Influenza Viral RNA? *Cell*, *34*(2), 619-627.

Jewell, N. A., Vaghefi, N., Mertz, S. E., Akter, P., Peebles Jr, R. S., Bakaletz, L. O., Durbin, R. K., Flano, E., & Durbin, J. E. (2007). Differential Type I Interferon Induction by Respiratory Syncytial Virus and Influenza A Virus in Vivo. *Journal of Virology*, *81*(18), 9790-9800.

Jiang, Z., Wei, F., Zhang, Y., Wang, T., Gao, W., Yu, S., Sun, H., Pu, J., Sun, Y., & Wang, M. (2021). IFI16 Directly Senses Viral RNA and Enhances RIG-I Transcription and Activation to Restrict Influenza Virus Infection. *Nature Microbiology*, *6*(7), 932-945.

Jiao, H., Wachsmuth, L., Kumari, S., Schwarzer, R., Lin, J., Eren, R. O., Fisher, A., Lane, R., Young, G. R., & Kassiotis, G. (2020). Z-Nucleic-Acid Sensing Triggers ZBP1-Dependent Necroptosis and Inflammation. *Nature*, *580*(7803), 391-395.

Johnson, N. P., & Mueller, J. (2002). Updating the Accounts: Global Mortality of the 1918-1920" Spanish" Influenza Pandemic. *Bulletin of the History of Medicine*, 105-115.

Jørgensen, S., Christiansen, M., Ryø, L., Gad, H., Gjedsted, J., Staeheli, P., Mikkelsen, J., Storgaard, M., Hartmann, R., & Mogensen, T. (2018). Defective RNA Sensing by RIG-I in Severe Influenza Virus Infection. *Clinical & Experimental Immunology*, *192*(3), 366-376.

Kamal, R. P., Katz, J. M., & York, I. A. (2014). Molecular Determinants of Influenza Virus Pathogenesis in Mice. *Current Topics in Microbiology and Immunology, 385*, 243–274. https://doi.org/10.1007/82_2014_388

Karki, R., & Kanneganti, T. D. (2021). The 'Cytokine Storm': Molecular Mechanisms and Therapeutic Prospects. *Trends in Immunology*, *42*(8), 681-705. https://doi.org/10.1016/j.it.2021.06.001

Karki, R., Lee, S., Mall, R., Pandian, N., Wang, Y., Sharma, B. R., Malireddi, R. S., Yang, D., Trifkovic, S., & Steele, J. A. (2022). ZBP1-Dependent Inflammatory Cell Death, Panoptosis, and Cytokine Storm Disrupt IFN Therapeutic Efficacy During Coronavirus Infection. *Science Immunology*,7(74), eabo6294. https://doi.org/10.1126/sciimmunol.abo6294

Kato, H., Takeuchi, O., Sato, S., Yoneyama, M., Yamamoto, M., Matsui, K., Uematsu, S., Jung, A., Kawai, T., & Ishii, K. J. (2006). Differential Roles of MDA5 and RIG-I Helicases in the Recognition of RNA Viruses. *Nature*, *441*(7089), 101-105.

Kerr, P. J., Cattadori, I. M., Liu, J., Sim, D. G., Dodds, J. W., Brooks, J. W., Kennett, M. J., Holmes, E. C., & Read, A. F. (2017). Next Step in the Ongoing Arms Race between Myxoma Virus and Wild

Rabbits in Australia Is a Novel Disease Phenotype. *Proceedings of the National Academy of Sciences*, *114*(35), 9397-9402.
Kesavardhana, S., Kuriakose, T., Guy, C. S., Samir, P., Malireddi, R. K. S., Mishra, A., & Kanneganti, T. D. (2017). ZBP1/DAI Ubiquitination and Sensing of Influenza Vrnps Activate Programmed Cell Death. *Journal of Experimental Medicine*, *214*(8), 2217-2229. https://doi.org/10.1084/jem.20170550
Keshavarz, M., Mirzaei, H., Salemi, M., Momeni, F., Mousavi, M. J., Sadeghalvad, M., Arjeini, Y., Solaymani-Mohammadi, F., Sadri Nahand, J., & Namdari, H. (2019). Influenza Vaccine: Where Are We and Where Do We Go? *Reviews in Medical Virology*, *29*(1), e2014.
Khaperskyy, D. A., Schmaling, S., Larkins-Ford, J., McCormick, C., & Gaglia, M. M. (2016). Selective Degradation of Host RNA Polymerase II Transcripts by Influenza A Virus PA-X Host Shutoff Protein. *PLoS Pathogens*, *12*(2), e1005427.
Killip, M. J., Smith, M., Jackson, D., & Randall, R. E. (2014). Activation of the Interferon Induction Cascade by Influenza A Viruses Requires Viral RNA Synthesis and Nuclear Export. *Journal of Virology*, *88*(8), 3942-3952. https://doi.org/10.1128/JVI.03109-13
Killip, M. J., Young, D. F., Gatherer, D., Ross, C. S., Short, J. A., Davison, A. J., Goodbourn, S., & Randall, R. E. (2013). Deep Sequencing Analysis of Defective Genomes of Parainfluenza Virus 5 and Their Role in Interferon Induction. *Journal of Virology*, *87*(9), 4798-4807. https://doi.org/10.1128/JVI.03383-12
Kim, C.-U., Jeong, Y.-J., Lee, P., Lee, M.-S., Park, J.-H., Kim, Y.-S., & Kim, D.-J. (2022). Extracellular Nucleoprotein Exacerbates Influenza Virus Pathogenesis by Activating Toll-Like Receptor 4 and the NLRP3 Inflammasome. *Cellular & Molecular Immunology*, *19*(6), 715-725.
Kim, J. H., Hatta, M., Watanabe, S., Neumann, G., Watanabe, T., & Kawaoka, Y. (2010). Role of Host-Specific Amino Acids in the Pathogenicity of Avian H5N1 Influenza Viruses in Mice. *Journal of General Virology*, *91*(5), 1284-1289. https://doi.org/10.1099/vir.0.018143-0
Kim, J. K., Negovetich, N. J., Forrest, H. L., & Webster, R. G. (2009). Ducks: The "Trojan Horses" of H5N1 Influenza. *Influenza and Other Respiratory Viruses*, *3*(4), 121-128. https://doi.org/10.1111/j.1750-2659.2009.00084.x
Kobasa, D., Jones, S. M., Shinya, K., Kash, J. C., Copps, J., Ebihara, H., Hatta, Y., Kim, J. H., Halfmann, P., Hatta, M., Feldmann, F., Alimonti, J. B., Fernando, L., Li, Y., Katze, M. G., Feldmann, H., & Kawaoka, Y. (2007). Aberrant Innate Immune Response in Lethal Infection of Macaques with the 1918 Influenza Virus. *Nature*, *445*(7125), 319-323. https://doi.org/10.1038/nature05495
Korbie, D. J., & Mattick, J. S. (2008). Touchdown PCR for Increased Specificity and Sensitivity in PCR Amplification. *Nature Protocols*, *3*(9), 1452-1456.
Korteweg, C., & Gu, J. (2008). Pathology, Molecular Biology, and Pathogenesis of Avian Influenza A (H5N1) Infection in Humans. *The American Journal of Pathology*, *172*(5), 1155-1170.
Koshiba, T., Yasukawa, K., Yanagi, Y., & Kawabata, S.-i. (2011). Mitochondrial Membrane Potential Is Required for MAVS-Mediated Antiviral Signaling. *Science Signaling*, *4*(158), ra7-ra7.
Kotenko, S. V., Gallagher, G., Baurin, V. V., Lewis-Antes, A., Shen, M., Shah, N. K., Langer, J. A., Sheikh, F., Dickensheets, H., & Donnelly, R. P. (2003). IFN-Λs Mediate Antiviral Protection through a Distinct Class II Cytokine Receptor Complex. *Nature Immunology*, *4*(1), 69-77.
Kotenko, S. V., Rivera, A., Parker, D., & Durbin, J. E. (2019). Type III IFNs: Beyond Antiviral Protection. *Seminars in Immunology*, 43, 101303. https://doi.org/10.1016/j.smim.2019.101303
Kowalinski, E., Lunardi, T., McCarthy, A. A., Louber, J., Brunel, J., Grigorov, B., Gerlier, D., & Cusack, S. (2011). Structural Basis for the Activation of Innate Immune Pattern-Recognition Receptor RIG-I by Viral RNA. *Cell*, *147*(2), 423-435.
Kumlin, U., Olofsson, S., Dimock, K., & Arnberg, N. (2008). Sialic Acid Tissue Distribution and Influenza Virus Tropism. *Influenza and Other Respiratory Viruses*, *2*(5), 147-154.
Kupke, S. Y., Ly, L. H., Borno, S. T., Ruff, A., Timmermann, B., Vingron, M., Haas, S., & Reichl, U. (2020). Single-Cell Analysis Uncovers a Vast Diversity in Intracellular Viral Defective

Interfering RNA Content Affecting the Large Cell-to-Cell Heterogeneity in Influenza A Virus Replication. *Viruses*, *12*(1). https://doi.org/10.3390/v12010071

Kuriakose, T., & Kanneganti, T.-D. (2017). Regulation and Functions of NLRP3 Inflammasome During Influenza Virus Infection. *Molecular Immunology*, *86*, 56-64.

Kuriakose, T., Man, S. M., Subbarao Malireddi, R., Karki, R., Kesavardhana, S., Place, D. E., Neale, G., Vogel, P., & Kanneganti, T.-D. (2016). ZBP1/DAI Is an Innate Sensor of Influenza Virus Triggering the NLRP3 Inflammasome and Programmed Cell Death Pathways. *Science Immunology*, *1*(2), aag2045-aag2045.

Lai, J. H., Wang, M. Y., Huang, C. Y., Wu, C. H., Hung, L. F., Yang, C. Y., Ke, P. Y., Luo, S. F., Liu, S. J., & Ho, L. J. (2018). Infection with the Dengue RNA Virus Activates TLR9 Signaling in Human Dendritic Cells. *EMBO Reports*, *19*(8), e46182.

Lai, S., Qin, Y., Cowling, B. J., Ren, X., Wardrop, N. A., Gilbert, M., Tsang, T. K., Wu, P., Feng, L., & Jiang, H. (2016). Global Epidemiology of Avian Influenza A H5N1 Virus Infection in Humans, 1997–2015: A Systematic Review of Individual Case Data. *The Lancet Infectious Diseases*, *16*(7), e108-e118.

Lamichhane, P. P., & Samarasinghe, A. E. (2019). The Role of Innate Leukocytes During Influenza Virus Infection. *Journal of Immunoogyl Research*, *2019*, 8028725. https://doi.org/10.1155/2019/8028725

Langlois, R. A., Varble, A., Chua, M. A., García-Sastre, A., & TenOever, B. R. (2012). Hematopoietic-Specific Targeting of Influenza a Virus Reveals Replication Requirements for Induction of Antiviral Immune Responses. *Proceedings of the National Academy of Sciences*, *109*(30), 12117-12122.

Laske, T., Heldt, F. S., Hoffmann, H., Frensing, T., & Reichl, U. (2016). Modeling the Intracellular Replication of Influenza A Virus in the Presence of Defective Interfering RNAs. *Virus Research*, *213*, 90-99. https://doi.org/10.1016/j.virusres.2015.11.016

Lee, L. Y.-H., Simmons, C., De Jong, M. D., Chau, N. V. V., Schumacher, R., Peng, Y. C., McMichael, A. J., Farrar, J. J., Smith, G. L., & Townsend, A. R. (2008). Memory T Cells Established by Seasonal Human Influenza A Infection Cross-React with Avian Influenza A (H5N1) in Healthy Individuals. *The Journal of Clinical Investigation*, *118*(10), 3478-3490.

Lee, N., Chan, P. K., Hui, D. S., Rainer, T. H., Wong, E., Choi, K.-W., Lui, G. C., Wong, B. C., Wong, R. Y., & Lam, W.-Y. (2009b). Viral Loads and Duration of Viral Shedding in Adult Patients Hospitalized with Influenza. *The Journal of Infectious Diseases*, *200*(4), 492-500.

Lee, N., Wong, C., Hui, D., & Chan, P. (2014). Role of Toll-Like Receptors in Naturally Occurring Influenza Virus Infection. *Hong Kong Medical Journal. Xianggang Yi Xue Za Zhi*, *20*(Suppl 6), S11-15.

Lee, S., Ishitsuka, A., Noguchi, M., Hirohama, M., Fujiyasu, Y., Petric, P. P., Schwemmle, M., Staeheli, P., Nagata, K., & Kawaguchi, A. (2019). Influenza Restriction Factor MXA Functions as Inflammasome Sensor in the Respiratory Epithelium. *Science Immunology*, *4*(40), eaau4643.

Lee, S. M., Gardy, J. L., Cheung, C. Y., Cheung, T. K., Hui, K. P., Ip, N. Y., Guan, Y., Hancock, R. E., & Peiris, J. S. (2009a). Systems-Level Comparison of Host-Responses Elicited by Avian H5N1 and Seasonal H1N1 Influenza Viruses in Primary Human Macrophages. *PloS One*, *4*(12), e8072. https://doi.org/10.1371/journal.pone.0008072

Li, D., Lott, W. B., Lowry, K., Jones, A., Thu, H. M., & Aaskov, J. (2011). Defective Interfering Viral Particles in Acute Dengue Infections. *PloS One*, *6*(4), e19447. https://doi.org/10.1371/journal.pone.0019447

Li, H., Bradley, K. C., Long, J. S., Frise, R., Ashcroft, J. W., Hartgroves, L. C., Shelton, H., Makris, S., Johansson, C., Cao, B., & Barclay, W. S. (2018). Internal Genes of a Highly Pathogenic H5N1 Influenza Virus Determine High Viral Replication in Myeloid Cells and Severe Outcome of Infection in Mice. *PLoS Pathogens*, *14*(1), e1006821. https://doi.org/10.1371/journal.ppat.1006821

Li, Q., Wang, X., Zhong, L., Wang, X., Sun, Z., Gao, Z., Cui, Z., Zhu, J., Gu, M., Liu, X., & Liu, X. (2014). Adaptation of a Natural Reassortant H5N2 Avian Influenza Virus in Mice. *Veterinary Microbiology*, *172*(3-4), 568-574. https://doi.org/10.1016/j.vetmic.2014.06.018

Li, W., Wang, H., & Zheng, S. J. (2022). Roles of RNA Sensors in Host Innate Response to Influenza Virus and Coronavirus Infections. *International Journal of Molecular Sciences*, *23*(15), 8285.

Li, X., Fu, Z., Liang, H., Wang, Y., Qi, X., Ding, M., Sun, X., Zhou, Z., Huang, Y., Gu, H., Li, L., Chen, X., Li, D., Zhao, Q., Liu, F., Wang, H., Wang, J., Zen, K., & Zhang, C. Y. (2018). H5N1 influenza virus-specific miRNA-like small RNA increases cytokine production and mouse mortality via targeting poly(rC)-binding protein 2. *Cell Research, 28(2)*, 157–171. https://doi.org/10.1038/cr.2018.3

Li, Z., Jiang, Y., Jiao, P., Wang, A., Zhao, F., Tian, G., Wang, X., Yu, K., Bu, Z., & Chen, H. (2006). The NS1 Gene Contributes to the Virulence of H5N1 Avian Influenza Viruses. *Journal of Virology*, *80*(22), 11115-11123.

Liem, N. T., Tung, C. V., Hien, N. D., Hien, T. T., Chau, N. Q., Long, H. T., Hien, N. T., Mai, L. Q., Taylor, W. R., & Wertheim, H. (2009). Clinical Features of Human Influenza A (H5N1) Infection in Vietnam: 2004–2006. *Clinical Infectious Diseases*, *48*(12), 1639-1646.

Lin, S.-J., Lo, M., Kuo, R.-L., Shih, S.-R., Ojcius, D. M., Lu, J., Lee, C.-K., Chen, H.-C., Lin, M. Y., & Leu, C.-M. (2014). The Pathological Effects of CCR2+ Inflammatory Monocytes Are Amplified by an IFNAR1-Triggered Chemokine Feedback Loop in Highly Pathogenic Influenza Infection. *Journal of Biomedical Science*, *21*(1), 1-18.

Liu, G., Lu, Y., Liu, Q., & Zhou, Y. (2019). Inhibition of Ongoing Influenza a Virus Replication Reveals Different Mechanisms of RIG-I Activation. *Journal of Virology*, *93*(6), e02066-18. https://doi.org/10.1128/JVI.02066-18

Liu, G., Lu, Y., Thulasi Raman, S. N., Xu, F., Wu, Q., Li, Z., Brownlie, R., Liu, Q., & Zhou, Y. (2018). Nuclear-Resident RIG-I Senses Viral Replication Inducing Antiviral Immunity. *Nature Communications*, *9*(1), 3199. https://doi.org/10.1038/s41467-018-05745-w

Liu, G., Park, H. S., Pyo, H. M., Liu, Q., & Zhou, Y. (2015). Influenza a Virus Panhandle Structure Is Directly Involved in RIG-I Activation and Interferon Induction. *Journal of Virology*, *89*(11), 6067-6079. https://doi.org/10.1128/JVI.00232-15

Liu, J., Liu, Y., Xia, H., Zou, J., Weaver, S. C., Swanson, K. A., Cai, H., Cutler, M., Cooper, D., & Muik, A. (2021). BNT162b2-Elicited Neutralization of B. 1.617 and Other SARS-Cov-2 Variants. *Nature*, *596*(7871), 273-275.

Liu, R., Sheng, Z., Huang, C., Wang, D., & Li, F. (2020). Influenza D Virus. *Current Opinion in Virology*, *44*, 154-161.

Lofgren, E., Fefferman, N. H., Naumov, Y. N., Gorski, J., & Naumova, E. N. (2007). Influenza Seasonality: Underlying Causes and Modeling Theories. *Journal of Virology*, *81*(11), 5429-5436.

Long, J. C., & Fodor, E. (2016). The PB2 Subunit of the Influenza a Virus RNA Polymerase Is Imported into the Mitochondrial Matrix. *Journal of Virology*, *90*(19), 8729-8738.

Long, J. S., Giotis, E. S., Moncorgé, O., Frise, R., Mistry, B., James, J., Morisson, M., Iqbal, M., Vignal, A., & Skinner, M. A. (2016). Species Difference in ANP32A Underlies Influenza A Virus Polymerase Host Restriction. *Nature*, *529*(7584), 101-104.

Long, J. S., Mistry, B., Haslam, S. M., & Barclay, W. S. (2019). Host and Viral Determinants of Influenza A Virus Species Specificity. *Nature Reviews Microbiology*, *17*(2), 67-81.

Loo, Y.-M., Fornek, J., Crochet, N., Bajwa, G., Perwitasari, O., Martinez-Sobrido, L., Akira, S., Gill, M. A., García-Sastre, A., & Katze, M. G. (2008). Distinct RIG-I and MDA5 Signaling by RNA Viruses in Innate Immunity. *Journal of Virology*, *82*(1), 335-345.

Lopez-Castejon, G., & Brough, D. (2011). Understanding the Mechanism of Il-1β Secretion. *Cytokine and Growth Factor Reviews*, *22*(4), 189-195.

López, C. B. (2014). Defective Viral Genomes: Critical Danger Signals of Viral Infections. *Journal of Virology*, *88*(16), 8720-8723. https://www.ncbi.nlm.nih.gov/pmc/articles/PMC4136278/pdf/zjv8720.pdf

Luczo, J. M., Stambas, J., Durr, P. A., Michalski, W. P., & Bingham, J. (2015). Molecular Pathogenesis of H5 Highly Pathogenic Avian Influenza: The Role of the Haemagglutinin Cleavage Site Motif. *Reviews in Medical Virology*, *25*(6), 406-430.

Lui, W. Y., Yuen, C. K., Li, C., Wong, W. M., Lui, P. Y., Lin, C. H., Chan, K. H., Zhao, H., Chen, H., To, K. K. W., Zhang, A. J. X., Yuen, K. Y., & Kok, K. H. (2019). Smrt Sequencing Revealed the Diversity and Characteristics of Defective Interfering RNAs in Influenza A (H7N9) Virus Infection. *Emerging Microbes & Infections*, *8*(1), 662-674. https://doi.org/10.1080/22221751.2019.1611346

Lutz IV, M. M., Dunagan, M. M., Kurebayashi, Y., & Takimoto, T. (2020). Key Role of the Influenza A Virus PA Gene Segment in the Emergence of Pandemic Viruses. *Viruses*, *12*(4), 365.

Ma, J. Z., Ng, W. C., Zappia, L., Gearing, L. J., Olshansky, M., Pham, K., Cheong, K., Hsu, A., Turner, S. J., & Wijburg, O. (2019). Unique Transcriptional Architecture in Airway Epithelial Cells and Macrophages Shapes Distinct Responses Following Influenza Virus Infection Ex Vivo. *Journal of Virology*, *93*(6), e01986-01918.

Machkovech, H. M., Bloom, J. D., & Subramaniam, A. R. (2019). Comprehensive Profiling of Translation Initiation in Influenza Virus Infected Cells. *PLoS Pathogens*, *15*(1), e1007518.

Madaan, A., Verma, R., Singh, A. T., Jain, S. K., & Jaggi, M. (2014). A Stepwise Procedure for Isolation of Murine Bone Marrow and Generation of Dendritic Cells. *Journal of Biological Methods*, *1*(1). https://doi.org/10.14440/jbm.2014.12

Maelfait, J., Liverpool, L., Bridgeman, A., Ragan, K. B., Upton, J. W., & Rehwinkel, J. (2017). Sensing of Viral and Endogenous RNA by ZBP1/DAI Induces Necroptosis. *The EMBO Journal, 36(17)*, 2529-2543. https://doi.org/10.15252/embj.201796476

Maines, T. R., Belser, J. A., Gustin, K. M., van Hoeven, N., Zeng, H., Svitek, N., von Messling, V., Katz, J. M., & Tumpey, T. M. (2012). Local Innate Immune Responses and Influenza Virus Transmission and Virulence in Ferrets. *Journal of Infectious Diseases*, *205*(3), 474-485.

Maines, T. R., Szretter, K. J., Perrone, L., Belser, J. A., Bright, R. A., Zeng, H., Tumpey, T. M., & Katz, J. M. (2008). Pathogenesis of Emerging Avian Influenza Viruses in Mammals and the Host Innate Immune Response. *Immunological Reviews*, *225*(1), 68-84.

Makris, S., Paulsen, M., & Johansson, C. (2017). Type I Interferons as Regulators of Lung Inflammation. *Frontiers in Immunology*, *8*, 259.

Malmgaard, L., Melchjorsen, J., Bowie, A. G., Mogensen, S. C., & Paludan, S. R. (2004). Viral Activation of Macrophages through TLR-Dependent and-Independent Pathways. *The Journal of Immunology*, *173*(11), 6890-6898.

Manicassamy, B., Manicassamy, S., Belicha-Villanueva, A., Pisanelli, G., Pulendran, B., & Garcia-Sastre, A. (2010). Analysis of in Vivo Dynamics of Influenza Virus Infection in Mice Using a GFP Reporter Virus. *Proceedings of the National Academy of Sciences of the United States of America*, *107*(25), 11531-11536. https://doi.org/10.1073/pnas.0914994107

Marongiu, L., Valache, M., Facchini, F. A., & Granucci, F. (2021). How Dendritic Cells Sense and Respond to Viral Infections. *Clinical Science (London)*, *135*(19), 2217-2242. https://doi.org/10.1042/CS20210577

Marsh, G. A., & Wang, L.-F. (2012). Hendra and Nipah Viruses: Why Are They So Deadly? *Current Opinion in Virology*, *2*(3), 242-247.

Marshall, I., & Fenner, F. (1958). Studies in the Epidemiology of Infectious Myxomatosis of Rabbits*: V. Changes in the Innate Resistance of Australian Wild Rabbits Exposed to Myxomatosis. *Epidemiology & Infection*, *56*(2), 288-302.

Martin, M. A., Kaul, D., Tan, G. S., Woods, C. W., & Koelle, K. (2019). The Dynamics of Influenza A H3N2 Defective Viral Genomes from a Human Challenge Study. *BioRxiv*. https://doi.org/10.1101/814673

Mase, M., Tanimura, N., Imada, T., Okamatsu, M., Tsukamoto, K., & Yamaguchi, S. (2006). Recent H5N1 Avian Influenza a Virus Increases Rapidly in Virulence to Mice after a Single Passage in Mice. *Journal of General Virology*, *87*(12), 3655-3659.

Matlin, K. S., Reggio, H., Helenius, A., & Simons, K. (1981). Infectious Entry Pathway of Influenza Virus in a Canine Kidney Cell Line. *The Journal of Cell Biology*, *91*(3), 601-613.

Matrosovich, M., Herrler, G., & Klenk, H. D. (2013). Sialic Acid Receptors of Viruses. *SialoGlyco Chemistry and Biology II*, 1-28.

Matsuoka, Y., Swayne, D. E., Thomas, C., Rameix-Welti, M. A., Naffakh, N., Warnes, C., Altholtz, M., Donis, R., & Subbarao, K. (2009). Neuraminidase Stalk Length and Additional Glycosylation of the Hemagglutinin Influence the Virulence of Influenza H5N1 Viruses for Mice. *Journal of Virology*, *83*(9), 4704-4708. https://doi.org/10.1128/JVI.01987-08

McAuley, J. L., Chipuk, J. E., Boyd, K. L., Van De Velde, N., Green, D. R., & McCullers, J. A. (2010). PB1-F2 Proteins from H5N1 and 20 Century Pandemic Influenza Viruses Cause Immunopathology. *PLoS Pathogens*, *6*(7), e1001014. https://doi.org/10.1371/journal.ppat.1001014

McAuley, J. L., Tate, M. D., MacKenzie-Kludas, C. J., Pinar, A., Zeng, W., Stutz, A., Latz, E., Brown, L. E., & Mansell, A. (2013). Activation of the NLRP3 Inflammasome by IAV Virulence Protein PB1-F2 Contributes to Severe Pathophysiology and Disease. *PLoS Pathogens*, *9*(5), e1003392.

McCrone, J. T., Woods, R. J., Martin, E. T., Malosh, R. E., Monto, A. S., & Lauring, A. S. (2018). Stochastic Processes Constrain the Within and Between Host Evolution of Influenza Virus. *Elife*, *7*, e35962.

McDermott, J. E., Shankaran, H., Eisfeld, A. J., Belisle, S. E., Neuman, G., Li, C., McWeeney, S., Sabourin, C., Kawaoka, Y., & Katze, M. G. (2011). Conserved Host Response to Highly Pathogenic Avian Influenza Virus Infection in Human Cell Culture, Mouse and Macaque Model Systems. *BMC Systems Biology*, *5*(1), 1-23.

Mehand, M. S., Al-Shorbaji, F., Millett, P., & Murgue, B. (2018). The Who R&D Blueprint: 2018 Review of Emerging Infectious Diseases Requiring Urgent Research and Development Efforts. *Antiviral Research*, *159*, 63-67.

Mendes, M., & Russell, A. B. (2021). Library-Based Analysis Reveals Segment and Length Dependent Characteristics of Defective Influenza Genomes. *PLoS Pathogens*, *17*(12), e1010125.

Mestas, J., & Hughes, C. C. (2004). Of Mice and Not Men: Differences between Mouse and Human Immunology. *Journal of Immunology*, *172*(5), 2731-2738. https://doi.org/10.4049/jimmunol.172.5.2731

Meyerson, N. R., Warren, C. J., Vieira, D. A., Diaz-Griferro, F., & Sawyer, S. L. (2018). Species-Specific Vulnerability of RanBP2 Shaped the Evolution of SIV as It Transmitted in African Apes. *PLoS Pathogens*, *14*(3), e1006906.

Miller, B. J. (2022). Why Unprecedented Bird Flu Outbreaks Sweeping the World Are Concerning Scientists. *Nature*, *606*(7912), 18-19.

Miotto, O., Heiny, A., Tan, T. W., August, J. T., & Brusic, V. (2008). Identification of Human-to-Human Transmissibility Factors in PB2 Proteins of Influenza A by Large-Scale Mutual Information Analysis. *BMC Bioinformatics*, 9 Suppl 1(Suppl 1), S18. https://doi.org/10.1186/1471-2105-9-S1-S18

Mo, W., & Han, J. (2021). Zbp1, a Dsrna Sensor for Cell Death and Inflammation.

Mogensen, T. H. (2009). Pathogen Recognition and Inflammatory Signaling in Innate Immune Defenses. *Clinical Microbiology Reviews*, *22*(2), 240-273.

Mok, K. P., Wong, C. H. K., Cheung, C. Y., Chan, M. C., Lee, S. M. Y., Nicholls, J. M., Guan, Y., & Peiris, J. S. M. (2009). Viral Genetic Determinants of H5N1 Influenza Viruses That Contribute to Cytokine Dysregulation. *Journal of Infectious Diseases*, *200*(7), 1104-1112. https://doi.org/10.1086/605606

Momota, M., Lelliott, P., Kubo, A., Kusakabe, T., Kobiyama, K., Kuroda, E., Imai, Y., Akira, S., Coban, C., & Ishii, K. J. (2020). ZBP1 Governs the Inflammasome-Independent IL-1α and Neutrophil

Inflammation That Play a Dual Role in Anti-Influenza Virus Immunity. *International Immunology*, *32*(3), 203-212.
Morens, D. M., & Taubenberger, J. K. (2018). The Mother of All Pandemics Is 100 Years Old (and Going Strong)! *American Journal of Public Health*, *108*(11), 1449-1454.
Nacken, W., Schreiber, A., Masemann, D., & Ludwig, S. (2021). The Effector Domain of the Influenza a Virus Nonstructural Protein NS1 Triggers Host Shutoff by Mediating Inhibition and Global Deregulation of Host Transcription When Associated with Specific Structures in the Nucleus. *mBio*, *12*(5), e02196-02121.
Nakano, M., Sugita, Y., Kodera, N., Miyamoto, S., Muramoto, Y., Wolf, M., & Noda, T. (2021). Ultrastructure of Influenza Virus Ribonucleoprotein Complexes During Viral RNA Synthesis. *Communications Biology*, *4*(1), 858. https://doi.org/10.1038/s42003-021-02388-4
National Institute for Health and Care Research. (2022). *New Study Will Help Rapidly Find Flu Treatments This Winter*. National Institute for Health and Care Research Retrieved 07/01/2023 from https://www.nihr.ac.uk/news/new-study-will-help-rapidly-find-flu-treatments-this-winter/32076
Neumann, G., Watanabe, T., Ito, H., Watanabe, S., Goto, H., Gao, P., Hughes, M., Perez, D. R., Donis, R., & Hoffmann, E. (1999). Generation of Influenza A Viruses Entirely from Cloned cDNAs. *Proceedings of the National Academy of Sciences*, *96*(16), 9345-9350.
Ng, W.-F., To, K.-F., Lam, W. W., Ng, T.-K., & Lee, K.-C. (2006). The Comparative Pathology of Severe Acute Respiratory Syndrome and Avian Influenza A Subtype H5N1—a Review. *Human Pathology*, *37*(4), 381-390.
Ngunjiri, J. M., Mohni, K. N., Sekellick, M. J., Schultz-Cherry, S., Webster, R. G., & Marcus, P. I. (2012). Lethal H5N1 Influenza Viruses Are Not Resistant to Interferon Action in Human, Simian, Porcine or Chicken Cells. *Nature Medicine*, *18*(10), 1456-1457.
Niles, M. A., Gogesch, P., Kronhart, S., Ortega Iannazzo, S., Kochs, G., Waibler, Z., & Anzaghe, M. (2021). Macrophages and Dendritic Cells Are Not the Major Source of Pro-Inflammatory Cytokines Upon SARS-CoV-2 Infection. *Frontiers in Immunology*, *12*, 647824.
Nilsson-Payant, B. E., Blanco-Melo, D., Uhl, S., Escudero-Perez, B., Olschewski, S., Thibault, P., Panis, M., Rosenthal, M., Munoz-Fontela, C., Lee, B., & tenOever, B. R. (2021). Reduced Nucleoprotein Availability Impairs Negative-Sense RNA Virus Replication and Promotes Host Recognition. *Journal of Virology*, *95*(9). https://doi.org/10.1128/JVI.02274-20
Nilsson-Payant, B. E., TenOever, B. R., & te Velthuis, A. J. (2022). The Host Factor ANP32A Is Required for Influenza a Virus vRNA and cRNA Synthesis. *Journal of Virology*, *96*(4), e02092-02021.
Noble, S., & Dimmock, N. (1995). Characterization of Putative Defective Interfering (DI) A/WSN RNAs Isolated from the Lungs of Mice Protected from an Otherwise Lethal Respiratory Infection with Influenza Virus A/WSN (H1N1): A Subset of the Inoculum DI RNAs. *Virology*, *210*(1), 9-19.
Noda, T., Sagara, H., Yen, A., Takada, A., Kida, H., Cheng, R. H., & Kawaoka, Y. (2006). Architecture of Ribonucleoprotein Complexes in Influenza a Virus Particles. *Nature*, *439*(7075), 490-492.
Nogales, A., Martinez-Sobrido, L., Topham, D. J., & DeDiego, M. L. (2018). Modulation of Innate Immune Responses by the Influenza a NS1 and PA-X Proteins. *Viruses*, *10*(12), 708. https://doi.org/10.3390/v10120708
Nuwarda, R. F., Alharbi, A. A., & Kayser, V. (2021). An Overview of Influenza Viruses and Vaccines. *Vaccines*, *9*(9), 1032.
Odagiri, T., Tominaga, K., Tobita, K., & Ohta, S. (1994). An Amino Acid Change in the Non-Structural NS2 Protein of an Influenza a Virus Mutant Is Responsible for the Generation of Defective Interfering (DI) Particles by Amplifying DI RNAs and Suppressing Complementary RNA Synthesis. *Journal of General Virology*, *75*(1), 43-53.
Oliver, I., Roberts, J., Brown, C. S., Byrne, A. M., Mellon, D., Hansen, R. D., Banyard, A. C., James, J., Donati, M., & Porter, R. (2022). A Case of Avian Influenza a (H5N1) in England, January 2022. *Eurosurveillance*, *27*(5), 2200061.

Oshansky, C. M., Gartland, A. J., Wong, S.-S., Jeevan, T., Wang, D., Roddam, P. L., Caniza, M. A., Hertz, T., DeVincenzo, J. P., & Webby, R. J. (2014). Mucosal Immune Responses Predict Clinical Outcomes During Influenza Infection Independently of Age and Viral Load. *American Journal of Respiratory and Critical Care Medicine*, *189*(4), 449-462.

Oshiumi, H., Miyashita, M., Inoue, N., Okabe, M., Matsumoto, M., & Seya, T. (2010). The Ubiquitin Ligase Riplet Is Essential for RIG-I-Dependent Innate Immune Responses to RNA Virus Infection. *Cell Host & Microbe*, *8*(6), 496-509.

Osterlund, P., Pirhonen, J., Ikonen, N., Ronkko, E., Strengell, M., Makela, S. M., Broman, M., Hamming, O. J., Hartmann, R., Ziegler, T., & Julkunen, I. (2010). Pandemic H1N1 2009 Influenza A Virus Induces Weak Cytokine Responses in Human Macrophages and Dendritic Cells and Is Highly Sensitive to the Antiviral Actions of Interferons. *Journal of Virology*, *84*(3), 1414-1422. https://doi.org/10.1128/JVI.01619-09

Oymans, J., & Te Velthuis, A. J. (2018). A Mechanism for Priming and Realignment During Influenza A Virus Replication. *Journal of Virology*, *92*(3), e01773-01717.

Padilla-Quirarte, H. O., Lopez-Guerrero, D. V., Gutierrez-Xicotencatl, L., & Esquivel-Guadarrama, F. (2019). Protective Antibodies against Influenza Proteins. *Frontiers in Immunology*, *10*, 1677.

Palese, P., Tobita, K., Ueda, M., & Compans, R. W. (1974). Characterization of Temperature Sensitive Influenza Virus Mutants Defective in Neuraminidase. *Virology*, *61*(2), 397-410.

Patrono, L. V., Vrancken, B., Budt, M., Düx, A., Lequime, S., Boral, S., Gilbert, M. T. P., Gogarten, J. F., Hoffmann, L., Horst, D., Merkel, K., Morens, D., Prepoint, B., Schlotterbeck, J., Schuenemann, V. J., Suchard, M. A., Taubenberger, J. K., Tenkhoff, L., Urban, C., Widulin, N., … Calvignac-Spencer, S. (2022). Archival influenza virus genomes from Europe reveal genomic variability during the 1918 pandemic. *Nature Communications, 13(1)*, 2314. https://doi.org/10.1038/s41467-022-29614-9

Peiris, J. S., Hui, K. P., & Yen, H. L. (2010). Host Response to Influenza Virus: Protection Versus Immunopathology. *Current Opinion in Immunology*, *22*(4), 475-481. https://doi.org/10.1016/j.coi.2010.06.003

Pelz, L., Rudiger, D., Dogra, T., Alnaji, F. G., Genzel, Y., Brooke, C. B., Kupke, S. Y., & Reichl, U. (2021). Semi-Continuous Propagation of Influenza a Virus and Its Defective Interfering Particles: Analyzing the Dynamic Competition to Select Candidates for Antiviral Therapy. *Journal of Virology*, *95*(24), e0117421. https://doi.org/10.1128/JVI.01174-21

Penn, R., Tregoning, J. S., Flight, K. E., Baillon, L., Frise, R., Goldhill, D. H., Johansson, C., & Barclay, W. S. (2022). Levels of Influenza A Virus Defective Viral Genomes Determine Pathogenesis in the BALB/C Mouse Model. *Journal of Virology*, e01178-01122.

Pérez-Cidoncha, M., Killip, M. J., Oliveros, J. C., Asensio, V. J., Fernández, Y., Bengoechea, J. A., Randall, R. E., & Ortín, J. (2014). An Unbiased Genetic Screen Reveals the Polygenic Nature of the Influenza Virus Anti-Interferon Response. *Journal of Virology*, *88*(9), 4632-4646.

Perez, J. T., Varble, A., Sachidanandam, R., Zlatev, I., Manoharan, M., García-Sastre, A., & tenOever, B. R. (2010). Influenza A Virus-Generated Small Rnas Regulate the Switch from Transcription to Replication. *Proceedings of the National Academy of Sciences*, *107*(25), 11525-11530.

Perng, Y.-C., & Lenschow, D. J. (2018). ISG15 in Antiviral Immunity and Beyond. *Nature Reviews Microbiology*, *16*(7), 423-439.

Perrone, L. A., Plowden, J. K., Garcia-Sastre, A., Katz, J. M., & Tumpey, T. M. (2008). H5N1 and 1918 Pandemic Influenza Virus Infection Results in Early and Excessive Infiltration of Macrophages and Neutrophils in the Lungs of Mice. *PLoS Pathogens*, *4*(8), e1000115. https://doi.org/10.1371/journal.ppat.1000115

Perrone, L. A., Szretter, K. J., Katz, J. M., Mizgerd, J. P., & Tumpey, T. M. (2010). Mice Lacking Both TNF and IL-1 Receptors Exhibit Reduced Lung Inflammation and Delay in Onset of Death Following Infection with a Highly Virulent H5N1 Virus. *Journal of Infectious Diseases*, *202*(8), 1161-1170. https://doi.org/10.1086/656365

Pichlmair, A., Schulz, O., Tan, C. P., Naslund, T. I., Liljestrom, P., Weber, F., & Reis e Sousa, C. (2006). RIG-I-Mediated Antiviral Responses to Single-Stranded RNA Bearing 5'-Phosphates. *Science*, *314*(5801), 997-1001.

Pinto, R. M., Lycett, S., Gaunt, E., & Digard, P. (2021). Accessory Gene Products of Influenza A Virus. *Cold Spring Harbor Perspectives in Medicine*, *11*(12), a038380.

Poon, L. L., Pritlove, D. C., Fodor, E., & Brownlee, G. G. (1999). Direct Evidence That the Poly (A) Tail of Influenza a Virus mRNA Is Synthesized by Reiterative Copying of a U Track in the Virion RNA Template. *Journal of Virology*, *73*(4), 3473-3476.

Prokunina-Olsson, L., Muchmore, B., Tang, W., Pfeiffer, R. M., Park, H., Dickensheets, H., Hergott, D., Porter-Gill, P., Mumy, A., & Kohaar, I. (2013). A Variant Upstream of IFNL3 (IL28b) Creating a New Interferon Gene IFNL4 Is Associated with Impaired Clearance of Hepatitis C Virus. *Nature Genetics*, *45*(2), 164-171.

Rabinowitz, S. G., & Huprikar, J. (1979). The Influence of Defective-Interfering Particles of the PR8 Strain of Influenza A Virus on the Pathogenesis of Pulmonary Infection in Mice, *The Journal of Infectious Diseases*, *140*(3), 305-315.

Ratcliffe, F., Myers, K., Fennessy, B., & Calaby, J. (1952). Myxomatosis in Australia: A Step Towards the Biological Control of the Rabbit. *Nature*, *170*(4314), 7-11.

Rausell, A., Munoz, M., Martinez, R., Roger, T., Telenti, A., & Ciuffi, A. (2016). Innate Immune Defects in HIV Permissive Cell Lines. *Retrovirology*, *13*(1), 43. https://doi.org/10.1186/s12977-016-0275-8

Rawling, D. C., Fitzgerald, M. E., & Pyle, A. M. (2015). Establishing the Role of ATP for the Function of the RIG-I Innate Immune Sensor. *Elife*, *4*, e09391.

Rehwinkel, J., & Gack, M. U. (2020). RIG-I-Like Receptors: Their Regulation and Roles in RNA Sensing. *Nature Reviews: Immunology*, *20*(9), 537-551. https://doi.org/10.1038/s41577-020-0288-3

Rehwinkel, J., Tan, C. P., Goubau, D., Schulz, O., Pichlmair, A., Bier, K., Robb, N., Vreede, F., Barclay, W., Fodor, E., & Reis e Sousa, C. (2010). RIG-I Detects Viral Genomic RNA During Negative-Strand RNA Virus Infection. *Cell*, *140*(3), 397-408. https://doi.org/10.1016/j.cell.2010.01.020

Reid, A. H., Fanning, T. G., Janczewski, T. A., McCall, S., & Taubenberger, J. K. (2002). Characterization of the 1918 “Spanish” Influenza Virus Matrix Gene Segment. *Journal of Virology*, *76*(21), 10717-10723.

Reid, A. H., Fanning, T. G., Janczewski, T. A., & Taubenberger, J. K. (2000). Characterization of the 1918 “Spanish” Influenza Virus Neuraminidase Gene. *Proceedings of the National Academy of Sciences*, *97*(12), 6785-6790.

Rhen, T., & Cidlowski, J. A. (2005). Anti-inflammatory Action of Glucocorticoids—New Mechanisms for Old Drugs. *New England Journal of Medicine*, *353*(16), 1711-1723.

Richardson, S., Hirsch, J. S., Narasimhan, M., Crawford, J. M., McGinn, T., Davidson, K. W., Barnaby, D. P., Becker, L. B., Chelico, J. D., & Cohen, S. L. (2020). Presenting Characteristics, Comorbidities, and Outcomes among 5700 Patients Hospitalized with Covid-19 in the New York City Area. *JAMA*, *323*(20), 2052-2059.

Rogers, G. N., & Paulson, J. C. (1983). Receptor Determinants of Human and Animal Influenza Virus Isolates: Differences in Receptor Specificity of the H3 Hemagglutinin Based on Species of Origin. *Virology*, *127*(2), 361-373.

Rossman, J. S., Jing, X., Leser, G. P., & Lamb, R. A. (2010). Influenza Virus M2 Protein Mediates Escrt-Independent Membrane Scission. *Cell*, *142*(6), 902-913.

Routh, A., & Johnson, J. E. (2014). Discovery of Functional Genomic Motifs in Viruses with Virema-a Virus Recombination Mapper-for Analysis of Next-Generation Sequencing Data. *Nucleic Acids Research*, *42*(2), e11. https://doi.org/10.1093/nar/gkt916

Rozo, M., & Gronvall, G. K. (2015). The Reemergent 1977 H1N1 Strain and the Gain-of-Function Debate. *mBio*, *6*(4), e01013-01015.

Rudiger, D., Pelz, L., Hein, M. D., Kupke, S. Y., & Reichl, U. (2021). Multiscale Model of Defective Interfering Particle Replication for Influenza A Virus Infection in Animal Cell Culture. *PLoS Computational Biology*, *17*(9), e1009357. https://doi.org/10.1371/journal.pcbi.1009357

Ruigrok, R., Baudin, F., Petit, I., & Weissenhorn, W. (2001). Role of Influenza Virus M1 Protein in the Viral Budding Process. In *International Congress Series* (Vol. 1219, pp. 397-404). Elsevier.

Russell, A. B., Elshina, E., Kowalsky, J. R., Te Velthuis, A. J. W., & Bloom, J. D. (2019). Single-Cell Virus Sequencing of Influenza Infections That Trigger Innate Immunity. *Journal of Virology*, *93*(14). https://doi.org/10.1128/JVI.00500-19

Saira, K., Lin, X., DePasse, J. V., Halpin, R., Twaddle, A., Stockwell, T., Angus, B., Cozzi-Lepri, A., Delfino, M., Dugan, V., Dwyer, D. E., Freiberg, M., Horban, A., Losso, M., Lynfield, R., Wentworth, D. N., Holmes, E. C., Davey, R., & Wentworth, D. E. (2013). Sequence Analysis of in Vivo Defective Interfering-Like RNA of Influenza a H1N1 Pandemic Virus. *Journal of Virology*, *87*(14), 8064-8074. https://doi.org/10.1128/JVI.00240-13

Sakabe, S., Iwatsuki-Horimoto, K., Takano, R., & Nidom, C. A. (2011). Cytokine Production by Primary Human Macrophages Infected with Highly Pathogenic H5N1 or Pandemic H1N1 2009 Influenza Viruses. *The Journal of General Virology*, *92*(6), 1428.

Sakabe, S., Takano, R., Nagamura-Inoue, T., Yamashita, N., Nidom, C. A., Quynh Le, M., Iwatsuki-Horimoto, K., & Kawaoka, Y. (2013). Differences in Cytokine Production in Human Macrophages and in Virulence in Mice Are Attributable to the Acidic Polymerase Protein of Highly Pathogenic Influenza A Virus Subtype H5N1. *Journal of Infectious Diseases*, *207*(2), 262-271. https://doi.org/10.1093/infdis/jis523

Sakai, S., Kawamata, H., Mantani, N., Kogure, T., Shimada, Y., Terasawa, K., Sakai, T., Imanishi, N., & Ochiai, H. (2000). Therapeutic Effect of Anti-Macrophage Inflammatory Protein 2 Antibody on Influenza Virus-Induced Pneumonia in Mice. *Journal of Virology*, *74*(5), 2472-2476.

Samji, T. (2009). Influenza A: Understanding the Viral Life Cycle. *The Yale Journal of Biology and Medicine*, *82*(4), 153.

Sanchez, A., Guerrero-Juarez, C. F., Ramirez, J., & Newcomb, L. L. (2014). Nuclear Localized Influenza Nucleoprotein N-Terminal Deletion Mutant Is Deficient in Functional vRNP Formation. *Virology Journal*, *11*(1), 1-14.

Sandbulte, M. R., Boon, A. C., Webby, R. J., & Riberdy, J. M. (2008). Analysis of Cytokine Secretion from Human Plasmacytoid Dendritic Cells Infected with H5N1 or Low-Pathogenicity Influenza Viruses. *Virology*, *381*(1), 22-28. https://doi.org/10.1016/j.virol.2008.08.018

Satoh, T., Kato, H., Kumagai, Y., Yoneyama, M., Sato, S., Matsushita, K., Tsujimura, T., Fujita, T., Akira, S., & Takeuchi, O. (2010). LGP2 Is a Positive Regulator of RIG-I–and MDA5-Mediated Antiviral Responses. *Proceedings of the National Academy of Sciences*, *107*(4), 1512-1517.

Satpathy, A. T., Kc, W., Albring, J. C., Edelson, B. T., Kretzer, N. M., Bhattacharya, D., Murphy, T. L., & Murphy, K. M. (2012). Zbtb46 Expression Distinguishes Classical Dendritic Cells and Their Committed Progenitors from Other Immune Lineages. *Journal of Experimental Medicine*, *209*(6), 1135-1152. https://doi.org/10.1084/jem.20120030

Sauter, D., Schindler, M., Specht, A., Landford, W. N., Münch, J., Kim, K.-A., Votteler, J., Schubert, U., Bibollet-Ruche, F., & Keele, B. F. (2009). Tetherin-Driven Adaptation of Vpu and Nef Function and the Evolution of Pandemic and Nonpandemic HIV-1 Strains. *Cell Host & Microbe*, *6*(5), 409-421.

Saygili, E., Yildiz-Ozturk, E., Green, M. J., Ghaemmaghami, A. M., & Yesil-Celiktas, O. (2021). Human Lung-on-Chips: Advanced Systems for Respiratory Virus Models and Assessment of Immune Response. *Biomicrofluidics*, *15*(2), 021501.

Scheller, J., Chalaris, A., Schmidt-Arras, D., & Rose-John, S. (2011). The Pro-and Anti-Inflammatory Properties of the Cytokine Interleukin-6. *Biochimica et Biophysica Acta (BBA)-Molecular Cell Research*, *1813*(5), 878-888.

Schmidt, M. E., & Varga, S. M. (2018). The CD8 T Cell Response to Respiratory Virus Infections. *Frontiers in Immunology*, 678.

Schneider, W. M., Chevillotte, M. D., & Rice, C. M. (2014). Interferon-Stimulated Genes: A Complex Web of Host Defenses. *Annual Review of Immunology*, *32*, 513.

Schoggins, J. W., & Rice, C. M. (2011). Interferon-Stimulated Genes and Their Antiviral Effector Functions. *Current Opinion in Virology*, *1*(6), 519-525.

Schrauwen, E. J., Herfst, S., Leijten, L. M., van Run, P., Bestebroer, T. M., Linster, M., Bodewes, R., Kreijtz, J. H., Rimmelzwaan, G. F., & Osterhaus, A. D. (2012). The Multibasic Cleavage Site in H5N1 Virus Is Critical for Systemic Spread Along the Olfactory and Hematogenous Routes in Ferrets. *Journal of Virology*, *86*(7), 3975-3984.

Schreiber, G., & Piehler, J. (2015). The Molecular Basis for Functional Plasticity in Type I Interferon Signaling. *Trends in Immunology*, *36*(3), 139-149.

Schroder, K., Hertzog, P. J., Ravasi, T., & Hume, D. A. (2004). Interferon-Γ: An Overview of Signals, Mechanisms and Functions. *Journal of Leukocyte Biology*, *75*(2), 163-189.

Schwartz, S. L., & Lowen, A. C. (2016). Droplet Digital Pcr: A Novel Method for Detection of Influenza Virus Defective Interfering Particles. *Journal of Virological Methods*, *237*, 159-165. https://doi.org/10.1016/j.jviromet.2016.08.023

Scott, P. D., Meng, B., Marriott, A. C., Easton, A. J., & Dimmock, N. J. (2011). Defective Interfering Virus Protects Elderly Mice from Influenza. *Virology Journal*, *8*, 212. https://doi.org/10.1186/1743-422X-8-212

Sederdahl, B. K., & Williams, J. V. (2020). Epidemiology and Clinical Characteristics of Influenza C Virus. *Viruses*, *12*(1), 89.

Selman, M., Dankar, S. K., Forbes, N. E., Jia, J.-J., & Brown, E. G. (2012). Adaptive Mutation in Influenza A Virus Non-Structural Gene Is Linked to Host Switching and Induces a Novel Protein by Alternative Splicing. *Emerging Microbes & Infections*, *1*(1), 1-10.

Seo, H. S., Hoffmann, E., & Webster, R. G. (2002). Lethal H5N1 Influenza Viruses Escape Host Anti-Viral Cytokine Responses. *Nature Medicine*, *8*(9), 950-954.

Shafiuddin, M., & Boon, A. C. (2019). RNA Sequence Features Are at the Core of Influenza A Virus Genome Packaging. *Journal of Molecular Biology*, *431*(21), 4217-4228.

Shanks, G. D. (2015). Insights from Unusual Aspects of the 1918 Influenza Pandemic. *Travel Medicine and Infectious Disease*, *13*(3), 217-222.

Shebl, F. M., Pinto, L. A., García-Piñeres, A., Lempicki, R., Williams, M., Harro, C., & Hildesheim, A. (2010). Comparison of Mrna and Protein Measures of Cytokines Following Vaccination with Human Papillomavirus-16 L1 Virus-Like Particlescomparison of Gene Expression and Protein Measures. *Cancer Epidemiology, Biomarkers and Prevention*, *19*(4), 978-981.

Shiliaev, N., Lukash, T., Palchevska, O., Crossman, D. K., Green, T. J., Crowley, M. R., Frolova, E. I., & Frolov, I. (2021). Natural and Recombinant SARS-CoV-2 Isolates Rapidly Evolve in Vitro to Higher Infectivity through More Efficient Binding to Heparan Sulfate and Reduced S1/S2 Cleavage. *Journal of Virology*, *95*(21), e01357-01321.

Shimizu, T., Takizawa, N., Watanabe, K., Nagata, K., & Kobayashi, N. (2011). Crucial Role of the Influenza Virus NS2 (Nep) C-Terminal Domain in M1 Binding and Nuclear Export of vRNP. *FEBS Letters*, *585*(1), 41-46.

Short, K. R., Brooks, A. G., Reading, P. C., & Londrigan, S. L. (2012). The Fate of Influenza a Virus after Infection of Human Macrophages and Dendritic Cells. *Journal of General Virology*, *93*(Pt 11), 2315-2325. https://doi.org/10.1099/vir.0.045021-0

Simonsen, L., Clarke, M. J., Schonberger, L. B., Arden, N. H., Cox, N. J., & Fukuda, K. (1998). Pandemic Versus Epidemic Influenza Mortality: A Pattern of Changing Age Distribution. *Journal of Infectious Diseases*, *178*(1), 53-60.

Simonsen, L., Spreeuwenberg, P., Lustig, R., Taylor, R. J., Fleming, D. M., Kroneman, M., Van Kerkhove, M. D., Mounts, A. W., Paget, W. J., & Teams, G. C. (2013). Global Mortality Estimates for the 2009 Influenza Pandemic from the Glamor Project: A Modeling Study. *PLoS Medicine*, *10*(11), e1001558.

Smith, A. M., & McCullers, J. A. (2013). Molecular Signatures of Virulence in the PB1-F2 Proteins of H5N1 Influenza Viruses. *Virus Research*, *178*(1), 146-150.

Smith, G. J., Donis, R. O., Health/Food, & World Health Organization/World Organisation for Animal Health/Food and Agriculture Organization (WHO/OIE/FAO) H5 Evolution Working Group (2015). Nomenclature Updates Resulting from the Evolution of Avian Influenza A (H5) Virus Clades 2.1. 3.2 a, 2.2. 1, and 2.3. 4 During 2013–2014. *Influenza and Other Respiratory Viruses*, *9*(5), 271-276.

Soh, Y. S., Moncla, L. H., Eguia, R., Bedford, T., & Bloom, J. D. (2019). Comprehensive Mapping of Adaptation of the Avian Influenza Polymerase Protein PB2 to Humans. *Elife*, *8*, e45079.

Staeheli, P., Grob, R., Meier, E., Sutcliffe, J., & Haller, O. (1988). Influenza Virus-Susceptible Mice Carry Mx Genes with a Large Deletion or a Nonsense Mutation. *Molecular and Cellular Biology*, *8*(10), 4518-4523.

Staller, E., & Barclay, W. S. (2021). Host Cell Factors That Interact with Influenza Virus Ribonucleoproteins. *Cold Spring Harbor Perspectives in Medicine*, *11*(11), a038307.

Staller, E., Sheppard, C. M., Neasham, P. J., Mistry, B., Peacock, T. P., Goldhill, D. H., Long, J. S., & Barclay, W. S. (2019). ANP32 Proteins Are Essential for Influenza Virus Replication in Human Cells. *Journal of Virology*, *93*(17), e00217-00219.

Steinberg, J., Wadenpohl, T., & Jung, S. (2021). The Endogenous RIG-I Ligand Is Generated in Influenza A-Virus Infected Cells. *Viruses*, *13*(8). https://doi.org/10.3390/v13081564

Stevaert, A., & Naesens, L. (2016). The Influenza Virus Polymerase Complex: An Update on Its Structure, Functions, and Significance for Antiviral Drug Design. *Medicinal Research Reviews*, *36*(6), 1127-1173.

Stoddart, M. J., Richards, R., & Alini, M. (2012). In Vitro Experiments with Primary Mammalian Cells: To Pool or Not to Pool. *Eur Cell Mater*, *24*, i-ii.

Sun, J. C., Beilke, J. N., & Lanier, L. L. (2009). Adaptive Immune Features of Natural Killer Cells. *Nature*, *457*(7229), 557-561.

Sun, Y., Jain, D., Koziol-White, C. J., Genoyer, E., Gilbert, M., Tapia, K., Panettieri, R. A., Jr., Hodinka, R. L., & Lopez, C. B. (2015). Immunostimulatory Defective Viral Genomes from Respiratory Syncytial Virus Promote a Strong Innate Antiviral Response During Infection in Mice and Humans. *PLoS Pathogens*, *11*(9), e1005122. https://doi.org/10.1371/journal.ppat.1005122

Sun, Y., Kim, E. J., Felt, S. A., Taylor, L. J., Agarwal, D., Grant, G. R., & López, C. B. (2019). A Specific Sequence in the Genome of Respiratory Syncytial Virus Regulates the Generation of Copy-Back Defective Viral Genomes. *PLoS Pathogens*, *15*(4), e1007707.

Swann, O. C., Rasmussen, A. B., Peacock, T. P., Sheppard, C. M., & Barclay, W. S. (2022). Avian Influenza A Virus Polymerase Can Utilise Human ANP32 Proteins to Support cRNA but Not vRNA Synthesis. *mBio, 14(1)*, e03399-22.

Swieton, E., Tarasiuk, K., & Smietanka, K. (2020). Low Pathogenic Avian Influenza Virus Isolates with Different Levels of Defective Genome Segments Vary in Pathogenicity and Transmission Efficiency. *Veterinary Research*, *51*(1), 108. https://doi.org/10.1186/s13567-020-00833-6

Szretter, K. J., Gangappa, S., Belser, J. A., Zeng, H., Chen, H., Matsuoka, Y., Sambhara, S., Swayne, D. E., Tumpey, T. M., & Katz, J. M. (2009). Early Control of H5N1 Influenza Virus Replication by the Type I Interferon Response in Mice. *Journal of Virology*, *83*(11), 5825-5834. https://doi.org/10.1128/JVI.02144-08

Szretter, K. J., Gangappa, S., Lu, X., Smith, C., Shieh, W. J., Zaki, S. R., Sambhara, S., Tumpey, T. M., & Katz, J. M. (2007). Role of Host Cytokine Responses in the Pathogenesis of Avian H5N1 Influenza Viruses in Mice. *Journal of Virology*, *81*(6), 2736-2744. https://doi.org/10.1128/JVI.02336-06

Tanaka, A., To, J., O'Brien, B., Donnelly, S., & Lund, M. (2017). Selection of Reliable Reference Genes for the Normalisation of Gene Expression Levels Following Time Course LPS Stimulation of Murine Bone Marrow Derived Macrophages. *BMC Immunology*, *18*(1), 43. https://doi.org/10.1186/s12865-017-0223-y

Tang, R.-B., & Chen, H.-L. (2013). An Overview of the Recent Outbreaks of the Avian-Origin Influenza A (H7N9) Virus in the Human. *Journal of the Chinese Medical Association*, *76*(5), 245-248.

Tapia, K., Kim, W.-k., Sun, Y., Mercado-López, X., Dunay, E., Wise, M., Adu, M., & López, C. B. (2013). Defective Viral Genomes Arising in Vivo Provide Critical Danger Signals for the Triggering of Lung Antiviral Immunity. *PLoS Pathogens*, *9*(10), e1003703.

Tate, M. D., Ioannidis, L. J., Croker, B., Brown, L. E., Brooks, A. G., & Reading, P. C. (2011). The Role of Neutrophils During Mild and Severe Influenza Virus Infections of Mice. *PloS One*, *6*(3), e17618.

Tate, M. D., Ong, J. D. H., Dowling, J. K., McAuley, J. L., Robertson, A. B., Latz, E., Drummond, G. R., Cooper, M. A., Hertzog, P. J., & Mansell, A. (2016). Reassessing the Role of the NLRP3 Inflammasome During Pathogenic Influenza A Virus Infection Via Temporal Inhibition. *Scientific Reports*, *6*, 27912. https://doi.org/10.1038/srep27912

Tate, M. D., Pickett, D. L., van Rooijen, N., Brooks, A. G., & Reading, P. C. (2010). Critical Role of Airway Macrophages in Modulating Disease Severity During Influenza Virus Infection of Mice. *Journal of Virology*, *84*(15), 7569-7580.

Taubenberger, J. K., Reid, A. H., Janczewski, T. A., & Fanning, T. G. (2001). Integrating Historical, Clinical and Molecular Genetic Data in Order to Explain the Origin and Virulence of the 1918 Spanish Influenza Virus. *Philosophical Transactions of the Royal Society of London. Series B: Biological Sciences*, *356*(1416), 1829-1839.

Taubenberger, J. K., Reid, A. H., Krafft, A. E., Bijwaard, K. E., & Fanning, T. G. (1997). Initial Genetic Characterization of the 1918 "Spanish" Influenza Virus. *Science*, *275*(5307), 1793-1796.

Taubenberger, J. K., Reid, A. H., Lourens, R. M., Wang, R., Jin, G., & Fanning, T. G. (2006). Was the 1918 Pandemic Caused by a Bird Flu? Was the 1918 Flu Avian in Origin?(Reply). *Nature*, *440*(7088), E9-E10.

Tavares, L. P., Teixeira, M. M., & Garcia, C. C. (2017). The Inflammatory Response Triggered by Influenza Virus: A Two Edged Sword. *Inflammation Research*, *66*(4), 283-302. https://doi.org/10.1007/s00011-016-0996-0

Te Velthuis, A. J., & Fodor, E. (2016). Influenza Virus RNA Polymerase: Insights into the Mechanisms of Viral RNA Synthesis. *Nature Reviews Microbiology*, *14*(8), 479-493.

Te Velthuis, A. J., Long, J. C., Bauer, D. L., Fan, R. L., Yen, H.-L., Sharps, J., Siegers, J. Y., Killip, M. J., French, H., & Oliva-Martín, M. J. (2018). Mini Viral RNAs Act as Innate Immune Agonists During Influenza Virus Infection. *Nature Microbiology*, *3*(11), 1234-1242.

Te Velthuis, A. J., Robb, N. C., Kapanidis, A. N., & Fodor, E. (2016). The Role of the Priming Loop in Influenza A Virus RNA Synthesis. *Nature Microbiology*, *1*(5), 1-7.

Te Velthuis, A. J. W., Grimes, J. M., & Fodor, E. (2021). Structural Insights into RNA Polymerases of Negative-Sense RNA Viruses. *Nature Reviews: Microbiology*, *19*(5), 303-318. https://doi.org/10.1038/s41579-020-00501-8

Thapa, R. J., Ingram, J. P., Ragan, K. B., Nogusa, S., Boyd, D. F., Benitez, A. A., Sridharan, H., Kosoff, R., Shubina, M., Landsteiner, V. J., Andrake, M., Vogel, P., Sigal, L. J., tenOever, B. R., Thomas, P. G., Upton, J. W., & Balachandran, S. (2016). DAI Senses Influenza A Virus Genomic RNA and Activates RIPK3-Dependent Cell Death. *Cell Host & Microbe*, *20*(5), 674-681. https://doi.org/10.1016/j.chom.2016.09.014

The RECOVERY Collaborative Group. (2020). Dexamethasone in Hospitalized Patients with Covid-19—Preliminary Report. *The New England Journal of Medicine*, *384*, 693-704. https://doi.org/DOI: 10.1056/NEJMoa2021436

Thomas, P. G., Dash, P., Aldridge Jr, J. R., Ellebedy, A. H., Reynolds, C., Funk, A. J., Martin, W. J., Lamkanfi, M., Webby, R. J., & Boyd, K. L. (2009). The Intracellular Sensor NLRP3 Mediates Key Innate and Healing Responses to Influenza A Virus Via the Regulation of Caspase-1. *Immunity*, *30*(4), 566-575.

Thompson, K. A., & Yin, J. (2010). Population Dynamics of an RNA Virus and Its Defective Interfering Particles in Passage Cultures. *Virology Journal*, *7*, 257. https://doi.org/10.1186/1743-422X-7-257

Thompson, M. R., Kaminski, J. J., Kurt-Jones, E. A., & Fitzgerald, K. A. (2011). Pattern Recognition Receptors and the Innate Immune Response to Viral Infection. *Viruses*, *3*(6), 920-940.

Thorne, L. G., Reuschl, A. K., Zuliani-Alvarez, L., Whelan, M. V., Turner, J., Noursadeghi, M., Jolly, C., & Towers, G. J. (2021). SARS-CoV-2 Sensing by RIG-I and MDA5 Links Epithelial Infection to Macrophage Inflammation. *The EMBO Journal*, *40*(15), e107826.

Tilston-Lunel, N. L., Welch, S. R., Nambulli, S., De Vries, R. D., Ho, G. W., Wentworth, D. E., Shabman, R., Nichol, S. T., Spiropoulou, C. F., & De Swart, R. L. (2021). Sustained Replication of Synthetic Canine Distemper Virus Defective Genomes in Vitro and in Vivo. *Msphere*, *6*(5), e00537-00521.

Tisoncik, J. R., Korth, M. J., Simmons, C. P., Farrar, J., Martin, T. R., & Katze, M. G. (2012). Into the Eye of the Cytokine Storm. *Microbiology and Molecular Biology Reviews*, *76*(1), 16-32.

To, K. F., Chan, P. K., Chan, K. F., Lee, W. K., Lam, W. Y., Wong, K. F., Tang, N. L., Tsang, D. N., Sung, R. Y., & Buckley, T. A. (2001). Pathology of Fatal Human Infection Associated with Avian Influenza A H5N1 Virus. *Journal of Medical Virology*, *63*(3), 242-246.

Tokunaga, R., Zhang, W., Naseem, M., Puccini, A., Berger, M. D., Soni, S., McSkane, M., Baba, H., & Lenz, H.-J. (2018). CXCL9, CXXCL0, CXCl11/CXCR3 Axis for Immune Activation–A Target for Novel Cancer Therapy. *Cancer Treatment Reviews*, *63*, 40-47.

Tong, S., Li, Y., Rivailler, P., Conrardy, C., Castillo, D. A. A., Chen, L.-M., Recuenco, S., Ellison, J. A., Davis, C. T., & York, I. A. (2012). A Distinct Lineage of Influenza A Virus from Bats. *Proceedings of the National Academy of Sciences*, *109*(11), 4269-4274.

Trouplin, V., Boucherit, N., Gorvel, L., Conti, F., Mottola, G., & Ghigo, E. (2013). Bone Marrow-Derived Macrophage Production. *JoVE (Journal of Visualized Experiments)*(81), e50966.

Tumpey, T. M., Basler, C. F., Aguilar, P. V., Zeng, H., Solórzano, A., Swayne, D. E., Cox, N. J., Katz, J. M., Taubenberger, J. K., & Palese, P. (2005). Characterization of the Reconstructed 1918 Spanish Influenza Pandemic Virus. *Science*, *310*(5745), 77-80.

Tumpey, T. M., Lu, X., Morken, T., Zaki, S. R., & Katz, J. M. (2000). Depletion of Lymphocytes and Diminished Cytokine Production in Mice Infected with a Highly Virulent Influenza A (H5N1) Virus Isolated from Humans. *Journal of Virology*, *74*(13), 6105-6116.

Turrell, L., Lyall, J. W., Tiley, L. S., Fodor, E., & Vreede, F. T. (2013). The Role and Assembly Mechanism of Nucleoprotein in Influenza A Virus Ribonucleoprotein Complexes. *Nature Communications*, *4*(1), 1-11.

Uiprasertkul, M., Kitphati, R., Puthavathana, P., Kriwong, R., Kongchanagul, A., Ungchusak, K., Angkasekwinai, S., Chokephaibulkit, K., Srisook, K., Vanprapar, N., & Auewarakul, P. (2007). Apoptosis and pathogenesis of avian influenza A (H5N1) virus in humans. Emerging Infectious Diseases, 13(5), 708–712. https://doi.org/10.3201/eid1305.060572

UK Health Security Agency. (2022). *Emerging-Infections-Summary-January-2022*. (UKHSA publications Gateway number: 11717). https://www.gov.uk/government/publications/emerging-infections-monthly-summaries Accessed September 2022.

Van Kerkhove, M. D., Mumford, E., Mounts, A. W., Bresee, J., Ly, S., Bridges, C. B., & Otte, J. (2011). Highly Pathogenic Avian Influenza (H5N1): Pathways of Exposure at the Animal-Human Interface, a Systematic Review. *PloS One*, *6*(1), e14582.

van Riel, D., Leijten, L. M., van der Eerden, M., Hoogsteden, H. C., Boven, L. A., Lambrecht, B. N., Osterhaus, A. D., & Kuiken, T. (2011). Highly Pathogenic Avian Influenza Virus H5N1 Infects Alveolar Macrophages without Virus Production or Excessive TNF-Alpha Induction. *PLoS Pathogens*, *7*(6), e1002099. https://doi.org/10.1371/journal.ppat.1002099

Varble, A., Albrecht, R. A., Backes, S., Crumiller, M., Bouvier, N. M., Sachs, D., & García-Sastre, A. (2014). Influenza A Virus Transmission Bottlenecks Are Defined by Infection Route and Recipient Host. *Cell Host & Microbe*, *16*(5), 691-700.

Vasilijevic, J., Zamarreño, N., Oliveros, J. C., Rodriguez-Frandsen, A., Gómez, G., Rodriguez, G., Pérez-Ruiz, M., Rey, S., Barba, I., & Pozo, F. (2017). Reduced Accumulation of Defective Viral Genomes Contributes to Severe Outcome in Influenza Virus Infected Patients. *PLoS Pathogens*, *13*(10), e1006650.

Vey, M., Orlich, M., Adler, S., Klenk, H.-D., Rott, R., & Garten, W. (1992). Hemagglutinin Activation of Pathogenic Avian Influenza Viruses of Serotype H7 Requires the Protease Recognition Motif RXK/RR. *Virology*, *188*(1), 408-413.

Viana, F., O'Kane, C. M., & Schroeder, G. N. (2022). Precision-Cut Lung Slices: A Powerful Ex Vivo Model to Investigate Respiratory Infectious Diseases. *Molecular Microbiology*, *117*(3), 578-588.

Vicary, A. C., Lekbua, A., Reddan, J., Rodriguez, Z. K., Mendes, M., & Russell, A. B. (2022). Maximal Interferon Induction by Influenza Lacking NS1 Is Infrequent Owing to Requirements for Replication and Export. *BioRxiv*. https://doi.org/10.1101/2022.10.24.513459

Vignuzzi, M., & Lopez, C. B. (2019). Defective Viral Genomes Are Key Drivers of the Virus-Host Interaction. *Nature Microbiology*, *4*(7), 1075-1087. https://doi.org/10.1038/s41564-019-0465-y

von Magnus, P. (1954). Incomplete Forms of Influenza Virus. In *Advances in Virus Research* (Vol. 2, pp. 59-79). Elsevier.

Vreede, F. T., Jung, T. E., & Brownlee, G. G. (2004). Model Suggesting That Replication of Influenza Virus Is Regulated by Stabilization of Replicative Intermediates. *Journal of Virology*, *78*(17), 9568-9572.

Walker, A. P., & Fodor, E. (2019). Interplay between Influenza Virus and the Host RNA Polymerase II Transcriptional Machinery. *Trends in Microbiology*, *27*(5), 398-407.

Wan, X.-F., Dong, L., Lan, Y., Long, L.-P., Xu, C., Zou, S., Li, Z., Wen, L., Cai, Z., & Wang, W. (2011). Indications That Live Poultry Markets Are a Major Source of Human H5N1 Influenza Virus Infection in China. *Journal of Virology*, *85*(24), 13432-13438.

Wandzik, J. M., Kouba, T., Karuppasamy, M., Pflug, A., Drncova, P., Provaznik, J., Azevedo, N., & Cusack, S. (2020). A Structure-Based Model for the Complete Transcription Cycle of Influenza Polymerase. *Cell*, *181*(4), 877-893 e821. https://doi.org/10.1016/j.cell.2020.03.061

Wang, C., Forst, C. V., Chou, T. W., Geber, A., Wang, M., Hamou, W., Smith, M., Sebra, R., Zhang, B., Zhou, B., & Ghedin, E. (2020). Cell-to-Cell Variation in Defective Virus Expression and Effects on Host Responses During Influenza Virus Infection. *mBio*, *11*(1). https://doi.org/10.1128/mBio.02880-19

Wang, F., Sheppard, C. M., Mistry, B., Staller, E., Barclay, W. S., Grimes, J. M., Fodor, E., & Fan, H. (2022). The C-Terminal LCAR of Host ANP32 Proteins Interacts with the Influenza A Virus Nucleoprotein to Promote the Replication of the Viral RNA Genome. *Nucleic Acids Research*, *50*(10), 5713-5725.

Wang, Q., Li, Q., Liu, T., Chang, G., Sun, Z., Gao, Z., Wang, F., Zhou, H., Liu, R., & Zheng, M. (2018). Host Interaction Analysis of PA-N155 and PA-N182 in Chicken Cells Reveals an Essential Role of UBA52 for Replication of H5N1 Avian Influenza Virus. *Frontiers in Microbiology*, 936.

Wang, X., Hinson, E. R., & Cresswell, P. (2007). The Interferon-Inducible Protein Viperin Inhibits Influenza Virus Release by Perturbing Lipid Rafts. *Cell Host & Microbe*, *2*(2), 96-105.

Wang, Y., Hao, Q., Florence, J. M., Jung, B. G., Kurdowska, A. K., Samten, B., Idell, S., & Tang, H. (2019). Influenza Virus Infection Induces ZBP1 Expression and Necroptosis in Mouse Lungs. *Frontiers in Cellular and Infection Microbiology*, *9*, 286. https://doi.org/10.3389/fcimb.2019.00286

Ward, M. P., & Brookes, V. J. (2021). Rabies in Our Neighbourhood: Preparedness for an Emerging Infectious Disease. *Pathogens*, *10*(3), 375.

Webster, R. G., & Govorkova, E. A. (2014). Continuing Challenges in Influenza. *Annals of the New York Academy of Sciences*, *1323*(1), 115-139.

Weis, S., & Te Velthuis, A. J. (2021). Influenza Virus RNA Synthesis and the Innate Immune Response. *Viruses*, *13*(5), 780.

Welch, S. R., Spengler, J. R., Harmon, J. R., Coleman-McCray, J. D., Scholte, F. E., Genzer, S. C., Lo, M. K., Montgomery, J. M., Nichol, S. T., & Spiropoulou, C. F. (2022). Defective Interfering Viral Particle Treatment Reduces Clinical Signs and Protects Hamsters from Lethal Nipah Virus Disease. *mBio*, *13*(2), e03294-03221.

Welch, S. R., Tilston, N. L., Lo, M. K., Whitmer, S. L. M., Harmon, J. R., Scholte, F. E. M., Spengler, J. R., Duprex, W. P., Nichol, S. T., & Spiropoulou, C. F. (2020). Inhibition of Nipah Virus by Defective Interfering Particles. *Journal of Infectious Diseases*, *221*(Suppl 4), S460-S470. https://doi.org/10.1093/infdis/jiz564

Welsh, R. M., & McNally, J. M. (1999). Immune Deficiency, Immune Silencing, and Clonal Exhaustion of T Cell Responses During Viral Infections. *Current Opinion in Microbiology*, *2*(4), 382-387.

Westenius, V., Mäkelä, S. M., Julkunen, I., & Österlund, P. (2018). Highly Pathogenic H5N1 Influenza A Virus Spreads Efficiently in Human Primary Monocyte-Derived Macrophages and Dendritic Cells. *Frontiers in Immunology*, *9*, 1664.

Westenius, V., Makela, S. M., Ziegler, T., Julkunen, I., & Osterlund, P. (2014). Efficient Replication and Strong Induction of Innate Immune Responses by H9N2 Avian Influenza Virus in Human Dendritic Cells. *Virology*, *471-473*, 38-48. https://doi.org/10.1016/j.virol.2014.10.002

Wille, M., & Barr, I. G. (2022). Resurgence of Avian Influenza Virus. *Science*, *376*(6592), 459-460.

Wise, H. M., Hutchinson, E. C., Jagger, B. W., Stuart, A. D., Kang, Z. H., Robb, N., Schwartzman, L. M., Kash, J. C., Fodor, E., & Firth, A. E. (2012). Identification of a Novel Splice Variant Form of the Influenza A Virus M2 Ion Channel with an Antigenically Distinct Ectodomain. *PLoS Pathogens*, *8*(11), e1002998.

Wisskirchen, C., Ludersdorfer, T. H., Muller, D. A., Moritz, E., & Pavlovic, J. (2011). The Cellular RNA Helicase UAP56 Is Required for Prevention of Double-Stranded RNA Formation During Influenza A Virus Infection. *Journal of Virology*, *85*(17), 8646-8655. https://doi.org/10.1128/JVI.02559-10

Wolbach, S. B. (1919). Comments on the Pathology and Bacteriology of Fatal Influenza Cases, as Observed at Camp Devens, Mass. *Bulletin of The Johns Hopkins Hospital*.

Woo, P. C., Tung, E. T., Chan, K. H., Lau, C. C., Lau, S. K., & Yuen, K. Y. (2010). Cytokine Profiles Induced by the Novel Swine-Origin Influenza A/H1N1 Virus: Implications for Treatment Strategies. *Journal of Infectious Diseases*, *201*(3), 346-353. https://doi.org/10.1086/649785

Woon, A. P., Boyd, V., Todd, S., Smith, I., Klein, R., Woodhouse, I. B., Riddell, S., Crameri, G., Bingham, J., & Wang, L.-F. (2020). Acute Experimental Infection of Bats and Ferrets with Hendra Virus: Insights into the Early Host Response of the Reservoir Host and Susceptible Model Species. *PLoS Pathogens*, *16*(3), e1008412.

World Health Organization. (2019). *Ebola Virus Disease: Key Facts*. https://www.who.int/news-room/fact-sheets/detail/ebola-virus-disease Accessed September 2022.

Xiao, C., Ma, W., Sun, N., Huang, L., Li, Y., Zeng, Z., Wen, Y., Zhang, Z., Li, H., & Li, Q. (2016). PB2-588 V Promotes the Mammalian Adaptation of H10N8, H7N9 and H9N2 Avian Influenza Viruses. *Scientific Reports*, *6*(1), 1-13.

Xiao, H., Killip, M. J., Staeheli, P., Randall, R. E., & Jackson, D. (2013). The Human Interferon-Induced Mxa Protein Inhibits Early Stages of Influenza A Virus Infection by Retaining the Incoming Viral Genome in the Cytoplasm. *Journal of Virology*, *87*(23), 13053-13058.

Xiao, Y., Lidsky, P. V., Shirogane, Y., Aviner, R., Wu, C. T., Li, W., Zheng, W., Talbot, D., Catching, A., Doitsh, G., Su, W., Gekko, C. E., Nayak, A., Ernst, J. D., Brodsky, L., Brodsky, E., Rousseau, E., Capponi, S., Bianco, S., . . . Andino, R. (2021). A Defective Viral Genome Strategy Elicits Broad Protective Immunity against Respiratory Viruses. *Cell*, *184*(25), 6037-6051. https://doi.org/10.1016/j.cell.2021.11.023

Xu, C., Hu, W.-B., Xu, K., He, Y.-X., Wang, T.-Y., Chen, Z., Li, T.-X., Liu, J.-H., Buchy, P., & Sun, B. (2012). Amino Acids 473V and 598P of PB1 from an Avian-Origin Influenza A Virus Contribute to Polymerase Activity, Especially in Mammalian Cells. *Journal of General Virology*, *93*(3), 531-540.

Xu, T., Qiao, J., Zhao, L., He, G., Li, K., Wang, J., Tian, Y., & Wang, H. (2009). Effect of Dexamethasone on Acute Respiratory Distress Syndrome Induced by the H5N1 Virus in Mice. *European Respiratory Journal*, *33*(4), 852-860.

Xu, T., Qiao, J., Zhao, L., Wang, G., He, G., Li, K., Tian, Y., Gao, M., Wang, J., Wang, H., & Dong, C. (2006). Acute Respiratory Distress Syndrome Induced by Avian Influenza A (H5N1) Virus in Mice. *American Journa of Respiratory and Critical Care Medicine*, *174*(9), 1011-1017. https://doi.org/10.1164/rccm.200511-1751OC

Xue, J., Chambers, B. S., Hensley, S. E., & López, C. B. (2016). Propagation and Characterization of Influenza Virus Stocks That Lack High Levels of Defective Viral Genomes and Hemagglutinin Mutations. *Frontiers in Microbiology*, *7*, 326.

Yamaji, R., Yamada, S., Le, M. Q., Ito, M., Sakai-Tagawa, Y., & Kawaoka, Y. (2015a). Mammalian Adaptive Mutations of the PA Protein of Highly Pathogenic Avian H5N1 Influenza Virus. *Journal of Virology*, *89*(8), 4117-4125.

Yamaji, R., Yamada, S., Le, M. Q., Li, C., Chen, H., Qurnianingsih, E., Nidom, C. A., Ito, M., Sakai-Tagawa, Y., & Kawaoka, Y. (2015b). Identification of PB2 Mutations Responsible for the Efficient Replication of H5N1 Influenza Viruses in Human Lung Epithelial Cells. *Journal of Virology*, *89*(7), 3947-3956.

Yang, M.-L., Wang, C.-T., Yang, S.-J., Leu, C.-H., Chen, S.-H., Wu, C.-L., & Shiau, A.-L. (2017). Il-6 Ameliorates Acute Lung Injury in Influenza Virus Infection. *Scientific Reports*, *7*(1), 1-11.

Yao, S., Narayanan, A., Majowicz, S. A., Jose, J., & Archetti, M. (2021). A Synthetic Defective Interfering SARS-CoV-2. *PeerJ*, *9*, e11686.

Yi, C., Zhao, Z., Wang, S., Sun, X., Zhang, D., Sun, X., Zhang, A., & Jin, M. (2017). Influenza A Virus PA Antagonizes Interferon-Beta by Interacting with Interferon Regulatory Factor 3. *Frontiers in Immunology*, *8*, 1051. https://doi.org/10.3389/fimmu.2017.01051

York, A., Hengrung, N., Vreede, F. T., Huiskonen, J. T., & Fodor, E. (2013). Isolation and Characterization of the Positive-Sense Replicative Intermediate of a Negative-Strand RNA Virus. *Proceedings of the National Academy of Sciences*, *110*(45), E4238-E4245. l

Young, P. L., Halpin, K., Selleck, P. W., Field, H., Gravel, J. L., Kelly, M. A., & MacKenzie, J. S. (1996). Serologic Evidence for the Presence in Pteropus Bats of a Paramyxovirus Related to Equine Morbillivirus. *Emerging Infectious Diseases*, *2*(3), 239.

Yu, W. C., Chan, R. W., Wang, J., Travanty, E. A., Nicholls, J. M., Peiris, J. S., Mason, R. J., & Chan, M. C. (2011). Viral Replication and Innate Host Responses in Primary Human Alveolar Epithelial Cells and Alveolar Macrophages Infected with Influenza H5N1 and H1N1 Viruses. *Journal of Virology*, *85*(14), 6844-6855. https://doi.org/10.1128/JVI.02200-10

Yuen, K.-Y., Chan, P., Peiris, M., Tsang, D., Que, T., Shortridge, K., Cheung, P., To, W., Ho, E., & Sung, R. (1998). Clinical Features and Rapid Viral Diagnosis of Human Disease Associated with Avian Influenza A H5N1 Virus. *The Lancet*, *351*(9101), 467-471.

Zankharia, U., Yadav, A., Yi, Y., Hahn, B. H., & Collman, R. G. (2022). Highly Restricted SARS-CoV-2 Receptor Expression and Resistance to Infection by Primary Human Monocytes and Monocyte-Derived Macrophages. *Journal of Leukocyte Biology*, *112*(3), 569-576.

Zeng, H., Pappas, C., Belser, J.A., Houser., K.V., Zhong, W., Wadford, D.A., Stevens, T., Balczon, R., Katz, J.M., & Tumpey, T.M. (2012). Human Pulmonary Microvascular Endothelial Cells Support Productive Replication of Highly Pathogenic Avian Influenza Viruses: Possible Involvement in the Pathogenesis of Human H5N1 Virus Infection. *Journal of Virology, 86(2)*, 667-78. https://doi.org/10.1128/JVI.06348-11

Zhai, W., Zhang, D. N., Mai, C., Choy, J., Jian, G., Sra, K., & Galinski, M. S. (2012). Comparison of Different Cell Substrates on the Measurement of Human Influenza Virus Neutralizing Antibodies. *PloS One*, *7*(12), e52327. https://doi.org/10.1371/journal.pone.0052327

Zhang, T., Yin, C., Boyd, D. F., Quarato, G., Ingram, J. P., Shubina, M., Ragan, K. B., Ishizuka, T., Crawford, J. C., Tummers, B., Rodriguez, D. A., Xue, J., Peri, S., Kaiser, W. J., Lopez, C. B., Xu, Y., Upton, J. W., Thomas, P. G., Green, D. R., & Balachandran, S. (2020). Influenza Virus Z-RNAs Induce ZBP1-Mediated Necroptosis. *Cell*, *180*(6), 1115-1129 e1113. https://doi.org/10.1016/j.cell.2020.02.050

Zhang, Z., Gu, Q., de Manuel Montero, M., Bravo, I. G., Marques-Bonet, T., Häussinger, D., & Münk, C. (2017). Stably Expressed APOBEC3H Forms a Barrier for Cross-Species Transmission of Simian Immunodeficiency Virus of Chimpanzee to Humans. *PLoS Pathogens*, *13*(12), e1006746.

Zhang, Z., Penn, R., Barclay, W. S., & Giotis, E. S. (2022). Naive Human Macrophages Are Refractory to SARS-CoV-2 Infection and Exhibit a Modest Inflammatory Response Early in Infection. *Viruses*, *14*(2). https://doi.org/10.3390/v14020441

Zhao, D., Liang, L., Wang, S., Nakao, T., Li, Y., Liu, L., Guan, Y., Fukuyama, S., Bu, Z., & Kawaoka, Y. (2017). Glycosylation of the Hemagglutinin Protein of H5N1 Influenza Virus Increases Its Virulence in Mice by Exacerbating the Host Immune Response. *Journal of Virology*, *91*(7), e02215-02216.

Zhao, Y., Lu, M., Lau, L. T., Lu, J., Gao, Z., Liu, J., Hoi Yu, A. C., Cao, Q., Ye, J., & McNutt, M. A. (2008). Neutrophils May Be a Vehicle for Viral Replication and Dissemination in Human H5N1 Avian Influenza. *Clinical Infectious Diseases*, *47*(12), 1575-1578.

Zheng, B.-J., Chan, K.-W., Lin, Y.-P., Zhao, G.-Y., Chan, C., Zhang, H.-J., Chen, H.-L., Wong, S. S., Lau, S. K., & Woo, P. C. (2008). Delayed Antiviral Plus Immunomodulator Treatment Still Reduces Mortality in Mice Infected by High Inoculum of Influenza A/H5N1 Virus. *Proceedings of the National Academy of Sciences*, *105*(23), 8091-8096.

Zhong, G., Le, M. Q., Lopes, T. J. S., Halfmann, P., Hatta, M., Fan, S., Neumann, G., & Kawaoka, Y. (2018). Mutations in the PA Protein of Avian H5N1 Influenza Viruses Affect Polymerase Activity and Mouse Virulence. *Journal of Virology*, *92*(4). https://doi.org/10.1128/JVI.01557-17

Zhou, B., Li, Y., Halpin, R., Hine, E., Spiro, D. J., & Wentworth, D. E. (2011). PB2 Residue 158 Is a Pathogenic Determinant of Pandemic H1N1 and H5 Influenza A Viruses in Mice. *Journal of Virology*, *85*(1), 357-365. https://doi.org/10.1128/JVI.01694-10

Zhou, H., Yu, Z., Hu, Y., Tu, J., Zou, W., Peng, Y., Zhu, J., Li, Y., Zhang, A., Yu, Z., Ye, Z., Chen, H., & Jin, M. (2009). The Special Neuraminidase Stalk-Motif Responsible for Increased Virulence and Pathogenesis of H5N1 Influenza A Virus. *PloS One*, *4*(7), e6277. https://doi.org/10.1371/journal.pone.0006277

Zhou, T., Gilliam, N. J., Li, S., Spaudau, S., Osborn, R., Anderson, C. S., Mariani, T. J., Thakar, J., Dewhurst, S., & Mathews, D. H. (2022). Generation and Functional Analysis of Defective Viral Genomes During SARS-CoV-2 Infection. *BioRxiv*. https://doi.org/10.1101/2022.09.22.509123

Zhu, Z., Fodor, E., & Keown, J. R. (2022). A Structural Understanding of Influenza Virus Genome Replication. *Trends in Microbiology*, 31(3), 308–319. https://doi.org/10.1016/j.tim.2022.09.015

Zobel, A., Neumann, G., & Hobom, G. (1993). RNA Polymerase I Catalysed Transcription of Insert Viral cDNA. *Nucleic Acids Research*, *21*(16), 3607-3614.

Appendix

Mouse	Virus	Time point	Total viral reads	PB1 DVGs	PB2 DVGs	PA DVGs
1	6:2 Tky/05	6 hrs	16,173	<30	<30	<30
2	6:2 Tky05	6 hrs	17,291	<30	**277-1872 (39)**	<30
6	6:2 Tky/05	24 hrs	59,623	<30	**277-1872 (45)**	<30
7	6:2 Tky/05	24 hrs	99,375	<30	**209-1927 (42)** **277-1872 (44)**	<30
11	6:2 Tky/05	48 hrs	155,424	<30	**209-1927 (312), 277-1872 (245),** 162-2138 (56)	295-1812 (30)
16	6:2 Tky/05	96 hrs	157,018	<30	120-2138 (190), 162-2097 (67)**, 277-1872 (67)**, 165-2138 (66), 190-2039 (52), 129-2140 (45), 217-2031 (44)	138-1958 (46)
1	7:1 Tky/05 HIGH	6 hrs	88,686	**244-2107 (1083)**	**116-2033 (6076) 242-2000 (696),** 149-2068 (331), 158-2114 (68), 110-2130 (53),	**129-2002 (105), 128-1974 (55), 162-1971 (36)**
2	7:1 Tky/05 HIGH	6 hrs	72,724	**244-2107 (1074),** 210-2308 (54), 361-2040 (32)	**116-2033 (5138), 242-2000 (601),** 149-2068 (339), 158-2114 (133), 110-2130 (51), 243-2121 (33)	**129-2002 (91), 128-1974 (77)**
6	7:1 Tky/05 HIGH	24 hrs	38,529	**244-2107 (425)**	**116-2033 (2625), 242-2000 (441)**, 149-2068 (195), 158-2114 (48), 110-2130 (38)	**129-2002 (31)**
7	7:1 Tky/05 HIGH	24 hrs	65,308	**244-2107 (431)**	**116-2033 (3597), 242-2000 (517),** 149-2068 (259), 158-2114 (79)	**128-1974 (40)**
11	7:1 Tky/05 HIGH	48 hrs	132,566	**244-2107 (1074)**, 210-2038 (54), 361-2040 (32)	**116-2033 (14659), 242-2000 (1574),** 149-2068 (1018), 158-2114 (285), 110-2130 (66), 244-2027 (64), 243-2121 (51), 215-2003 (35)	**128-1974 (155), 129-2002 (81), 187-1971 (38)**
12	7:1 Tky/05 HIGH	48 hrs	56,589	**244-2107 (449)**	**116-2033 (6575),** 149-2068 (506), **242-2000 (140),** 158-2114 (102),110-2130 (38)	**129-2002 (64), 128-1974 (58)**
16	7:1 Tky/05 HIGH	96 hrs	351,152	**244-2107 (1727)**	**116-2033 (12135), 242-2000 (1759),** 149-2068 (648), 190-2039 (317), 158-2114 (94), 110-2130 (90), 243-2121 (83), 215-2019 (46), 215-2003 (34)	**129-2002 (85), 128-1974 (33)**

17	7:1 Tky/05 HIGH	96 hrs	215,109	**244-2107 (672)**	**116-2033 (8542), 242-2000 (1621),** 149-2068 (620), 158-2114 (277), 110-2130 (62), 243-2121 (35)	**129-2002 (148), 128-1974 (41), 187-1971 (39)**
1	7:1 Tky/05 LOW	6 hrs	28,532	**244-2107 (190)**	**116-2033 (679), 242-2000 (65)**	**129-2002 (31)**
2	7:1 Tky/05 LOW	6 hrs	45,852	**244-2107 (283)**	**116-2033 (1087), 242-2000 (155),** 149-2068 (39)	**128-1974 (70), 129-2002 (63)**
6	7:1 Tky/05 LOW	24 hrs	243,849	**244-2107 (1380)** 231-2097 (36) 210-2038 (31)	**116-2033 (5844), 242-2000 (594),** 149-2068 (239), 158-2114 (83), 110-2130 (49), 120-2118 (32)	**129-2002 (359), 128-1974 (298), 162-1971 (41)187-1971 (39)**
7	7:1 Tky/05 LOW	24 hrs	204,938	**244-2107 (1317),** 231-2097 (35)	**116-2003 (5049), 242-2000 (629),** 149-2068 (237), 175-2099 (62), 158-2114 (55), 110-2130 (48)	**129-2002 (318), 128-1974 (270), 187-1971 (72) 162-1971 (34)**
11	7:1 Tky/05 LOW	48 hrs	143,696	**244-2107 (1895),** 210-2038 (33)	**116-2033 (9375),** 149-2068 (535), **242-2000 (444),** 158-2114 (91),243-2121 (69), 175-2099 (68), 110-2130 (40)	**129-2002 (742), 128-1974 (605), 187-1971 (99), 162-1971 (59)**
12	7:1 Tky/05 LOW	48 hrs	64,999	**244-2107 (1190),** 231-2097 (36)	**116-2033 (4613), 242-2000 (192),** 149-2068 (167), 158-2114 (141), 110-2130 (43)	**129-2002 (465), 128-1974 (344), 187-1971 (64)**
16	7:1 Tky/05 LOW	96 hrs	161,646	**244-2107 (2147)**	**116-2033 (12176),** 149-2068 (633), 158-2114(335), 120-2118 (164), **242-2000 (148),** 110-2130 (86), 169-2121 (37), 155-2067 (35), 119-2147 (30)	**129-2002 (1583), 128-1974 (1218), 162-1971 (204), 187-1971 (173),** 134-1973 (45)
17	7:1 Tky/05 LOW	96 hrs	347,736	**244-2107 (4608),** 210-2308 (71)**,** 231-2097 (57), 190-2092 (54)	**116-2033 (16880), 242-2000 (1922),** 149-2068 (835), 158-2114 (789), 175-2046 (232), 110-2130 (165), 243-2121 (81), 120-2118 (64), 120-2138 (59), 175-2099 (36)	**128-1974 (2217), 129-2002 (1674),** 134-1973 (256), **187-1971 (207), 162-1971 (198),** 204-1973 (41) 164-1885 (32)

Table A.1. More detailed ViReMa analysis on NGS from individual murine lungs. Deletion junctions are displayed in bold and underlined have the same deletion junctions as those identified in the corresponding viral stock. Read counts for each polymerase DVG is shown in parenthesis.

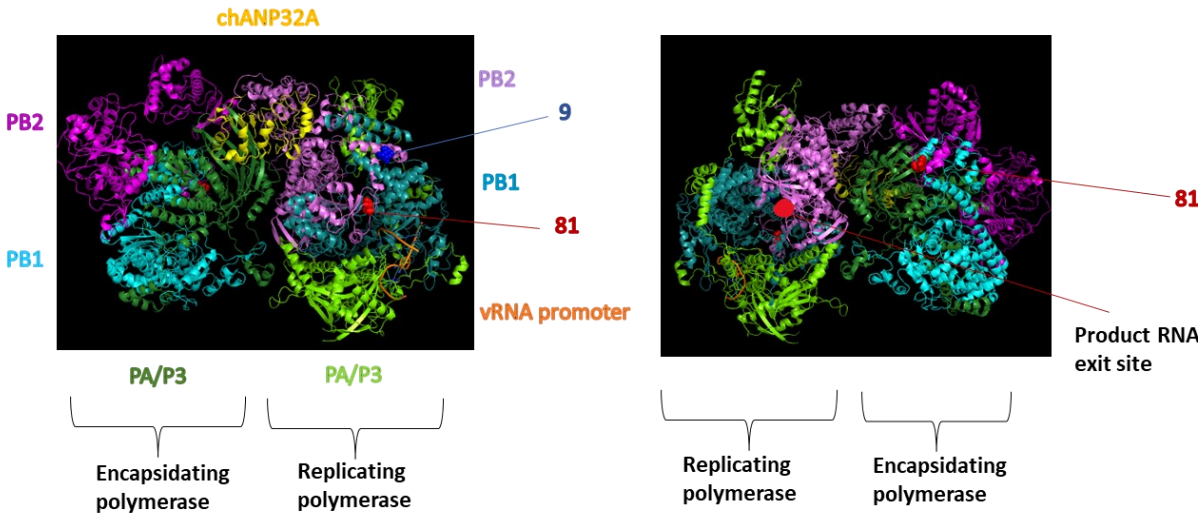

Figure A1A. The asymmetric dimer formed by replicating and encapsidating influenza C virus polymerase monomers during viral replication with PB2 residues 9 and 81 mapped. Due to insufficient resolution/low density the residue at position 9 was missing in the crystal structure of the encapsidating polymerase. The pro-viral factor ANP32 and vRNA promoter are also shown. The putative RNA exit site is shown in the right-hand panel where the structure has been rotated 180°. Although the structure corresponds to an influenza C polymerase, there is compelling evidence that Influenza A also adopts this conformation due to the importance of residues at the dimer interface during Influenza A replication (Carrique et al., 2020). This dimer is also believed to be formed by cRNA bound polymerases (Nilsson-Payant et al., 2022; Swann et al., 2022; Wang et al., 2022). This figure was generated in Pymol using PDB: 6XZR.

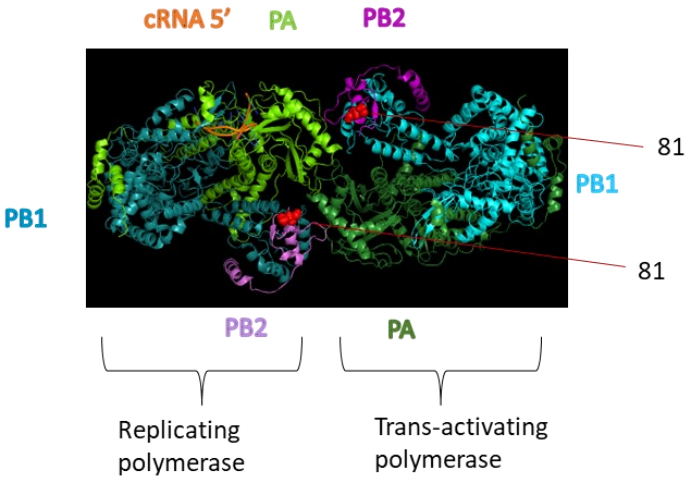

Figure A1B. The symmetric dimer formed by a replicating and trans-activating Influenza A polymerase for cRNA-vRNA synthesis with PB2 residue 81 mapped. Residue 9 is not shown due to insufficient resolution/low density in this region (Fan et al., 2019). This figure was generated in Pymol using PDB: 6QX8. The role of both influenza polymerase dimers (asymmetric and symmetric) is nicely reviewed in (Zhu et al., 2022).

Page No.	Type of work:	Name of work	Source of work	Copyright holder and contact	permission requested on	I have permission yes /no	Permission note
20	figure	Figure 1.1. Host species of IAV	Long J.*S et al*. (2019). Host and viral determinants of influenza A virus species specificity. Nature Reviews Microbiology **17**, 67-81 https://doi.org/10.1038/s41579-018-0115-z	Springer Nature Springer Nature Copyright Clearance Center's RightLink service https://s100.copyright.com/AppDispatchServlet	22.12.2022	yes	Written permission (licence given-5454230575795)
24-25	table	Table 1.1. Summary of the major functions of proteins encoded from the IAV genome	Pinto R.M *et al.* Accessory gene products of Influenza A virus. (2021) Cold Spring Harbor Perspectives in Medicine. 11 (12), a038380.	Cold Spring Harbor Laboratory Press https://www.cshlpress.com/permission_form.tpl	22.12.2022	yes	Written permission
32	figure	Figure 1.5. The composition of pandemic IAV strains.	Long J.*S et al*. (2019). Host and viral determinants of influenza A virus species specificity. Nature Reviews Microbiology **17**, 67-81 https://doi.org/10.1038/s41579-018-0115-z	Springer Nature Springer Nature Copyright Clearance Center's RightLink service https://s100.copyright.com/AppDispatchServlet	22.12.2022	yes	Written permission (licence given-5454230575795)
51	figure	Figure 1.8. A model of how Influenza DVGs/mvRNAs are made via a copy-choice mechanism	Te Velthius A.J.W *et al* (2018). Mini viral RNAs act as innat immune agonists during influenza virus infection. Nature Microbiology 3, 1234-1242. https://doi.org/10.1038/s41564-018-0240-5	Springer Nature Springer Nature Copyright Clearance Center's RightLink service https://s100.copyright.com/AppDispatchServlet	22.12.2022	yes	Written permission (licence given-5454240260522)
110	figure	Figure 4.14 Generation of pPol plasmids containing DVGs.	Neumann G. (1999). Generation of influenza A viruses entirely from cloned cDNAs. Proceedings of the National Academy of Sciences, 96(16), 9345-9350.	PNAS PNASPermissions@nas.edu	31.12.2022	yes	Written permission

Table A2. Table of permissions. All other figures reproduced throughout this thesis are under Creative Commons licence which permits their use.